Ecotoxicological and physico-chemical monitoring of home-manufactured quantum dots from luminescent devices

Bingbing Deng

Université Paris Cité

Ecole doctorale Chimie Physique et Chimie Analytique de Paris Centre (ED 388)

Laboratoire Interfaces, Traitement, Organisation et Dynamique des Systèmes (ITODYS)

Ecotoxicological and physico-chemical monitoring of home-manufactured quantum dots from luminescent devices

Par Bingbing DENG

Thèse de doctorat de **Nanosciences, matériaux, surfaces**

Présentée et soutenue publiquement le 17 octobre 2022

Devant le jury composé de :

M. Thibaud CORADIN, Directeur de Recherches, Sorbonne Université, Rapporteur
M. Fabien GRASSET, Directeur de Recherches, Université de Rennes, Rapporteur
Mme Souhir BOUJDAY, Professeure, Sorbonne Université, Examinatrice
Mme Yan-gai LIU, Professeure, Université de Géosciences (Beijing), Examinatrice
Mme Fayna, MAMMERI, Maitre de Conférences-HDR, Université Paris Cité, Directrice de thèse
M. Claude YEPREMIAN, Ingénieur d'Etudes, MNHN, Invité

Acknowledgments

Engaging in my PhD at lab ITODYS and University Paris Cite was a great experience for me. Many people have helped me during my studying here, and I would like to take this opportunity to thank everyone who made my PhD thesis possible.

First and foremost, I would like to express my sincere thanks to my supervisor for allowing me to study here and introducing me to this scientific research field. I would like to thank the late **Mme. Roberta Brayner** mentor for nurturing me in the field of microbiology, she was a very nice supervisor, I am sorry for her passing. Meanwhile, I am also very grateful to my current supervisor **Mme. Fayna Mammeri**, thanks for her enthusiastic help, advice, inspiration, encouragement, and continued support during my four years PhD, especially thanks to her for the comfort and care she gave me during my worst moments last year. **Fayna** has always been supportive of me, with her help I can adapt the life here quickly. In addition, I want to thank **Mme. Souad Ammar-Merah**, thanks for her help in my experiments and tests, she is very nice and friendly. I also want to thank **Lorette Sicard** for her concern in my experimental and life.

Moreover, I am grateful to **Antonino Madonia** and **Larissa Chaperman**, they are my earliest good friends here, they helped me a lot with the registration and other administrative matters, and with their help, I was able to quickly adapt to the experimental life here.

Meanwhile, I also want to thank my best intern **Rania Maaloul**, who worked 6 months in our lab, she did excellent work to help me with the toxicity tests, and we had a wonderful cooperation experience here. Thanks to her, I was able to complete the toxicology part of my work.

Besides, I must thank my good friend, **Marie-Charlotte Dragassi**, she is a very kind and beautiful girl who can help us with whatever we need, e.g., she helped me a lot with the booking of materials. At the same time, my sincere thanks also go to my good friend **Sonia Perez Quiros,** who is very friendly and helpful, she always comforts and encourages me when I am down. And I also sincerely thank my friend **Sendos Darwish** for her help with UV-vis testing.

Furthermore, I also got lots of help with the characterization of my samples. I would like to express my specific thanks to **Sophie Nowak,** she did a great help on the XRD and XRF tests of my samples. Thanks to **Patricia Beaunier** and **Guillaume Wang** for the TEM test. To **Yann Sivry**, for the ICP-AES measurement. To **Philippe Decorse**,

for the XPS characterizations. To **Thanh Ha Duong**, thanks for the assistance of the UV-vis and PL experiments. To **Claude Yéprémian**, for the guidance on microalgae cultivation. To **Chang-Zhi Dong**, for the assistance on the Envision Multilabel Plate Reader. To **Miguel Comesaña Hermo, thanks for his valuable advice on the silica coating part.** Their excellent work made a great contribution to my experiments.

I want to thank the member of my PhD defense committee, thanks to the reviewers, **M. Thibaud Coradin** and **M. Fabien Grasset**, for reviewing my thesis, and also the examiners, **Mme Souhir Boujda** and **Mme Yan-gai LIU**, for participating in my PhD defense in the coming October.

Besides, I would like to thank the lab ITODYS, thanks for supporting all the equipment and required reagents in my experiments. Meanwhile, I would like to express my sincere thanks to all the administration staff, including **Pierre-Francois Quenin**, **Juliette Le**, **Sylvio Rasolonarivo,** and **Philippe Cabaniols**, thanks for their help with the materials command and administrative procedures.

I am so glad to have the chance to study in the IMM group and know lots of nice mates here, they are all friendly and interesting people, I experienced an amazing spare and experimental time with them. And I would also like to thank those who were not in our team but were very supportive, because of them I had a great time in Paris for the past four years, including **Pengfei Gong, Yu Lei**.

Finally, I want to thank my family for their unconditional love, especially my mother, who always supported me in my further study. It is because of the unconditional dedication of my parents that I can continue my further study.

In the end, I really appreciate to China Scholarship Council (CSC, no. 201806400081), CNRS, and lab ITODYS for the financial support on my PhD project.

Bingbing DENG

Suivi écotoxicologique et physico-chimique de nanoparticules semi-conductrices possédant des propriétés luminescentes.

Courts résumés en français

Les NPs de ZnS sont un semi-conducteur de type n avec un large gap de bang direct, il est largement utilisé dans de nombreux domaines commerciaux en raison de ses propriétés optiques, électroniques et magnétiques spécifiques. Par ailleurs, l'effet écotoxicologique potentiel des nanoparticules (NPs) a attiré de plus en plus l'attention des chercheurs. Les NP peuvent augmenter la production d'espèces réactives de l'oxygène (ROS), induisant un stress oxydatif des cellules, et affecter les activités des mitochondries et des chloroplastes des organismes photosynthétiques, voire provoquer la mort cellulaire. Dans ce travail, nous avons préparé des NPs de ZnS : Mn de différentes tailles et des NPs de ZnS dopées par différents dopants par la méthode des polyols, qui est une méthode de synthèse très mature dans notre groupe. La petite taille des NPs ZnS : Mn (10%) est d'environ 1.1 à 1.5 nm, la grande taille est d'environ 8.5 nm, et les NPs ZnS monodopées Cu, Co sont d'environ 2.6 nm. Les tests XRD et TEM ont prouvé que toutes ces NPs ZnS ont une structure cubique. De plus, l'effet écotoxique de ces NPs ZnS sur Chlorella vulgaris a été évalué dans les milieux BG11, eau de la Seine (SRW) et eau de mer synthétique (SSW). L'activité photosynthétique, la viabilité cellulaire, l'activité des mitochondries et l'activité SOD ont été évaluées, et la structure et la morphologie des microalgues ont été mesurées par le test TEM. Nous avons démontré la toxicité des NPs de ZnS pour Chlorella vulgaris. Les NPs de ZnS : Mn (10%) de petite taille sont plus toxiques que les NPs de ZnS : Mn de grande taille, l'enveloppe de silice peut empêcher l'effet toxique des NPs de ZnS : Mn (10%) dans une certaine mesure. De plus, les NPs ZnS : Cu (10%) et ZnS : Co (10%) ont un effet toxique plus fort sur les mitochondries que les NPs ZnS : Mn (10%). De plus, le MET a montré que la paroi cellulaire est devenue plus mince et les NPs de ZnS ont été observées à l'intérieur du cytoplasme, et le cytoplasme a été détruit dans une certaine mesure après avoir été exposé dans le milieu traité par les NPs de ZnS pendant 96 heures.

Mots-clés en français:

Écotoxicité; quantum dots ZnS; Chlorella vulgaris; activité photosynthétique; activité des mitochondries.

Ecotoxicological and physico-chemical monitoring of home-manufactured quantum dots from luminescent devices

Short abstract in English

ZnS NPs is a n-type semiconductor with a wide direct bang gap, it is widely used in many commercial fields due to its specific optical, electronic and magnetic properties. Besides, the potential ecotoxicology effect of the nanoparticles (NPs) has attracted more and more attentions of the researchers. NPs can increase the reactive oxygen species (ROS) production inducing the oxidative stress to the cells, and affect the mitochondria and chloroplast activities of the photosynthetic organisms, even caused the cell death. In this work, we prepared the different size ZnS: Mn NPs and the different dopants doped ZnS NPs by the polyol method, which is a very mature synthesis method in our group. The small size of ZnS: Mn (10%) NPs is around 1.1 to 1.5 nm, the big size is about 8.5 nm, and the Cu, Co monodoped ZnS NPs is about 2.6 nm. The XRD and TEM test had proved that all these ZnS NPs have a cubic structure. Moreover, the ecotoxicity effect of these ZnS NPs on Chlorella vulgaris were evaluated in BG11, Seine River water (SRW) and synthetic seawater (SSW) mediums. The photosynthetic activity, cell viability, mitochondria activity and SOD activity were assessed, and the structure and morphology of the microalgae were measured by the TEM test. We have demonstrated the toxicity of the ZnS NPs to Chlorella vulgaris. The small size ZnS: Mn (10%) NPs are more toxic than the big size ZnS: Mn NPs, the silica shell can prevent the toxicity effect of ZnS: Mn (10%) NPs to some extent. Moreover, the ZnS: Cu (10%) and ZnS: Co (10%) NPs have a stronger toxicity effect to the mitochondria than the ZnS: Mn (10%) NPs. Furthermore, the TEM showed that the cell wall became more thinner and the ZnS NPs were observed inside the cytoplasm, and the cytoplasm were destroyed to some extent after exposed in the ZnS NPs treated medium 96 h.

Keywords in English:

Ecotoxicity; ZnS quantum dots; *Chlorella vulgaris*; photosynthetic activity; mitochondria activity.

Suivi écotoxicologique et physico-chimique de nanoparticules semi-conductrices possédant des propriétés luminescentes.

Résumé

Du fait de la large utilisation des nanomatériaux dans notre vie quotidienne, l'écotoxicité potentielle des nanoparticules (NPs) attire de plus en plus l'attention des chercheurs. Les nanoparticules peuvent augmenter la production d'espèces réactives de l'oxygène (ERO), lesquelles induisent un stress oxydant dans les cellules ; elles peuvent également affecter les activités des mitochondries et des chloroplastes des organismes photosynthétiques, voire s'attacher aux micromolécules dans les cellules (comme l'ADN, l'ARN et les protéines), provoquant un effet cytotoxique sur les cellules, et pouvant détruire l'intégrité de la membrane cellulaire et du cytoplasme, entraînant la mort cellulaire. Après que des produits manufacturés composés de NPs aient été jetés dans l'environnement, ils s'écouleront dans les rivières ou se déposeront dans le sol, provoquant une certaine toxicité envers les micro-organismes présents dans l'environnement. C'est pourquoi nous souhaitons étudier l'effet écotoxicologique des NPs de ZnS sur les microalgues (et notamment *Chlorella vulgaris*) dans les systèmes d'eau douce (BG11), d'eau de Seine (SRW) et d'eau de mer synthétique (SSW).

Les NPs de ZnS sont des semi-conducteurs de type n qui présentent une large bande interdite directe, et sont utilisés dans les dispositifs électroluminescents, par exemple. Mes travaux de thèse ont pour objectif l'étude de leur écotoxicité potentielle. Des nanoparticules de ZnS dopées au manganèse (ZnS:Mn) (0.5%, 2.0%, 4.0% et 10% en mol de Mn) ont été synthétisées par le procédé polyol, adapté pour préparer des NPs de petite taille (moins de 10 nm). Pour cela, nous avons mélangé l'acétate de zinc dihydraté ($Zn(CH_3COO)_2.2H_2O$) et la thiourée ($SC(NH_2)_2$) dans du diéthylène glycol (DEG), puis ajouté l'acétate de manganèse tétrahydraté ($Mn(CH_3COO)_2.4H_2O$) dont nous avons fait varier la concentration molaire, le tout à 180 ℃ pendant 30 minutes en présence d'oxyde de trioctylphosphine (TOPO). Toutes les NPs de ZnS dopées au Mn présentent une structure cubique, et ce, quelle que soit la concentration de Mn ; la taille de ces NPs varie de 1,1 nm à 1,5 nm et des mesures de spectroscopie de fluorescence X (XRF) et de spectroscopie de rayons X à dispersion d'énergie (EDX) ont montré que la teneur en Mn dans les NPs de ZnS augmente avec l'augmentation de la concentration molaire en Mn. Des analyses de spectroscopie de photoélectrons X (XPS) ont confirmé la présence des éléments Mn, Zn et S, et l'état de surface des NPs a également été caractérisé par XPS (spectres haute résolution). La diffusion

dynamique de la lumière (DLS) a montré des agrégats colloïdaux de taille comprise entre 300 nm et 700 nm à pH 6 et 8 ; les NPs de ZnS:Mn (10%) s'agrègent plus facilement dans le milieu de culture BG11, leur taille étant supérieure à 1000 nm à pH identique. Des mesures de potentiel zêta ont confirmé l'instabilité des colloïdes formés par ces NPs de ZnS:Mn. De plus, le pourcentage de dissolution de Mn^{2+} et de Zn^{2+} a été évalué par spectrométrie à plasma à couplage inductif (ICP-AES) : les résultats obtenus montrent que la dissolution de Mn^{2+} est plus élevée dans les eaux de Seine et de mer que dans l'eau MilliQ. La dissolution de Zn^{2+} augmente avec le temps dans l'eau milli-Q et l'eau de Seine, alors qu'elle reste constante dans l'eau de mer.

Puis nous avons testé l'effet écotoxicologique des nanoparticules de ZnS, de ZnS:Mn et de Mn^{2+} en solution sur les microalgues *Chlorella vulgaris* ; ces dernières ont été exposées aux NPs dans trois milieux de culture : eau pure (milieu BG11), eaux de rivière (Seine) et de mer en présence de 20 mg/L, 50 mg/L et 100 mg/L de nanoparticules ou d'ions Mn^{2+}. Par ailleurs, nous avons testé l'activité photosynthétique, le contenu intracellulaire en adénosine-5'-triphosphate (ATP), l'activité de la superoxyde dismutase (SOD) et la viabilité cellulaire des microalgues pendant 5 jours continus suivant l'introduction des nanoparticules ; l'activité photosynthétique et la viabilité cellulaire sont toutes deux diminuées dans tous les groupes de cultures en présence des NPs ZnS:Mn. En revanche, dans les milieux BG11 et eau de Seine, l'activité photosynthétique de *Chlorella vulgaris* a augmenté en présence de Mn^{2+}, bien que la viabilité cellulaire a diminué : ceci est probablement dû au fait que les microalgues peuvent collecter et stocker les ions métalliques pendant leur période d'adaptation. Parallèlement, l'activité SOD a augmenté de manière significative dans le milieu eau de mer, en présence de NPs ZnS:Mn, indiquant une augmentation sérieuse du stress oxydant dans les cellules d'algues ; le niveau d'ATP intracellulaire a également diminué de manière significative dans tous les milieux exposés aux NPs de ZnS:Mn, et plus particulièrement dans le milieu eau de mer en présence de 10% de NPs de ZnS:Mn. La structure et la morphologie des sections minces de *Chlorella vulgaris* ont été observées par microscopie électronique en transmission (TEM) : la structure initiale de *Chlorella vulgaris* présente toujours une paroi cellulaire claire, une membrane cellulaire et un cytoplasme ; la paroi cellulaire des cellules d'algues dans les milieux eau de Seine et eau de mer est plus épaisse qu'en milieu eau douce (BG11). Cependant, après exposition aux NPs de ZnS:Mn (0,5% et 10%), la paroi cellulaire, la membrane cellulaire et le cytoplasme des cellules ont été détruits ; les observations de TEM ont permis de mettre en évidence une paroi

cellulaire plus fine que celle initiale de la *Chlorella vulgaris*, un cytoplasme brisé, et les NPs de ZnS:Mn ont été observées à l'intérieur du cytoplasme, particulièrement après une exposition dans le milieu eau de mer. Ces résultats ont confirmé l'effet cytotoxique des NPs de ZnS:Mn sur la *Chlorella vulgaris*.

Afin de prévenir la toxicité des NPs de ZnS:Mn pour les microalgues, nous avons enrobé les NPs de ZnS:Mn (10%) d'une coquille de silice par la méthode de microémulsion inverse, puis évalué l'effet toxique des nanoparticules de structure cœur-coquille ZnS:Mn (10%) @SiO_2. La taille moyenne des nanoparticules de structure cœur-coquille ZnS:Mn (10%) @SiO_2 est d'environ 36 nm (la taille du cœur de ZnS:Mn (10 %) étant d'environ 4 nm). De façon intéressante, on observe que l'activité photosynthétique et la viabilité cellulaire de *Chlorella vulgaris* ont légèrement diminué dans les milieux d'eau douce (BG11) et d'eau de mer (SSW) en présence de NPs cœur-coquille (concentrations de 20 mg/L, 50 mg/L et 100 mg/L), tandis que l'activité photosynthétique et la viabilité cellulaire des microalgues dans le milieu eau de Seine n'ont pas été influencées par les NPs de ZnS:Mn (10 %) recouvertes de silice. En outre, le niveau d'ATP intracellulaire a diminué de manière significative dans l'eau douce (BG11) en présence de nanoparticules cœur-coquille (concentration de 50 mg/L). Dans l'eau de mer, l'activité des mitochondries a diminué dans tous les groupes de culture, et n'a pas été influencée par les NPs enrobées de silice. Parallèlement, les activités de la SOD dans les milieux BG11 et eau de Seine ont augmenté de manière significative au troisième et au dernier jour de test, respectivement ; elles ont clairement augmenté du troisième au dernier jour de test dans l'eau de mer, ce qui signifie que les NPs ont généré un stress oxydant plus important dans les algues dans l'eau de mer. Cependant, la viabilité cellulaire n'a pas été affectée par les NPs enrobées de silice. La diminution de l'activité photosynthétique et de l'activité des mitochondries est probablement due au fait que la grande quantité de NPs enrobées de silice a influencé le métabolisme normal des microalgues. Par conséquent, la coquille de silice peut prévenir la toxicité des NPs de ZnS:Mn (10%) dans une certaine mesure : bien que les NPs de ZnS:Mn (10%) enrobées de silice puissent générer un stress oxydant dans les cellules d'algues, elles ne sont pas mortelles pour les algues.

Nous avons également testé l'influence de la taille des NPs de ZnS:Mn (10%) sur leur toxicité. Ainsi, nous avons préparé des NPs de ZnS:Mn de plus grande taille par le procédé polyol assisté par micro-ondes (220W, 30 min) dans l'éthylène glycol (EG) et en présence de thioacétamide (TAA). Les NPs de ZnS:Mn produites présentent également une structure cubique et une taille d'environ 8,5 nm. Par DLS, des agrégats

sont de nouveau observés, de taille supérieure à 1700 nm à des valeurs de pH de 6 et 8; les mesures de potentiel zêta ont de nouveau confirmé l'instabilité colloïdale de ces NPs. Les analyses par XRF et EDX ont confirmé la présence de manganèse, les résultats XPS ont montré la présence des cations Zn^{2+} et Mn^{2+} dans les NPs de ZnS:Mn. De façon surprenante, on observe par ICP-AES, XRF et par des mesures magnétiques de magnétométrie, que des ions Mn^{2+} ont disparu dans les trois types de milieux, ce qui signifie que les ions Mn^{2+} et/ou Zn^{2+} se dissolvent dans le milieu aqueux.

L'écotoxicité de ces plus grosses particules de ZnS:Mn (10%) a été évaluée par le même protocole. L'activité photosynthétique a légèrement diminué dans les milieux eau douce (BG11) et eau de Seine (SRW), mais elle a augmenté dans le milieu eau de mer (SSW). La viabilité cellulaire n'a pas été affectée par ZnS:Mn (10%). De plus, le contenu intracellulaire en ATP a légèrement diminué dans le milieu BG11, et significativement diminué dans les milieux eaux de Seine et de mer (SRW et SSW) ; cependant, l'activité SOD n'a diminué dans aucun groupe de culture, quel que soit le milieu. Il y a deux raisons pour expliquer la diminution de l'activité SOD : l'une est la taille plus conséquente des NPs ZnS:Mn (10%) qui présentent un effet toxique sérieux résultant en l'inactivation de la SOD ; l'autre raison est que ces NPs ne peuvent pas induire la production de ROS en raison de leur forte agrégation autour des cellules. D'après l'activité des mitochondries et la viabilité cellulaire, nous pensons que ces NPs ont une forte influence sur les mitochondries, alors qu'elles ne sont pas trop toxiques pour les autres métabolismes de *Chlorella vulgaris*.

Enfin, nous avons synthétisé des NPs de ZnS dopées au manganèse (Mn), cuivre (Cu), ou cobalt (Co) en présence de TAA dans le diéthylène glycol (DEG) par la méthode polyol assistée par micro-ondes. La taille des NPs produites est comprise entre 2,6 nm et 3 nm, et toutes les NPs présentent une structure cubique confirmée par diffraction des rayons X et par TEM. Les analyses XRF et XPS ont confirmé la présence de Mn, Cu, Co dans les NPs de ZnS produites, et les spectres XPS à haute résolution ont confirmé que tous les ions de métaux de transition sont bien divalents. En outre, les spectres d'absorption UV-vis ont montré un décalage vers le rouge pour de faibles concentrations de dopant, et un décalage vers le bleu lorsque la concentration molaire de dopant augmente. Les spectres de photoluminescence des NPs de ZnS:Mn (10%) présentent une émission jaune-orange (à 585 nm) à la longueur d'onde d'excitation de 330 nm. Les NPs de ZnS:Cu (10%) présentent une émission bleue (à 437 nm) à la longueur d'onde d'excitation de 300 nm, et les NPs de ZnS:Co (10%) présentent une émission verte (centrée à 517 nm) à la longueur d'onde

d'excitation de 344 nm. En outre, l'écotoxicité de ces NPs a été étudiée sur *Chlorella vulgaris*. Les microalgues ont été exposées, dans différents milieux, à des concentrations plus faibles (20 mg/L, 40 mg/L et 60 mg/L) de NPs de ZnS monodopées au Mn, Cu, ou Co. L'activité photosynthétique, la viabilité cellulaire et le niveau intracellulaire ont diminué dans les milieux exposés aux NPs ZnS:Mn (10%). Par ailleurs, l'activité SOD a clairement augmenté pendant les trois premiers jours de test. En outre, l'exposition à des NPs de ZnS:Cu (10%) réduit également l'activité photosynthétique, la viabilité cellulaire et l'activité des mitochondries dans les trois milieux BG11, SRW et SSW, et l'activité SOD a augmenté au cours des trois derniers jours de test, ce qui signifie que les NPs de ZnS:Cu (10%) induisent l'augmentation de la production de ROS après un court temps d'adaptation. Parallèlement, les NPs de ZnS:Co (10%) ont un effet toxique plus important sur *Chlorella vulgaris* dans les milieux eau de mer (SSW) et de Seine (SRW) dans lesquels on observe que l'activité photosynthétique diminue significativement. De plus, l'activité intracellulaire diminue clairement dans les trois milieux, ce qui signifie que les NPs de ZnS:Co (10%) ont un effet plus toxique sur les mitochondries, particulièrement dans les eaux de Seine et de mer (SRW et SSW) ; l'activité SOD augmente également clairement dans les milieux SRW et SSW. En conclusion, les NPs de ZnS monodopées au Cu et Co ont un effet toxique plus important sur l'activité des mitochondries que les NPs de ZnS:Mn (10%).

Les principales conclusions de ce travail sont les suivantes : nous avons démontré la toxicité des NPs de ZnS dopées par des cations de transitions divalents (Mn^{2+}, Cu^{2+}, Co^{2+}) pour *Chlorella vulgaris*. Les NPs de petite taille sont plus toxiques que celles de taille supérieure ; de surcroît, plus la concentration de NPs est élevée et plus la toxicité est élevée (100 mg/L vs 20 mg/L). Une coquille de silice peut prévenir l'effet toxique des NPs. Les cations divalents du cuivre et du cobalt sont plus toxiques que celui du manganèse.

Mots clefs :

Écotoxicité, quantum dots ZnS, *Chlorella vulgaris*, activité photosynthétique, activité des mitochondries.

Table of contents

Chapter I. State of the art

Nanoparticles (NPs) have been widely studied due to their special physicochemical properties, such as quantum confinement effects and high specific surface area surface reactivity, surface chemical functions, and physicochemical stability.[1–4] Nanoparticles are widely used in luminescence, photovoltaic, drug delivery, optoelectronic, and other fields owing to their novel optical, electrical, and magnetic properties, including the semiconductors.[5–7] With the wider use of nanoparticles in our life, like for solar cells, LEDs, quantum computing, drug delivery, cosmetics, and medical imaging,[8] the concerns about their environmental effects and health impacts attract lots of people's attention. In the last 20 years, the nanoparticles have shown some different **toxicity** properties compared with the bulk materials due to their small size and their high reactivity, and with the decrease of the NPs size, the toxicity is increase.[2] Due to their small size, the NPs can easily penetrate the skin, mucous membrane, and cell membranes, which will produce some toxic effects on the cell,[9] and there are three ways can induce the toxicity of NPs, (1) surface interactions with microorganisms directly or NPs internalization by the microorganism, (2) the toxic metal ions (e.g. Cd^{2+}, Zn^{2+}, Ag^{+}) released from NPs, (3) oxidative stress induced by reactive oxygen species (ROS) due to the NPs or the toxic metal ions.[3] Based on this, nanotoxicology is emerging as a new important subdiscipline of nanotechnology, to do research on the relationship between nanostructures and biological systems and to know more information about the safety and the potential danger of nanoparticles.

To evaluate the ecotoxicological impact of NPs, their fate and behavior in the environment,[10] it is crucial to understand the **physicochemical properties** related to their nano size, shape, and huge surface area as nanoparticles more easily act with the biological system and produce more toxicity.[9] Another point is to study the biological target since, after the NPs are spread in the environment or the aquatic system, then they will be uptake by the planktonic or sediment microorganisms; the latter will be exposed to uncontrolled ecotoxicological effects,[2,11] and human beings may be affected from that too.

In the last two decades, lots of researchers have focused on the toxicological study of different NPs; they have many choices for the biological target, such as algae, duckweed, amphipods, daphnids, chironomids, chironomids, terrestrial plants, nematodes, and earthworms.[12] Each of them presents its advantages. For example, **algae** can be considered an appropriate research target since they just need a short exposure period to NPs (72h --96h) for the toxicity assessment; duckweed is also easy

to cultivate and can grow indefinitely into genetically homogeneous clonal colonies because of its vegetative reproduction method.[12]

Hence this chapter will present some fundamentals about 1) The research status of the nanoparticles ecotoxicology to understand the research progress: e.g., the ecotoxicology of CdS, ZnO, and TiO_2 NPs. 2) The biological target used in ecotoxicological experiments, since many living creatures can be used for ecotoxicity tests, like microalgae, fishes, mussels, and plants. They all have their advantages such as sensitivity to the NPs or short cultivation time. 3) The synthesis and toxicity research of the ZnS NPs to introduce the properties of and the potential toxicity of ZnS NPs.

1. Ecotoxicology research status of nanomaterials

Nanoparticles usually have external dimensions or internal structures measured on the nanoscale and exhibit different physical, chemical, biological, catalytic and optical properties compared with bulk materials; they have a great potential to use in different fields, such as clean energy, medicine, agriculture, astronomy, and environment remediation fields.[12] Although nanoparticles present special physicochemical properties and can be used in many commercial fields, the ecotoxicological effect of nanoparticles should also be paid attention to. According to Roberta Brayner's opinion, there are two factors which influence the toxic mechanisms of the chemical destabilization NPs: (i) the dissolution process, (ii) the redox evolution of the surface, which can produce reactive oxygen species (ROS), oxidize proteins, and induce the oxidative stress.[13]

The toxicological research have shown that nanoparticles may cause serious lung troubles, compared with bulk materials: NPs will cause more inflammation effects even using the same materials and same dose concentration.[14] However, it is not easy to draw general conclusions on the toxicity of the nanomaterials before comparing their properties with their relative bulk counterparts: indeed, nanoparticles present a higher surface/volume ratio and hence, intrinsic defects that affect the surface properties. Thus, nanoparticles may exhibit different ecotoxicological effects due to higher surface reactivity.[15]

Here, we have selected some of the most representative nanomaterials to introduce the ecotoxicity of the NPs, such as the ecotoxicity of CdS NPs due to the heavy metal cations Cd^{2+}, and the toxicity of the TiO_2 NPs that exhibit toxicity under specific conditions. Meanwhile, the toxicity of the widespread applicated NPs, like the ZnO NPs and antibacterial Ag NPs, is also introduced in this part.

1.1. Ecotoxicity of cadmium sulfide (CdS) NPs

CdS nanoparticles have been used in many fields, such as sunscreens, biosensors, pigments, rubber fillers, and electronic materials.[10] However, the toxicological effects of these NPs directly or not exposed in the environment are not clear.

Brayner et al. investigated the ecotoxicological features of cadmium sulfide (CdS) NPs using photosynthetic microorganisms (*Anabaena flos-aquae cyanobacteria and Euglena gracilis euglenoid microalgae*).[13] Brayner et al. synthesized CdS NPs by the polyol process, with and without tri-n-octylphosphine oxide (TOPO), used to control the size and shape, but also to protect the NP surface and potentially reduce the toxicity. The toxicity of Cd^{2+} was tested through an exposition to cadmium acetate. The NPs concentration they used varied from 10^{-3} to 5×10^{-4} mol/L; the authors evidenced that the Cd^{2+} ions were more toxic to *Anabaena flos aquae* than to *Euglena gracilis*. Moreover, the toxicity of CdS and CdS-TOPO varied with the concentration: TEM pictures revealed that the morphology of the microorganisms changed, and that NPs were inside the cells, which means NPs caused some metabolic reactions in microorganisms. They also confirmed the toxicity of Cd^{2+} ions and CdS NPs. Thus, toxicity and biocompatibility tests are necessary concerning the public and environmental health for the further use of CdS NPs or quantum dots (Fig. 1).

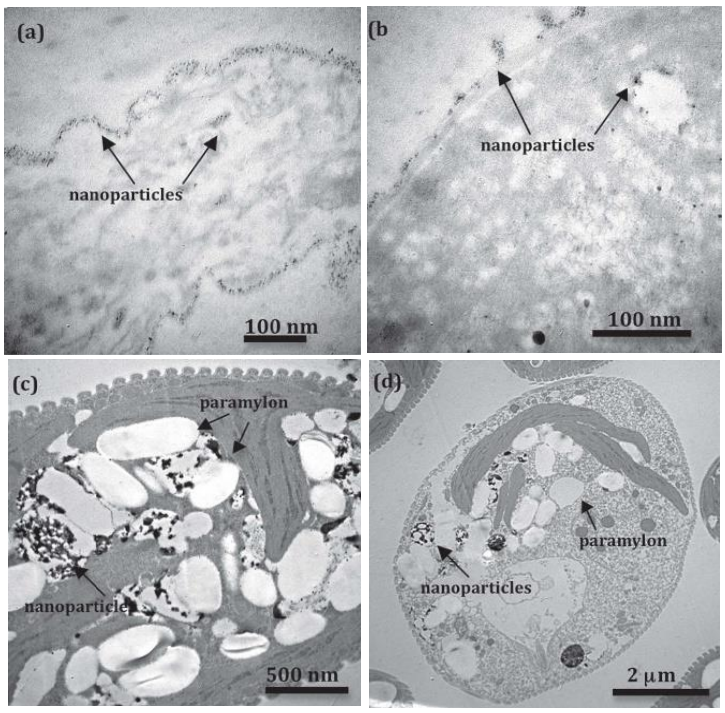

Fig. 1 *TEM micrographs of Anabaena flos-aquae after contact with 10^{-3} M (a) CdS, (b) CdS-TOPO; Euglena gracilis after contact with 10^{-3} M (c) CdS, (d) CdS-TOPO. From Ref 13*

Da Rocha et al. focused on the fate of CdS and ZnO NPs, synthesized by the polyol process, in the Seine River Water.[10] The authors studied the behavior and evolutions over time of the nanoparticles with different compositions and structures in the natural environment. They chose ZnO and CdS presenting different structures (fcc and hcp), after contacting these NPs with Seine River Water for a period. They did some essential characterizations (XRD, SAXs, cryo-TEM), which showed that the fcc CdS sample was totally agglomerated, as well as ZnO sample; on the contrary, the hcp CdS sample remained unchanged. The dissolution of these NPs in the Seine River Water was also different: ZnO NPs almost present a 90% dissolution, which may increase the toxicity in a natural environment.

Da Rocha et al. also studied the ecotoxicological effect of ZnO and CdS NPs on the photosynthetic microorganism *Chlorella vulgaris* in Seine River water.[16] They evaluated the toxicity degree of the ZnO and CdS NPs as well as Zn^{2+} and Cd^{2+} free ions. Through the viability test and photosynthetic activity test, they confirmed that the **free Zn^{2+} is less toxic** compared with the free Cd^{2+} and ZnO NPs; however, the toxic degree of free Cd^{2+} is almost the same with CdS NPs. Hence, the toxic degree can be sorted in descending order as follows: CdS > Cd^{2+} > ZnO > Zn^{2+}; this has been confirmed by the Adenosine-5'-triphosphate (ATP) assay and superoxide dismutase (SOD) enzymatic activity test. In addition, when the nanoparticle concentration reached 10^{-2} mol/L, the NPs was internalized by the algae, as observed by TEM.

Yu et al. investigated the effect of four different NPs on the toxicity of cadmium on *Chlamydomonas reihardtii.*[17] Cadmium can reduce the algae biomass and affect the photosynthetic activity of algae. Therefore, the authors studied the influence of TiO_2, SiO_2, Ag, and core-shell CdTe/CdS quantum dots (QDs) on cadmium toxicity: they reported that the n-TiO_2 and n-SiO_2 can decrease the intracellular Cd content and reduce the toxicity of Cd on the *Chlamydomonas reihardtii* cell, while the CdTe/CdS QDs is mostly increasing the Cd toxicity on the algae cell due to the Cd dissolution of the cadmium-containing QDs. Ag NPs did not show any synergistic effect on the toxicity of Cd-containing materials. This work highlights the possibility of a **synergistic effect** of different NPs on the Cd toxicity on the microalgae and the complexity to evaluate the toxicity of a multi-component material.

Silva et al. studied the toxic effect of the cadmium based QDs on the aquatic biota and investigated the influence of natural sunlight exposure on the NPs toxicity.[18] They proved that the toxicity of CdS 480 and CdSeS QDs on *Daphnia magna (D. magna)* and *Raphidocelis subcapitata* (*R. subcapitata)* can be decreased by sunlight exposure,

while the toxicity of CdS 380 on *D. magna* would be increased. Their work suggests that **sunlight exposure** may affect the surface functional groups of the NPs causing the aggregation and precipitation of the larger QDs, which may lead to a lowered release of Cd^{2+} ions into the aquatic medium and lowered ROS production; therefore, the toxicity of the CdS QDs can be reduced. Overall, this work revealed the effect of the relevant abiotic factor (sunlight) on the toxicity of the nanoparticles.

Moreover, the toxicity of N-acetyl cysteine coated core-shell CdS:Mn/ZnS QDs (NAC-QDs) on plant life was studied by Das et al., who confirmed the toxic effect of the ultra-small size QDs on the seed germination and growth of the snow pea model plant system (Pisum sativum).[19] Through the monitoring of the fluorescence of NAC-Qdot, they could track the dispersion of the NPs in the seeds during the germination process; after 48h exposure of the seeds to the NAC-Qdot, the NPs appeared inside a few cell layers under the surface of the seeds, and the concentration of the NAC-Qdots was found to have a great influence on the process of the seed germination and seed growth. When the NPs concentration is lower than 40 μg/mL, the NAC and Zn cations can passivate the Cd cation to prevent phytotoxicity. Once the concentration exceeded this threshold, the seedling growth was severely affected, and even the photosynthetic activity was influenced. In this work they highlighted the existence of a threshold of the NAC-Qdot on the seedling growth of snow pea, confirming the nanotoxicity of the CdS:Mn/ZnS QDs on the plant.

Besides, the toxicity of ten kinds of common NPs, including CdS NPs, on echinoderms, namely sea urchin (*Strongylocentrotus intermedius*), was also investigated by Pikula et al.[20] They studied the spermatozoa activity, egg fertilization, and early stage of embryo development of the sea urchin to assess the toxicity of the selected NPs. They evidenced that two kinds of silicon nanotubes (SNT-1, SNT-2) presented the highest embryotoxicity, while CdS, ZnS, and Au NPs and the silicon tube (SNT-2) had the inhibition effect on egg fertilization, meanwhile the spermatozoa activity was also inhibited by the CdS and ZnS NPs under the highest-used concentrations (50 mg/L and 100 mg/L). This work highlighted the toxicology of the NPs on **marine life**.

1.2. Ecotoxicity of zinc oxide (ZnO) NPs

Zinc oxide (ZnO) nanoparticles, as an essential ingredient of many manufactured products,[21] have been widely used in many commercial applications, like pigments in paints, and fillers in rubber due to their chemical stability and strong adsorption; they

can also be applied as sensors, photovoltaic and solar cells because of their piezoelectric and luminescent properties.[2,22,23] And thousands of tons of ZnO NPs are produced every year.[2] However, ZnO NPs are intrinsically toxic to some bacteria and microalgae (such as Escherichia coli, cyanobacteria, and Euglena gracilis microalgae).[15,22,24] They can break down cell membranes and accumulate in the cytoplasm causing cell death; the action mechanism was owing to the activation by light,[21] so sometimes they are also used as an effective against microorganisms materials.[15] In addition, ZnO NPs can cause toxic effects at a lower concentration, especially to the algae, since they can damage the membrane integrity and cause a decrease in cell viability.[12,15] Some researchers have demonstrated that toxic effects are mainly caused by the Zn^{2+} ions and that the **dissolution process** of ZnO NPs plays an important role to its toxicity.[12,21]

Gelabert et. al measured the nanoeffect of the NPs on bacteria: they exposed the E. coli strains MG1655 and W3110 to different concentrations (0.1-1 mmol/L) of nano-ZnO and Zn^{2+} in Luria Bertani (LB) medium to explore the nanotoxicity mechanisms.[25] They confirmed that the nanotoxicity of the ZnO NPs to Gram-negative bacterial cells partly comes from the ZnO NPs and partly comes from the dissolution of the Zn^{2+} in the medium. This means that both can inhibit the growth of the bacteria. The strain W3110 presents a stronger resistance to ZnO nanotoxicity than MG1655; in addition, they conclude that the sensitivity to the nanotoxicity was related to **respiratory metabolism**.

Brayner et al. studied the ecotoxicological properties of nanostructured films of ZnO.[22] They prepared 3 kinds of ZnO NPs differing by the surface modification (ZnO, ZnO-TOPO, ZnO-Brij-76) and one sample of zinc acetate without nanoparticles (ZnO-SOL), that were contacted with 3 kinds of microorganisms (*Anabaena flos-aquae, Calothrix pulvinata cyanobacteria and Euglena gracilis*). These microorganisms' fifer by the fact that the *Anabaena flos-aquae* and *Calothrix pulvinate* present polysaccharides surrounding the cell wall, which can prevent the internalization of the NPs; however, *Euglena gracilis* can internalize the NPs by endocytosis. The epifluorescence microscopy analyses, and Live/Dead test indicated that all the films are toxic to the *Euglena gracilis*, while ZnO-TOPO and ZnO-Brij-76 are not toxic for *Anabaena flos-aquae* and *Calothrix pulvinate*, because the tri-n-octylphosphine oxide (TOPO) and polyoxyethylene stearyl ether (Brij-76) molecules can prevent the ZnO NPs toxicity.

Brayner et al. also studied the toxicological effect of the ultrafine ZnO NPs in a colloidal medium on *Escherichia coli* bacteria.[14] Various ZnO NPs differing by their surface chemistry (BSA, TOPO, SDS, Brij-76) were prepared using the polyol method, and their size ranged from 10 nm to 14 nm. The toxicological tests were carried out using different concentrations of these NPs, and the results showed that the lower concentration of pure ZnO NPs was safe and did not cause any damage to the bacteria. If the ZnO NPs concentration was higher than 1.3×10^{-3} mol/L, the cells were damaged and the cell content was leaked out; in addition, the NPs with some small molecules and macromolecules in DEG medium can also have the same influence on the cells compared with the NPs in free Luria-Bertani (LB) medium group, which was due to the increase of the membrane permeability in DEG medium leading to the accumulation of ZnO NPs in the bacteria cells. This research highlights the role of the **surface state** of the NPs.

Suman et al. also studied the toxicity of ZnO NPs using a marine algae *Chlorella vulgaris*,[23] because they assumed that ZnO NPs will release a high concentration of ionic zinc in the seawater, this latter being a potential reason for the toxicity of ZnO NPs. To elucidate the mechanism of the toxicity, they chose the *Chlorella vulgaris* as the biological target, and contacted it with different concentrations of ZnO NPs for 24h and 72h; then they performed the flow cytometric, cytotoxicity and oxidative stress analysis to evaluate the toxicity. The viability of *Chlorella vulgaris* decreased with the increase of the concentration of ZnO NPs, and the activity of superoxide dismutase (SOD) increased after exposure of *Chlorella vulgaris* to 200 mg/L and 300 mg/L of ZnO NPs. Moreover, the non-enzymatic antioxidant glutathione (GSH) content decreased, and the level of lipid peroxidation (LPO) increased after exposure to the ZnO NPs. These results showed that the ZnO NPs are toxic to the *Chlorella vulgaris*: when ZnO NPs will interact with the algae, a distorted morphological is developed. All these works established an endpoint for the **toxicity of ZnO NPs to *Chlorella vulgaris*** (Fig. 2).

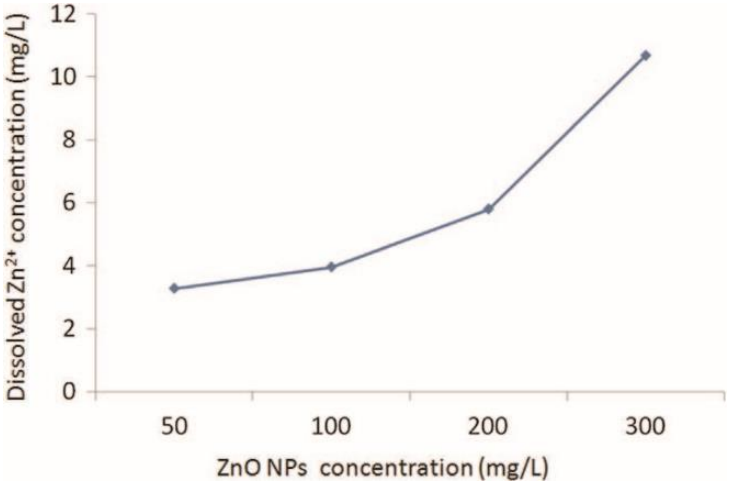

Fig. 2 *Dissolved Zn^{2+} concentration as a function of the ZnO NPs concentration. From Ref 23*

Finally, Serrà et al. carried out interesting research on the ecotoxicological and photocatalytic analysis of different structures of ZnO NPs using ZnO films, ZnO@ZnS core@shell fern-like biomimetic microleaf arrays and ZnO NPs. They studied the photocorrosion resistance and the toxicity of these different nanostructure NPs on microalgae *Spirulina (Arthrospira) platensis;*[26] their work showed that the algae viability has significant improved in presence of ZnO@ZnS core@shell fern-like NPs. The ecotoxicity was also drastically reduced compared with the other structures. ZnO NPs at the same light exposure condition, and ZnO@ZnS micro/nanoferns at the concentration of 400 mg/L also had an excellent photcatalytic efficiency to mineralize the polluted water. In their work, they demonstrated that the special structure ZnO@ZnS fern-like arrays supported on solid substrates can significantly improve photocatalytic performance and decrease the photocorrosion activity and ecotoxicity. Hence, they can be used as an eco-friendly material to remediate polluted water.

1.3. Ecotoxicity of titanium dioxide (TiO_2) NPs

Due to the low toxicity, biocompatibility, strong oxidizing properties and long-term photostability,[27] TiO_2 NPs are highly produced in the world, and they are widely applied in many fields, such as photocatalysts, cosmetics, sunscreens, solar cells, paints or food additives.[28–31] Usually, TiO_2 NPs are chemically inert materials; however, they can become highly reactive after being photoactivated, especially under UV irradiation, which can produce reactive oxygen species (ROS) for the biological cells.[9] So they can be used as antibacterial materials, but at the same time, they will also present a potential toxicity threat to the ecosystems, especially to aquatic microorganisms.[31]

Planchon et al. tested the ecotoxicological impact of three kinds of artificial TiO_2 NPs (R = rutile structure, M = mixed structure, and P25 from Degussa) on *Escheriichia coli* in natural and artificial waters.[8] Significant toxicity of TiO_2 NPs was observed at 10 ppm concentrations under the ambient light, and the toxicity depended on the structure of the NPs, the toxicity of the pure rutile TiO_2 NPs (R) was slightly lower than the mixed TiO_2 NPs (M and P25). The toxicity of TiO_2 NPs in the synthetic water with pH 5 was lower than that in Seine water (pH 8), and there was a stronger interaction between TiO_2 NPs and *Escheriichia colli* cells in the medium with pH 5. They also observed, by TEM and zetametry, that the toxicity was not directly related to the aggregation of NPs on the cell surfaces. Moreover, they confirmed that the toxicity of the anatase polymorph NPs was slightly higher than that of the pure rutile nanoparticles, which means that the **crystalline structure** is related to the toxicity of the NPs.

Pikula et al. studied the toxicity of individual and derivative composites of NPs on marine microalgae *Heterosigma akashiwo*.[32] They prepared five kinds of nanoparticles including CdS, ZnS, TiO_2, and two kinds of mesoporous silicon dioxide (with (SMB24) and without (SMB3) metal inclusions) to explore the individual and mixture NPs toxicity through the growth inhibition of the microalgae bioassay. The highest toxicity was observed for individual SMB24 (EC50, 3.6 mg/L)[a] and CdS (EC50, 21.3 mg/L). Meanwhile, they confirmed that TiO_2 and SMB3 NPs had a **synergy effect** on the toxicity of CdS and ZnS NPs. However, SMB24 NPs had an antagonistic toxic effect with CdS and ZnS NPs. According to the authors, it was due to the metal ion scavenging effect. Indeed, they had proved the different NPs can have a synergy toxic effect on the microalgae, and can have an antagonistic toxic effect, which probably **pave a way for combining the NPs** in the future.

Gottschalk et al. predicted the environmental concentrations of the manufactured nanomaterials using a probabilistic material flow analysis through the life-cycle perspective of the engineered nanomaterials (nano-TiO_2, nano-ZnO, nano-Ag, fullerenes, and carbon nanotubes).[11] They modeled the environmental concentrations of these NPs for the U.S., Europe, and Switzerland using the probabilistic density functions. The most frequent concentrations they modeled were 0.003 ng/L (fullerenes) and 21 ng/L (nano-TiO_2) in the surface waters, and it ranged from 4 ng/L (fullerenes) to 4 μg/L (nano-TiO_2) in the sewage treatment effluents. They also found that the

[a] EC50 = concentration for 50% of maximal effect. It is used to test the effect of antibacterial materials or medicine.

engineered nanomaterials in the sludge-treated soil increased with the year: for fullerenes it increased 1 ng/kg every year, and 89 μg/kg for nano-TiO_2. This work evidenced the ecotoxicological risks of nano-TiO_2, nano-ZnO and nano-Ag on the **aquatic biota**.

Yinghan Liu et al. studied the toxicity of the mixture made of TiO_2 and/or SiO_2 and/or ZrO_2 NPs on the freshwater algae *Scenedesmus obliquus*.[33] They tested the toxic effect of these individual, binary, and ternary nanoparticle mixtures. The results showed that the combined NPs influenced the mitochondria activity while the individual NPs did not induce any inhibition effect on the photosynthetic activity at the same concentrations. The ternary mixture of NPs significantly increased the mitochondria membrane potential and the ROS level in the algae cell for the NP concentration of 1 mg/L, meanwhile, the antioxidant defense enzyme SOD and catalase, as well as the lipid peroxidation products and the small molecule metabolisms were increased; this means that the ternary mixture could induce severely oxidative damage to the algae cells, and it was demonstrated by the superficial structure of the algae cells. Overall, their work had proved that the **mixture** of TiO_2, SiO_2 and ZrO_2 NPs would present a **more serious toxicity** on the algae cells compared with the individual NPs **at the same lower concentrations** (Fig. 3).

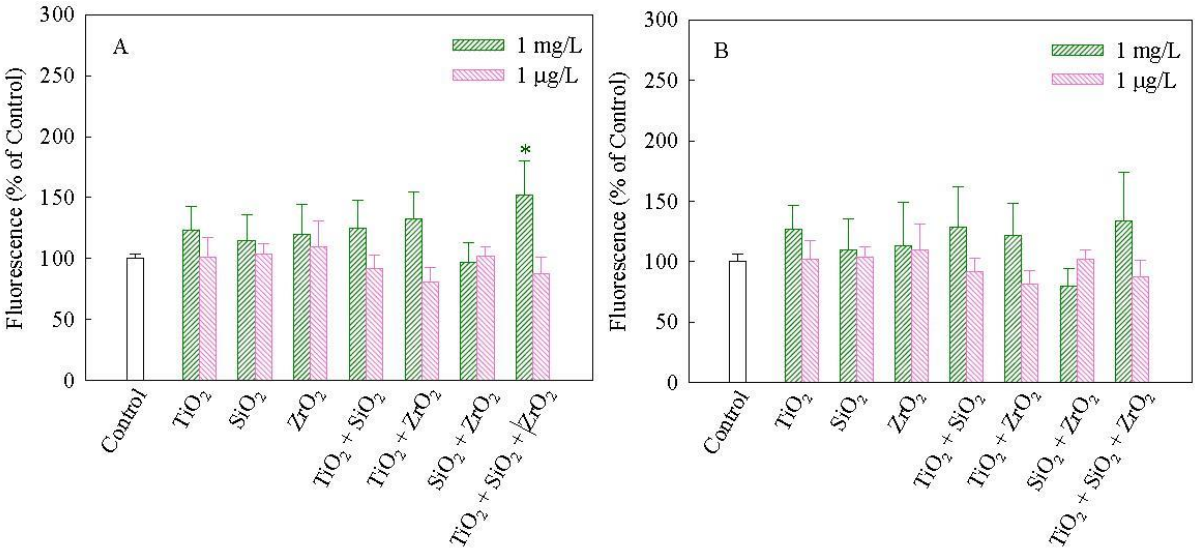

Fig.3 *Mitochondrial membrane potential (A) and cellular membrane permeability (B) of S. obliquus exposed to 1 mg/L and 1 μg/L of alone and combined NPs. From Ref 33*

Kose et al. investigated the toxicity impact of the TiO_2 NPs on human cells according to their physicochemical properties, such as the particle size, charge, shape crystallinity and agglomeration state.[34] They used five kinds of TiO_2 NPs with different

sizes/specific surface area, shape, agglomeration state and surface functionalization or charges, and they tested their toxicity impact on two different cells, A549 cells and macrophages differentiated from the human monocytic THP-I cells, in the monoculture or co-culture systems. They observed the smaller size and the larger aggregated TiO_2 NPs had a less toxic effect compared with the commercial P25 sample, and the rod-shaped TiO_2 NPs seemed to present a more toxic effect. Meanwhile, they found the positively charged NPs were more toxic compared with the negatively charged NPs. Interestingly, although these NPs caused some toxic effects on the human cells, they did not induce any ROS production in the two kinds of human cells. This research work proved that the **physicochemical features** (e.g., shape, size, and surface charge) can influence the toxic effect of NPs on **human cells**.

Moreover, Valentini et al. studied the hepatic and renal toxicity of TiO_2 NPs in rats,[35] exposing them to different concentrations of TiO_2 NPs, during different assessed times (4 days, 1 month and 2 months). In these conditions, TiO_2 NPs caused morphological and physiological changes in the liver and kidney, while ICP-AES measurements confirmed the accumulation of TiO_2 NPs in the liver. The morphological and physiological changes in the liver would mainly influence the function of the hepatocytes around the centrilobular veins, which are an important part of oxidative stress, as proved by the immunocytochemical detection of 4-hydroxynonenal. Besides, amounts of TiO_2 NPs were internalized by the Kupffer cells, which is also an important site for the oxidative stress. In addition, the highest doses of TiO_2 NPs can disrupt the enzymatic markers of the liver and kidney (e.g., AST and uric acid), and the change of the urine samples can be detected in the 4 days in rats exposed at the lowest dose compared with the control group by the metabonomic approach. Above all, their work proved that TiO_2 NPs has a significant toxic effect on the **liver and kidney cells**.

1.4. Ecotoxicity of carbon nanotubes (CNTs)

Carbon is one of the most important elements in the world and presents several different allotropes, such as graphene, diamond, fullerene and carbon nanotubes. Among all of them, carbon nanotubes have been intensively studied,[36] and envisaged in many fields, such as biomedical, field emission devices, optical devices, solar cells, and gas sensors,[36–39] due to their unique mechanical, optical, electrical, good tensile strength, good conducting, and lightweight properties.[40,41] Meanwhile, the carbon nanotubes are more likely to be exposed in the public environment, causing the

granuloma in lungs, oxidative stress, inflammation, apoptosis, and liver or kidney toxicity to human beings or the other organisms.[41–43]

Pereira et al. tested the toxicity of the carbon nanotubes (CNTs) and of the cotton cellulose nanofibers (CNFs) on *Chlorella vulgaris*,[38] cultivated in two different media (BB medium and Seine River water). The results showed that both nanomaterials can cause the decline of algae growth and cell viability; besides, the CNTs can induce an increase in ROS production and decrease in the intracellular ATP content, which means the mitochondria functional was affected by the CNTs. Moreover, the damage to the cell ultrastructure was observed, the CNTs could penetrate the cell membrane and appear in the cytoplasm of the algae cells in BB medium. However, in the Seine River water, the cotton cellulose nanofibers were not observed inside the algae cells. This work confirmed that the CNTs and CNFs can affect algae growth and cell viability and that CNTs are more toxic than CNFs for algae cells.

The carbon nanotubes can easily pose a potential health hazard in the lung due to the high aspect ratio and biopersistant in the lung. On this basis, Gaté et al. studied the pulmonary toxicity of two kinds of multiwalled carbon nanotubes (MWCNTs) in Sprague-Dawley rats.[44] One is the long and thick NM-401 and the other one is the short and thin NM-403. They treated the rats by intratracheal instillation and 4-week inhalation, respectively. Both MWCNTs caused the pulmonary neutrophil influx no matter in which treated methods, and this influx extent of the pulmonary neutrophil depended on the exposure time and the deposited surface area across MWCNTs types. The influx significantly increased (20-fold increase) at the 3-day exposure and decreased to a 10-fold increase at day 30, and the lymphocyte numbers increased at 3 days exposure and decrease later, at the same time, the DNA damage was observed in all the tested groups exposed to different doses and treated time point. In addition, the NM-401 CNTs introduced by intratracheal instillation presented a higher deposited dose in the lung causing the fibrosis compared with the inhalation method, while the NM-403 did not cause the fibrosis in the lung. Their work proved the toxicity of the CNTs, which can induce **inflammation and DNA damage responses**, and even fibrosis in the lung.

Cheng et al. investigated the toxic effect of the single-walled carbon nanotube on rat.[45] They concluded that 200 μg/mL single-walled carbon nanotube can cause the rat aorta endothelial cells apoptosis, mainly determined by the mitochondria-dependent apoptosis pathway activated by the ROS generation. The latter was induced by CNTs, and the mitochondria-dependent apoptosis pathway was proved by a series of

morphological and biochemical hallmarks, such as internucleosomal DNA fragmentation, chromatin condensation and caspase-3 activation. All these hallmarks can confirm that the single-walled CNTs can cause a toxic effect on the mitochondria functional inducing cell apoptosis in rats.

Cimbaluk et al. evaluated the ecotoxicological effect of the multiwalled carbon nanotubes on two fish species (*Danio rerio and Astyanax altiparanae*).[46] They used the commercial multiwalled carbon nanotubes to test the toxic effect of MWCNTs on the erythrocytes and piscine micronucleus of the fish. The results indicated that the CNTs did not cause any genotoxicity to the fish, such as the single/double DNA strand break and clastogenic/aneugenic effects. However, the CNTs can induce oxidative stress in the cells after a subchronic exposure, which was confirmed by the SOD and catalase activity. In addition, the CNTs can cause acute **neurotoxicity** to *Astyanax altiparanae* and subchronic neurotoxicity to Danio rerio.

Zhao at al. studied the toxicity of three kinds of commercial MWCNTs of different diameters (XFM4< XFM22< XFM34) on the human umbilical vein endothelial cells (HUVECs).[47] The results indicated that the XFM4 (of smaller diameter) can significantly induce cytotoxicity compared to the two other MWCNTs. This confirmed the significantl increase of cytokine release, monocyte adhesion and intracellular ROS production after contact with XFM4, and the XFM4 can be observed inside the endothelial cells. In addition, the XFM4 can influence the expression of the autophagic genes and proteins, and the cellular modulation of autophagy-ER stress can increase the cytotoxicity of XFM4 but decrease the cytotoxicity of XFM34. These results proved that MWCNTs of smaller diameters can induce more serious toxicity to the human umbilical vein endothelial cells.

1.5. Ecotoxicity of silver nanoparticles (Ag NPs)

Silver nanoparticles (Ag NPs) present good antibacterial, anti-inflammatory, and antiviral properties, so they can be used in many fields, like medicine, vascular grafts, clothes, cosmetics, drug delivery systems, wound healing, household appliances and toys.[48–50] With the widespread use of Ag NPs, the potential ecotoxicological and environmental impacts need to be concerned, as Ag NPs are easy to be released into the environment, during washing clothes and children's products for example.[48] Once they are released into the environment, Ag NPs can be oxidized to the Ag^+ or remain as Ag NPs in the environment and induce toxicity to human cells, aquatic organisms and microalgaes.[51]

Taylor et al. evaluated the toxicity magnitude and mechanisms of silver cation (Ag^+) and two kinds of Ag NPs on the *Chlamydomonas reinhardtii* and *Synechococcus leopoliensis*.[52] The two kinds of Ag NPs are different in size, the commercial AG1 is 3-8 nm, the home synthesized AG2 is 50 nm. The results showed that all silver species caused the cell viability decrease for the *C. reinhardtii*, while only cationic silver significantly induced the ROS production in the algae cells and influenced the viability of *the S. leopoliensis*. All Ag species had an influence on the extracellular polymeric substances (EPS) composition of *C. reinhardtii,* which would be able to produce a great amount of lower molecular weight materials after being exposed to silver. In addition, Ag NPs affected the integrity of the cell membrane only for *C. reinhardtii*. The different toxicity behaviors of the Ag species were probably related to the **ionic release dynamics**, which means that the silver cations seemed more toxic than Ag NPs.

Buffet et al. studied the toxicity of the silver nanoparticles on two endobenthic species: the ragworm *Hediste diversicolor* and the bivalve mollusc *Scrobicularia plana*.[53] In this work, they exposed the two endobenthic species in the natural environment to 10 μg/L of Ag NPs or ($AgNO_3$) soluble salt for 21 days. the results showed the bioaccumulation of Ag in the two kinds of endobenthic species cells no matter treated with which kind of Ag. Both caused oxidative stress, detoxification, apoptosis, genotoxicity, and immunomodulation to the cells, which proved that the dissolved Ag was partly responsible for the toxicity effects. In addition, they found that Ag NPs caused the increase of the phenoloxidase and lysozyme activities in clams and worms, respectively. And Ag NPs also induced much more serious **genotoxicity** in the digestive gland of calms than the soluble Ag. Although they did not prove the toxicity was induced by the specific nano effect or the dissolved Ag^+, they have proved that Ag NPs or soluble Ag can cause the toxicity effect to the endobenthic species.

Meanwhile, Gomes et al. evaluated the ecotoxicological effect of Ag NPs on the mussels *Mytilus gallprovinvialis*.[54] They exposed the mussels to 10 μg/L of Ag NPs and ionic silver (Ag^+) environment for 15 days. The results showed that the bioaccumulation of Ag NPs and Ag^+ was observed in gills and digestive glands; they also induced the antioxidant enzymes, such as SOD, catalase, and glutathione peroxidase. The bioaccumulation of Ag in gills induced the production of metallothionein. Meanwhile, the Ag NPs caused a more severe lipid peroxidation in gills than the Ag^+, while the lipid peroxidation in digestive glands was only caused by Ag^+. Therefore, they confirmed that Ag NPs can induce oxidative stress in the mussels.

Besides, the ecotoxicity effects of the other nanoparticles have also been evaluated, such as cerium oxide (CeO_2),[55] copper oxide (CuO),[56] barium titanate ($BaTiO_3$)[57], and metal lanthanum (La).[58] All of these research works proved the **toxicity of the commonly used nanomaterials in our life**, which also **confirmed the necessity of ecotoxicological research**.

2. Ecotoxicology research biota

With the widespread application of nanomaterials in our daily life, the ecotoxicology investigation of nanomaterials has become more necessary than ever. For assessment of the NPs ecotoxicological features, many different biotas can be used, including aquatic organisms and terrestrial organisms; the most popular ones are the aquatic organisms due to their sensitivity, easiness of cultivation, and ubiquity,[59] such as microalgae, plants, bivalves and amphibians. Meanwhile, not all organisms can be used for the ecotoxicology tests, which must respect some guidelines from the international organizations, such as United States Environmental Protection Agency (EPA), International Organization for Standardization (ISO).[12] Moreover, different organisms have different sensitivity to the nanoparticles: for example, algae and crustaceans are the most sensitive ones,[12,15] so the organisms should be selected according to the needs of the ecotoxicological test. Here, we will introduce some of the most popular organisms used for ecotoxicology tests.

2.1. Microalgae

Microalgae are unicellular microorganisms with chloroplasts, at the lowest trophic level of the food chains. They can produce oxygen and food for the other aquatic biota through the photosynthesis activity, and they can provide food for more than 70% of biomass in this world; moreover, they are carrying out more than half of the photosynthesis activity.[59] Due to their sensitivity and bioaccumulation activity, they can be used to purify water and also as bioindicator to pollutants and poisons.[43,60] Besides, microalgae are easy to cultivate with a short growth period and they can present the signs of the toxicity of the nanoparticles in a short period of time (72-96 h).[12] Therefore, they are the most widely used for evaluating the ecotoxicity of NPs, and can also be selected as the bioreactor for the synthesis of NPs.

2.1.1. Biosynthesis of nanoparticles by microalgae

Green synthesis of NPs by microalgae has become one of the most eco-friendly methods compared with the chemical and physical methods. It is the easiest, quickest,

and most biocompatible way to synthesize nanoparticles.[61,62] Many microorganisms can be used for the biosynthesis of nanoparticles, such as bacteria, microalgae, fungi, and yeast. Here, we will just focus on the biosynthesis by microalgae.

As the earliest researcher using microalgae to synthesize NPs and to evaluate the ecotoxicology effect of the NPs, R. Brayner has carried forward this technology and made great contributions to this field. Brayner et al. synthesized akaganeite *β*-FeOOH nanorods of tunable size by the common microalgae *Anabaena*, *Calothrix* and *Klebsormidium* at room temperature.[63] The size of the nanorods was around 100 nm, and the nanorods presented a spongelike structure with a complex porous arrangement. In addition, the biosynthesized akageneite nanorods were superparamagnetic and exhibited a better degree of crystallinity than the ones synthesized by traditional method (liquid phase method). This work proved that the biosynthesis method by microalgae could be a good way to synthesize highly crystalline NPs (Fig. 4) presenting expected properties such as magnetic properties.

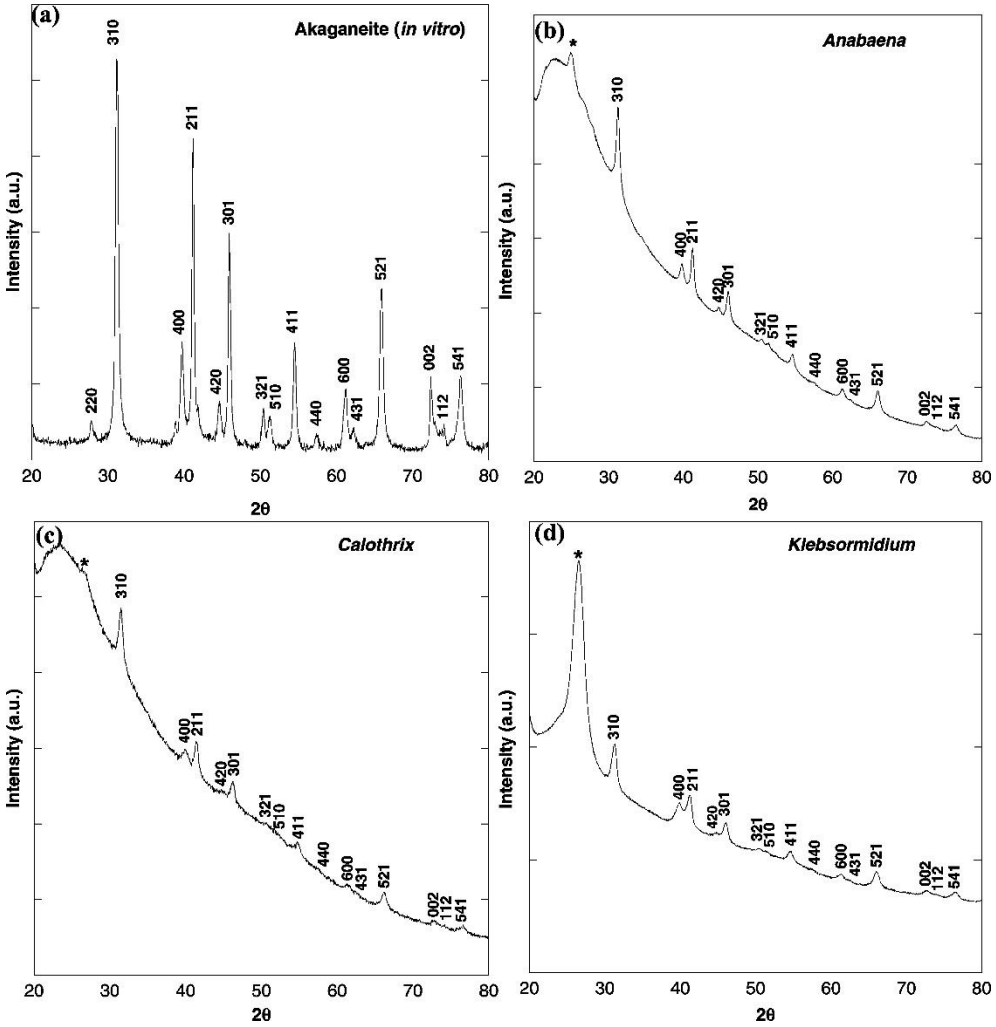

Fig. 4 *XRD patterns: (a) in vitro synthesized β-FeOOH and synthesized by (b) Anabaena, (c) Calothrix (d) Klebsormidium contacted with iron salts. (*) algal biomass. From Ref 63*

Meanwhile, Brayner et al. also synthesized superparamagnetic 2-lines ferrihydrite NPs by intracellular biosynthesis method using *Euglena gracilis*.[64] These NPs were well-controlled in size (about 0.6-1.0 nm) and shape, and the intracellular 2-lines ferrihydrite NPs presented good superparamagnetic properties, also paving the way to obtaining the magnetic living cell used in biosensors and therapy fields. in addition, this work makes it possible to make microalgae synthesize magnetic NPs rather than using only magnetostatic bacteria.

Sicard et al. also used microalgae to synthesize gold nanoparticles.[65] The microalgae (*Klebsormidium flaccidum*) were first encapsulated in the silica gels and then, successfully synthesized nano-gold. The results showed that the silica gels protect the algae cells from the toxicity of the produced Au NPs and proved that the algae inside the silica gels still had good viability and photosynthetic activity for synthesis the Au NPs. This makes it possible to prepare photosynthesis-based environmental **biosensors** in the future.

2.1.2. Ecotoxicology effect evaluation with microalgae

Microalgae, as an important part of the aquatic system, are one of the most sensitive microorganisms to the toxicity of NPs and pollutants; therefore, they are an ideal choice for carrying out the toxicological test of the NPs.[2]

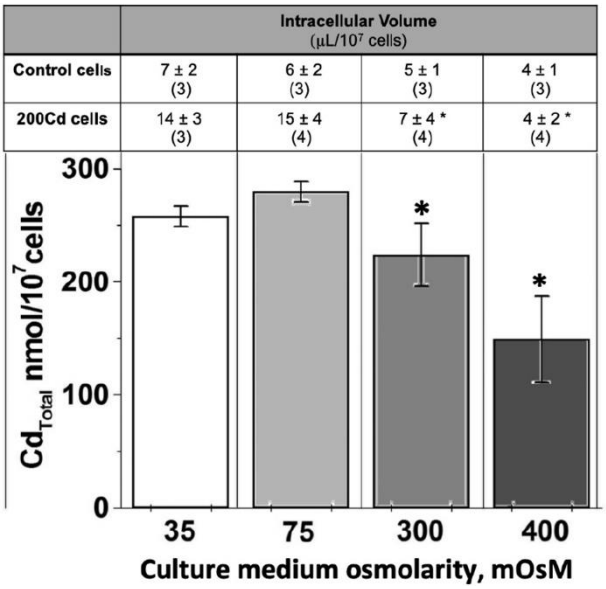

Fig. 5 *Accumulation of Cd^{2+} in different culture medium osmolarities. From Ref 66*

Sanchez-Thomas et al. investigated the cytotoxicity mechanism of Cd^{2+} using microalgae (*Euglena gracilis*).[66] They exposed the *Euglena gracilis* in 50 and 200

μmol/L solutions of Cd^{2+} and observed that the intracellular water and cellular size increased after being exposed to the Cd^{2+} environment; they assumed that it was caused by the increased intracellular osmolarity and the triggered antioxidant defense. Furthermore, the intracellular volume, cellular size, and antioxidant status did not change in the control group with hyperaccumulation of Zn^{2+}, which proved the specific effects of Cd^{2+} on the change of the intracellular volume and osmotic pressure. This work proved that the accumulation of Cd^{2+} has a close relationship with the **intracellular water volume changes** during the oxidative stress-mediated process (Fig. 5).

Djearamane et al. evaluated the cytotoxic effects of ZnO NPs using cyanobacteria *Spirulina (Arthrospira) platensis*.[67] They exposed the *Spirulina (Arthrospira) platensis* in various concentrations of ZnO NPs (10-200 mg/L) with different exposure times (6-96 h) to investigate the dose and exposure time influence on the cytotoxic effect. They observed that all the research groups presented the cytotoxic effect after 24 h exposure, and 96 h later, the algae cells appeared to exhibit the highest cytotoxicity. Furthermore, the cell viability, algae biomass, photosynthetic pigments (chlorophyll-a), carotenoids and phycocyanin contents decreased more than 70% after contact with 200 mg/L of ZnO NPs for 96 h. In addition, the cell membrane and intracellular damage were observed by TEM. This work confirmed the influence of the **concentration** of ZnO NPs on cyanobacteria *Spirulina (Arthrospira) platensis*.

In addition, the green algae *Chlorella vulgaris* was also used to evaluate the toxicity of nanoparticles. Chen et al. studied the toxicity of Cu^{2+} on *Chlorella vulgaris* through the photosynthetic activity and oxidant stress perspective.[68] The results showed that the Cu^{2+}inhibited the growth of *Chlorella vulgaris*, and the photosynthetic activity was also affected. The results showed that the chlorophyll II fluorescence parameters were reduced at a high concentration of Cu^{2+}, which means the photosystem II was destructed by the Cu^{2+} meanwhile, they found the Hill reaction activity (HRA) of chloroplast significantly declined with the increase of the Cu^{2+} concentration. Furthermore, the SOD, catalase (CAT), and malondialdehyde (MDA) content increased firstly and then decreased with the increase of the Cu^{2+} concentration, which evidenced the significant increase of the ROS production in the algae cells. The increase of these biomarkers is due to the antioxidant defense mechanisms to the O_2^- induced by the Cu^{2+}, while the decrease is caused by the enzyme inactivation. All these physiological phenomena indicated the serious oxidative stress to the microalgae cells

induced by the Cu^{2+}, which means the Cu^{2+} caused severe cytotoxicity to the microalgae.

2.2. Mussels

Mussels are bivalves, can filter large amounts of water and capture the particulates in suspension to get nutrients. The particles can be distributed in their tissues and cellular compartments.[54] In addition, they are widely present in the world, their mobility is limited, and they are able to adapt to different environments.[58,69] Therefore, they can also be selected as biological targets for ecotoxicity tests.

Katsumiti et al. used mussels (*Mytilus galloprovincialis*) as a biological target to evaluate the toxicity of CuO NPs.[70] Mussels were contacted to bulk CuO and ionic Cu ($CuCl_2$), to test the cytotoxicity and cellular mechanisms of the hemocytes and gill cells of the mussels. The results showed that the toxicity extent of CuO NPs was dependent on the dose of CuO NPs; it can induce ROS production increase in the mussel and human cells. The ionic Cu was found to be more toxic than the other two forms. All Cu species could increase the activity of the catalase and acid phosphatase in the hemocytes and gill cells. In addition, all the forms of Cu caused DNA damage in hemocytes cells, and only ionic Cu and CuO NPs also induced genotoxic in gill cells. Besides, only CuO NPs caused the phagocytosis increase in hemocytes cells. This work proved that the mussels can be selected as a biological target for assessing the toxicity of NPs, meanwhile, **ionic Cu and CuO NPs have a more toxic effect** than the bulk CuO on the mussels.

Ale et al. used the mussel *Mytilus galloprovincialis* to study the toxicity of nanosilver-enabled consumer products, demonstrating that the latter had a similar accumulation and toxicity in the mussel's cells as silver NPs.[71] The mussels were exposed at the environmentally relevant concentrations of nanArgen™ (1 μg/L and 10 μg/L) for 96 h (the presence of Ag NPs were confirmed in the nanArgen™ with an average size of ca. 30 ± 10 nm). The results showed that the Ag significantly accumulated in all the soft tissue of mussels, and the accumulation became more obvious with the increase of nanArgen™ concentration; this was confirmed by the related measurement in the hemocytes cells and digestive glands. In addition, the malondialdehyde (MDA) and metallothionein (MT) content significantly increased only at the highest nanArgen™ concentration (10 μg/L), and the efflux activity of ATP-binding cassette transport proteins in gill biopsies clearly decreased at the lowest 1 μg/L concentration. These results confirmed that the nanArgen™ can cause cytotoxicity on the marine mussels

at environmentally relevant concentrations, which is similar to the toxicity behavior of Ag NPs to the mussels.

2.3. Vertebrates

The ecotoxicology of the NPs on the microbe, microalgae, invertebrates is widely investigated, but is still not clear in the vertebrates; new research on ecotoxicology of vertebrates, based on ethical standards is in progress. Up to now, the lower vertebrates (such as zebrafish) are often selected instead of the higher vertebrates.[72–74]

Vicario-Parés et al. chose the zebrafish embryos to evaluate the toxicity of the metal oxide nanoparticles.[75] They studied the ecotoxicity of CuO, ZnO, TiO_2 NPs, meanwhile, the bulk rutile TiO_2 and Cu^{2+} and Zn^{2+} were used as the comparison group. In their work, all these metal oxide NPs were found to be not lethal to the zebrafish embryos. However, among all these NPs, the CuO NPs presented a more serious toxic effect on hatching and malformation prevalence at the concentration of 1 mg/L. Then ZnO NPs could affect the hatching at a concentration of 5 mg/L, and TiO_2 NPs affected the hatching and caused mortality at the concentration of 100 mg/L. The comparison group also presents a similar toxicity effect on the zebrafish embryos. According to the toxicity results, they found that **metal ions presented the most toxic effect**, followed by the metal oxide NPs. Furthermore, they found Cu and Zn metal deposition in embryos, and the CuO NPs seemed easier to deposit inside the embryos. Overall, they concluded that the metal oxide NPs had a serious toxic effect on the zebrafish embryos by affecting the hatching and increasing the malformations prevalence.

Ispas et al. studied the toxicity effect of nickel metallic nanoparticles on the zebrafish, they used Ni NPs of different sizes (30, 60, and 100 nm) and large aggregates (60 nm) of Ni presenting a dendritic structure.[76] The zebrafish embryos were exposed to these different NPs, and the soluble nickel salt ($NiCl_2$) was used as the control sample. The results showed that the soluble Ni salt seemed more toxic than the three kinds of Ni NPs. However, the **dendritic structure** presented a most serious toxic effect on the embryos. In addition, these NPs also led to thinning of the intestinal epithelium and the separation of skeletal muscle fibers. All these NPs indicated that **nanoparticle shape may have a more toxicity influence than size**, and that the Ni NPs can induce serious cytotoxicity to the zebrafish embryos.

Wang et al. selected young and adult rats to assess the toxicity of the TiO_2 NPs.[77] They treated the 3-weeks (youth) and 8-weeks (adult) *Sprague-Dawley* rats with different doses (0, 10, 50, 200 mg/kg) of NPs. The results showed that liver edema,

heart damage and the activated non-allergic mase cells in stomach tissues were observed in the youth rats. However, only a slightly liver and kidney hurt were found in the adult rats. Meanwhile, the reductive stress in plasmas were induced by the TiO_2 NPs in both rats. Therefore, TiO_2 NPs can induce a different toxicity behavior to the rats with **different ages**.

2.4. Plants

Now lots of the ecotoxicology tests are based on algae, bacteria, invertebrates, and vertebrates, while the data on higher plants is also lacking.[78] Plants, as the important environmental part of this planet, are essential for life.[79] Meanwhile, they can also be affected by the phytotoxicity induced by the NPs; therefore, it is necessary to address the ecotoxicity effects of NPs on plants.

Ji et al. studied the joined toxicity of the TiO_2 and NPs and cadmium in the rice (*Oryzasativa L.*) seedlings process.[80] The rice seedlings were divided randomly into 12 groups, all exposed to different concentrations of $CdCl_2$ (0, 10, 20 mg/L) and TiO_2 (0, 10, 100 and 1000 mg/L) NPs. The results showed that the ionic Cd had a significant toxic effect on the rice seedlings through the plant height, biomass, and root length measurements while the TiO_2 NPs seemed to reduce the toxicity of ionic Cd although TiO_2 was observed in the rice seedling. The deposition of Ti in the roots significantly decreased in the group exposed to both TiO_2 NPs and $CdCl_2$. Furthermore, the photosynthetic activity of the rice seedling in the co-exposure group clearly increased compared with the group contacted only with Cd. This work confirmed that the TiO_2 NPs and $CdCl_2$ can induce the toxicity effect on the rice seedlings and that TiO_2 NPs are potentially able to reduce the toxicity of ionic Cd.

Furthermore, Bandyopadhyay et al. used the symbiotic alfalfa (*Medicago sativa L.*)–*Sinorhizobium meliloti* to evaluate the ecotoxicity of the ZnO NPs, bulk ZnO and $ZnCl_2$.[81] By contacting the symbiotic alfalfa with different concentrations of nano-species (ranging from 0 to 750 mg/kg) in soil. The results showed that the ZnO NPs and ionic Zn caused a 80% and 25% decrease in the root and shoot biomass respectively; on the contrary, the 750 mg/kg bulk ZnO significantly increased the root and shoot biomass compared with the control group. In addition, ionic Zn reduced the catalase activity in the stalk and leave at the concentration of 500 mg/kg and 750 mg/kg; hence, they confirmed that the **ionic Zn was more toxic than the ZnO NPs**, and the bulk ZnO instead promote the growth of the plant.

3. ZnS nanoparticles

Semiconductor nanomaterials may find many aplications,[82] such as photovoltaic devices, sensors and lasers, light emitting diodes (LEDs), or flat-panel displays.[83,84] Among all of them, during the last two-decade years, a deeper effort has been put in the fabricating of II-VI binary compounds presenting attractive optical properties.[82,85] In the last few years, chalcogenide nanostructures with well-controlled size and morphology have attracted lots of researchers' interest.[86] As one of the most important II-VI semiconductor compound, cadmium sulfide (CdS) possess excellent optical properties, and is also used as the important buffer layer in thin film solar cells.[87,88] In recent years, owing to its potential applications in field effect transistors, light emitting diodes, photocatalysis and biological sensors, CdS has been extensively investigated[89] as a direct bandgap nanomaterial (around 2.4eV), a high flat-band potential (0.9 V vs. normal hydrogen electrode), making it widely used in photocatalysis hydrogen evolution as an important photocatalyst.[90] However, the major drawback that limits the use of CdS is its toxicity. During the photocatalysis reaction process, S^{2-} in CdS can be oxidized by photogenerated holes and release the heavy metal ions Cd^{2+} which can form the highly reactive oxygen species (ROS).[90,91]

As a promising alternative II-VI semiconductor nanomaterial, ZnS is sought to be used in photoluminescent and electroluminescent devices, optoelectronic devices, photocatalyst, and flat-panel displays fields.[92–95] ZnS is a non-toxic compound and is classified as an n-type semiconductor with a wide direct band gap.[83,93] ZnS presents two crystal structures, one being the cubic structure with the space group F-43m (lattice constant, a=0.541nm), and presenting a direct bandgap of 3.68 eV at room temperature.[88,96,97] The other one is the hexagonal structure with the space group P63m (lattice constant, a=0.382nm and c=2.49nm), presenting a direct bandgap in the range of 3.74-3.87 eV at room temperature.[87,93,98] To date, lots of methods have been used to synthesize well-defined size and morphologies ZnS nanomaterials: one can mention the polyol process,[99] RF sputtering, chemical vapor deposition, chemical bath deposition (CBD), chemical solution (sol-gel), spray pyrolysis, hot injection method and solvothermal method [83,87] Many different morphologies of ZnS nanocrystals were synthesized through these methods, including ZnS nanoparticles, nanowires, nanorods, nanobelts, thin films, nanospheres, and core-shell structures.[86,93]

To enhance the properties of ZnS nanoparticles, doping and coating methods have been used. Doping is known to improve the optical, electronic, and magnetic properties [100,101] For example, the photoluminescent properties of ZnS NPs can be improved by

doping with Mn isoelectronic impurities. The d-electron states of the Mn^{2+} ion can interact strongly with the s-p electronic states of the host ZnS nanoparticle, which make the Mn^{2+} also act as efficient luminescent centers; doped nanocrystals of semiconductors can also yield both high luminescence efficiencies and lifetime shorting at the same time.[102,103] Se^{4+} doped ZnS nanoparticles showed much higher photodegradation efficiency (6-8) times than commercial ZnS, and the antibacterial activity of Se^{4+} doped ZnS is enhanced by increasing reactive oxygen species (ROS) generation.[104] In order to modify the different properties of ZnS, different dopants can be used, such as Ni^{2+}, Cu^{2+}, Eu^{2+}, Co^{2+}, and Ag^{+}.

3.1. Synthesis of ZnS:Mn nanoparticles

ZnS:Mn nanoparticles may find applications in biomedicine and nanotechnology fields due to their antibacterial, optical, electrical and magnetic properties. To obtain well-controlled size and morphology nanoparticles with suitable properties, various synthetic routes have been used for the synthesis of QDs (less than 10 nm in size), such as chemical bath polyol method, deposition method (CBD), solvothermal method, chemical vapor deposition method, RF sputtering method, spray pyrolysis method, etc.

3.1.1. Polyol method

The polyol process is an appropriate route for the preparation of nanoparticles, even can be less than10 nm in size. The organic solvent, namely the polyol, acts as a stabilizer, which can limit the growth of particles and prohibit agglomeration, and as a reducing agent. In addition, it is quite inexpensive and easy to operate.[105]

Feldmann et al. synthesized successfully ZnS doped with impurities (Ag^{+}, Cl) through the polyol method using DEG as solvent. The size of the synthesized nanocrystals was found between 30 and 200nm, and the NPs were spherical and almost monodispersed. The ZnS:Ag^{+}, Cl nanoparticles presented good luminescence properties, and exhibited remarkable high quantum efficiencies (Fig. 6).[84]

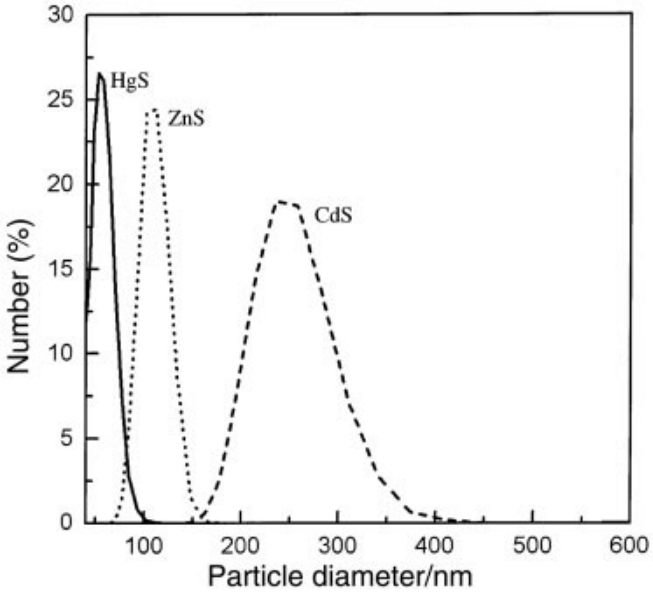

Fig. 6 *Size distribution of nanoscale ZnS, CdS and HgS particles in DEG–H_2O-suspension (DEG:H_2O ~ 1:50). From Ref 84*

Soltani et al. prepared cubic structure and spherical ZnS nanoparticles of relatively small size through microwave-hydrothermal (M-H) and microwave-polyol (M-P) methods. Deionized water and ethylene glycol were used as solvents for the M-H and M-P methods, respectively. the average size of the ZnS nanoparticles was less than 5nm. The yield of reaction of M-P method was higher than the one of M-H process, in a given irradiation time and the crystallinity degree of the NPs was also higher (Fig. 7).[106]

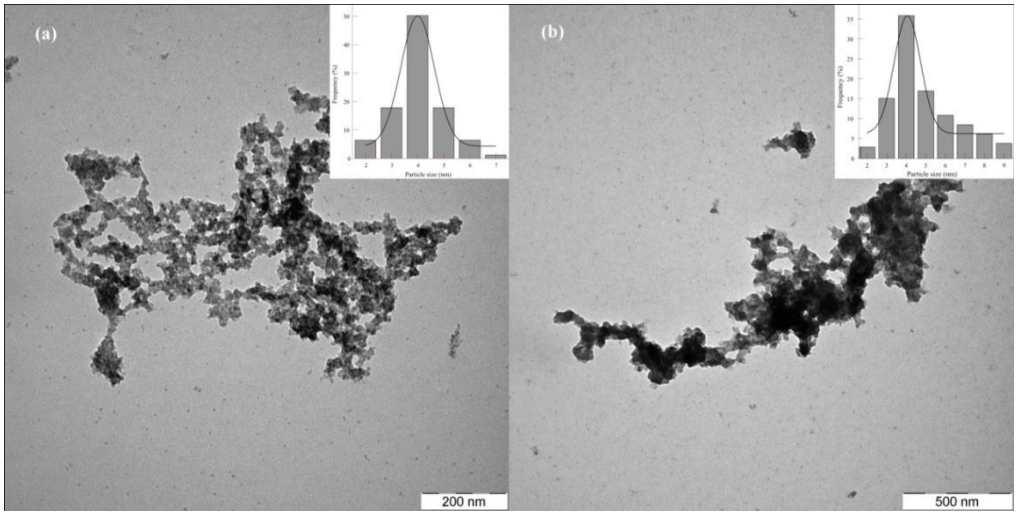

Figure 7. *TEM images and Particle size distribution of the ZnS nanoparticles synthesized with M-P method for (a) 20 and (b) 40 min irradiation time. From Ref 106*

Chaguetmi et al. synthesized ZnS and CdS quantum dots (QDs) through the polyol method, to design ZnS- and CdS-TiO_2 hetero-nanostructures. The size of these nanoparticle reaches 2-3 nm.[99]

Gaceur et al. synthesized ZnS:Mn nanoparticles for potential luminescent and magnetic bimodal imaging probes through the polyol method.[107] The average size of these nanoparticles was 1.5nm. Genotoxicity tests demonstrated that these NPs were nontoxic for doses lower than 100 μg/mL, which makes it possible to be used as bimodal probes for magnetic resonance (MRI) coupled to optical fluorescence imaging.

Longo et al. synthesized the ultrafine ZnS:Mn quantum dots by the microwave-assisted polyol process in ethanol;[108] the crystal size of these NPs was about 2.5-3.0 nm, and they emitted a significantly orange light under UV light. They confirmed that the photoactivated luminescence is caused by the lattice-strain effects. The outside sulfide layer was replaced by sulfates due to the surface oxidation under the UV irradiation; therefore, in this case, the outside metal sulfate lattice induced the mechanical strains to the inner zinc sulfide, resulting in the electronic transition from the $^4T_1$ to $^6A_1$ of $[MnS_4]^{6-}$ emitting center. This work also proved the effectiveness of the polyol method to synthesize materials exhibiting an excellent photo-activated phosphorescence.

3.1.2. Hydrothermal and solvothermal methods

The hydrothermal method is also a quite simple and widely used synthesis route of nanoparticles, which is carried out at low temperature (100 ℃ to 200 ℃) and allows high yield, through a well-controlled process.[109,110]

Rashad and co-workers prepared Mn-doped ZnS (ZnS:Mn) nanocrystal powders using the hydrothermal method.[111] The produced samples presented a wurtzite structure, and the NP size was about 3.8-7.9 nm. However, the size of the undoped ZnS nanoparticles synthesized using the same method was found to be a little bigger (7.9-15.1 nm). In addition, when the ion molar ratio was less than 0.2, the ZnS:Mn NPs presented a high saturation magnetization.

Hu et al. prepared the ZnS:Mn (0.6 at.%) QDs at different reaction temperatures by the hydrothermal method and investigated the structure and the optical properties of the ZnS:Mn NPs.[112] The particles presented a cubic structure, and the average size of these QDs ranged from 3.75 nm to 6.36 nm; the lattice was found to be smaller than the pure ZnS due to the smaller ion radius Mn^{2+} dopant. Meanwhile, the UV-vis spectra of these ZnS:Mn NPs can be affected by the quantum confinement effect: the band

gap increased from 3.2 eV to 3.5 eV with the decrease of the grain size, and the photoluminescence emissions shifted to blue with the decrease of the reaction temperature.

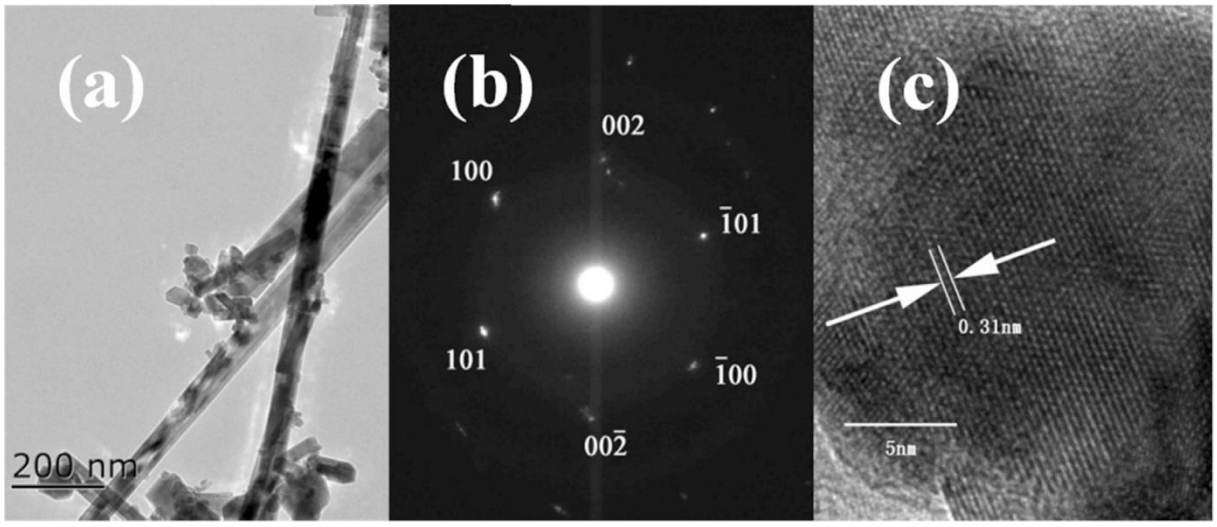

Fig. 8 *(a) TEM image, (b) SAED pattern and (c) HRTEM of as-synthesized ZnS nanowires. From Ref 93*

The solvothermal method is one of the most useful methods to synthesize well-defined size and morphology ZnS nanoparticles because of the low-temperature reaction, facile procedure, maneuverability, and cheap precursors of low toxicity. Gao et al. synthesized structural and morphological controlled ZnS nanostructures using the mixed solvent of ethylenediamine (en) and deionized water. The size ranged between 30 and 60 nm. In addition, the PL spectra showed two main peaks at 363 nm and 570 nm, corresponding to the near band-to-band transition of ZnS NPs and the S vacancies or defects in ZnS NPs, respectively; the UV-vis absorbance at 333 nm corresponds to ZnS NPs. These two tests clearly evidenced the purity of the synthesized ZnS NPs (Fig. 8).[93] Cao et al. synthesized ZnS and $Zn_{1-x}Mn_xS$ nanocrystalline samples by the solvothermal method without any surface-active agents; the size of these nanomaterials was found to be about 10-16 nm.[113] Ramachandran et al. synthesized ZnS decorated graphene nanocomposites using a facile solvothermal method, and the size of the nanocrystal was almost 7 nm. In addition, these ZnS/Graphene heterostructures were promising in the supercapacitor field, since they delivered a maximum specific capacitance of 197.1F/g at a 5mV/s scan rate and capacitance retention higher than the devices made of pure ZnS nanoparticles and bare graphene electrode.[114]

3.1.3. Chemical precipitation method

Chemical precipitation has also been used to synthesize nanoparticles; the main advantages of this route, regarding other methods, is to be carried out in a friendly environment, using non-toxic reagents, and allowing high yield products.[115]

Rahdar synthesized ZnS nanoparticles by a co-precipitation method using 2-mercaptoethanol as a capping agent. The produced NPs exhibited suitable optical properties to be used in the optoelectronic field, and the mean crystallite size was comprised between 1.85 nm and 2.44 nm.[116] Reddy et al. synthesized nanoparticles of ZnS doped with Al^{3+} through chemical co-precipitation method using polyethylene glycol (PEG) as a stabilizer. The crystal size was almost 2 nm - 4 nm, and the photoluminescence increased when the concentration of Al increased to 6 at.%.[117] Manzoor et al. prepared ZnS nanocrystals doped with Cu^{2+} and halogen that exhibited multiple blue emission related to the sulfur vacancies V_s.[118]

Lakshmi et al. synthesized ZnS:Mn nanoparticles that presented a zinc blende structure, and about 17 nm in size.[119] The optical absorption showed that the band gap of the nanocrystal ZnS was 3.9 eV and the blue shift was observed compared with the bulk ZnS. In addition, magnetic measurements showed that ZnS:Mn (2%) NPs are ferromagnetic at room temperature.

Other methods may also be used to synthesize ZnS:Mn NPs, such as the organometallic method or aqueous colloidal method. Bol et al. synthesized nanocrystalline 4 nm ZnS doped with Mn^{2+} via an organometallic and inorganic synthesis method. The photoluminescence emission properties were evaluated: the decay time (~100 ns) is shorter than the undoped sample.[103] Murase et al. prepared 4 nm ZnS:Mn NPs through an aqueous colloidal method and the fluorescence properties were studied under 266 nm light excitation. The orange emission induced by the $^4T_1$ to $^6A_1$ transition of Mn^{2+} has been observed as well as the blue emission, which is related to the donor-acceptor pair transition.[120]

3.2. Applications of ZnS nanoparticles

ZnS NPs present various unique properties: excellent transport properties, good thermal stability, and high electronic mobility,[121] and can be used in many fields: photoluminescence, electroluminescence, flat panel displays, infrared windows, sensors and biological applications.[122–124]

3.2.1. Photoluminescence applications

Reducing the particle size of phosphors to the nanometer scale seriously increases the number of vacancies, that are detrimental to the luminescence performance. Therefore, it is necessary to take some measures (such as doping with impurities) to improve the optical properties of nanoparticles.[125]

Kolmykov et al. synthesized the glutathione (GSH) capped ZnS:Mn QDs by an aqueous-based method;[126] the nanoparticles presented a cubic structure and a size of 4.3 nm. An orange luminescence was observed, due to a low surface defect density. When the molar ratio of Mn^{2+} and Zn^{2+} was ca. 3%, the NPs demonstrated the highest photoluminescence performance. After coating these ZnS:Mn NPs with an additional ZnS shell, the photoluminescence (PL) quantum yield of the core-shell NPs could reach 23%. To conclude, these ZnS:Mn @ZnS @GSH NPs present a great potential for applications as fluorescent labels in biological fields (Fig. 9).

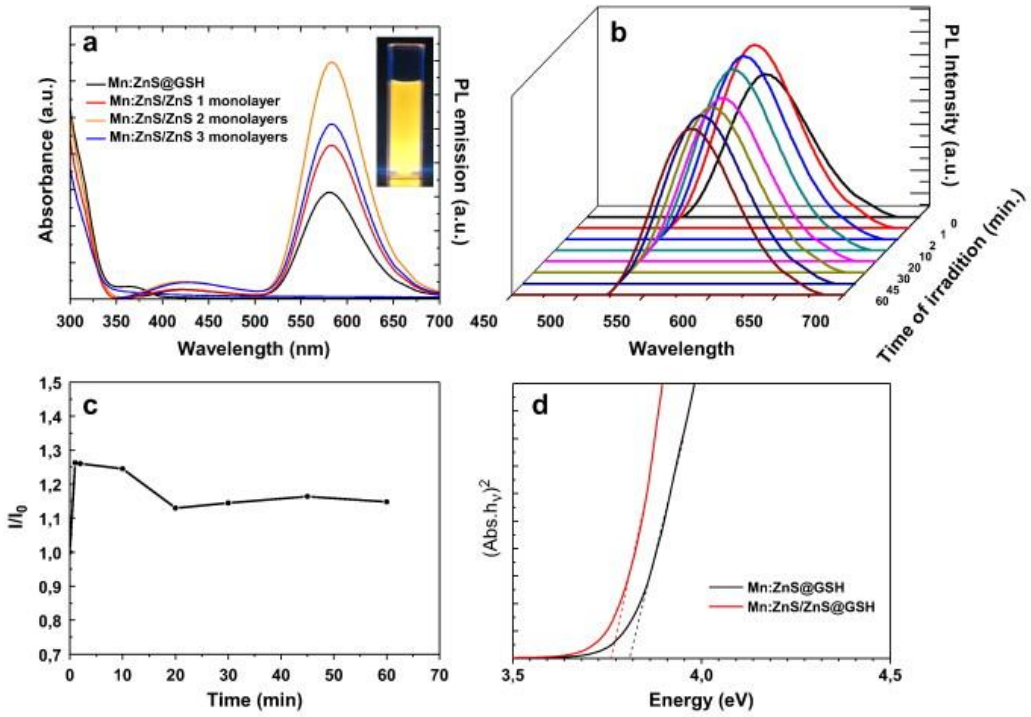

Fig. 9 *(a) UV-vis absorbance spectra, (b) evolution of PL emission spectra of Mn:ZnS/ZnS QDs, (c) photostability of Mn:ZnS/ZnS QDs, (d) Tauc plots of ZnS and Mn:ZnS/ZnS absorption spectra. From Ref 126*

Murugadoss studied the photoluminescence of ZnS:Cu NPs synthesized by the chemical precipitation method.[127] The produced ZnS:Cu NPs presented a cubic structure with a size ranging from 3.2 to 5.3 nm. The absorption peaks of all these ZnS:Cu NPs exhibited a blue shift compared with the bulk ZnS; in addition, the

photoluminescence emission spectra of the NPs presented a red shift with the increase of the Cu^{2+}. Finally, the PL emission spectra of ZnS:Cu NPs capped with surfactants increased since the surfactants contributed to eliminating the surface defects and improving the crystallinity of the ZnS:Cu NPs. This work also demonstrated the surfactant capped ZnS: Cu NPs can be used in the optoelectronic devices and even as fluorescence probes in the biological or medicinal fields.

3.2.2. Field emission displays

Field emission displays (FEDs) are one of the new flat panel displays under development. FEDs rely on the excitation of phosphor nanomaterials by an electron beam to generate photons. To improve the properties of sulfide-based phosphors, the degradation of the ZnS phosphor must be avoided.[128]

Ollinger et al. prepared micro-sized ZnS:Ag particles coated with indium tin oxide (ITO) using the physical vapor deposition method.[128] The results showed that the degradation lifetime of these samples was significantly increased through the cathodoluminescence degradation test, compared with uncoated ZnS:Ag samples. The brightness of the ZnS:Ag @ITO samples only lost 30% under a coulombic dose of 5 C/cm^2 exposure, which indicated that the ITO coating can reduce the degradation rate of the samples; therefore, it is possible to use them for field emission displays.

3.2.3. Sensors

ZnS nanoparticles are also widely used as fluorescent sensors for some specific molecules (such as folic acid or alcohol). Yu et al. synthesized novel core-shell ZnO@ZnS hollow dumbbells-graphene nanoparticles by a polymer-assisted hydrothermal method for further use as high-performance photocatalysts and alcohol sensors.[129] These nanomaterials exhibited excellent sensitivity and selectivity to alcohol during the gas sensing measurement, which could be ascribed to the improved electric conductivity and the improved adsorption and diffusion way of gas molecules due to the hollow structure; it resulted also an excellent photocatalytic activity.

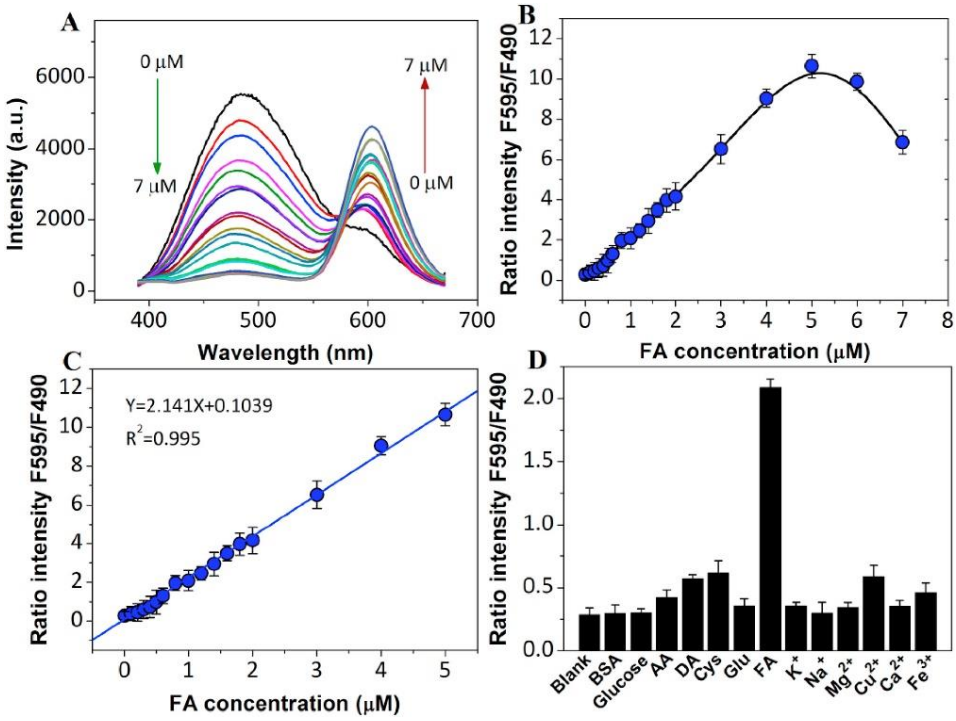

Fig. 10 *(A) Fluorescence spectra of Cu-Mn codoped ZnS QDs with different concentration FA. (B) the intensity ratios of the sensors versus the FA concentrations, (C) calibration regression curve, and (D) the intensity ratios of sensors towards FA (1 μM) and the different interfering substances at 10 μM. From Ref 130*

Wang et al. fabricated the ZnS QDs co-doped with Cu^{2+} and Mn^{2+} for further use as fluorescent sensors for folic acid (FA),[130] owing to two independent dopant emission centers. Once contacted with the FA, the two emission centers exhibited a different behavior, the Cu dopant emission being quenched, while the Mn dopant emission being improved. This sensor has been successfully applied to the detection of FA in the spiked samples, and the recoveries were high than 95%, which means this sensor showed high sensitivity and selectivity to FA (Fig. 10).

3.2.4. Photocatalytic/photoelectrocatalytic application

In recent years, photoelectrocatalytic (PEC) water splitting for hydrogen generation has drawn great attention, because hydrogen has been considered renewable energy that could reduce the world's energy dependency on fossil resources. Metal sulfides are sought as an excellent material for highly efficient water reduction to H_2.

Xiao et al. studied the photocatalytic properties of the core-shell copper nanowires/ZnS structures under exposure to visible light.[131] They used the microwave-induced metal dissolution strategy to synthesize the samples, which showed an excellent photocatalytic activity and stability for H_2 evolution; the H_2 generation rate

could reach 10722 μmol h^{-1} g^{-1}, and the apparent quantum efficiency (AQE) was up to 69% under the 420 nm irradiation.

Pang et al. synthesized ZnS:Ni nanocrystals as an efficient photocatalyst for CO_2 reduction reaction (CO_2 RR) under solar light.[132] these particles presented a high selectivity to formic acid (FA), which can be up to 95%. In addition, the ZnS:Ni (0.1%) colloidal samples exhibited a significant apparent quantum yield of 59.1% at 340 nm and 5.6% at 420 nm during the photocatalytic process, which is ascribed to the enhanced visible light absorption and abundant sulfur vacancies of the ZnS:Ni nanocrystals.

Ma et al. prepared Au decorated hollow ZnO@ZnS (HZOS) materials for photocatalytic hydrogen evolution;[133] these samples showed a high hydrogen generation rate of 569.81 μmol h^{-1} with 10 mg catalyst, which is 345, 374, and 11 times higher than that of the pure ZnO, ZnS, and ZnO@ZnS samples, respectively. This excellent photocatalytic efficiency can be ascribed to the special hollow structure of HZOS, which created a special migration pathway for the charge carriers to quickly arrive at the outside of the photocatalyst, meanwhile, it also provides enough active surface sites for the photocatalytic process.

Besides, the ZnS NPs can also be used in many other fields, like tribological applications, lithium/ sodium-ion battery materials, and opto-electronics field. So far, we have known that the ZnS semiconductors may have many applications in our daily life, while the ecotoxicity effects of the ZnS NPs on organisms or human beings still need to care.

3.3. Ecotoxicity effects of ZnS NPs

As we discussed previously, ZnS NPs have been used in photoluminescence, opto-electronic devices, photocatalytic and biological fields, due to their specific physicochemical properties. However, these specific properties of the ZnS NPs can also cause some toxicity effects on the organisms and can induce ROS production, lipid peroxidation, cell membrane damage, and even cell death to the organisms. Sometimes, to increase the biocompatibility, hydrophilicity, and antibacterial properties of the ZnS NPs used in the biological fields, they will be functionalized by different capping agents, which will make it easier for the NPs to attach to the biomolecules, like the DNA, RNA, and proteins.[134] However, this may also induce the NPs toxicity to these biomolecules inside the cells.

Touaylia et al. synthesized ZnS:Mn NPs by the nucleating doping method and a further stabilization was carried out by reaction with 3-mercaptopropionic acid (MPA).[135] The toxicity of the ZnS:Mn (10%) NPs was evaluated using the western mosquitofish *Gambusia affinis*, which was exposed to 14 mg/L and 28 mg/L of the ZnS:Mn (10%) NPs for 94h. These NPs could cause the neurotoxic effect in all the detected organs of the mosquitofish and induced oxidative stress in the cells; they also increased the catalase (CAT) activity and lipid peroxidation at the highest concentration (28 mg/L).

Labiadh et al. investigated the optical properties and the toxicity of undoped and Mn-doped ZnS NPs, prepared at 95 °C by the nucleation-doping strategy.[92] All these nanoparticles presented a blue emission at 450 nm and an orange emission at 592 nm. In addition, they evaluated the toxicity of these NPs in the clam *Ruditapes decussatus*: oxidative stress was induced in the digestive gland, and the antioxidant enzymes (SOD and CAT) activities increased in the digestive gland after exposure to the 100 µg/L of ZnS:Mn NPs. The malondialdehyde (MAD) levels also increased in the digestive gland, which all proved the cytotoxicity of the ZnS:Mn NPs to the *Ruditapes decussatus*.

Mohammad et al. assessed the toxicity of the ZnS:Mn QDs in vitro.[136] They prepared the ZnS:Mn NPs by the co-precipitation method and the toxicity was assessed by exposing the liver cells (BRL3A) of rats to 25-250 µg/mL of ZnS:Mn NPs. The nanoparticles induced a significant cytotoxicity effect on the hepatic cells at a concentration of 100 µg/mL after 16 h of exposure. The oxidative forms Mn^{2+}/ Mn^{3+} had been reported to induce intracellular ROS production, which can further affect the DNA and the mitochondria activity, causing DNA fragmentation and the loss of the mitochondria transmembrane potential (Fig. 11).

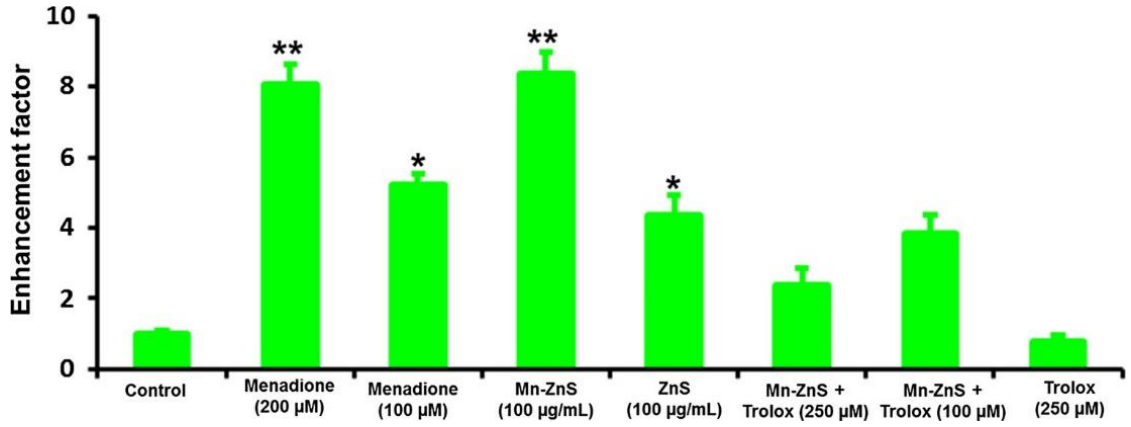

Fig. 11 *Comparison of DNA fragmentation of liver cells treated by pure ZnS, ZnS:Mn NPs against the control group, positive group (Menadione) and negative control (Trolox). From Ref 136*

4. Conclusion

Through this synthesis, we learned that nanomaterials present all a potential toxicity, which can be due to their composition, their size, their shape, the potential release of ions by dissolution, etc. The toxicity exhibited by a type of nanomaterial may vary from one living species to another.

We were particularly interested in quantum dot nanoparticles, studied in the team for various applications. I chose to focus on ZnS nanoparticles doped with transition metal cations and intended to be used in the manufacture of electroluminescent panels. For this, these nanoparticles are inserted between two layers of dielectric, often metal oxides. However, after these products constituted of ZnS NPs are abandoned, lots of them will end up in the environment, and will flow into the rivers and seas and/or deposit in soil or sediments and induce uncontrolled toxicological effects not only on the microbes in the environment, but even to the alimentary vegetal, animal, and human chain.

Therefore, I chose to synthesize several samples of ZnS NPs, doped with different metals, at different concentrations, even coated with silica and to evaluate their toxicity. I then evaluated their toxicity for the algae *Chlorella Vulgaris*, in the freshwater, Seine River water and synthetic seawater systems in collaboration with the Museum National d'Histoire Naturelle (MNHN).

In this manuscript, I am presenting the synthesis of ZnS:Mn (0.5, 2.0, 4.0, and 10%) NPs with a small size by the polyol method, in order to investigate their ecotoxicity on microalgae, using different molar concentrations of Mn (Chapter 2). Then the ZnS: Mn (10%) NPs were coated with a silica shell using the reverse microemulsion method to check if the silica shell can prevent the toxicity of ZnS:Mn NPs (Chapter 2). After that, in order to check the ecotoxicity effects of different sizes of ZnS:Mn NPs, bigger ZnS:Mn NPs were synthesized using the microwave-assisted polyol method, and the ecotoxicity of these NPs has been evaluated through the measurement of photosynthetic activity, cell viability, intracellular ATP content, and SOD activity (Chapter 3). Finally, Mn^{2+}, Cu^{2+}, and Co^{2+} monodoped ZnS NPs were synthesized by the microwave-assisted polyol method to study the toxicity of these NPs on *Chlorella Vulgaris* (Chapter 4).

5. References

(1) Brayner, R.; Fiévet, F. Toxicological Models Part A: Toxicological Studies of Nanoparticles on Biological Targets and Attempts to Attenuate Toxicity by Encapsulation Techniques. In *Nanoethics and Nanotoxicology*; Houdy, P., Lahmani, M., Marano, F., Eds.; Springer: Berlin, Heidelberg, 2011; pp 359–377. https://doi.org/10.1007/978-3-642-20177-6_15.

(2) da Rocha, A.; Brayner, R. Ecotoxicological Impact of ZnO and CdE (E = S, Se, Te) Quantum Dots on Microorganisms. In *Nanomaterials: A Danger or a Promise? A Chemical and Biological Perspective*; Brayner, R., Fiévet, F., Coradin, T., Eds.; Springer: London, 2013; pp 287–305. https://doi.org/10.1007/978-1-4471-4213-3_11.

(3) Peng, C.; Zhang, W.; Gao, H.; Li, Y.; Tong, X.; Li, K.; Zhu, X.; Wang, Y.; Chen, Y. Behavior and Potential Impacts of Metal-Based Engineered Nanoparticles in Aquatic Environments. *Nanomaterials* **2017**, *7* (1), 21. https://doi.org/10.3390/nano7010021.

(4) Chung, J. H.; Ah, C. S.; Jang, D.-J. Formation and Distinctive Decay Times of Surface- and Lattice-Bound Mn^{2+} Impurity Luminescence in ZnS Nanoparticles. *J. Phys. Chem. B* **2001**, *105* (19), 4128–4132. https://doi.org/10.1021/jp002692j.

(5) Saavedra-Rodriguez, G.; Pal, U.; Sánchez-Zeferino, R.; Álvarez-Ramos, M. E. Tunable White-Light Emission of Co^{2+} and Mn^{2+} Co-Doped ZnS Nanoparticles by Energy Transfer between Dopant Ions. *J. Phys. Chem. C* **2020**, *124* (6), 3857–3866. https://doi.org/10.1021/acs.jpcc.9b10890.

(6) Poornaprakash, B.; Chalapathi, U.; Poojitha, P. T.; Vattikuti, S. V. P.; Reddy, M. S. P. (Al, Cu) Co-Doped ZnS Nanoparticles: Structural, Chemical, Optical, and Photocatalytic Properties. *J Mater Sci: Mater Electron* **2019**, *30* (10), 9897–9902. https://doi.org/10.1007/s10854-019-01327-8.

(7) Li, R.; Sun, H.; Wang, S.; Wang, Y.; Yu, K. Retention of CdS/ZnS Quantum Dots (QDs) on the Root Epidermis of Woody Plant and Its Implications by Benzo[a]Pyrene: Evidence from the in Situ Synchronous Nanosecond Time-Resolved Fluorescence Spectra Method. *J. Agric. Food Chem.* **2018**, *66* (4), 814–821. https://doi.org/10.1021/acs.jafc.7b04258.

(8) Planchon, M.; Ferrari, R.; Guyot, F.; Gélabert, A.; Menguy, N.; Chanéac, C.; Thill, A.; Benedetti, M. F.; Spalla, O. Interaction between Escherichia Coli and TiO_2

Nanoparticles in Natural and Artificial Waters. *Colloids and Surfaces B: Biointerfaces* **2013**, *102*, 158–164. https://doi.org/10.1016/j.colsurfb.2012.08.034.

(9) Polonini, H. C.; Brayner, R. Nanoecotoxicology: The State of the Art. In *Nanotechnologies in Food and Agriculture*; Rai, M., Ribeiro, C., Mattoso, L., Duran, N., Eds.; Springer International Publishing: Cham, 2015; pp 301–319. https://doi.org/10.1007/978-3-319-14024-7_13.

(10) Rocha, A. D.; Sivry, Y.; Gelabert, A.; Beji, Z.; Benedetti, M. F.; Menguy, N.; Brayner, R. The Fate of Polyol-Made ZnO and CdS Nanoparticles in Seine River Water (Paris, France). *j nanosci nanotechnol* **2015**, *15* (5), 3900–3908. https://doi.org/10.1166/jnn.2015.9276.

(11) Gottschalk, F.; Sonderer, T.; Scholz, R. W.; Nowack, B. Modeled Environmental Concentrations of Engineered Nanomaterials (TiO_2, ZnO, Ag, CNT, Fullerenes) for Different Regions. *Environ. Sci. Technol.* **2009**, *43* (24), 9216–9222. https://doi.org/10.1021/es9015553.

(12) Boros, B.-V.; Ostafe, V. Evaluation of Ecotoxicology Assessment Methods of Nanomaterials and Their Effects. *Nanomaterials* **2020**, *10* (4), 610. https://doi.org/10.3390/nano10040610.

(13) Brayner, R.; Dahoumane, S. A.; Nguyen, J. N.-L.; Yéprémian, C.; Djediat, C.; Couté, A.; Fiévet, F. Ecotoxicological Studies of CdS Nanoparticles on Photosynthetic Microorganisms. *Journal of Nanoscience and Nanotechnology* **2011**, *11* (3), 1852–1858. https://doi.org/10.1166/jnn.2011.3564.

(14) Brayner, R.; Ferrari-Iliou, R.; Brivois, N.; Djediat, S.; Benedetti, M. F.; Fiévet, F. Toxicological Impact Studies Based on Escherichia Coli Bacteria in Ultrafine ZnO Nanoparticles Colloidal Medium. *Nano Lett.* **2006**, *6* (4), 866–870. https://doi.org/10.1021/nl052326h.

(15) Djurišić, A. B.; Leung, Y. H.; Ng, A. M. C.; Xu, X. Y.; Lee, P. K. H.; Degger, N.; Wu, R. S. S. Toxicity of Metal Oxide Nanoparticles: Mechanisms, Characterization, and Avoiding Experimental Artefacts. *Small* **2015**, *11* (1), 26–44. https://doi.org/10.1002/smll.201303947.

(16) da Rocha, A.; Menguy, N.; Yéprémian, C.; Couté, A.; Brayner, R. Ecotoxicological Studies of ZnO and CdS Nanoparticles on Chlorella Vulgaris

Photosynthetic Microorganism in Seine River Water. *Nanomaterials (Basel)* **2020**, *10* (2). https://doi.org/10.3390/nano10020227.

(17) Yu, Z.; Hao, R.; Zhang, L.; Zhu, Y. Effects of TiO_2, SiO_2, Ag and CdTe/CdS Quantum Dots Nanoparticles on Toxicity of Cadmium towards Chlamydomonas Reinhardtii. *Ecotoxicology and Environmental Safety* **2018**, *156*, 75–86. https://doi.org/10.1016/j.ecoenv.2018.03.007.

(18) Silva, B. F.; Andreani, T.; Gavina, A.; Vieira, M. N.; Pereira, C. M.; Rocha-Santos, T.; Pereira, R. Toxicological Impact of Cadmium-Based Quantum Dots towards Aquatic Biota: Effect of Natural Sunlight Exposure. *Aquatic Toxicology* **2016**, *176*, 197–207. https://doi.org/10.1016/j.aquatox.2016.05.001.

(19) Das, S.; P. Wolfson, B.; Tetard, L.; Tharkur, J.; Bazata, J.; Santra, S. Effect of N -Acetyl Cysteine Coated CdS:Mn/ZnS Quantum Dots on Seed Germination and Seedling Growth of Snow Pea (Pisum Sativum L.): Imaging and Spectroscopic Studies. *Environmental Science: Nano* **2015**, *2* (2), 203–212. https://doi.org/10.1039/C4EN00198B.

(20) Pikula, K.; Zakharenko, A.; Chaika, V.; Em, I.; Nikitina, A.; Avtomonov, E.; Tregubenko, A.; Agoshkov, A.; Mishakov, I.; Kuznetsov, V.; Gusev, A.; Park, S.; Golokhvast, K. Toxicity of Carbon, Silicon, and Metal-Based Nanoparticles to Sea Urchin Strongylocentrotus Intermedius. *Nanomaterials* **2020**, *10* (9), 1825. https://doi.org/10.3390/nano10091825.

(21) Vimercati, L.; Cavone, D.; Caputi, A.; De Maria, L.; Tria, M.; Prato, E.; Ferri, G. M. Nanoparticles: An Experimental Study of Zinc Nanoparticles Toxicity on Marine Crustaceans. General Overview on the Health Implications in Humans. *Frontiers in Public Health* **2020**, *8*, 192. https://doi.org/10.3389/fpubh.2020.00192.

(22) Brayner, R.; Sicard, C.; Sassi, H. B.; Beji, Z.; Yéprémian, C.; Couté, A.; Fiévet, F. Design of ZnO Nanostructured Films: Characterization and Ecotoxicological Studies. *Thin Solid Films* **2011**, *519* (10), 3340–3345. https://doi.org/10.1016/j.tsf.2011.01.257.

(23) Suman, T. Y.; Radhika Rajasree, S. R.; Kirubagaran, R. Evaluation of Zinc Oxide Nanoparticles Toxicity on Marine Algae Chlorella Vulgaris through Flow Cytometric, Cytotoxicity and Oxidative Stress Analysis. *Ecotoxicology and Environmental Safety* **2015**, *113*, 23–30. https://doi.org/10.1016/j.ecoenv.2014.11.015.

(24) Brayner, R.; Dahoumane, S. A.; Yéprémian, C.; Djediat, C.; Meyer, M.; Couté, A.; Fiévet, F. ZnO Nanoparticles: Synthesis, Characterization, and Ecotoxicological Studies. *Langmuir* **2010**, *26* (9), 6522–6528. https://doi.org/10.1021/la100293s.

(25) Gelabert, A.; Sivry, Y.; Gobbi, P.; Mansouri-Guilani, N.; Menguy, N.; Brayner, R.; Siron, V.; Benedetti, M. F.; Ferrari, R. Testing Nanoeffect onto Model Bacteria: Impact of Speciation and Genotypes. *Nanotoxicology* **2016**, *10* (2), 216–225. https://doi.org/10.3109/17435390.2015.1048323.

(26) Serrà, A.; Zhang, Y.; Sepúlveda, B.; Gómez, E.; Nogués, J.; Michler, J.; Philippe, L. Highly Reduced Ecotoxicity of ZnO-Based Micro/Nanostructures on Aquatic Biota: Influence of Architecture, Chemical Composition, Fixation, and Photocatalytic Efficiency. *Water Research* **2020**, *169*, 115210. https://doi.org/10.1016/j.watres.2019.115210.

(27) Dar, G. I.; Saeed, M.; Wu, A. Toxicity of TiO_2 Nanoparticles. In *TiO_2 Nanoparticles*; John Wiley & Sons, Ltd, 2020; pp 67–103. https://doi.org/10.1002/9783527825431.ch2.

(28) Jallouli, N.; Elghniji, K.; Trabelsi, H.; Ksibi, M. Photocatalytic Degradation of Paracetamol on TiO_2 Nanoparticles and TiO_2/Cellulosic Fiber under UV and Sunlight Irradiation. *Arabian Journal of Chemistry* **2017**, *10*, S3640–S3645. https://doi.org/10.1016/j.arabjc.2014.03.014.

(29) Lusvardi, G.; Barani, C.; Giubertoni, F.; Paganelli, G. Synthesis and Characterization of TiO_2 Nanoparticles for the Reduction of Water Pollutants. *Materials* **2017**, *10* (10), 1208. https://doi.org/10.3390/ma10101208.

(30) Haider, A. J.; AL– Anbari, R. H.; Kadhim, G. R.; Salame, C. T. Exploring Potential Environmental Applications of TiO_2 Nanoparticles. *Energy Procedia* **2017**, *119*, 332–345. https://doi.org/10.1016/j.egypro.2017.07.117.

(31) Gottschalk, F.; Sonderer, T.; Scholz, R. W.; Nowack, B. Possibilities and Limitations of Modeling Environmental Exposure to Engineered Nanomaterials by Probabilistic Material Flow Analysis. *Environmental Toxicology and Chemistry* **2010**, *29* (5), 1036–1048. https://doi.org/10.1002/etc.135.

(32) Pikula, K.; Johari, S. A.; Santos-Oliveira, R.; Golokhvast, K. Individual and Binary Mixture Toxicity of Five Nanoparticles in Marine Microalga Heterosigma Akashiwo. *International Journal of Molecular Sciences* **2022**, *23* (2), 990. https://doi.org/10.3390/ijms23020990.

(33) Liu, Y.; Wang, S.; Wang, Z.; Ye, N.; Fang, H.; Wang, D. TiO_2, SiO_2 and ZrO_2 Nanoparticles Synergistically Provoke Cellular Oxidative Damage in Freshwater Microalgae. *Nanomaterials* **2018**, *8* (2), 95. https://doi.org/10.3390/nano8020095.

(34) Kose, O.; Tomatis, M.; Leclerc, L.; Belblidia, N.-B.; Hochepied, J.-F.; Turci, F.; Pourchez, J.; Forest, V. Impact of the Physicochemical Features of TiO_2 Nanoparticles on Their In Vitro Toxicity. *Chem. Res. Toxicol.* **2020**, *33* (9), 2324–2337. https://doi.org/10.1021/acs.chemrestox.0c00106.

(35) Valentini, X.; Rugira, P.; Frau, A.; Tagliatti, V.; Conotte, R.; Laurent, S.; Colet, J.-M.; Nonclercq, D. Hepatic and Renal Toxicity Induced by TiO_2 Nanoparticles in Rats: A Morphological and Metabonomic Study. *Journal of Toxicology* **2019**, *2019*, e5767012. https://doi.org/10.1155/2019/5767012.

(36) Gupta, N.; Gupta, S. M.; Sharma, S. K. Carbon Nanotubes: Synthesis, Properties and Engineering Applications. *Carbon Lett.* **2019**, *29* (5), 419–447. https://doi.org/10.1007/s42823-019-00068-2.

(37) Haniu, H.; Saito, N.; Matsuda, Y.; Tsukahara, T.; Maruyama, K.; Usui, Y.; Aoki, K.; Takanashi, S.; Kobayashi, S.; Nomura, H.; Okamoto, M.; Shimizu, M.; Kato, H. Culture Medium Type Affects Endocytosis of Multi-Walled Carbon Nanotubes in BEAS-2B Cells and Subsequent Biological Response. *Toxicology in Vitro* **2013**, *27* (6), 1679–1685. https://doi.org/10.1016/j.tiv.2013.04.012.

(38) Pereira, M. M.; Mouton, L.; Yéprémian, C.; Couté, A.; Lo, J.; Marconcini, J. M.; Ladeira, L. O.; Raposo, N. R.; Brandão, H. M.; Brayner, R. Ecotoxicological Effects of Carbon Nanotubes and Cellulose Nanofibers in Chlorella Vulgaris. *J Nanobiotechnol* **2014**, *12* (1), 15. https://doi.org/10.1186/1477-3155-12-15.

(39) Zhang, M.; Wang, H.; Liu, P.; Song, Y.; Huang, H.; Shao, M.; Liu, Y.; Li, H.; Kang, Z. Biotoxicity of Degradable Carbon Dots towards Microalgae Chlorella Vulgaris. *Environmental Science: Nano* **2019**, *6* (11), 3316–3323. https://doi.org/10.1039/C9EN00829B.

(40) Simon, J.; Flahaut, E.; Golzio, M. Overview of Carbon Nanotubes for Biomedical Applications. *Materials* **2019**, *12* (4), 624. https://doi.org/10.3390/ma12040624.

(41) Mohanta, D.; Patnaik, S.; Sood, S.; Das, N. Carbon Nanotubes: Evaluation of Toxicity at Biointerfaces. *Journal of Pharmaceutical Analysis* **2019**, *9* (5), 293–300. https://doi.org/10.1016/j.jpha.2019.04.003.

(42) Francis, A. P.; Devasena, T. Toxicity of Carbon Nanotubes: A Review. *Toxicol Ind Health* **2018**, *34* (3), 200–210. https://doi.org/10.1177/0748233717747472.

(43) Wang, F.; Guan, W.; Xu, L.; Ding, Z.; Ma, H.; Ma, A.; Terry, N. Effects of Nanoparticles on Algae: Adsorption, Distribution, Ecotoxicity and Fate. *Applied Sciences* **2019**, *9* (8), 1534. https://doi.org/10.3390/app9081534.

(44) Gaté, L.; Knudsen, K. B.; Seidel, C.; Berthing, T.; Chézeau, L.; Jacobsen, N. R.; Valentino, S.; Wallin, H.; Bau, S.; Wolff, H.; Sébillaud, S.; Lorcin, M.; Grossmann, S.; Viton, S.; Nunge, H.; Darne, C.; Vogel, U.; Cosnier, F. Pulmonary toxicity of two different multi-walled carbon nanotubes in rat: Comparison between intratracheal instillation and inhalation exposure. *Toxicology and Applied Pharmacology* **2019**, *375*, 17–31. https://doi.org/10.1016/j.taap.2019.05.001.

(45) Cheng, W.-W.; Lin, Z.-Q.; Wei, B.-F.; Zeng, Q.; Han, B.; Wei, C.-X.; Fan, X.-J.; Hu, C.-L.; Liu, L.-H.; Huang, J.-H. Single-Walled Carbon Nanotube Induction of Rat Aortic Endothelial Cell Apoptosis: Reactive Oxygen Species Are Involved in the Mitochondrial Pathway. *The International Journal of Biochemistry & Cell Biology* **2011**, *43* (4), 564–572. https://doi.org/10.1016/j.biocel.2010.12.013.

(46) Cimbaluk, G. V.; Ramsdorf, W. A.; Perussolo, M. C.; Santos, H. K. F.; Da Silva De Assis, H. C.; Schnitzler, M. C.; Schnitzler, D. C.; Carneiro, P. G.; Cestari, M. M. Evaluation of Multiwalled Carbon Nanotubes Toxicity in Two Fish Species. *Ecotoxicology and Environmental Safety* **2018**, *150*, 215–223. https://doi.org/10.1016/j.ecoenv.2017.12.034.

(47) Zhao, X.; Chang, S.; Long, J.; Li, J.; Li, X.; Cao, Y. The Toxicity of Multi-Walled Carbon Nanotubes (MWCNTs) to Human Endothelial Cells: The Influence of Diameters of MWCNTs. *Food and Chemical Toxicology* **2019**, *126*, 169–177. https://doi.org/10.1016/j.fct.2019.02.026.

(48) Schaumann, G. E.; Philippe, A.; Bundschuh, M.; Metreveli, G.; Klitzke, S.; Rakcheev, D.; Grün, A.; Kumahor, S. K.; Kühn, M.; Baumann, T.; Lang, F.; Manz, W.; Schulz, R.; Vogel, H.-J. Understanding the Fate and Biological Effects of Ag- and TiO_2-Nanoparticles in the Environment: The Quest for Advanced Analytics and Interdisciplinary Concepts. *Science of The Total Environment* **2015**, *535*, 3–19. https://doi.org/10.1016/j.scitotenv.2014.10.035.

(49) El-Naggar, N. E.-A.; Hussein, M. H.; Shaaban-Dessuuki, S. A.; Dalal, S. R. Production, Extraction and Characterization of Chlorella Vulgaris Soluble Polysaccharides and Their Applications in AgNPs Biosynthesis and

Biostimulation of Plant Growth. *Scientific Reports* **2020**, *10* (1), 3011. https://doi.org/10.1038/s41598-020-59945-w.

(50) Husain, S.; Afreen, S.; Hemlata; Yasin, D.; Afzal, B.; Fatma, T. Cyanobacteria as a Bioreactor for Synthesis of Silver Nanoparticles-an Effect of Different Reaction Conditions on the Size of Nanoparticles and Their Dye Decolorization Ability. *Journal of Microbiological Methods* **2019**, *162*, 77–82. https://doi.org/10.1016/j.mimet.2019.05.011.

(51) Maiga, D. T.; Nyoni, H.; Mamba, B. B.; Msagati, T. A. M. The Role and Influence of Hydrogeochemistry in the Behaviour and Fate of Silver Nanoparticles in Freshwater Systems. *SN Appl. Sci.* **2020**, *2* (3), 326. https://doi.org/10.1007/s42452-020-2130-8.

(52) Taylor, C.; Matzke, M.; Kroll, A.; S. Read, D.; Svendsen, C.; Crossley, A. Toxic Interactions of Different Silver Forms with Freshwater Green Algae and Cyanobacteria and Their Effects on Mechanistic Endpoints and the Production of Extracellular Polymeric Substances. *Environmental Science: Nano* **2016**, *3* (2), 396–408. https://doi.org/10.1039/C5EN00183H.

(53) Buffet, P.-E.; Zalouk-Vergnoux, A.; Châtel, A.; Berthet, B.; Métais, I.; Perrein-Ettajani, H.; Poirier, L.; Luna-Acosta, A.; Thomas-Guyon, H.; Risso-de Faverney, C.; Guibbolini, M.; Gilliland, D.; Valsami-Jones, E.; Mouneyrac, C. A Marine Mesocosm Study on the Environmental Fate of Silver Nanoparticles and Toxicity Effects on Two Endobenthic Species: The Ragworm Hediste Diversicolor and the Bivalve Mollusc Scrobicularia Plana. *Science of The Total Environment* **2014**, *470–471*, 1151–1159. https://doi.org/10.1016/j.scitotenv.2013.10.114.

(54) Gomes, T.; Pereira, C. G.; Cardoso, C.; Sousa, V. S.; Teixeira, M. R.; Pinheiro, J. P.; Bebianno, M. J. Effects of Silver Nanoparticles Exposure in the Mussel Mytilus Galloprovincialis. *Marine Environmental Research* **2014**, *101*, 208–214. https://doi.org/10.1016/j.marenvres.2014.07.004.

(55) Rodea-Palomares, I.; Boltes, K.; Fernández-Piñas, F.; Leganés, F.; García-Calvo, E.; Santiago, J.; Rosal, R. Physicochemical Characterization and Ecotoxicological Assessment of CeO_2 Nanoparticles Using Two Aquatic Microorganisms. *Toxicological Sciences* **2011**, *119* (1), 135–145. https://doi.org/10.1093/toxsci/kfq311.

(56) Mahawar, H.; Prasanna, R.; Singh, S. B.; Nain, L. Influence of Silver, Zinc Oxide and Copper Oxide Nanoparticles on the Cyanobacterium Calothrix Elenkinii. *BioNanoSci.* **2018**, *8* (3), 802–810. https://doi.org/10.1007/s12668-018-0543-2.

(57) Polonini, H. C.; Brandão, H. M.; Raposo, N. R. B.; Mouton, L.; Yéprémian, C.; Couté, A.; Brayner, R. Ecotoxicological Studies of Micro- and Nanosized Barium Titanate on Aquatic Photosynthetic Microorganisms. *Aquatic Toxicology* **2014**, *154*, 58–70. https://doi.org/10.1016/j.aquatox.2014.05.005.

(58) Pinto, J.; Costa, M.; Leite, C.; Borges, C.; Coppola, F.; Henriques, B.; Monteiro, R.; Russo, T.; Di Cosmo, A.; Soares, A. M. V. M.; Polese, G.; Pereira, E.; Freitas, R. Ecotoxicological Effects of Lanthanum in Mytilus Galloprovincialis: Biochemical and Histopathological Impacts. *Aquatic Toxicology* **2019**, *211*, 181–192. https://doi.org/10.1016/j.aquatox.2019.03.017.

(59) Pikula, K. S.; Zakharenko, A. M.; Aruoja, V.; Golokhvast, K. S.; Tsatsakis, A. M. Oxidative Stress and Its Biomarkers in Microalgal Ecotoxicology. *Current Opinion in Toxicology* **2019**, *13*, 8–15. https://doi.org/10.1016/j.cotox.2018.12.006.

(60) Xiao, A.; Wang, C.; Chen, J.; Guo, R.; Yan, Z.; Chen, J. Carbon and Metal Quantum Dots Toxicity on the Microalgae Chlorella Pyrenoidosa. *Ecotoxicology and Environmental Safety* **2016**, *133*, 211–217. https://doi.org/10.1016/j.ecoenv.2016.07.026.

(61) Srinivasan, M.; Venkatesan, M.; Arumugam, V.; Natesan, G.; Saravanan, N.; Murugesan, S.; Ramachandran, S.; Ayyasamy, R.; Pugazhendhi, A. Green Synthesis and Characterization of Titanium Dioxide Nanoparticles (TiO_2 NPs) Using Sesbania Grandiflora and Evaluation of Toxicity in Zebrafish Embryos. *Process Biochemistry* **2019**, *80*, 197–202. https://doi.org/10.1016/j.procbio.2019.02.010.

(62) Kalpana, V. N.; Devi Rajeswari, V. A Review on Green Synthesis, Biomedical Applications, and Toxicity Studies of ZnO NPs. *Bioinorganic Chemistry and Applications* **2018**, *2018*, e3569758. https://doi.org/10.1155/2018/3569758.

(63) Brayner, R.; Yéprémian, C.; Djediat, C.; Coradin, T.; Herbst, F.; Livage, J.; Fiévet, F.; Couté, A. Photosynthetic Microorganism-Mediated Synthesis of Akaganeite (β-FeOOH) Nanorods. *Langmuir* **2009**, *25* (17), 10062–10067. https://doi.org/10.1021/la9010345.

(64) Brayner, R.; Coradin, T.; Beaunier, P.; Grenèche, J.-M.; Djediat, C.; Yéprémian, C.; Couté, A.; Fiévet, F. Intracellular Biosynthesis of Superparamagnetic 2-Lines Ferri-Hydrite Nanoparticles Using Euglena Gracilis Microalgae. *Colloids and Surfaces B: Biointerfaces* **2012**, *93*, 20–23. https://doi.org/10.1016/j.colsurfb.2011.10.014.

(65) Sicard, C.; Brayner, R.; Margueritat, J.; Hémadi, M.; Couté, A.; Yéprémian, C.; Djediat, C.; Aubard, J.; Fiévet, F.; Livage, J.; Coradin, T. Nano- Gold Biosynthesis by Silica -Encapsulated Micro-Algae: A “Living” Bio-Hybrid Material. *Journal of Materials Chemistry* **2010**, *20* (42), 9342–9347. https://doi.org/10.1039/C0JM01735C.

(66) Sánchez-Thomas, R.; García-García, J. D.; Marín-Hernández, Á.; Pardo, J. P.; Rodríguez-Enríquez, S.; Vera-Estrella, R.; López-Macay, A.; Moreno-Sánchez, R. The Intracellular Water Volume Modulates the Accumulation of Cadmium in Euglena Gracilis. *Algal Research* **2020**, *46*, 101774. https://doi.org/10.1016/j.algal.2019.101774.

(67) Djearamane, S.; Lim, Y. M.; Wong, L. S.; Lee, P. F. Cytotoxic Effects of Zinc Oxide Nanoparticles on Cyanobacterium Spirulina (Arthrospira) Platensis. *PeerJ* **2018**, *6*, e4682. https://doi.org/10.7717/peerj.4682.

(68) Chen, Z.; Song, S.; Wen, Y.; Zou, Y.; Liu, H. Toxicity of Cu (II) to the Green Alga Chlorella Vulgaris: A Perspective of Photosynthesis and Oxidant Stress. *Environ Sci Pollut Res* **2016**, *23* (18), 17910–17918. https://doi.org/10.1007/s11356-016-6997-2.

(69) Hartmann, J. T.; Beggel, S.; Auerswald, K.; Stoeckle, B. C.; Geist, J. Establishing Mussel Behavior as a Biomarker in Ecotoxicology. *Aquatic Toxicology* **2016**, *170*, 279–288. https://doi.org/10.1016/j.aquatox.2015.06.014.

(70) Katsumiti, A.; Thorley, A. J.; Arostegui, I.; Reip, P.; Valsami-Jones, E.; Tetley, T. D.; Cajaraville, M. P. Cytotoxicity and Cellular Mechanisms of Toxicity of CuO NPs in Mussel Cells in Vitro and Comparative Sensitivity with Human Cells. *Toxicology in Vitro* **2018**, *48*, 146–158. https://doi.org/10.1016/j.tiv.2018.01.013.

(71) Ale, A.; Liberatori, G.; Vannuccini, M. L.; Bergami, E.; Ancora, S.; Mariotti, G.; Bianchi, N.; Galdopórpora, J. M.; Desimone, M. F.; Cazenave, J.; Corsi, I. Exposure to a Nanosilver-Enabled Consumer Product Results in Similar Accumulation and Toxicity of Silver Nanoparticles in the Marine Mussel Mytilus

Galloprovincialis. *Aquatic Toxicology* **2019**, *211*, 46–56. https://doi.org/10.1016/j.aquatox.2019.03.018.

(72) Wacksman, M. N.; Maul, J. D.; Lydy, M. J. Impact of Atrazine on Chlorpyrifos Toxicity in Four Aquatic Vertebrates. *Arch Environ Contam Toxicol* **2006**, *51* (4), 681–689. https://doi.org/10.1007/s00244-005-0264-8.

(73) Norberg-King, T. J.; Embry, M. R.; Belanger, S. E.; Braunbeck, T.; Butler, J. D.; Dorn, P. B.; Farr, B.; Guiney, P. D.; Hughes, S. A.; Jeffries, M.; Journel, R.; Lèonard, M.; McMaster, M.; Oris, J. T.; Ryder, K.; Segner, H.; Senac, T.; Van Der Kraak, G.; Whale, G.; Wilson, P. An International Perspective on the Tools and Concepts for Effluent Toxicity Assessments in the Context of Animal Alternatives: Reduction in Vertebrate Use. *Environmental Toxicology and Chemistry* **2018**, *37* (11), 2745–2757. https://doi.org/10.1002/etc.4259.

(74) Jayasinghe, C. D.; Jayawardena, U. A. Toxicity Assessment of Herbal Medicine Using Zebrafish Embryos: A Systematic Review. *Evidence-Based Complementary and Alternative Medicine* **2019**, *2019*, e7272808. https://doi.org/10.1155/2019/7272808.

(75) Vicario-Parés, U.; Castañaga, L.; Lacave, J. M.; Oron, M.; Reip, P.; Berhanu, D.; Valsami-Jones, E.; Cajaraville, M. P.; Orbea, A. Comparative Toxicity of Metal Oxide Nanoparticles (CuO, ZnO and TiO_2) to Developing Zebrafish Embryos. *J Nanopart Res* **2014**, *16* (8), 2550. https://doi.org/10.1007/s11051-014-2550-8.

(76) Ispas, C.; Andreescu, D.; Patel, A.; Goia, D. V.; Andreescu, S.; Wallace, K. N. Toxicity and Developmental Defects of Different Sizes and Shape Nickel Nanoparticles in Zebrafish. *Environ. Sci. Technol.* **2009**, *43* (16), 6349–6356. https://doi.org/10.1021/es9010543.

(77) Wang, Y.; Chen, Z.; Ba, T.; Pu, J.; Chen, T.; Song, Y.; Gu, Y.; Qian, Q.; Xu, Y.; Xiang, K.; Wang, H.; Jia, G. Susceptibility of Young and Adult Rats to the Oral Toxicity of Titanium Dioxide Nanoparticles. *Small* **2013**, *9* (9–10), 1742–1752. https://doi.org/10.1002/smll.201201185.

(78) Handy, R. D.; Owen, R.; Valsami-Jones, E. The Ecotoxicology of Nanoparticles and Nanomaterials: Current Status, Knowledge Gaps, Challenges, and Future Needs. *Ecotoxicology* **2008**, *17* (5), 315–325. https://doi.org/10.1007/s10646-008-0206-0.

(79) Aubert, T.; Burel, A.; Esnault, M.-A.; Cordier, S.; Grasset, F.; Cabello-Hurtado, F. Root Uptake and Phytotoxicity of Nanosized Molybdenum Octahedral Clusters. *Journal of Hazardous Materials* **2012**, *219–220*, 111–118. https://doi.org/10.1016/j.jhazmat.2012.03.058.

(80) Ji, Y.; Zhou, Y.; Ma, C.; Feng, Y.; Hao, Y.; Rui, Y.; Wu, W.; Gui, X.; Le, V. N.; Han, Y.; Wang, Y.; Xing, B.; Liu, L.; Cao, W. Jointed Toxicity of TiO_2 NPs and Cd to Rice Seedlings: NPs Alleviated Cd Toxicity and Cd Promoted NPs Uptake. *Plant Physiology and Biochemistry* **2017**, *110*, 82–93. https://doi.org/10.1016/j.plaphy.2016.05.010.

(81) Bandyopadhyay, S.; Plascencia-Villa, G.; Mukherjee, A.; Rico, C. M.; José-Yacamán, M.; Peralta-Videa, J. R.; Gardea-Torresdey, J. L. Comparative Phytotoxicity of ZnO NPs, Bulk ZnO, and Ionic Zinc onto the Alfalfa Plants Symbiotically Associated with Sinorhizobium Meliloti in Soil. *Science of The Total Environment* **2015**, *515–516*, 60–69. https://doi.org/10.1016/j.scitotenv.2015.02.014.

(82) Zhu, Y.-P.; Li, J.; Ma, T.-Y.; Liu, Y.-P.; Du, G.; Yuan, Z.-Y. Sonochemistry-Assisted Synthesis and Optical Properties of Mesoporous ZnS Nanomaterials. *Journal of Materials Chemistry A* **2014**, *2* (4), 1093–1101. https://doi.org/10.1039/C3TA13636A.

(83) Goktas, A.; Tumbul, A.; Aslan, F. A New Approach to Growth of Chemically Depositable Different ZnS Nanostructures. *J Sol-Gel Sci Technol* **2019**, *90* (3), 487–497. https://doi.org/10.1007/s10971-019-04990-9.

(84) Feldmann, C.; Metzmacher, C. Polyol Mediated Synthesis of Nanoscale MS Particles (M = Zn, Cd, Hg). *Journal of Materials Chemistry* **2001**, *11* (10), 2603–2606. https://doi.org/10.1039/B103167H.

(85) Vasudevan, K.; Divyasree, M. C.; Chandrasekharan, K. Enhanced Nonlinear Optical Properties of ZnS Nanoparticles in 1D Polymer Photonic Crystal Cavity. *Optics & Laser Technology* **2019**, *114*, 35–39. https://doi.org/10.1016/j.optlastec.2019.01.027.

(86) Amaranatha Reddy, D.; Kim, D. H.; Rhee, S. J.; Jung, C. U.; Lee, B. W.; Liu, C. Hydrothermal Synthesis of Wurtzite $Zn_{1-x}Ni_xS$ Mesoporous Nanospheres: With Blue–Green Emissions and Ferromagnetic Curie Point above Room Temperature. *Journal of Alloys and Compounds* **2014**, *588*, 596–604. https://doi.org/10.1016/j.jallcom.2013.11.079.

(87) Göde, F.; Gümüş, C.; Zor, M. Investigations on the Physical Properties of the Polycrystalline ZnS Thin Films Deposited by the Chemical Bath Deposition Method. *Journal of Crystal Growth* **2007**, *299* (1), 136–141. https://doi.org/10.1016/j.jcrysgro.2006.10.266.

(88) Shao, L.-X.; Chang, K.-H.; Hwang, H.-L. Zinc Sulfide Thin Films Deposited by RF Reactive Sputtering for Photovoltaic Applications. *Applied Surface Science* **2003**, *212–213*, 305–310. https://doi.org/10.1016/S0169-4332(03)00085-0.

(89) Thambidurai, M.; Muthukumarasamy, N.; Agilan, S.; Murugan, N.; Vasantha, S.; Balasundaraprabhu, R.; Senthil, T. S. Strong Quantum Confinement Effect in Nanocrystalline CdS. *J Mater Sci* **2010**, *45* (12), 3254–3258. https://doi.org/10.1007/s10853-010-4333-7.

(90) Peng Xie, Y.; Bao Yu, Z.; Liu, G.; Liang Ma, X.; Cheng, H.-M. CdS–Mesoporous ZnS Core–Shell Particles for Efficient and Stable Photocatalytic Hydrogen Evolution under Visible Light. *Energy & Environmental Science* **2014**, *7* (6), 1895–1901. https://doi.org/10.1039/C3EE43750G.

(91) Geszke, M.; Murias, M.; Balan, L.; Medjahdi, G.; Korczynski, J.; Moritz, M.; Lulek, J.; Schneider, R. Folic Acid-Conjugated Core/Shell ZnS:Mn/ZnS Quantum Dots as Targeted Probes for Two Photon Fluorescence Imaging of Cancer Cells. *Acta Biomaterialia* **2011**, *7* (3), 1327–1338. https://doi.org/10.1016/j.actbio.2010.10.012.

(92) Labiadh, H.; Sellami, B.; Khazri, A.; Saidani, W.; Khemais, S. Optical Properties and Toxicity of Undoped and Mn-Doped ZnS Semiconductor Nanoparticles Synthesized through the Aqueous Route. *Optical Materials* **2017**, *64*, 179–186. https://doi.org/10.1016/j.optmat.2016.12.011.

(93) Gao, W.; Cao, M.; Xiao, W.; Lei, F.; Huang, J.; Sun, Y.; Wang, L.; Shen, Y. Effects of Reaction Conditions on the Structural, Morphological and Optical Properties of Solvothermal Synthesized ZnS Nanostructures. *Materials Science in Semiconductor Processing* **2016**, *56*, 349–356. https://doi.org/10.1016/j.mssp.2016.09.020.

(94) Geng, B. Y.; Liu, X. W.; Du, Q. B.; Wei, X. W.; Zhang, L. D. Structure and Optical Properties of Periodically Twinned ZnS Nanowires. *Appl. Phys. Lett.* **2006**, *88* (16), 163104. https://doi.org/10.1063/1.2196827.

(95) Fang, X.; Zhai, T.; Gautam, U. K.; Li, L.; Wu, L.; Bando, Y.; Golberg, D. ZnS Nanostructures: From Synthesis to Applications. *Progress in Materials Science* **2011**, *56* (2), 175–287. https://doi.org/10.1016/j.pmatsci.2010.10.001.

(96) Qi, L.; Mao, G.; Ao, J. Chemical Bath-Deposited ZnS Thin Films: Preparation and Characterization. *Applied Surface Science* **2008**, *254* (18), 5711–5714. https://doi.org/10.1016/j.apsusc.2008.03.059.

(97) Brayek, A.; Chaguetmi, S.; Ghoul, M.; Assaker, I. B.; Chtourou, R.; Decorse, P.; Beaunier, P.; Nowak, S.; Mammeri, F.; Ammar, S. The Structural and the Photoelectrochemical Properties of ZnO–ZnS/ITO 1D Hetero-Junctions Prepared by Tandem Electrodeposition and Surface Sulfidation: On the Material Processing Limits. *RSC Advances* **2018**, *8* (21), 11785–11798. https://doi.org/10.1039/C8RA00176F.

(98) Ham, S.; Kim, Y.; Jin Park, M.; Hee Hong, B.; Jang, D.-J. Graphene Quantum Dots-Decorated ZnS Nanobelts with Highly Efficient Photocatalytic Performances. *RSC Advances* **2016**, *6* (29), 24115–24120. https://doi.org/10.1039/C5RA28026E.

(99) Chaguetmi, S.; Chaperman, L.; Nowak, S.; Schaming, D.; Lau-Truong, S.; Decorse, P.; Beaunier, P.; Costentin, C.; Mammeri, F.; Achour, S.; Ammar, S. Photoelectrochemical Properties of ZnS- and CdS-TiO_2 Nanostructured Photocatalysts: Aqueous Sulfidation as a Smart Route to Improve Catalyst Stability. *Journal of Photochemistry and Photobiology A: Chemistry* **2018**, *356*, 489–501. https://doi.org/10.1016/j.jphotochem.2018.01.038.

(100) Norris, D. J.; Efros, A. L.; Erwin, S. C. Doped Nanocrystals. *Science* **2008**, *319* (5871), 1776–1779. https://doi.org/10.1126/science.1143802.

(101) Della Gaspera, E.; Griggs, J.; Ahmed, T.; Walia, S.; Mayes, E. L. H.; Calzolari, A.; Catellani, A.; van Embden, J. Augmented Band Gap Tunability in Indium-Doped Zinc Sulfide Nanocrystals. *Nanoscale* **2019**, *11* (7), 3154–3163. https://doi.org/10.1039/C8NR08830F.

(102) Bhargava, R. N.; Gallagher, D.; Welker, T. Doped Nanocrystals of Semiconductors - a New Class of Luminescent Materials. *Journal of Luminescence* **1994**, *60–61*, 275–280. https://doi.org/10.1016/0022-2313(94)90146-5.

(103) Bol, A. A.; Meijerink, A. Long-Lived Mn^{2+} Emission in Nanocrystalline ZnS:Mn^{2+}. *Phys. Rev. B* **1998**, *58* (24), R15997–R16000. https://doi.org/10.1103/PhysRevB.58.R15997.

(104) Raksha, K. R.; Ananda, S.; Madegowda, N. M. Study of Kinetics of Photocatalysis, Bacterial Inactivation and •OH Scavenging Activity of Electrochemically Synthesized Se^{4+} Doped ZnS Nanoparticles. *Journal of Molecular Catalysis A: Chemical* **2015**, *396*, 319–327. https://doi.org/10.1016/j.molcata.2014.10.005.

(105) Fiévet, F.; Ammar-Merah, S.; Brayner, R.; Chau, F.; Giraud, M.; Mammeri, F.; Peron, J.; Piquemal, J.-Y.; Sicard, L.; Viau, G. The Polyol Process: A Unique Method for Easy Access to Metal Nanoparticles with Tailored Sizes, Shapes and Compositions. *Chem. Soc. Rev.* **2018**, *47* (14), 5187–5233. https://doi.org/10.1039/C7CS00777A.

(106) Soltani, N.; Saion, E.; Hussein, M. Z.; Bahrami, A.; Naghavi, K.; Yunus, R. B. MICROWAVE IRRADIATION EFFECTS ON HYDROTHERMAL AND POLYOL SYNTHESIS OF ZnS NANOPARTICLES. 11.

(107)Gaceur, M.; Giraud, M.; Hemadi, M.; Nowak, S.; Menguy, N.; Quisefit, J. P.; David, K.; Jahanbin, T.; Benderbous, S.; Boissière, M.; Ammar, S. Polyol-Synthesized $Zn_{0.9}Mn_{0.1}S$ Nanoparticles as Potential Luminescent and Magnetic Bimodal Imaging Probes: Synthesis, Characterization, and Toxicity Study. *Journal of Nanoparticle Research* **2012**, *14* (7). https://doi.org/10.1007/s11051-012-0932-3.

(108) Longo, A. V.; Notebaert, B.; Gaceur, M.; Patriarche, G.; Sciortino, A.; Cannas, M.; Messina, F.; von Bardeleben, H. J.; Battaglini, N.; Ammar, S. Photo-Activated Phosphorescence of Ultrafine ZnS:Mn Quantum Dots: On the Lattice Strain Contribution. *J. Phys. Chem. C* **2022**, *126* (3), 1531–1541. https://doi.org/10.1021/acs.jpcc.1c09687.

(109) Polsongkram, D.; Chamninok, P.; Pukird, S.; Chow, L.; Lupan, O.; Chai, G.; Khallaf, H.; Park, S.; Schulte, A. Effect of Synthesis Conditions on the Growth of ZnO Nanorods via Hydrothermal Method. *Physica B: Condensed Matter* **2008**, *403* (19–20), 3713–3717. https://doi.org/10.1016/j.physb.2008.06.020.

(110) Meng, L.-Y.; Wang, B.; Ma, M.-G.; Lin, K.-L. The Progress of Microwave-Assisted Hydrothermal Method in the Synthesis of Functional Nanomaterials. *Materials Today Chemistry* **2016**, *1–2*, 63–83. https://doi.org/10.1016/j.mtchem.2016.11.003.

(111) Rashad, M. M.; Rayan, D. A.; El-Barawy, K. Hydrothermal Synthesis and Magnetic Properties of Mn Doped ZnS Nanoparticles. *J. Phys.: Conf. Ser.* **2010**, *200* (7), 072077. https://doi.org/10.1088/1742-6596/200/7/072077.

(112) Hu, Y.; Hu, B.; Wu, B.; Wei, Z.; Li, J. Hydrothermal Preparation of ZnS:Mn Quantum Dots and the Effects of Reaction Temperature on Its Structural and Optical Properties. *J Mater Sci: Mater Electron* **2018**, *29* (19), 16715–16720. https://doi.org/10.1007/s10854-018-9764-y.

(113) Cao, J.; Yang, J.; Zhang, Y.; Yang, L.; Wang, Y.; Wei, M.; Liu, Y.; Gao, M.; Liu, X.; Xie, Z. Optimized Doping Concentration of Manganese in Zinc Sulfide Nanoparticles for Yellow-Orange Light Emission. *Journal of Alloys and Compounds* **2009**, *486* (1), 890–894. https://doi.org/10.1016/j.jallcom.2009.07.097.

(114) Ramachandran, R.; Saranya, M.; Kollu, P.; Raghupathy, B. P. C.; Jeong, S. K.; Grace, A. N. Solvothermal Synthesis of Zinc Sulfide Decorated Graphene (ZnS/G) Nanocomposites for Novel Supercapacitor Electrodes. *Electrochimica Acta* **2015**, *178*, 647–657. https://doi.org/10.1016/j.electacta.2015.08.010.

(115) Goswami, M.; Adhikary, N. C.; Bhattacharjee, S. Effect of Annealing Temperatures on the Structural and Optical Properties of Zinc Oxide Nanoparticles Prepared by Chemical Precipitation Method. *Optik* **2018**, *158*, 1006–1015. https://doi.org/10.1016/j.ijleo.2017.12.174.

(116) Rahdar, A. Effect of 2-Mercaptoethanol as Capping Agent on ZnS Nanoparticles: Structural and Optical Characterization. *J Nanostruct Chem* **2013**, *3* (1), 10. https://doi.org/10.1186/2193-8865-3-10.

(117) Amaranatha Reddy, D.; Liu, C.; Vijayalakshmi, R. P.; Reddy, B. K. Effect of Al Doping on the Structural, Optical and Photoluminescence Properties of ZnS Nanoparticles. *Journal of Alloys and Compounds* **2014**, *582*, 257–264. https://doi.org/10.1016/j.jallcom.2013.08.051.

(118) Manzoor, K.; Vadera, S. R.; Kumar, N.; Kutty, T. R. N. Synthesis and Photoluminescent Properties of ZnS Nanocrystals Doped with Copper and Halogen. *Materials Chemistry and Physics* **2003**, *82* (3), 718–725. https://doi.org/10.1016/S0254-0584(03)00366-3.

(119) Lakshmi, P. V. B.; Raj, K. S.; Ramachandran, K. Synthesis and Characterization of Nano ZnS Doped with Mn. *Crystal Research and Technology* **2009**, *44* (2), 153–158. https://doi.org/10.1002/crat.200800271.

(120) Murase, N.; Jagannathan, R.; Kanematsu, Y.; Watanabe, M.; Kurita, A.; Hirata, K.; Yazawa, T.; Kushida, T. Fluorescence and EPR Characteristics of Mn^{2+}-Doped ZnS Nanocrystals Prepared by Aqueous Colloidal Method. *J. Phys. Chem. B* **1999**, *103* (5), 754–760. https://doi.org/10.1021/jp9828179.

(121) Fang, X.; Wu, L.; Hu, L. ZnS Nanostructure Arrays: A Developing Material Star. *Advanced Materials* **2011**, *23* (5), 585–598. https://doi.org/10.1002/adma.201003624.

(122) Lin, K. B.; Su, Y. H. Photoluminescence of Cu:ZnS, Ag:ZnS, and Au:ZnS Nanoparticles Applied in Bio-LED. *Appl. Phys. B* **2013**, *113* (3), 351–359. https://doi.org/10.1007/s00340-013-5497-z.

(123) Hao, X.; Wang, Y.; Zhou, J.; Cui, Z.; Wang, Y.; Zou, Z. Zinc Vacancy-Promoted Photocatalytic Activity and Photostability of ZnS for Efficient Visible-Light-Driven Hydrogen Evolution. *Applied Catalysis B: Environmental* **2018**, *221*, 302–311. https://doi.org/10.1016/j.apcatb.2017.09.006.

(124) Poliukhova, V.; Khan, S.; Qiaohong, Z.; Zhang, J.; Kim, D.; Kim, S.; Cho, S.-H. ZnS/ZnO Nanosheets Obtained by Thermal Treatment of ZnS/Ethylenediamine as a Z-Scheme Photocatalyst for H_2 Generation and Cr(VI) Reduction. *Applied Surface Science* **2022**, *575*, 151773. https://doi.org/10.1016/j.apsusc.2021.151773.

(125) Igarashi, T.; Isobe, T.; Senna, M. EPR Study of Mn^{2+} Electronic States for the Nanosized ZnS:Mn Powder Modified by Acrylic Acid. *Phys. Rev. B* **1997**, *56* (11), 6444–6445. https://doi.org/10.1103/PhysRevB.56.6444.

(126) Kolmykov, O.; Coulon, J.; Lalevée, J.; Alem, H.; Medjahdi, G.; Schneider, R. Aqueous Synthesis of Highly Luminescent Glutathione-Capped Mn^{2+}-Doped ZnS Quantum Dots. *Materials Science and Engineering: C* **2014**, *44*, 17–23. https://doi.org/10.1016/j.msec.2014.07.064.

(127) Murugadoss, G. Synthesis and Photoluminescence Properties of Zinc Sulfide Nanoparticles Doped with Copper Using Effective Surfactants. *Particuology* **2013**, *11* (5), 566–573. https://doi.org/10.1016/j.partic.2012.11.003.

(128) Ollinger, M.; Craciun, V.; Singh, R. K. Nanoencapsulation of ZnS:Ag Particulates with Indium Tin Oxide for Field Emission Displays. *Appl. Phys. Lett.* **2002**, *80* (11), 1927–1929. https://doi.org/10.1063/1.1453477.

(129) Yu, X.; Zhang, G.; Cao, H.; An, X.; Wang, Y.; Shu, Z.; An, X.; Hua, F. ZnO@ZnS Hollow Dumbbells– Graphene Composites as High-Performance Photocatalysts and Alcohol Sensors. *New Journal of Chemistry* **2012**, *36* (12), 2593–2598. https://doi.org/10.1039/C2NJ40770A.

(130) Wang, Y.; Yang, M.; Ren, Y.; Fan, J. Cu-Mn Codoped ZnS Quantum Dots-Based Ratiometric Fluorescent Sensor for Folic Acid. *Analytica Chimica Acta* **2018**, *1040*, 136–142. https://doi.org/10.1016/j.aca.2018.08.010.

(131) Xiao, S.; Dai, W.; Liu, X.; Pan, D.; Zou, H.; Li, G.; Zhang, G.; Su, C.; Zhang, D.; Chen, W.; Li, H. Microwave-Induced Metal Dissolution Synthesis of Core–Shell Copper Nanowires/ZnS for Visible Light Photocatalytic H_2 Evolution. *Advanced Energy Materials* **2019**, *9* (22), 1900775. https://doi.org/10.1002/aenm.201900775.

(132) Pang, H.; Meng, X.; Song, H.; Zhou, W.; Yang, G.; Zhang, H.; Izumi, Y.; Takei, T.; Jewasuwan, W.; Fukata, N. Probing the Role of Nickle Dopant in Aqueous Colloidal ZnS Nanocrystals for Efficient Solar-Driven Nickel Reduction. *Applied Catalysis B: Environmental* **2019**, *244*, 1013–1020.

(133) Ma, D.; Shi, J.-W.; Sun, D.; Zou, Y.; Cheng, L.; He, C.; Wang, H.; Niu, C.; Wang, L. Au Decorated Hollow ZnO@ ZnS Heterostructure for Enhanced Photocatalytic Hydrogen Evolution: The Insight into the Roles of Hollow Channel and Au Nanoparticles. *Applied Catalysis B: Environmental* **2019**, *244*, 748–757.

(134) Sajimol Augustine, M.; Anas, A.; Das, A. V.; Sreekanth, S.; Jayalekshmi, S. Cytotoxicity and Cellular Uptake of ZnS:Mn Nanocrystals Biofunctionalized with Chitosan and Aminoacids. *Spectrochimica Acta Part A: Molecular and Biomolecular Spectroscopy* **2015**, *136*, 327–333. https://doi.org/10.1016/j.saa.2014.08.147.

(135) Touaylia, S.; Labiadh, H. Effect of the Exposure to Mn-Doped ZnS Nanoparticles on Biomarkers in the Freshwater Western Mosquitofish Gambusia Affinis. *International Journal of Environmental Health Research* **2019**, *29* (1), 60–70. https://doi.org/10.1080/09603123.2018.1508648.

(136) Mohammad, F.; Al-Lohedan, H. A. Toxicity Assessment of Engineered Mn–ZnS Quantum Dots in Vitro. *J Mater Sci* **2016**, *51* (20), 9207–9216. https://doi.org/10.1007/s10853-016-0149-4.

Chapter II. Fate of ZnS:Mn quantum dots in Seine River water and seawater. Ecotoxicological effects of different molar concentration of Mn doped ZnS Quantum dots on Chlorella Vulgaris microalgae

To be adapted as a paper for submission

1. Introduction

Great interest has been paid on the semiconductor nanomaterials (NPs) due to their quantum confinement effect, and their electronic and optical properties can be tailored by changing the nanoparticle size.[1,2] As an important II-VI semiconductor, ZnS nanomaterials exhibits a wide direct optical band gap (3.6 eV), making it to be a very attractive materials on the optical fields,[3,4] such as displays, optical-based sensor and lasers. Their optical properties can be tuned by doping them with impurities, which can induce new emitting centers in their quantum confined crystalline structure,[4,5] The Mn^{2+} doped ZnS NPs, one kind of the most popular used dopant in ZnS, which can emit an orange luminescence at the visible light range. According to the previous research, the ZnS NPs has a weak toxicity,[6,7] while the toxicity of the Mn-doped ZnS NPs is still not clear, based on this, we designed this work to research the toxic effect of the different concentration Mn doped ZnS NPs on microalgae in different water systems.

In our work, we synthesized the different molar concentration Mn doped ZnS NPs by polyol method, which is a unique soft chemical method to prepare large amounts of nanomaticales.[8] The produced ZnS: Mn NPs has a cubic structure, and the size of the NPs is very small, around 1-2 nm. After contacting them with the chlorella vulgaris culture in BG11, Seine River water and synthetic seawater mediums, we studied the toxic effect of the ZnS: Mn NPs on the photosynthetic activity, mitochondria activity, superoxide dismutase (SOD) activity and the viability of chlorella vulgaris.

2. Experimental

2.1. Synthesis of different molar concentration Mn doped ZnS quantum dots by the polyol method

All chemicals are of analytical grade and were used without any further purification. Manganese acetate tetrahydrate (≥ 99%, $Mn(CH_3COO)_2.4H_2O$), trioctylphosphine oxide (TOPO, $(CH_3(CH_2)_7)_3PO$), diethylene glycol (DEG) ($OH(CH_2)_2O(CH_2)_2OH$), tetraethyl orthosilicate (TEOS, 98%), IGEPAL® CO-520 ($(C_2H_4O)_n \cdot C_{15}H_{24}O$, n~5), n-

heptane (C_7H_{16}, 99%), ammonia solution (25%), 3-Mercapto-1-propanol (C_3H_8OS, 95%) purchased from Sigma-Aldrich, thiourea (99%, $SC(NH_2)_2$) purchased from Alfa Aesar, and zinc acetate dihydrate (98+%, $Zn(CH_3COO)_2.2H_2O$) purchased from Acros Organics.

Zinc acetate dihydrate ($Zn(CH_3COO)_2.2H_2O$, 87.8 mg) and manganese acetate tetrahydrate ($Mn(CH_3COO)_2.4H_2O$, 1.0 mg, 4.1 mg, 8.5 mg and 24.5 mg) were mixed in a three neck flask with 80 mL of diethylene glycol (DEG) to synthesis ZnS:Mn (0.5%), ZnS:Mn (2.0%), ZnS:Mn (4.0%), ZnS:Mn (10%), respectively, in presence of thiourea (38.8 mg) and TOPO (193.3 mg). All the reagents were dissolved in DEG during 20 min of sonication, then the solutions were heated to 180 ℃ for 30 min; after that, ZnS:Mn (0.5%), ZnS:Mn (2.0%), ZnS:Mn (4.0%), ZnS:Mn (10%) NPs were recovered after 3 cycles of centrifugation (at 22 000 rpm) and washing with ethanol, then dried at 60 °C overnight.

2.2. Chlorella vulgaris culture

Chlorella vulgaris came from Museum National d'Histoire Naturelle (MNHN) Culture Collection. Chlorella vulgaris is a planktonic eukaryotic single-cell green algae, which was cultivated in the 75 cm^2 cell culture flask bought from Thermofisher in (i) sterile BG11 medium (Annex 1.1) (pH 7.30), (ii) Seine River water (SRW, pH 8.11) (Annex 1.2) and (iii) synthetic seawater (SSW, pH 7.81) (Annex 1.3). Took 15 mL of Chlorella vulgaris collection culture and mixed with 45 mL of different media, then all the cultures were kept at a controlled temperature of 25 ℃ and a daily cycle of 16 h of luminosity (50-80 µmol m^2 s^1 photosynthetic photon flux, PPF) under ambient CO_2 environment.[9]

3. Results and discussion

3.1. Characterization of Mn-doped ZnS nanoparticles (ZnS: Mn)

The X-ray diffraction patterns of these NPs are presented in Fig. 12. The diffraction peaks of these samples are matching well with the (111), (220), (311) crystalline planes of cubic ZnS phase (COD no. 5000088). No other impurity phases were found in the XRD patterns, which indicates the high purity of the ZnS:Mn NPs. The broadness of the peaks revealed the nanocrystalline size of the samples.[10] The crystal size of each sample has been calculated through computational Rietveld refinements using MAUD software (Materials Analysis Using Diffraction), which was ranging from 1.1 to 1.5 nm. The average crystalline size of these ZnS NPs was also estimated using the diffraction peaks full width at half maximum (FWHM) by Debye-Scherrer's formula[10,11]:

$$D = \frac{k\lambda}{\beta cos\theta},$$

where D is the average size of the particles, k is the particles shape factor (0.89), λ is the X-ray wavelength (0.179 nm), β is the FWHM of the diffraction peak, θ is the diffraction Bragg angle. The calculation of average crystalline sizes of ZnS:Mn (0.5%, 2.0%, 4.0% and 10%) NPs ranged from 2.3 nm to 2.5 nm**,** which agrees with the average diameter deduced from TEM analysis (2.3 ± 0.5 nm) (Fig. 15).

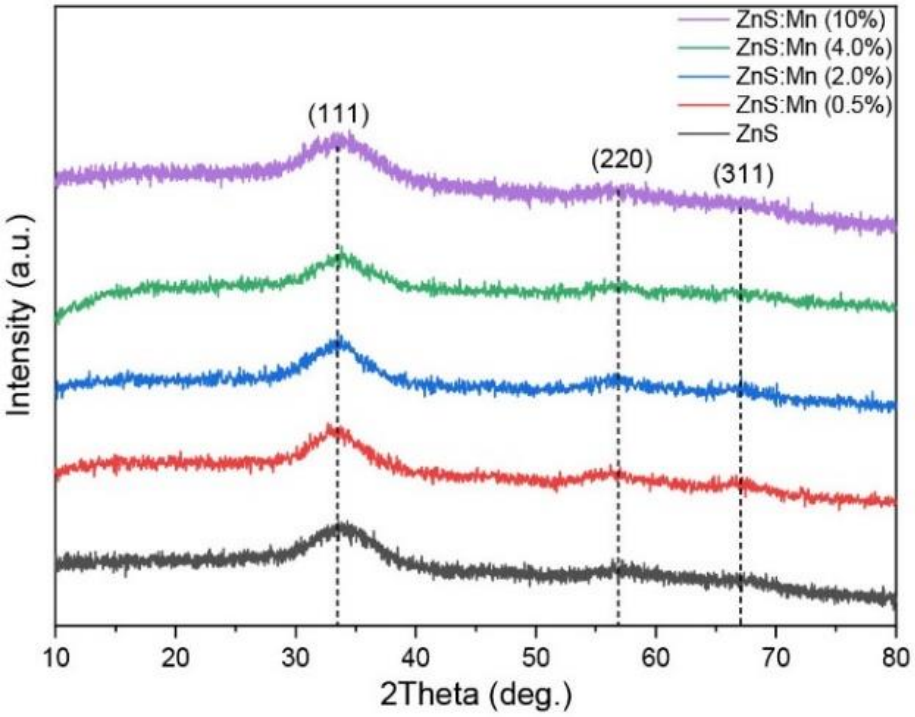

Fig. 12 *XRD patterns of all the produced ZnS:Mn NPs.*

Table 1 *XRF of all the produced ZnS:Mn NPs.*

NPs		**Zn**	**S**	**Mn**
ZnS:Mn (0.5%)	mass	32.315	11.034	0.048
	%mol	58.900	41.000	0.100
ZnS:Mn (2.0%)	mass	46.842	14.838	0.668
	%mol	60.100	38.800	1.100
ZnS:Mn (4.0%)	mass	22.464	8.427	0.427
	%mol	55.900	42.800	1.300
ZnS:Mn (10.0%)	mass	8.336	3.500	1.420
	%mol	48.600	41.600	9.800

X-ray fluorescence (XRF) was performed for confirming the composition of the NPs (Table 1): the Mn content in the NPs increased while increasing the Mn molar concentration, although it does not match well with the Mn molar concentration increased.

The surface chemical composition of these NPs was investigated by XPS analysis.[12] The survey spectra of ZnS: Mn (0.5%, 2.0%, 4.0% and 10%) NPs are presented in Fig. 13. The Zn $2p_{3/2}$ peak at 1022.0 eV confirmed the expected presence of Zn^{2+} cations, whereas the S 2p peak at 161.4 eV is characteristic of S^{2-} species.[13,14] The XPS semi-quantitative data gave atomic Zn/S ratio of 1:0.9; 1:1; 1:1 and 1:0.9, for the samples 0.5%, 2.0%, 4.0% and 10% respectively, that lies reasonably close to the ideal 1:1 ratio for every sample. Peaks corresponding to C and O adventitious contaminations were also observed in all spectra. The slight error on the Zn/S ratio (equal to 0.9) may raise suspicion of oxidation of the nanoparticles. However, the O 1s peak observed at 532.0 eV cannot be attributed to O atoms belonging to a ZnO crystalline system, since the signal originated from ZnO would appear at 530 eV. Moreover, no peak corresponding to higher oxidation states was detected in the S 2p core level region (e.g., sulfates that would be found at 169.2 eV). Hence, the O 1s peak at 532 eV may be assigned to chemisorbed oxygen species.[13]

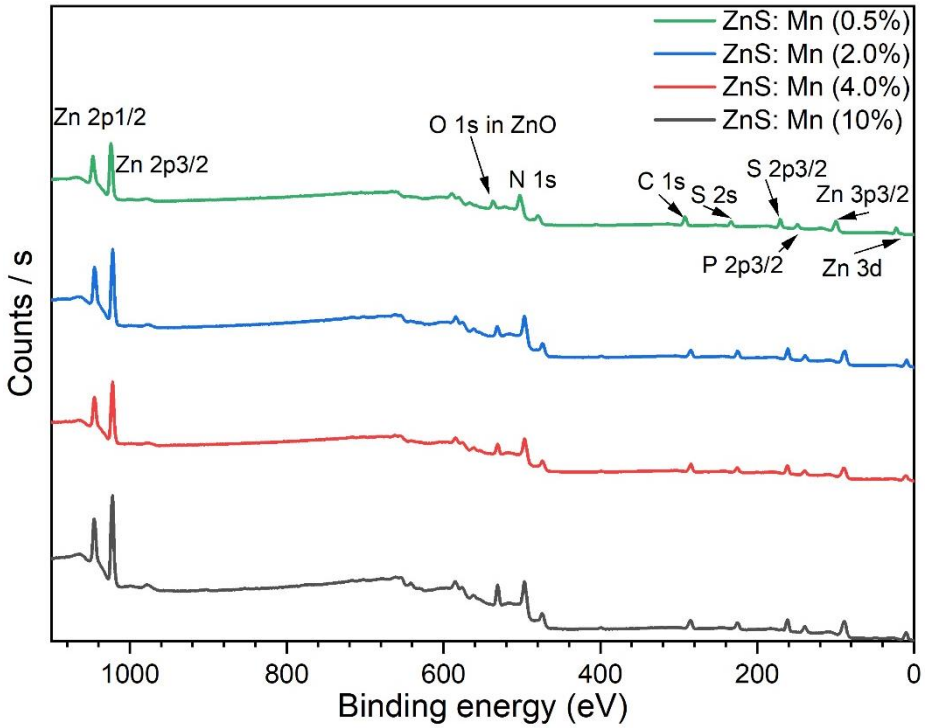

Fig. 13 *XPS survey spectra of ZnS: Mn (0.5%, 2.0%, 4.0% and 10%) NPs, the spectra were calibrated by setting the main C 1s at 285 eV.*

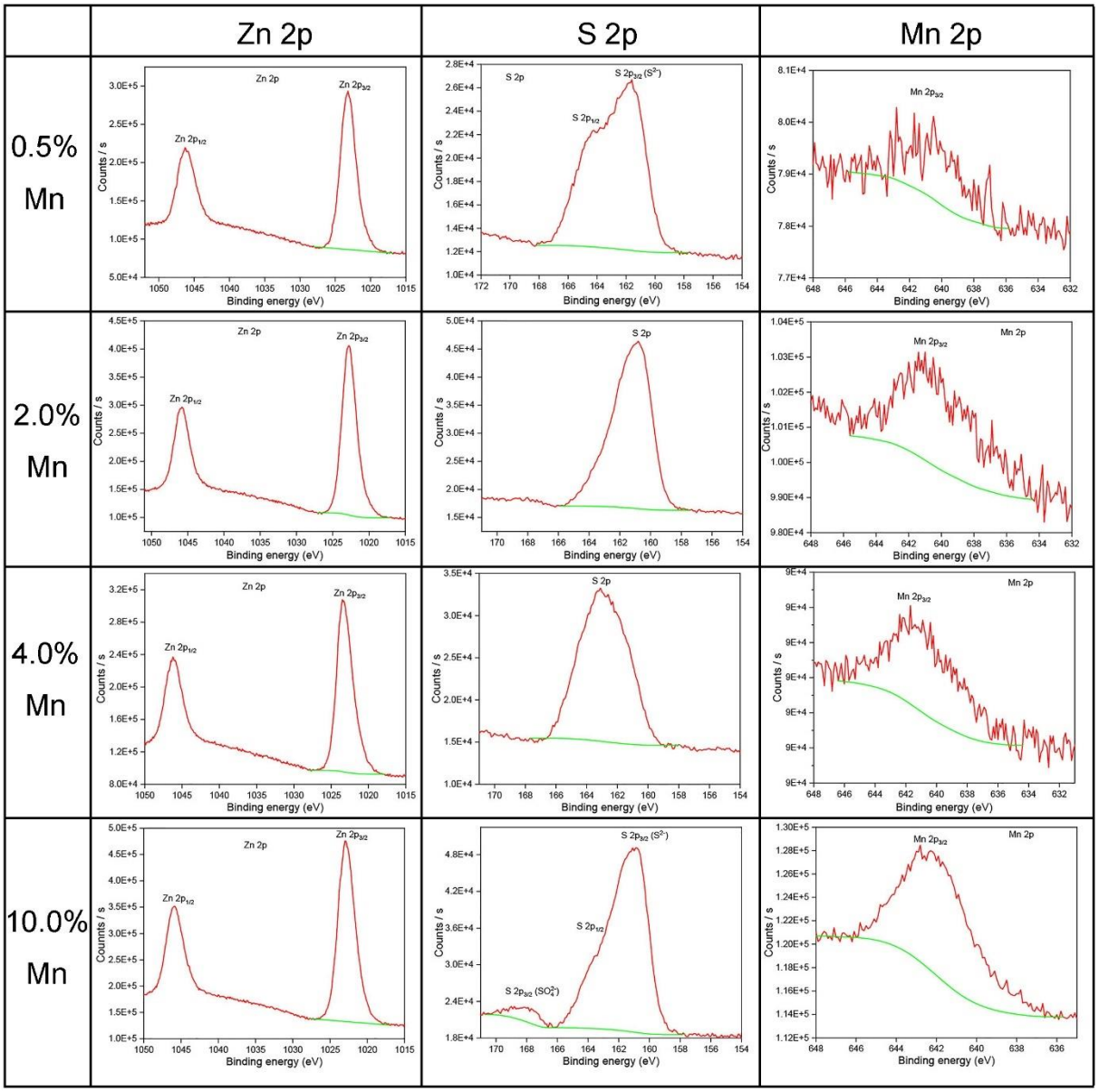

Fig. 14 *High resolution spectra of Zn 2p, S 2p, Mn 2p signals recorded on ZnS:Mn NPs with 0.5%, 2.0%, 4.0%,10% of Mn.*

The high-resolution spectra of Zn 2p, S 2p, Mn 2p elements are shown in Fig. 14. The binding energy of Zn $2p_{1/2}$ and Zn $2p_{3/2}$ are centered at 1045.8 eV and 1022.9 eV, respectively, which confirm that Zn atom exists only in the form of Zn^{2+}. Furthermore, the intensity ratio of the spin–orbit splitting peaks for S $2p_{3/2}$ and S $2p_{1/2}$ was approximately 2:1, in good agreement with the presence of Zn^{2+} linked only to S atoms.[15] The S 2p asymmetric spectra may be fitted with two peaks for ZnS:Mn (0.5%) and ZnS:Mn (10%) NPs, corresponding to S $2p_{3/2}$ and S $2p_{1/2}$ at the binding energy of 160.8 eV and 163.2 eV, respectively. The binding energy of 160.8 eV originated from S^{2-} in the ZnS structure while the subpeak at approximately 163.2 eV may be due to surface defects of the S–S species in the ZnS shell layer as it was previously reported for ZnS nanorods.[16] One can notice, on these two spectra, a lower intensity S 2p peak

at 167.9 eV, attributed to the oxidized SO_4^{2-} form,[3,17] due to a very slight and negligible oxidization of the surface of ZnS:Mn NPs. Mn $2p_{3/2}$ spctra are also shown in Fig. 14. The spectra were less and less noisy as the Mn content increases [18–20] while the Mn $2p_{3/2}$ peak was centered at around 642 eV, corresponding to Mn^{2+}.[21] The asymmetric S 2p peak in Fig. 14 was deconvoluted into two subpeaks corresponding to S 2p3/2 and S 2p1/2 and were located at 161.1 and 162.2 eV, respectively. The binding energy of 161.1 eV originated from S 2p in the ZnS structure. The subpeak at approximately 162.2 eV might be due to surface defects of the S–S species in the ZnS shell layer and was previously reported in chemically derived ZnS nanorods. The XPS semi-quantitative data gave atomic Mn/S ratio of 0.02:1; 0.03:1; 0.04; 0.08, for the samples 0.5%, 2.0%, 4.0% and 10% respectively, that lies reasonably close to the ideal ratio for every sample.

Transmission electron microscopy (TEM) images of different molar concentration of Mn doped ZnS NPs are shown in Fig. 15. The TEM pictures gave lattice information and confirmed the blende structure of the crystallized ZnS:Mn (0.5%, 2.0%, 4.0%, and 10%). The statistical analysis of the size distribution of these NPs indicated the average size are around 2.3 ± 0.5 nm. In addition, the EDX showed that all these NPs mainly contain Mn, Zn and S elements, Cu being a constitutive element of the grid and Cr coming from the TEM machine; hence, we can assume that no impurity was found in these ZnS:Mn NPs.

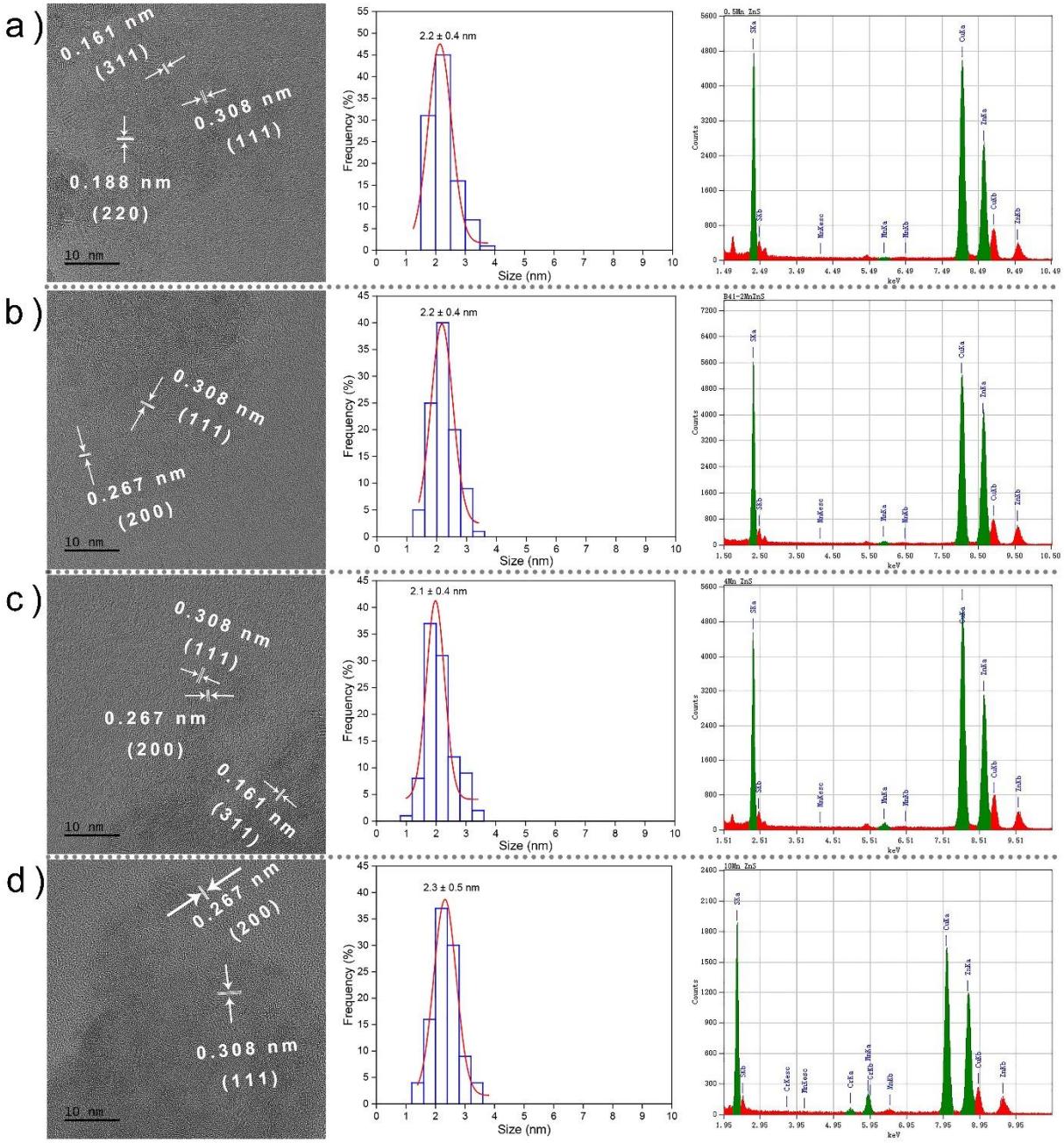

Fig. 15 *TEM image, size distribution and EDS of ZnS: Mn (0.5%) (a), ZnS: Mn (2.0%) (b), ZnS: Mn (4.0%) (c), ZnS: Mn (10%) (d).*

The size and colloidal stability of the NPs were determined by dynamic light scattering (DLS), in 3 different types of water, at various pH (Fig. 16). Whatever the medium and the pH, the nanoparticles were aggregated, but to a different degree. In a BG11 water (or fresh water), at pH = 2, all the NPs formed what will be called small aggregates since the size of the colloids was around 340 nm for ZnS:Mn (0.5%) and ZnS:Mn (4.0%) NPs, and 460 nm and 400 nm for ZnS:Mn (2.0 %) and ZnS:Mn (10 %) respectively. However, in a more basic medium (pH = 8), the size of almost all the colloids was greater than 1000 nm, only that of ZnS:Mn (4.0%) remained less than 340

nm. In the Seine River water, all the colloids were more stable, with sizes between 340 nm and 530 nm at different pH, except the ZnS: Mn (4.0%) NPs which formed aggregates of 220 nm at pH 4 and larger than 2000 nm at pH 10. Moreover, the size of these colloids was smaller in seawater, in an acid medium (less than 400 nm at pH 6), and it could exceed 1000 nm at pH 10. Above all, we could conclude that the size of these NP aggregates was more stable in BG11 and in seawater in an acidic environment. Colloids were stable (300 to 500 nm) in Seine River water, whether the medium is acidic or alkaline, except for ZnS:Mn (4.0%) NPs, which were unfortunately easier to aggregate when the pH varied from 6 to 8. Indeed, one should know that the pH of culture of Chlorella vulgaris in the different water systems varies from 7.4 to 8.7.

Figure 17 presents the zeta potential measurements performed on all the NPs produced, in the three different water systems at different pH. We observed that the NPs were relatively stable in an alkaline medium either in BG11 and Seine River water, whereas they were unstable in synthetic seawater, whatever the pH, not only alkaline but also acid. We also observed that these NPs were negatively charged when the pH varied from 6 to 8, which means that the NPs are not easy to internalize by the algae cell (the zeta potential of the algae cell is about -8.82 eV) due to repulsive electrostatic interactions with the cell membrane. [22,23]

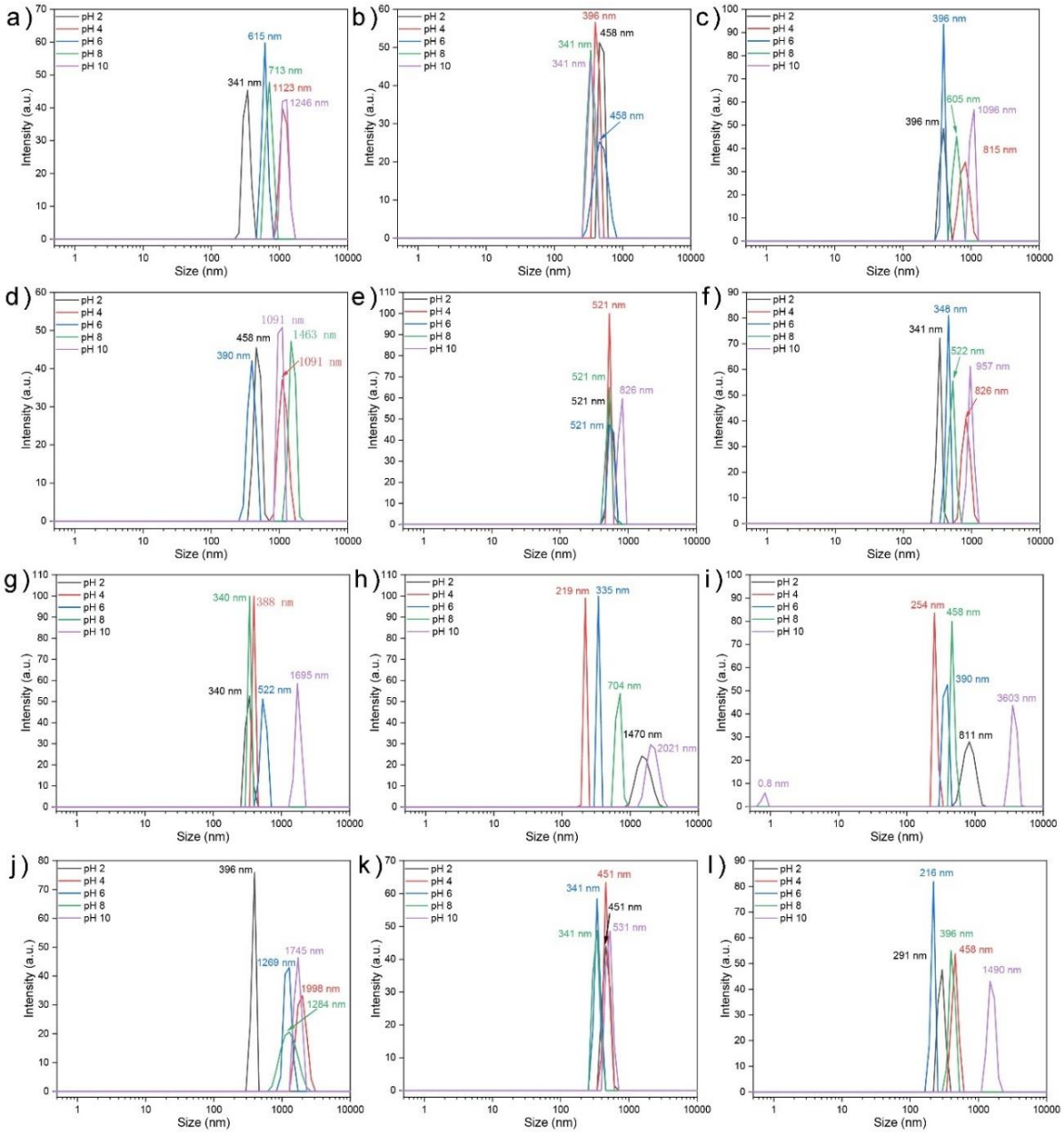

Fig. 16 *Size of ZnS: Mn NPs in (a, d, g, j) BG11, (b, e, h, k) Seine River water, (c, f, i, l) Synthetic seawater. ZnS: Mn (0.5%) (a-c), ZnS: Mn (2.0%) (d-f), ZnS: Mn (4.0%) (g-i), ZnS: Mn (10%) (j-l).*

Although nanoparticles tend to aggregate in water, whatever the pH, they can be dissolved. Therefore, we followed the dissolution of ZnS:Mn (10%) by ICP-AES. Figure 18 presents the concentration of Mn^{2+} and Zn^{2+} in the 3 different water systems after dissolving the ZnS:Mn (10%) NPs. The dissolution of Mn^{2+} was generally higher in synthetic seawater and in Seine River water than in Milli-Q water. Moreover, in Milli-Q water, the dissolution of Mn^{2+} was maximum on the 2nd day, whereas it reached a maximum on the 4th or 5th day in seawater and in Seine River water. Surprisingly, the dissolution of Zn^{2+} was totally different: in seawater, the concentration of dissolved Zn^{2+}

remained stable for a week, which is probably due to a saturation of seawater with Zn^{2+} ions; however, in the Seine River water and Milli-Q water, the dissolution of Zn^{2+} continued and increased over time.

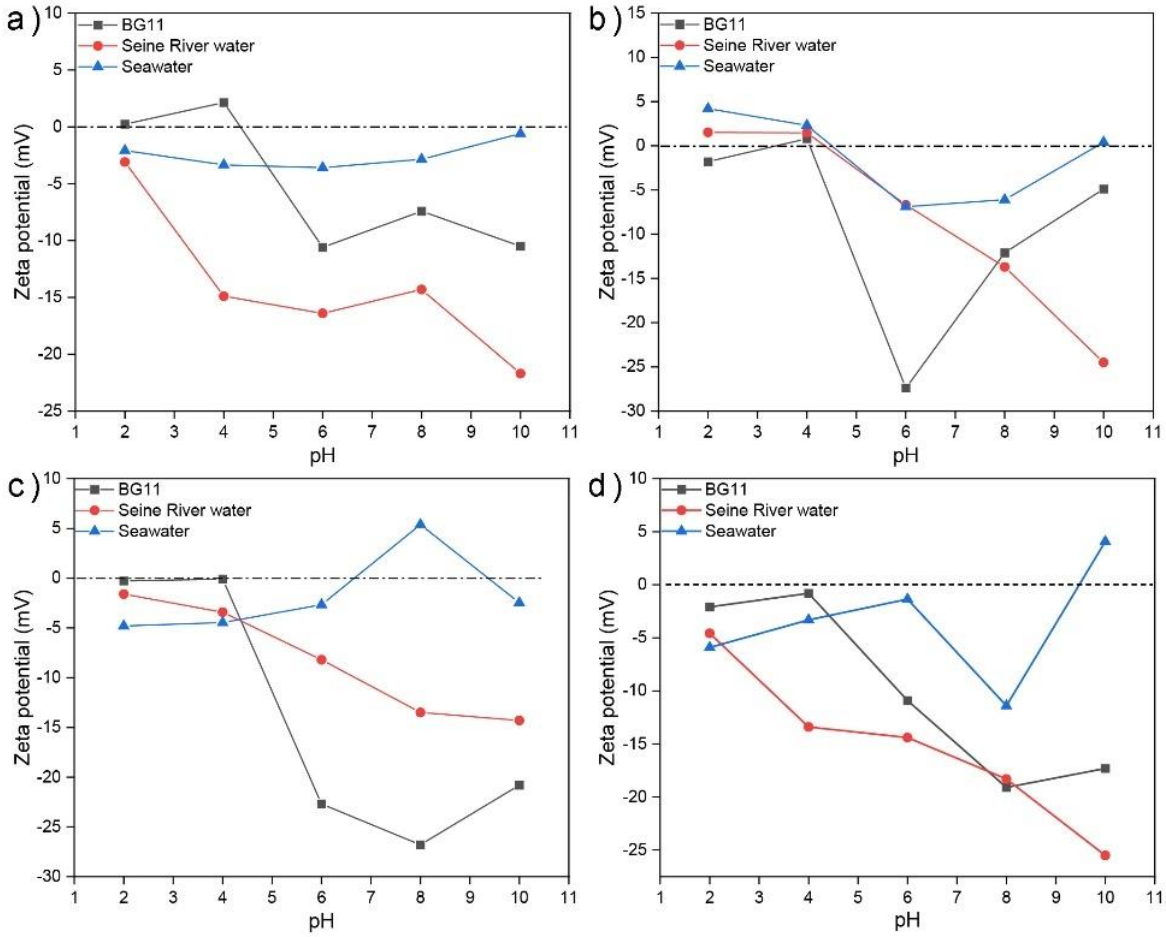

Fig. 17 *Zeta potential of ZnS:Mn NPs in different water systems, ZnS Mn (0.5%) (a), ZnS:Mn (2.0%) (b), ZnS:Mn (4.0%) (c), ZnS:Mn (10%) (d).*

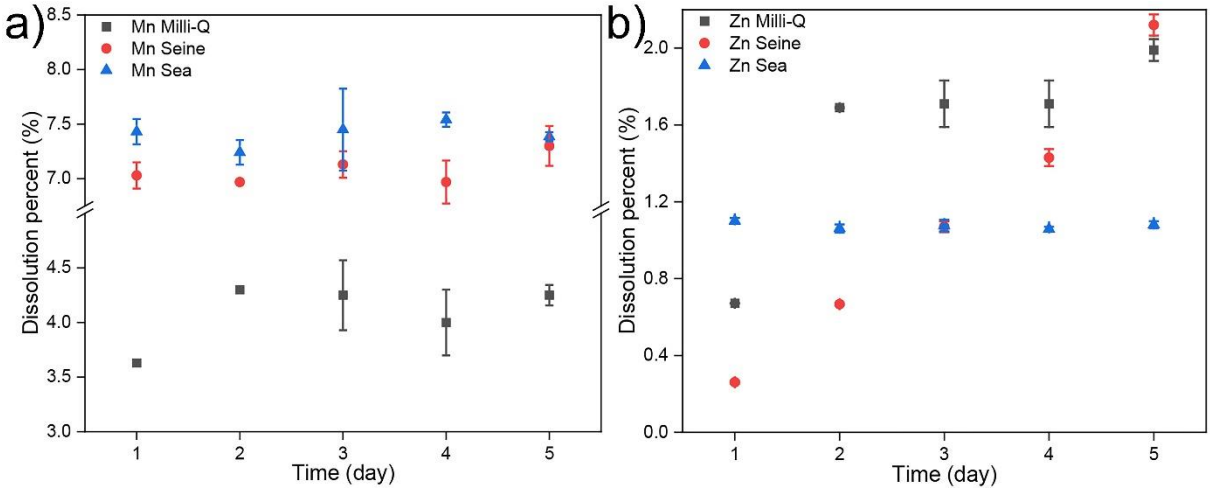

Fig. 18 *Dissolution of ZnS:Mn (10%) NPs in different water systems: monitoring of a) Mn^{2+} and b) Zn^{2+} concentrations in different water systems.*

3.2. Toxicity analysis

In order to investigate whether the toxicity came from Mn^{2+} ions or from the NPs themselves, $Mn(CH_3COO)_2.4H_2O$ salt, pure ZnS NPs and ZnS:Mn NPs were added into the culture medium of Chlorella vulgaris. Chlorella vulgaris was cultured in three different aquatic media: BG11, Seine River water (SRW), and synthetic seawater (SSW). One week later, the different concentrations of NPs (20 mg/L, 50 mg/L, and 100 mg/L) were added into the three types of aqueous medium; each medium had 4 culture flasks (three research groups and a control group), and relative toxicity measurements such as photosynthetic activity, cell viability, superoxide dismutase (SOD) activity and mitochondria activity were performed over the next 5 continuous days after exploring in the NPs environment. Then we could evaluate the toxic effect of NPs by comparing with the control group.

3.2.1. Toxicity of pure ZnS nanoparticles

Pulse amplitude fluorometry (PAM) can be used to monitor photosynthesis in algae, through the measurement of chlorophyll fluorescence. F_v/F_m is a normalized ratio obtained by dividing variable fluorescence by maximum fluorescence. It represents the maximum potential quantum efficiency of Photosystem II if all capable reaction centers were open.

The results of PAM and viability tests obtained on the pure ZnS NPs are presented in Fig. 19. These two tests were carried out after the addition of the ZnS NPs after 3 hours of culture. Fig. 19 a-c) shows that the photosynthetic activity (F_v/F_m) of Chlorella vulgaris in BG11 and synthetic seawater (SSW) media decreased from the first to the last day of testing; in Seine River water (SRW), photosynthetic activity decreased during the first 24 hours only compared to the control group. A high concentration of NPs (100 mg/L) had a more negative influence on the photosynthetic activity of Chlorella vulgaris in BG11 and SSW media than lower concentrations (20 mg/L and 50 mg/L). On the other hand, in SRW medium, low concentrations of NPs already had a very clear negative influence on the photosynthetic activity of algae. Reduced photosynthetic activity may be caused by increased reactive oxygen species (ROS) [24,25] or shading impact induced by aggregation of NPs around the cells.[24]

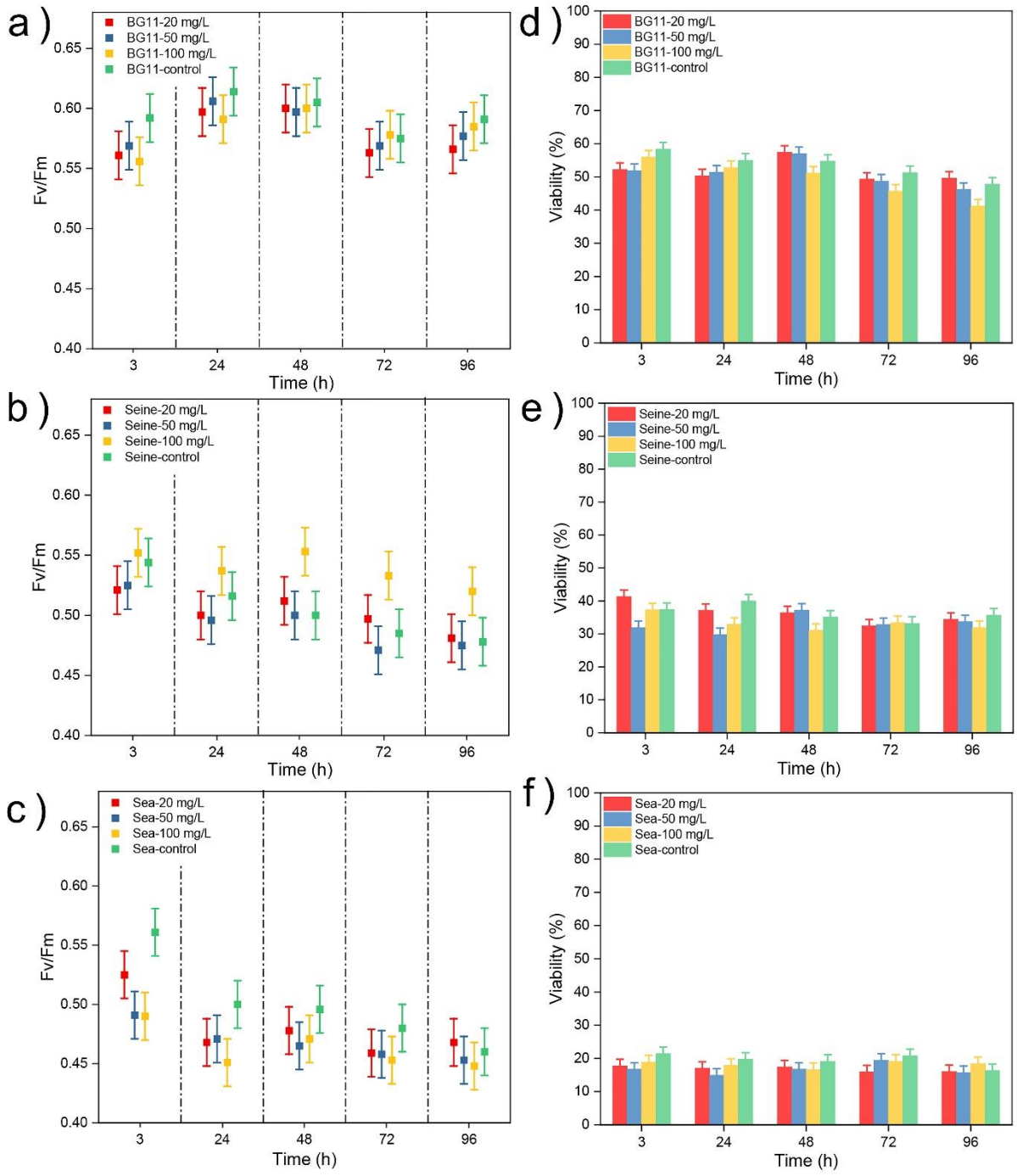

Fig. 19 *PAM (a-c) and viability (d-f) test of chlorella vulgaris in different culture medium with pure ZnS NPs.*

Figure 19 d-f) presents the viability of Chlorella vulgaris in different aqueous media, in contact with ZnS NPs. The viability test represents the percentage of surviving cells among all the Chlorella vulgaris cells, under the bright field imaging model the software can identify and count the live/dead cells quickly and accurately. In BG11 and SSW media, viability decreased immediately, from the first day of testing until the last day compared to the control group. Viability recovers 48 h later in the presence of lower concentrations of NPs (20 mg/L and 50 mg/L). In Seine River water, the viability decreased throughout the first days of the test in the presence of high concentrations

of NPs (50 mg/L and 100 mg/L) except on the 4th day of the test. Algae showed much lower viability (less than 40%) in SRW and SSW media; it could be assumed either that the culture media influenced the expression of cell membrane proteins [24,26] or that the ZnS NPs were very strongly aggregated on the surface of the algae, and thus disturbed the transport function of the cellular membrane. This led to a decrease in the availability of nutrients necessary for algae growth.[24] Therefore, we could conclude that ZnS NPs had a relatively weak toxic effect on Chlorella vulgaris, in agreement with previous work.[6,7] Not surprisingly, high concentrations of NPs were more toxic than lower concentrations.

3.2.2. Toxicity of Mn^{2+}

The toxicity of Mn^{2+} ions was also addresses, by introducing solutions of Mn^{2+} at the same concentrations as during the study of pure ZnS NPs. Figure 20 shows Chlorella vulgaris in the presence of Mn^{2+} ions 96 hours after their introduction. We observed that the color of the cultures carried out in Seine River Water and synthetic seawater and containing Mn^{2+} ions was deeper than that of the control groups. The Seine River water was even darker... This means that the Chlorella vulgaris algae were dying in these two aqueous environments, in presence of Mn^{2+}.

Fig. 20 *Chlorella vulgaris in the different culture media.*

Fluorescence fluorimetry (PAM) and viability results are shown in Fig. 21. Fig. 21 a-c) depict the PAM results: after the introduction of Mn^{2+} ions in each of the three aqueous media, the photosynthetic activity (F_v/F_m) increased in BG11 and in Seine River water, compared to the control group while it decreased in the seawater. This agrees with measurements of the viability of the algae Chlorella vulgaris. The increased photosynthetic activity of Chlorella vulgaris in BG11 and SRW media could be explained by the adaptation of algae, which allowed them to harvest and store manganese there when it was available.[27]

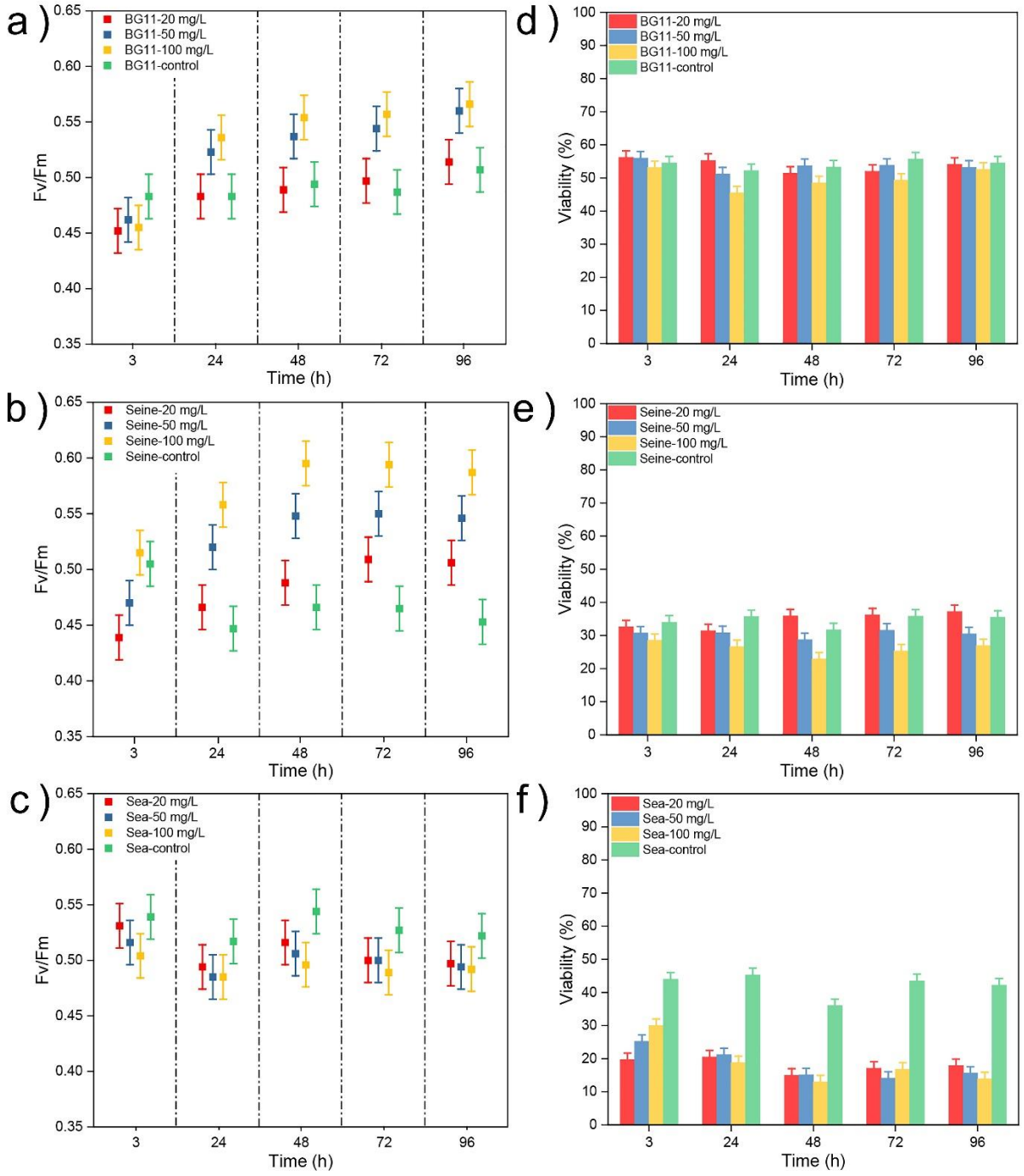

Fig. 21 *PAM (a-c) and viability (d-f) tests of Chlorella vulgaris in different culture media in presence of* Mn^{2+} *ions.*

Fig. 21 d-f) shows the viability of Chlorella vulgaris: in BG11 water, the viability remained almost stable in the presence of NPs concentrations below 100 mg/L; when the concentration of NPs was 100 mg/L, the viability decreased drastically during the first four days of the test. In Seine and sea waters, viability decreased in a variable way: it is probably caused by a paucity of nutrients, such as nitrates, phosphates or carbon sources (for example glucose), absent in Seine and sea waters.[24,28] Consequently, the physiological state of the algae became very bad due to the lack of nutrients.[24] Then, they showed less resistance to the bad water environment or even

toxic Mn^{2+} ions. In BG11, the algae had all the adequate nutrients, which led to a completely different behavior. Consequently, a high concentration of Mn^{2+} ions (for example, 100 mg/L) was highly toxic for Chlorella vulgaris in all culture media, but even more particularly in SSW medium.

3.2.3. Toxicity of ZnS: Mn (0.5%)

Then, we studied the toxicity of ZnS:Mn NPs (0.5%) against Chlorella vulgaris. For this, we introduced different concentrations of NPs (20 mg/L, 50 mg/L and 100 mg/L) into the three aqueous media and kept a control group.

Photosynthetic activity and viability of Chlorella vulgaris are shown in Fig. 22. The photosynthetic activity of the algae in the BG11 medium decreased from the very beginning of the 1st day of the test, but then, the algae seemed to recover from the toxic effect until the last test day (after 96 h, i.e. 4 days). Again, we observed that high NPs concentrations (100 mg/L) exhibited higher toxicity than lower NPs concentrations (20 mg/L). In SRW, photosynthetic activity decreased during the first three days of the test, in the presence of NPs in concentrations equal to 20 mg/L and 50 mg/L, while it decreased only slightly in the presence of NPs of concentration equal to 100 mg/L; this may be due to a stronger aggregation of the nanoparticles when the concentration increased. In SSW, the photosynthetic activity significantly decreased during the first three days of test in a medium exposed to a concentration of NPs of 100 mg/L.

Fig. 22 d-f) showed the viability of Chlorella vulgaris in the presence of NPs was clearly reduced in BG11 and SSW aqueous media throughout the test period, while it decreased during the first 48 h of testing in SRW. Finally, we could see that the toxic effect was much stronger for high concentrations of NPs (e.g., 100 mg/L).

Finally, we evaluated the amounts of adenosine-5'-triphosphate (ATP) and the activity of superoxide dismutase (SOD) of the algae Chlorella vulgaris in the different media in the presence of different concentrations of NPs. The intracellular ATP content reflects the level of activity of algae mitochondria: the mitochondria is an important organelle, which is responsible for the production of ATP, the production of ROS but also the release of proteins controlling apoptosis. Therefore, mitochondria are directly linked to cell death.[24,29,30] In addition, SOD activity reflects the level of production of reactive oxygen species (ROS) which can lead to the decrease in photosynthetic activity and activity of mitochondria, but also induce the disturbance of metabolism and hence, lead to cell death. SOD, one of the most important antioxidant enzymes in all cells, can catalyze the disproportionation of superoxide anions (O^{2-}) into oxygen and/or

hydrogen peroxide, and then maintain antioxidant balance in cells. Therefore, SOD can protect cells from ROS toxicity.[29,31]

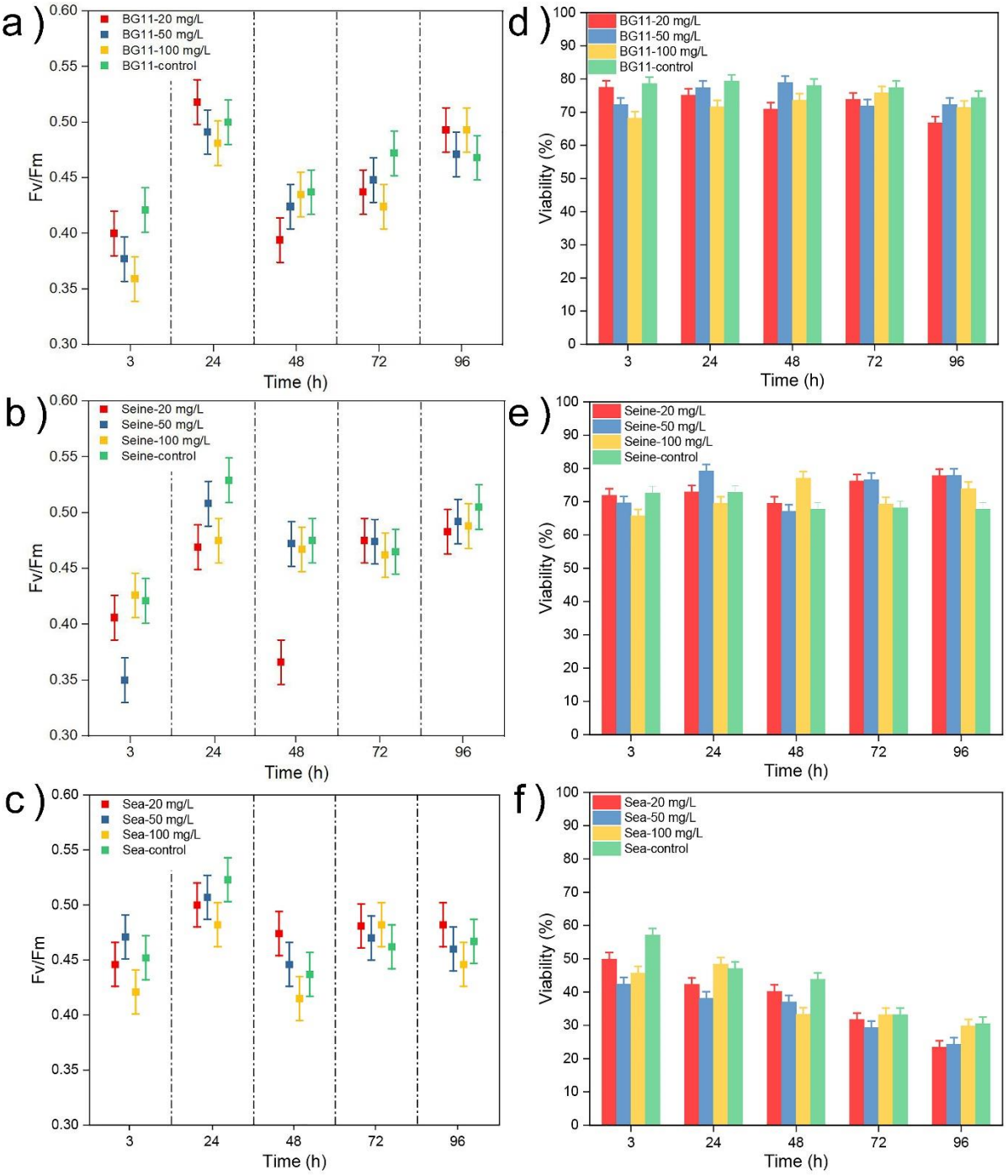

Fig. 22 *PAM (a-c) and viability (d-f) tests of chlorella vulgaris in different culture media in presence of ZnS:Mn (0.5%) NPs.*

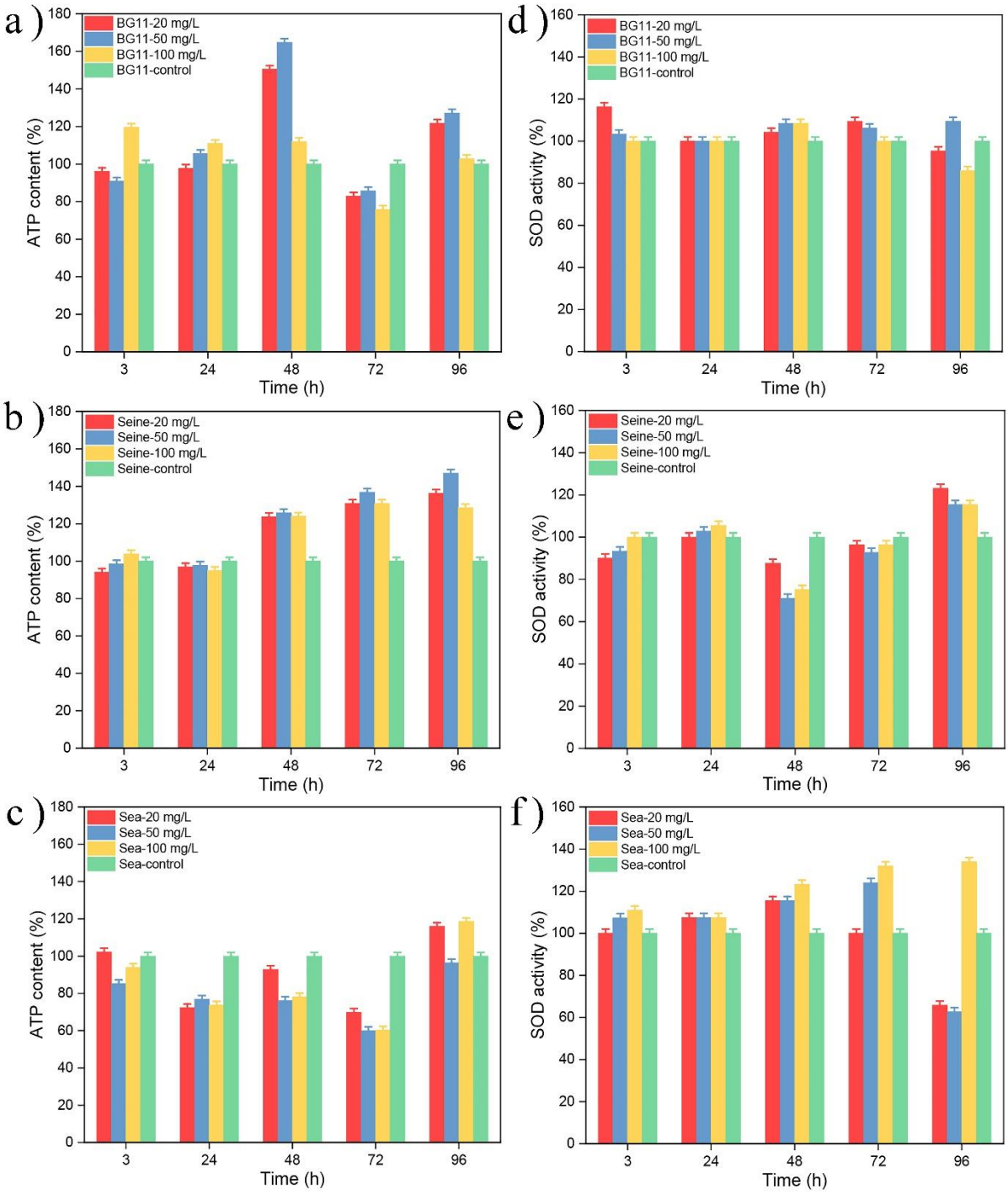

Fig. 23 *ATP (a-c) and SOD (d-f) tests of Chlorella vulgaris in different culture media in presence of ZnS:Mn (0.5%) NPs.*

Fig. 23 shows the intracellular ATP level and SOD activity of Chlorella exposed to ZnS:Mn (0.5%) NPs. In Fig. 23 a-c) we observed that the ATP content decreased on the 4th day of the test (i.e., after 72 h) in the BG11 medium, slightly decreased during the first two days of the test in the SRW medium, and significantly decreased in the SSW medium from the very first day to the fourth day of testing. This confirmed that the toxic effect of ZnS:Mn (0.5%) NPs could affect the activity of mitochondria. In Fig. 23 d-f), we observed that SOD activity increased to varying degrees over the test

period. For low concentrations of NPs, SOD activity increased little, even for a concentration of 100 mg/L, which was probably due to the aggregation of NPs.[24] ROS production increased only on the last day of testing in SRW medium, whereas it increased during the first days of testing in SSW medium. The SOD activity was higher in the groups exposed to concentrations of 100 mg/L of NP than in the other groups. Therefore, we clearly see that ZnS:Mn (0.5%) NPs could induce the toxic effect on chlorella vulgaris and cause cell death in all media. The NPs introduced in higher concentration were more toxic, in the BG11 and SSW media. NPs could induce ROS production in Chlorella vulgaris cells present in SSW as well as a toxic effect on cellular metabolic activity; it represents one of the main impacts of NP toxicity.

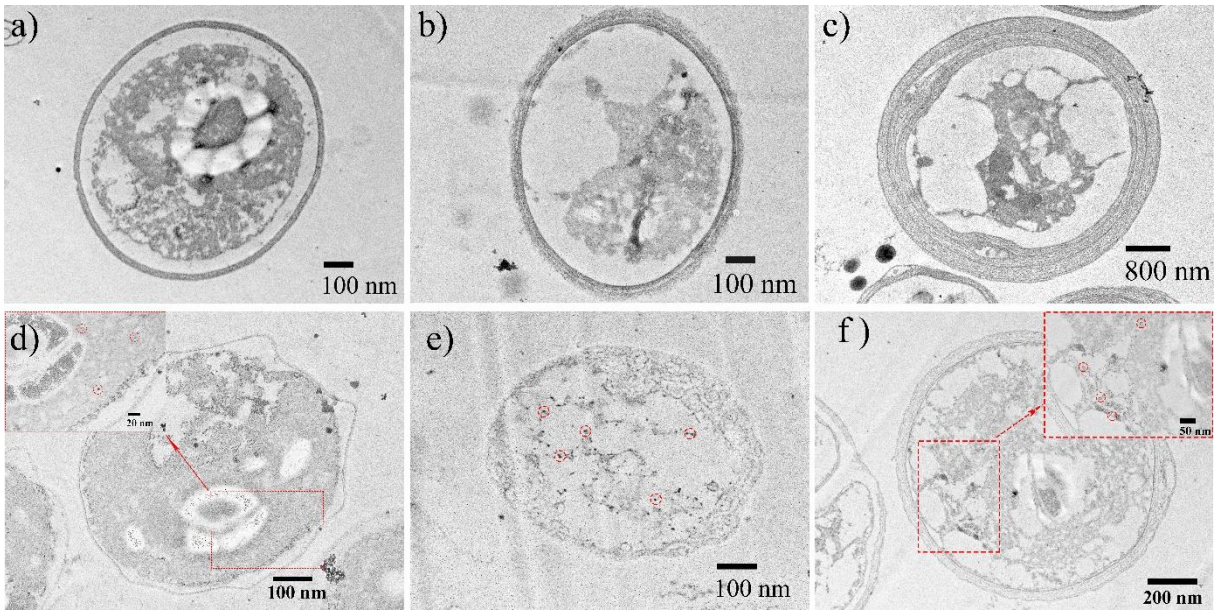

Fig. 24 *TEM images of Chlorella vulgaris thin sections in different media, (a, d) in BG11, (b, e) in SRW, (c, f) in SSW. (d, e, f) showed the Chlorella vulgaris thin sections contacted with 100 mg/L with ZnS:Mn (0.5%) NPs.*

Figure 24 shows thin sections of Chlorella vulgaris with and without ZnS:Mn (0.5%) NPs observed by TEM. In Figure 24 a), in BG11 without NPs, we observed that the cell wall and cytoplasm of Chlorella were intact, which means that the algae were alive and healthy. In SRW (Fig. 24 b) and SSW (Fig. 24 c), without NPs, the cell wall was intact, but the cytoplasm was shrinking, revealing algae cell malaise, which explained the lower viability of Chlorella in these aquatic environments. Fig. 24 d-f) shows thin sections of Chlorella algae in the same aquatic media after exposure to ZnS:Mn NPs (0.5%). Fig. 24 d) shows the thin section of an alga in BG11 after exposure to NPs: we observed that the cell wall was clearly deformed and thinner than the original wall of

Chlorella vulgaris.[32,33] Furthermore, part of the NPs appeared in the cytoplasm. In SRW (Fig. 24 e), aggregated NPs clearly appeared inside the algal cell, cytoplasm was broken down, cell membrane and cell wall composed by polysaccharides were also damaged.[34] Finally, in SSW (Fig. 24 f), NPs were also observed in algal cells; in contrast, the cell wall and cytoplasm were intact, and not yet damaged by NPs. We could therefore conclude that NPs can be first internalized by endocytosis,[34] and then the cell membrane, cell wall and cytoplasm could be damaged by the aggregated NPs in the cell. In some cases, the cell wall will break down and the intracellular contents will leak out,[33,34] which means the inevitable death of the algal cells.

3.2.4. Toxicity of ZnS:Mn (2.0%)

The toxicity of ZnS:Mn (2.0%) NPs was then also studied on Chlorella vulgaris, by introducing 1.2 mg (20 mg/L), 3.0 mg (50 mg/L) and 6.0 mg (100 mg/L) of NPs in culture flasks containing 60 ml of algae culture. Figure 25 presents the results of fluorimetry (PAM) as well as the viability of the algae in the presence of NPs.

In BG11, photosynthetic activity decreased compared to the control group throughout the test period (Fig. 25 a-c). Moreover, the photosynthetic activity of microalgae in contact with the concentration of 100 mg/L of NPs was much more influenced than the other research groups. In the SRW, the photosynthetic activity was only slightly reduced on the 4th day of the test, even in the presence of high levels of NPs. Finally, in the SSW, the photosynthetic activity decreased during the first two days of the test and was very strongly influenced by the high concentrations of NPs.

The viability of Chlorella vulgaris (Fig. 25 d-f) decreased significantly during the first two days of testing in BG11 medium treated with 100 mg/L of NPs. The toxic effect continued throughout the duration of the test since even the viability of the groups exposed to the lowest concentration decreased slightly 48 hours later. While the decrease in viability only appeared on the first day of the test in the SRW and SSW media containing high levels of NPs, the viability of Chlorella vulgaris in the medium containing 20 mg/L of NPs does not seem be affected.

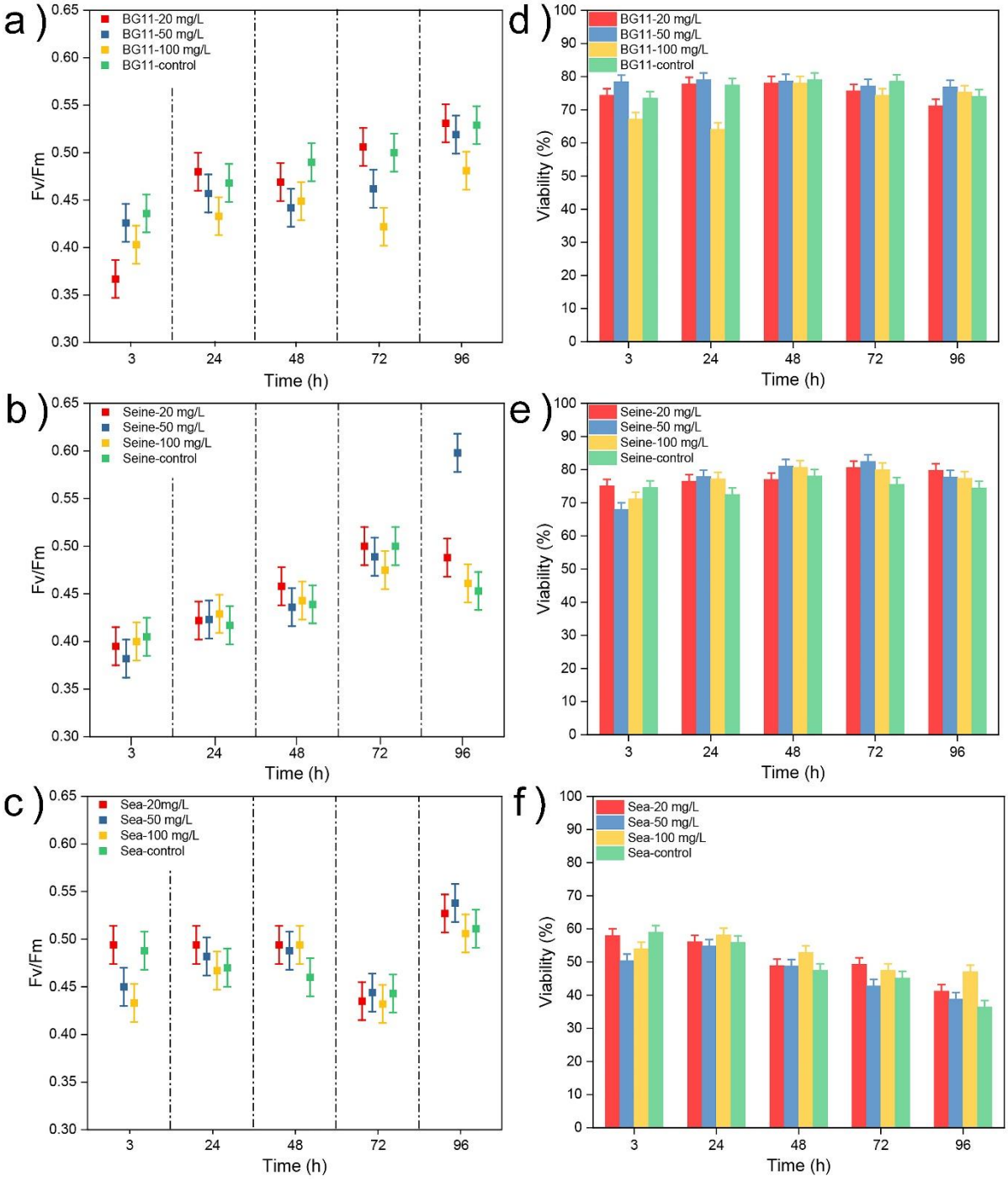

Fig. 25 *PAM (a-c) and viability (d-f) tests of Chlorella vulgaris in different culture media contacted with ZnS:Mn (2.0%) NPs.*

Fig. 26 shows the intracellular ATP content and SOD activity of Chlorella vulgaris in media exposed to ZnS:Mn (2.0%) NPs. In Fig. 26 a-c) we observed that the intracellular ATP content decreased in the BG11 medium from the first day of the test, but the toxic effect of the NPs on the mitochondria was much higher after 48 h. The activity of Chlorella vulgaris mitochondria in the SRW in the presence of 100 mg/L of NPs was more affected than in the other two research groups, while the microalgae exposed to

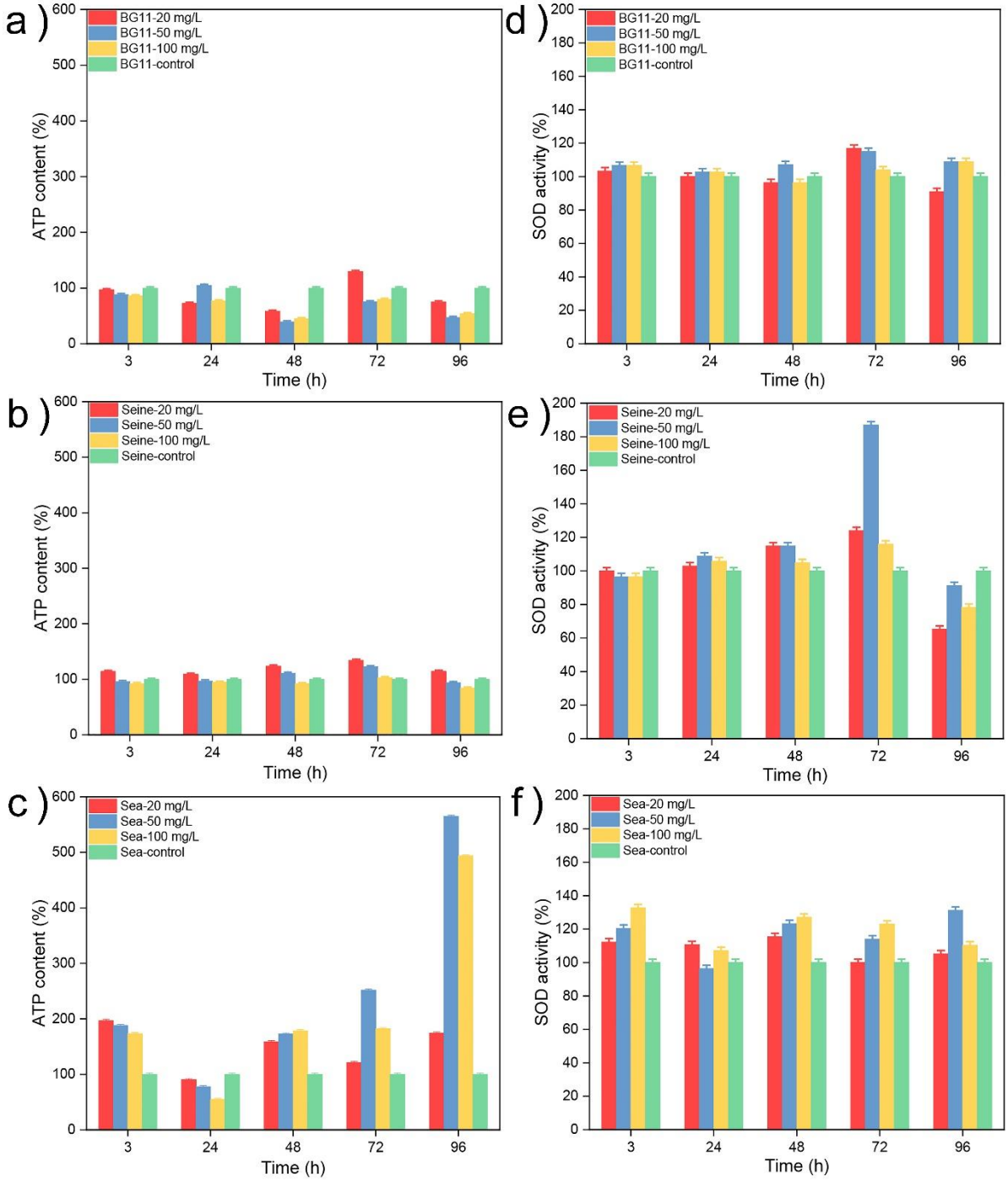

Fig. 26 *ATP (a-c) and SOD (d-f) tests of Chlorella vulgaris in different culture media exposed to ZnS:Mn (2.0%) NPs.*

20 mg/L of NPs did not seem affected. While the activity of Chlorella vulgaris mitochondria in SSW medium only varied after 24 hours of testing, and a concentration of NPs of 100 mg/L was much more toxic, the ATP content suddenly increased significantly in presence of high levels of NPs (50 mg/L and 100 mg/L) in SSW at 96h, of the test: this was probably due to the energy obtained by the microalgae from the NPs. Moreover, in BG11 and SRW, the SOD activity of Chlorella vulgaris (Fig. 26 d-f),

increased slightly during the first two days of testing, and more markedly 48 h later. In SSW, the SOD activity of chlorella vulgaris increased significantly throughout the test period and more particularly in the presence of 100 mg/L of NPs. Above all, we could conclude that ZnS:Mn NPs (2.0%) induced ROS production after 48 hours of testing in BG11 and SRW media, while it increased quickly from the beginning of measurements in SSW medium. The ROS produced may have a severe effect on the mitochondria from the third day of testing (intracellular ATP levels) and then indirectly affect other metabolic activities, such as photosynthetic activity and viability.

3.2.5. Toxicity of ZnS: Mn (4.0%)

The toxic effect of ZnS:Mn (4.0%) NPs on chlorella vulgaris was also evaluated (Fig.27). The photosynthetic activity of chlorella vulgaris decreased immediately from the very first day of testing to the last day compared to the control group, and the toxic effect increased with the increase in the concentration of NPs used. Chlorella vulgaris showed lower photosynthetic activity throughout the test period in contact with 100 mg/L of NPs. In the SRW, the photosynthetic activity did not seem to be affected by the high concentrations (50 mg/L and 100 mg/L) of ZnS:Mn (4.0%) NPs, while in the BG11 containing 20 mg/L, the photosynthetic activity significantly decreased throughout the duration of the test; this was probably because NPs, in high concentrations, were much easier to aggregate, and therefore more difficult for Chlorella vulgaris to absorb them. DLS measurements supported the aggregation of NPs in SRW (size greater than 700 nm at pH 8, the pH of the algae culture has been shown in Table 2). In SSW, photosynthetic activity increased significantly during the first two days of testing, then slightly decreased 72 h later, which was probably due to the scarcity of nutrients necessary for chloroplast activity, such as the absence of nitrates, phosphates, and carbon sources in the SRW and SSW. [24,28] Therefore, algae started to harvest and store metal species present in SSW containing NPs.[27]

In Fig. 27 d-f), algae viability decreased slightly during the first two days of testing in BG11 and SRW media while in SSW viability decreased within 24 h, again in the presence of a high concentration of ZnS:Mn (4.0%) (100 mg/L of NPs).

Then, intracellular ATP content and SOD activity were measured to study the effect of ROS production on mitochondrial activity. In Fig. 28 a-c), one can see that the intracellular ATP content decreased to varying degrees in BG11 and SSW while it just decreased slightly at 3 h and then 72 h in SRW, which corresponds to the

photosynthetic activity and the viability of Chlorella vulgaris. It is also clear that a high NP content (100 mg/L) is more toxic.

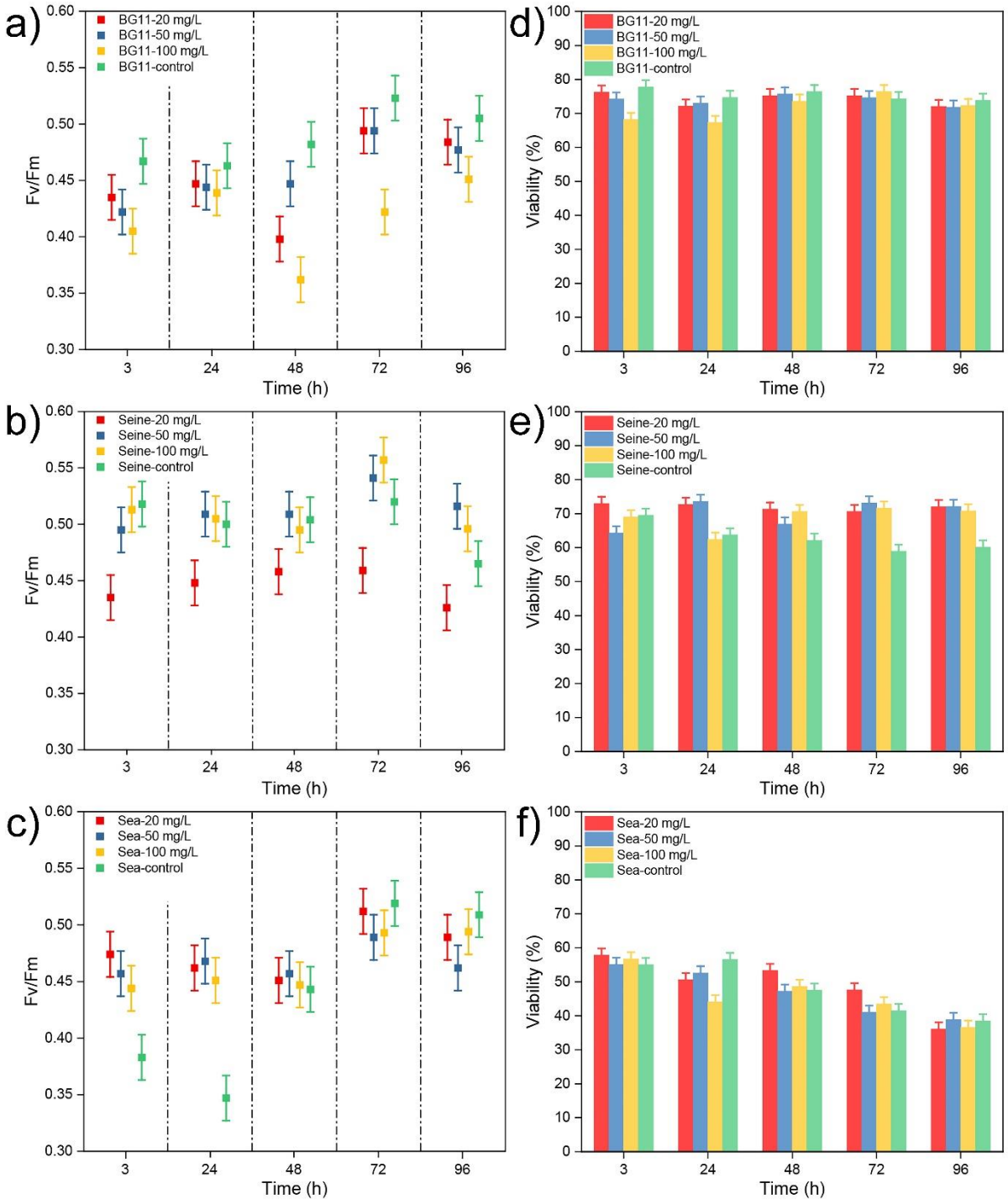

Fig. 27 *PAM (a-c) and viability (d-f) tests of Chlorella vulgaris in different culture media contacted with ZnS: Mn (4.0%) NPs.*

In Fig. 28 d-f), one can notice that the SOD increased in the BG11 and SRW media from the first day of testing to the fourth day of testing, and that it decreased after 96h. In SSW, SOD activity increased significantly throughout the test period, and more markedly in the presence of 100 mg/L of NPs, whatever the medium. Therefore, we

could confirm that NPs may induce the production of ROS, which may have a toxic effect on photosynthetic activity, cell viability and other metabolic activities.

Table 2. *pH of the aqueous media containing various amounts of ZnS:Mn (4.0%).*

Medium	BG11				SRW				SSW			
	20 mg/L	50 mg/L	100 mg/L	control	20 mg/L	50 mg/L	100 mg/L	control	20 mg/L	50 mg/L	100 mg/L	control
pH	7.60	7.54	7.36	8.12	8.68	8.65	8.69	9.34	8.23	8.20	8.19	8.29

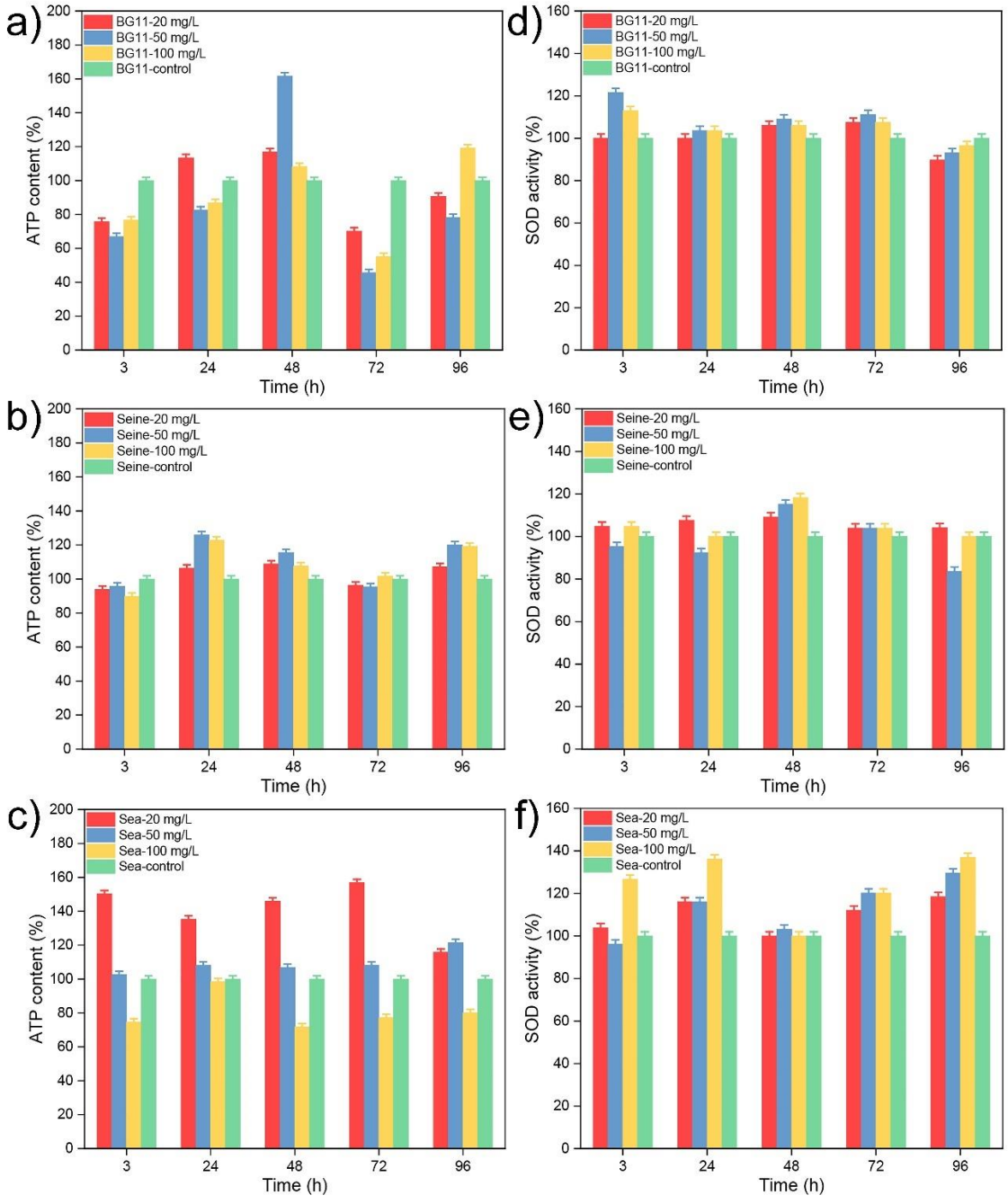

Fig. 28 *ATP (a-c) and SOD (d-f) tests of Chlorella vulgaris in different culture media contacted with ZnS: Mn (4.0%) NPs.*

3.2.6. Toxicity of ZnS:Mn (10%)

Finally, we evaluated the toxicity of ZnS:Mn (10%) NPs. In Fig. 29 a-c), we observed that the photosynthetic activity decreased throughout the duration of the test after the introduction of the ZnS:Mn (10%) NPs in the BG11 medium, and this, all the more quickly as the concentration of NPs was high. However, in SRW and SSW, the photosynthetic activity of Chlorella vulgaris in contact with NPs increased compared to the control group, which could be ascribed to the adaptation of algae to the environment of NPs; algae can harvest and store manganese or any other necessary element when it is abundant.[27] This is in good agreement with the dissolution of manganese in water, which we have shown in Fig. 18, and to a greater extent in SRW and SSW than in BG11.

In Fig.29 d-f), the viability of the algae decreased immediately after the introduction of a content of 100 mg/L of ZnS:Mn (10%) NPs, and this, in the three aqueous media: it was close to 50% in BG11 and SRW, and close to 20% in SSW. For a concentration of 50 mg/L of NPs, the viability in BG11 and SSW decreased slightly during the first three days of testing, then gradually increased to the normal value.[35] For a concentration of 20 mg/L, the viability also decreased, even in SSW from 24h to 72h. We can therefore conclude that a concentration of 100 mg/L of ZnS:Mn (10%) NPs exhibited strong toxicity towards Chlorella vulgaris and threaten its survival; a lower concentration of these NPs was also toxic to Chlorella vulgaris in SSW. However, if viability decreased, photosynthetic activity did not decrease, probably through a protective mechanism of carotenoids, a type of non-enzymatic antioxidants, which may act as singlet oxygen quenchers, thus protecting the machinery photosynthetic.[36]

The influence of NPs on the mitochondrial activity of algae cells was measured through the intracellular ATP content (Fig. 30 a-c). In BG11, the ATP content decreased after 24 h of exposure, compared to the control group. It is even more affected by a concentration of 50 mg/L, 72 h later. While mitochondrial activity decreased significantly after 3 h of exposure in SRW and especially in SSW, the toxic effect on mitochondria continued for a long time. The decrease in the ATP content means the decrease in mitochondrial activity, which means that the ZnS:Mn NPs (10%) caused the disruption of the algae's energy metabolism. The SOD activity (Fig. 30 d-f) increased slightly in BG11, 48 h later, especially in the presence of a concentration of 100 mg/L of NPs. Moreover, SOD activity increased significantly in SRW, 24 h later, while in SSW, SOD activity increased significantly from the very beginning of the test until the last day. Therefore, **we can assume that NPs induced the production of**

ROS, especially in SRW and SSW, which affected the activity of mitochondria, leading to a certain reduction in ATP production, which in turn affected photosynthetic activity and cell viability.

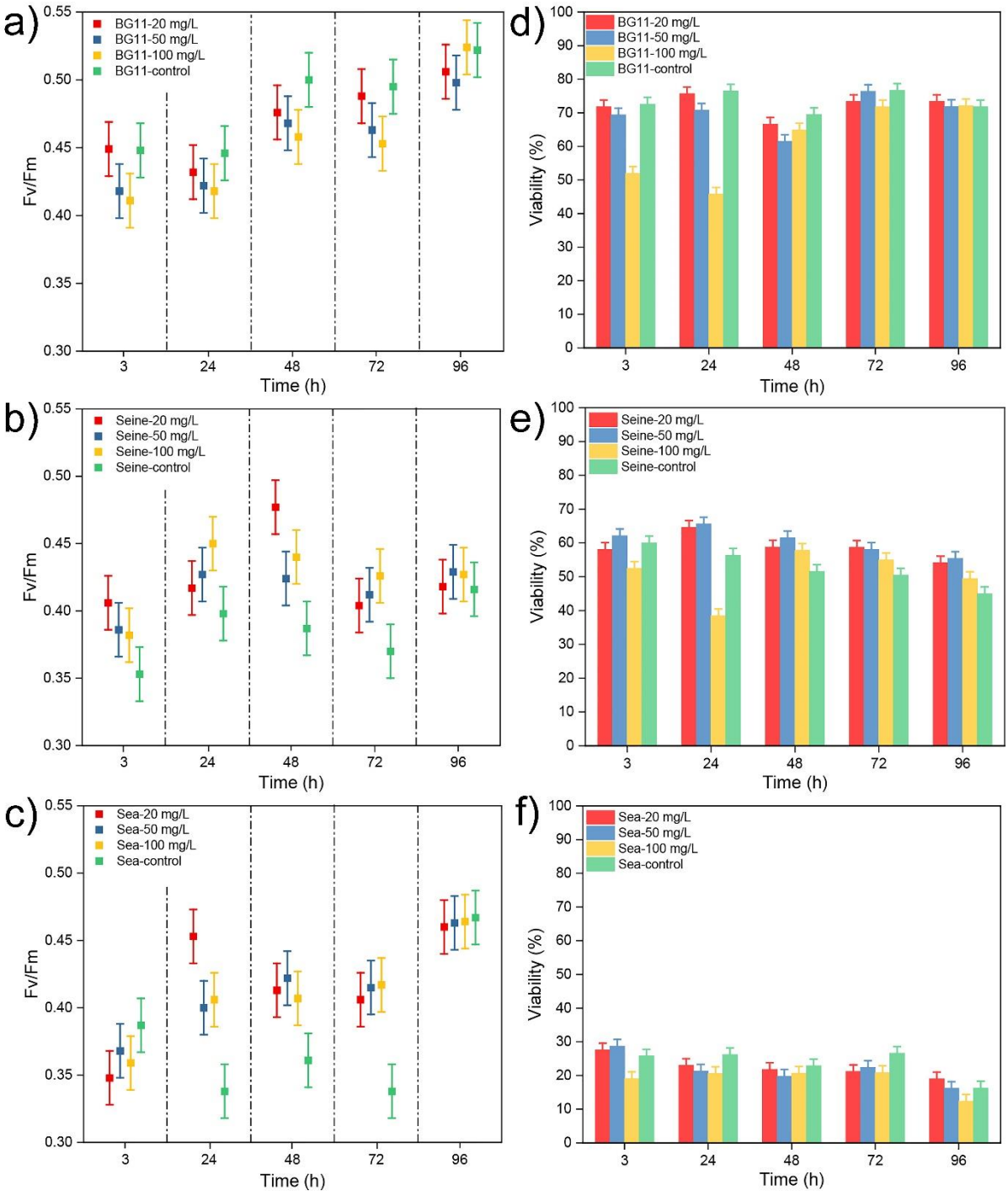

Fig. 29 *PAM (a-c) and viability (d-f) tests of Chlorella vulgaris in different culture media contacted with ZnS:Mn (10%) NPs.*

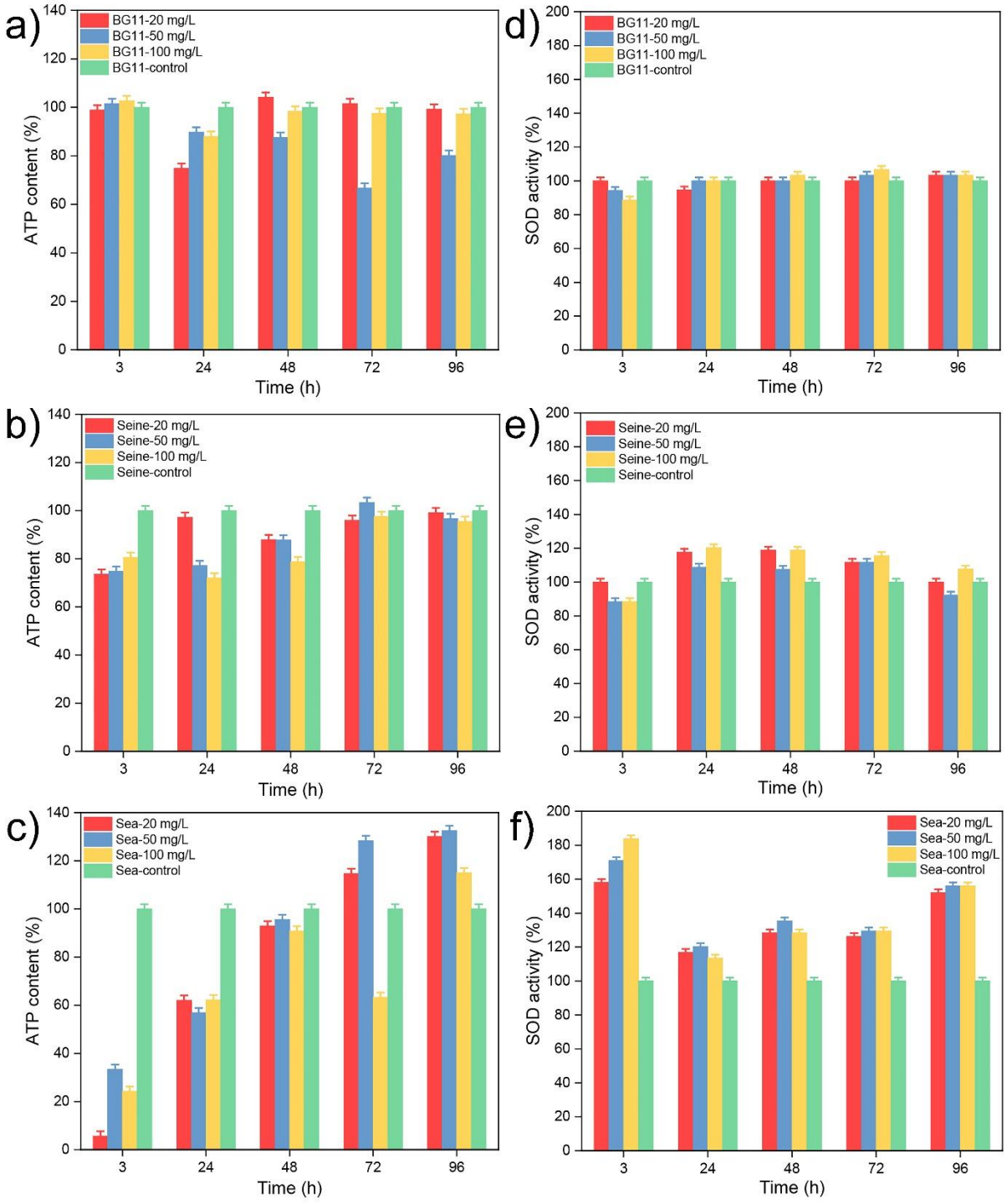

Fig. 30 *ATP (a-c) and SOD (d-f) tests of Chlorella vulgaris in different culture media contacted with ZnS:Mn (10%) NPs.*

Thin-section TEM images of Chlorella vulgaris in the presence or absence of ZnS:Mn (10%) NPs are shown in Fig. 31. In the absence of NPs (Fig. 31 a-c), one can see the integral cell wall and the clear cytoplasm of the algae, whatever the aqueous medium. On the other hand, in the presence of ZnS:Mn (10%) NPs, the cell wall and/or the cytoplasm were damaged. In BG11, we clearly see the dark, circled, spherical aggregate NPs on the cell wall; furthermore, the cytoplasm and the cell wall are clearly separated. In SRW, part of the small-sized NPs also appeared in the cytoplasm, and

the cell wall was broken down. Moreover, we can clearly see the number of aggregated NPs inside the algae cell; the cytoplasm has disappeared, and many NPs (circled in the image) were outside the algae cell.

Therefore, we can conclude that the algae cell can internalize ZnS:Mn (10%) NPs by endocytosis, which will destroy the cytoplasm and cell wall of the algae cell and induce lethal danger.

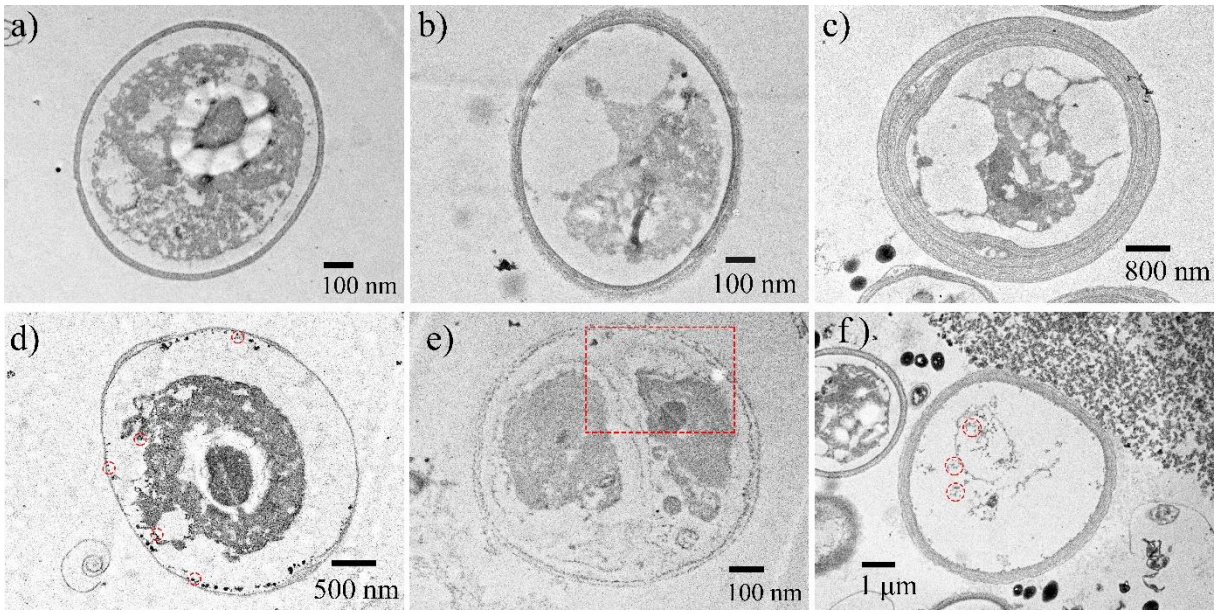

Fig. 31 *TEM images of Chlorella vulgaris thin sections in different media, (a, d) in BG11, (b, e) in SRW, (c, f) in SSW. (d, e, f) showed the Chlorella vulgaris thin sections after exposure to 100 mg/L of ZnS:Mn (10%) NPs.*

3.2.7. Toxicity of ZnS: Mn (10%) coating with silica shell

Previous research has shown that silica NPs are not toxic to the cells.[37] The results I presented in this Chapter evidenced that ZnS:Mn NPs are toxic to Chlorella vulgaris-type algae whatever the type of aqueous medium. So I considered coating the ZnS:Mn (10%) NPs with a silica shell to protect the algae cells from the toxicity of the NPs.

3.2.7.1. Synthesis core-shell structure 10% Mn-ZnS @SiO2 core-shell NPs

At the end of the polyol process, the ZnS:Mn NPs are functionalized by TOPO. Therefore, we first carried out a ligand exchange before coating the NPs with a silica shell using the inverse microemulsion method.[38] Hence, 6.5 mg of ZnS:Mn NPs (10%) were dispersed in 5 mL of heptane by sonication for 15 min. Then, 4 mL of Milli-Q water and 300 µL of 3-mercapto-1-propanol ($HS(CH_2)_3OH$) were introduced dropwise. After sonication for 15 minutes, the NPs were completely transferred into the aqueous phase.

After removal of the supernatant, we obtained 4 mL of ZnS:Mn (10%) NPs colloidal solution functionalized with hydrophilic groups.

Then, we mixed 4 mL of the colloidal solution of NPs with 10 mL of Igepal CO-520 in 50 mL of n-heptane. These suspensions were stabilized by stirring for 4 hours using the Branson 450 Digital Sonifier. 200 µL of tetraethoxysilane (TEOS) were added, under magnetic stirring at 950 rpm for 15 min. To promote the condensation of the TEOS to form the silica shells, 0.5 mL of ammoniacal solution were then introduced. After stirring for 6 hours, 30 mL of ethanol were added to precipitate the core-shell NPs. After washing, centrifugation (22000 rpm, 20 min) and drying (65℃), we recovered the core-shell ZnS:Mn (10%)@SiO_2 NPs (Scheme 1).

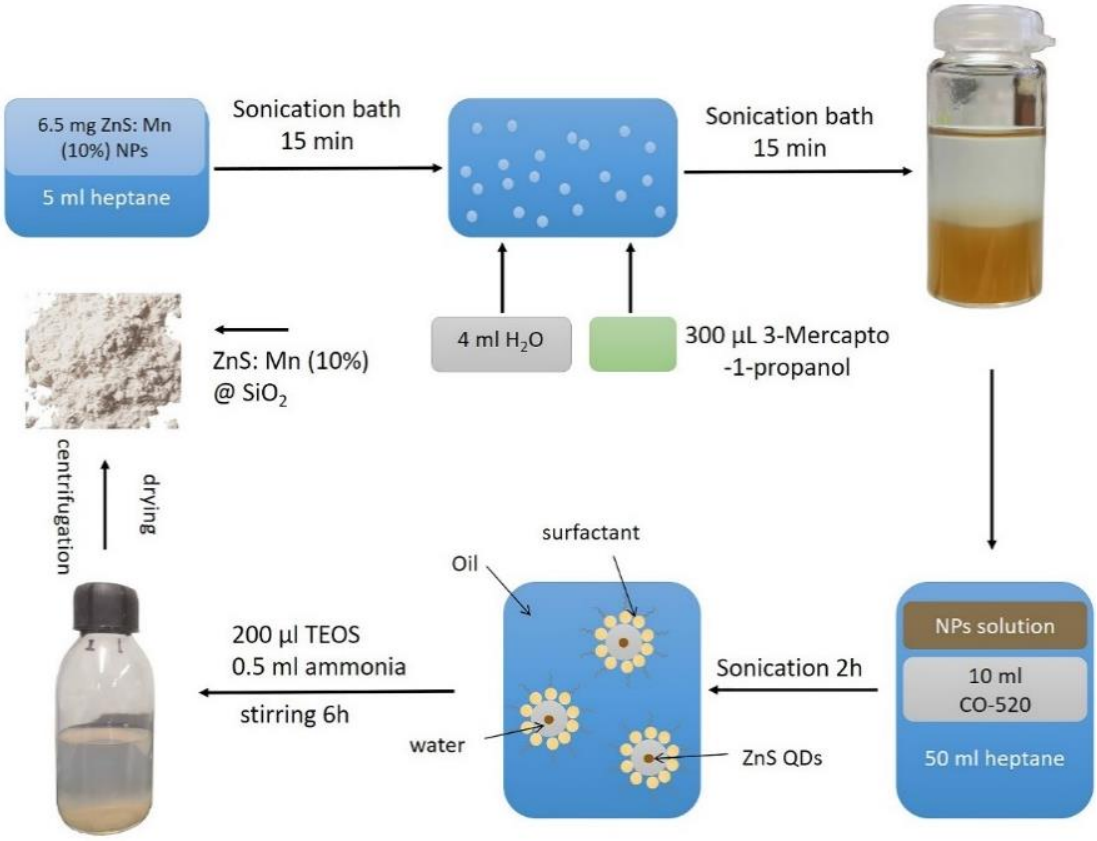

***Scheme 1**. Synthesis pathway of ZnS:Mn (10%) @SiO_2 core-shell NPs.*

3.2.7.2. characterization of the ZnS: Mn (10%) @SiO_2 core-shell NPs

Fig. 32 shows the X-ray diffraction patterns of ZnS:Mn(10%)@SiO_2 core-shell NPs. The diffraction peaks of these samples at 33°, 56°, 67° matched well to the crystal planes (111), (220), (311) of the cubic ZnS phase (COD n° 5000088), while the peak at 26° is characteristic of silica. Therefore, we could confirm that silica was synthesized successfully. TEM pictures were recorded and are shown in Fig. 33; the ZnS:Mn NPs

(10%) were covered with a silica shell. The 2-3 nm NPs were in the center of the silica shell, and the resulting size of core-shell NPs was about 30 nm.

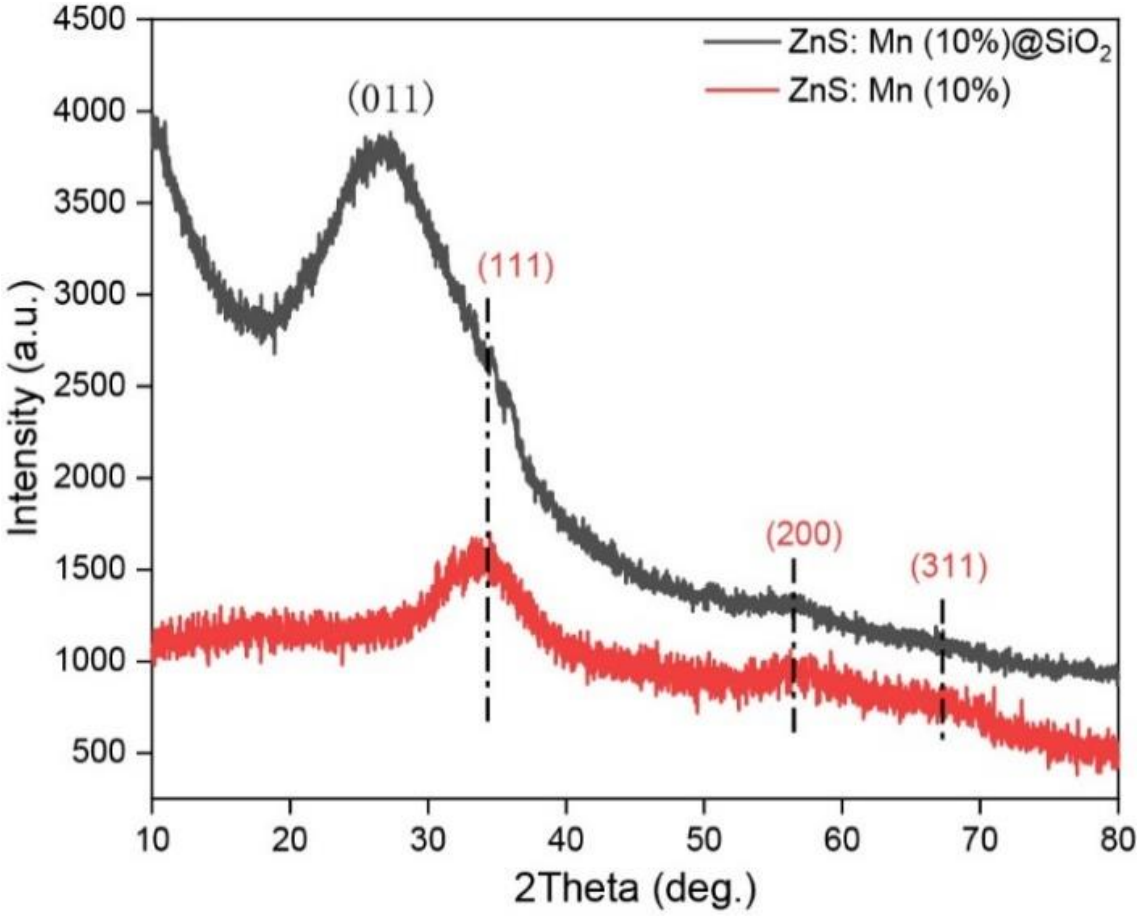

Fig. 32 *XRD patterns of the ZnS:Mn (10%)@SiO_2 core-shell NPs.*

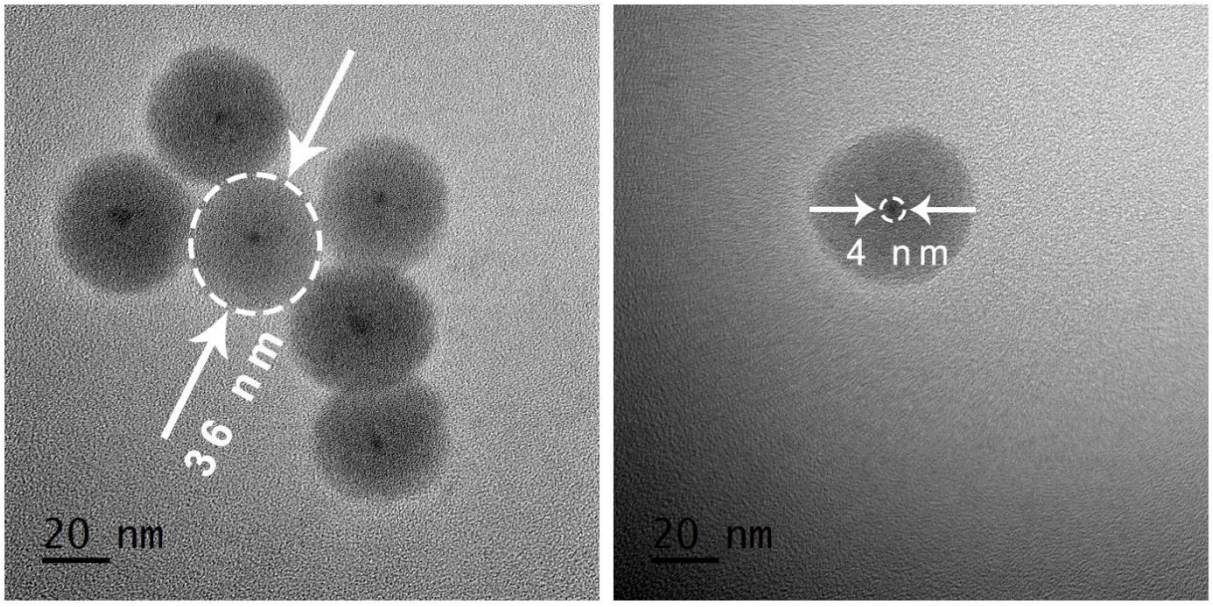

Fig. 33 *TEM pictures of the ZnS:Mn (10%) @SiO_2 core-shell NPs*

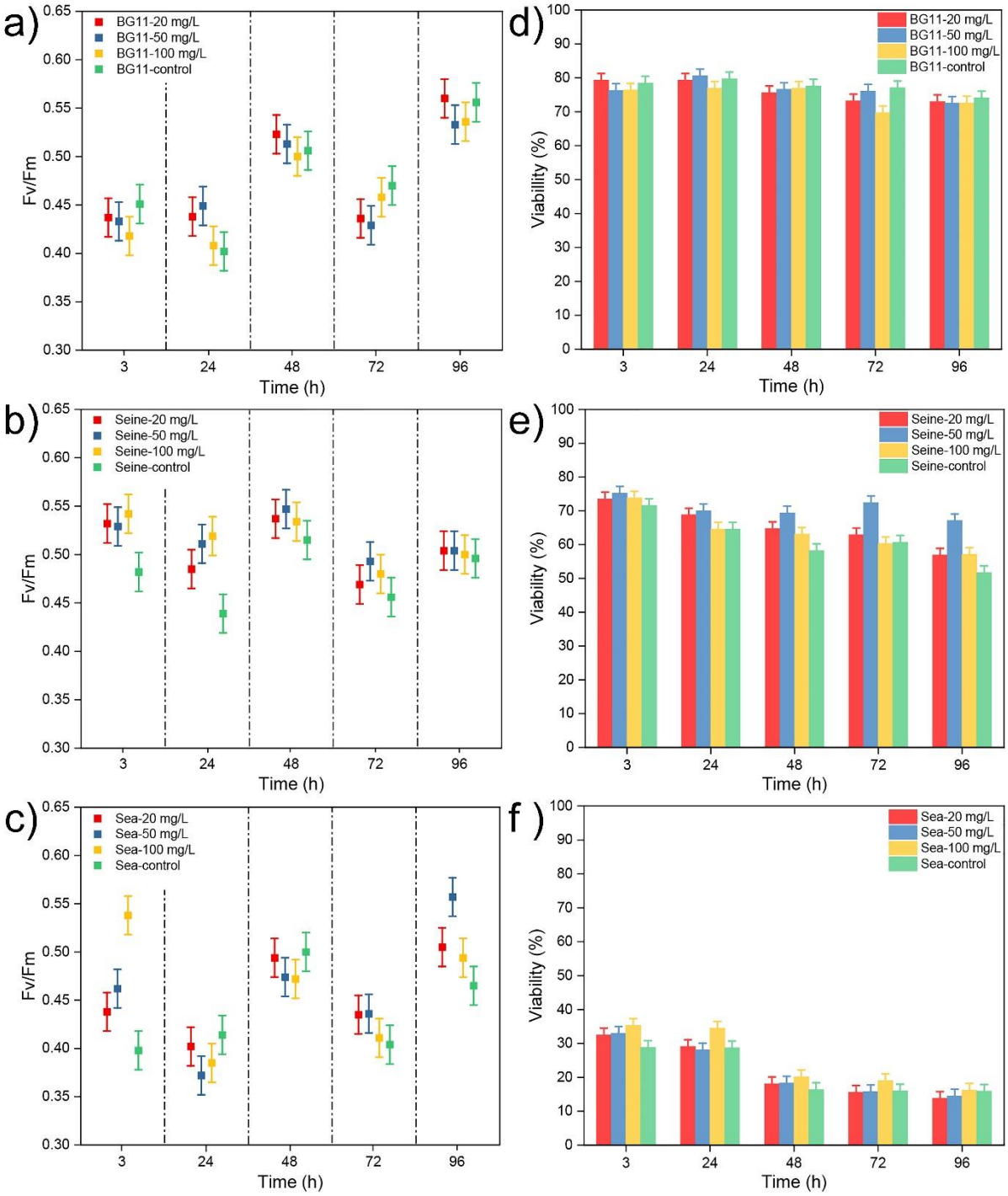

Fig. 34 *PAM (a-c) and viability (d-f) experiments made on Chlorella vulgaris in different culture media contacted with ZnS Mn (10%) @SiO_2 core-shell NPs.*

In order to perform the toxicity tests under the same conditions as before, we calculated the amount of ZnS:Mn NPs present in a sample of core-shell NPs. At the end of this normalization, we put the Chlorella Vulgaris algae in contact with 6 mg, 15 mg and 30 mg of core-shell NPs to keep the same concentrations of ZnS: Mn (10%) Fig. 34 a-c) shows photosynthetic activity of ZnS:Mn (10%) @SiO_2 core-shell NPs. Photosynthetic activity decreased slightly on the first day of testing in BG11, it increased throughout the duration of the test in SRW, and it decreased slightly on the

second and third day of testing in SSW. This is likely due to the shading factor caused by the amount of core-shell NP surrounding the algal cells.[24]

According to Fig. 34 d-f), the viability of Chlorella vulgaris first decreased only slightly, within an acceptable range of values, while the decrease at 72h was probably caused by core-shell NPs. In SRW and SSW, the viability was always similar or higher than that of the control group, which agreed with the evolution of the photosynthetic activity.as before (i.e., 20 mg /L, 50mg/L, 100mg/L, respectively).

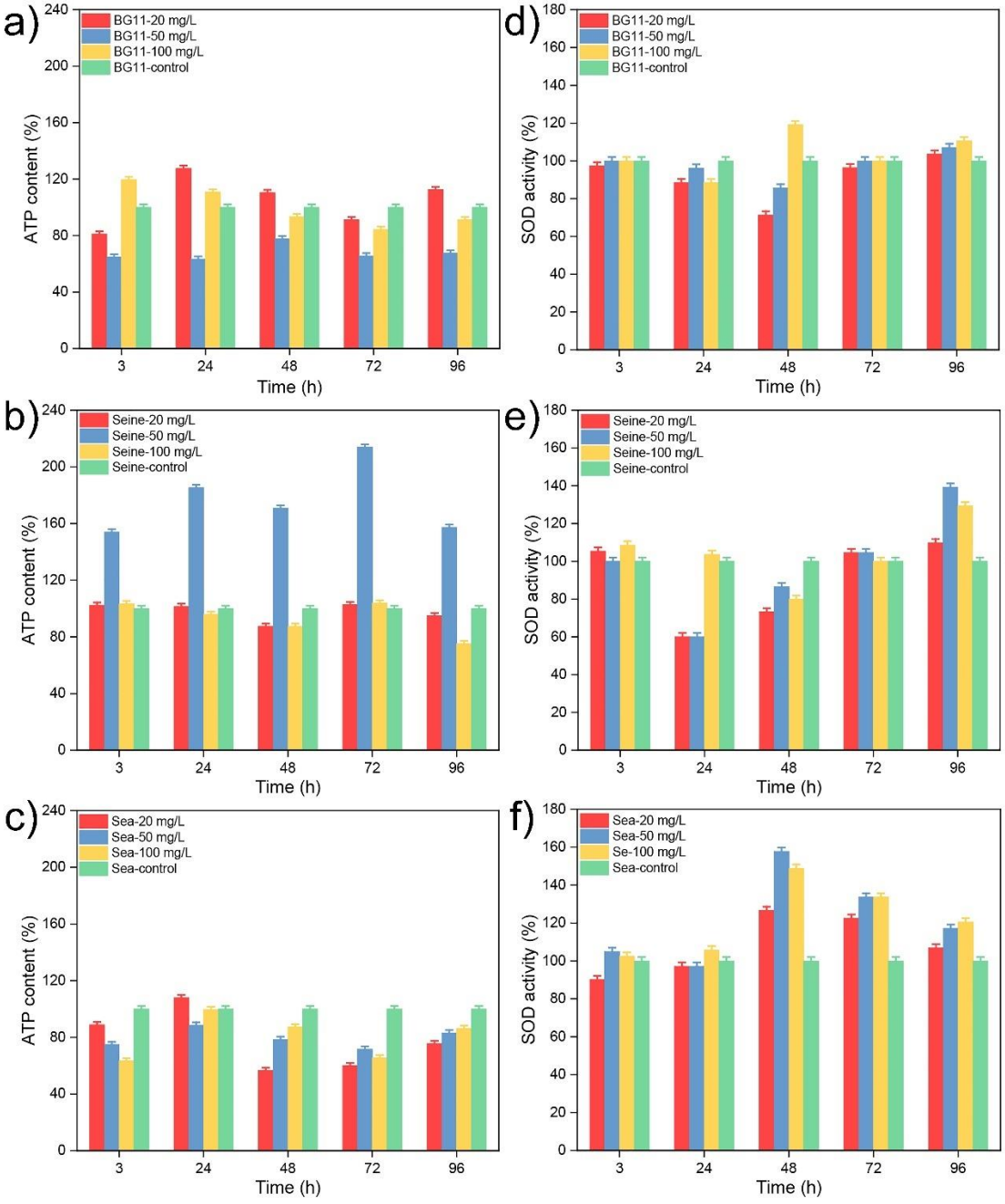

Fig. 35 *ATP (a-c) and SOD (d-f) tests carried out on Chlorella vulgaris in different culture media exposed to ZnS:Mn (10%) @SiO_2 core-shell NPs.*

The intracellular ATP content was measured since it is a parameter directly linked to the activity of mitochondria which produce not only ATP but also ROS. Mitochondria also control cellular apoptosis by releasing associated proteins, reducing ATP production, and increasing ROS production.[24,31,39] Fig. 35 a-c) presents the ATP content in Chlorella vulgaris in the presence of different concentrations of ZnS:Mn (10%)@SiO_2 NPs. In BG11 (Fig. 35 a), the ATP content increased or decreased to varying degrees in the presence of concentrations of NPs equal to 20 mg/L and 100 mg/L. For a concentration of NPs of 50 mg/L, the ATP content decreased throughout the duration of the test. In BG11, the ATP content fluctuated due to shading caused by the number of NPs surrounding the algal cell, which hindered the supply of nutrients to the algae.[24] The ATP content in SRW (Fig. 35 b) is similar to that of the control group, while the ATP level in SSW decreased.

Fig. 35 d-f) shows the SOD activity of Chlorella vulgaris in contact with different concentrations of ZnS:Mn (10%) @SiO_2 core-shell NPs. In BG11, SOD activity increased in the presence of 100 mg/L of core-shell NPs, after 48 h of testing. It also increased in SRW in the presence of 50 mg/L and 100 mg/L of NPs. In SSW, SOD activity increased drastically over the past three days of testing. This increase in SOD activity indicated the NPs induced a high exposure to ROS, which influenced the other metabolic activity of the algae cell. Although core-shell NPs induced the production of ROS that could induce a negative effect on algae cells, viability and photosynthetic activity did not seem to be influenced. **Therefore, the silica shell can prevent the toxic effect of ZnS:Mn (10%) NPs to some extent**.

4. Conclusions

During this work, we have successfully synthesized, by the polyol process, ZnS NPs containing different concentrations of manganese. All the NPs obtained presented a zinc blende structure, and their size varied between 1.1 nm and 1.5 nm (XRD and TEM). Nevertheless, in water, these NPs aggregated to form larger colloids whose size was determined by DLS: at least 300 nm or even greater than 1000 nm in an acidic (pH = 2) or alkaline (pH = 10) medium. The size of the colloids was between 400 nm and 600 nm for pH between 6 and 8, corresponding to the pH of the culture medium of Chlorella vulgaris. This suggested that NPs brought into contact with algae tend to aggregate on the surface of the algae cell, influencing the normal metabolic activity of the algae cell. Moreover, zeta potential measurements showed that NPs were negatively charged when the pH varied from 6 to 8; this makes NPs difficult to

internalize by the algae cell due to repulsive electrostatic interactions with the cell membrane. However, internalized NPs were still internalized and found inside algae cells, as we were able to observe by TEM thin section observations.

Furthermore, the dissolution of Mn^{2+} and Zn^{2+} ions was measured by ICP-AES in the three culture media. We observed that the amounts of Mn^{2+} and Zn^{2+} increased with time, especially in SRW and SSW. This showed that the algae made efforts to harvest and store the nutrients or elements that are necessary for them, when they are available in the environmental conditions that they undergo (such as SRW and SSW). This agreed with the photosynthetic activity of Chlorella vulgaris measured in the media in which we introduced Mn^{2+} cations.

Then, we showed that ZnS:Mn NPs are toxic to microalgae cells. This toxic effect on the metabolic activity of Chlorella vulgaris, was manifested by the reduction in photosynthetic activity, in the activity of the mitochondria, and in cell viability. At the same time, the SOD activity increased, which means that the NPs induced an increase in the production of ROS which is a dangerous factor for cell health. The positive side of all this is that SOD can protect the algae cell from the toxic effect caused by the production of ROS. Furthermore, we found that NPs concentrations of 100 mg/L were more toxic than lower concentrations and ZnS:Mn NPs (10%) seemed more dangerous than ZnS:Mn NPs (0.5%). Indeed, a high concentration of NPs seemed to induce a greater production of ROS, causing a decrease in the activity of mitochondria or chloroplasts or even cell death. The observation of thin sections of Chlorella vulgaris by TEM showed that NPs were internalized inside the cytoplasm of the algae cell, and that part of the cytoplasm was damaged. The cell wall has even been destroyed and some cells were deformed.

Finally, we evidenced that the silica shell is useful to prevent the toxic effect of NPs on Chlorella vulgaris cells. Although ATP content decreased, and SOD activity increased to some extent, photosynthetic activity and viability were not affected by the core-shell NPs. The fluctuation in mitochondrial activity and SOD activity was probably caused by the shading factor of a large number of NPs surrounding the algae cell.

5. References

(1) Longo, A. V.; Notebaert, B.; Gaceur, M.; Patriarche, G.; Sciortino, A.; Cannas, M.; Messina, F.; von Bardeleben, H. J.; Battaglini, N.; Ammar, S. Photo-Activated Phosphorescence of Ultrafine ZnS:Mn Quantum Dots: On the Lattice Strain Contribution. J. Phys. Chem. C 2022, 126 (3), 1531–1541. https://doi.org/10.1021/acs.jpcc.1c09687.

(2) Wang, Y.; Herron, N. Nanometer-Sized Semiconductor Clusters: Materials Synthesis, Quantum Size Effects, and Photophysical Properties. J. Phys. Chem. 1991, 95 (2), 525–532. https://doi.org/10.1021/j100155a009.

(3) Chaguetmi, S.; Mammeri, F.; Nowak, S.; Decorse, P.; Lecoq, H.; Gaceur, M.; Naceur, J. B.; Achour, S.; Chtourou, R.; Ammar, S. Photocatalytic Activity of TiO_2 Nanofibers Sensitized with ZnS Quantum Dots. RSC Advances 2013, 3 (8), 2572–2580. https://doi.org/10.1039/C2RA21684A.

(4) Chung, J. H.; Ah, C. S.; Jang, D.-J. Formation and Distinctive Decay Times of Surface- and Lattice-Bound Mn^{2+} Impurity Luminescence in ZnS Nanoparticles. J. Phys. Chem. B 2001, 105 (19), 4128–4132. https://doi.org/10.1021/jp002692j.

(5) Xu, S. J.; Chua, S. J.; Liu, B.; Gan, L. M.; Chew, C. H.; Xu, G. Q. Luminescence Characteristics of Impurities-Activated ZnS Nanocrystals Prepared in Microemulsion with Hydrothermal Treatment. Appl. Phys. Lett. 1998, 73 (4), 478–480. https://doi.org/10.1063/1.121906.

(6) Jahanbin, T.; Gaceur, M.; Gros-Dagnac, H.; Benderbous, S.; Merah, S. A. High Potential of Mn-Doped ZnS Nanoparticles with Different Dopant Concentrations as Novel MRI Contrast Agents: Synthesis and in Vitro Relaxivity Studies. J Nanopart Res 2015, 17 (6), 258. https://doi.org/10.1007/s11051-015-3038-x.

(7) Gaceur, M.; Giraud, M.; Hemadi, M.; Nowak, S.; Menguy, N.; Quisefit, J. P.; David, K.; Jahanbin, T.; Benderbous, S.; Boissière, M.; Ammar, S. Polyol-Synthesized $Zn_{0.9}Mn_{0.1}S$ Nanoparticles as Potential Luminescent and Magnetic Bimodal Imaging Probes: Synthesis, Characterization, and Toxicity Study. Journal of Nanoparticle Research 2012, 14 (7). https://doi.org/10.1007/s11051-012-0932-3.

(8) Fiévet, F.; Ammar-Merah, S.; Brayner, R.; Chau, F.; Giraud, M.; Mammeri, F.; Peron, J.; Piquemal, J.-Y.; Sicard, L.; Viau, G. The Polyol Process: A Unique Method for Easy Access to Metal Nanoparticles with Tailored Sizes, Shapes and

Compositions. Chem. Soc. Rev. 2018, 47 (14), 5187–5233. https://doi.org/10.1039/C7CS00777A.

(9) Dahoumane, S. A.; Yéprémian, C.; Djédiat, C.; Couté, A.; Fiévet, F.; Coradin, T.; Brayner, R. Improvement of Kinetics, Yield, and Colloidal Stability of Biogenic Gold Nanoparticles Using Living Cells of Euglena Gracilis Microalga. J Nanopart Res 2016, 18 (3), 79. https://doi.org/10.1007/s11051-016-3378-1.

(10) Murugadoss, G. Synthesis and Photoluminescence Properties of Zinc Sulfide Nanoparticles Doped with Copper Using Effective Surfactants. Particuology 2013, 11 (5), 566–573. https://doi.org/10.1016/j.partic.2012.11.003.

(11) Sakthivel, P.; Prasanna Venkatesan, G. K. D.; Subramaniam, K.; Muthukrishnan, P. Structural, Optical, Photoluminescence and Electrochemical Behaviours of Mg, Mn Dual-Doped ZnS Quantum Dots. J Mater Sci: Mater Electron 2019, 30 (13), 11984–11993. https://doi.org/10.1007/s10854-019-01551-2.

(12) Chaguetmi, S.; Chaperman, L.; Nowak, S.; Schaming, D.; Lau-Truong, S.; Decorse, P.; Beaunier, P.; Costentin, C.; Mammeri, F.; Achour, S.; Ammar, S. Photoelectrochemical Properties of ZnS- and CdS-TiO_2 Nanostructured Photocatalysts: Aqueous Sulfidation as a Smart Route to Improve Catalyst Stability. Journal of Photochemistry and Photobiology A: Chemistry 2018, 356, 489–501. https://doi.org/10.1016/j.jphotochem.2018.01.038.

(13) Zhu, Y.-P.; Li, J.; Ma, T.-Y.; Liu, Y.-P.; Du, G.; Yuan, Z.-Y. Sonochemistry-Assisted Synthesis and Optical Properties of Mesoporous ZnS Nanomaterials. Journal of Materials Chemistry A 2014, 2 (4), 1093–1101. https://doi.org/10.1039/C3TA13636A.

(14) Do, Y. R.; Park, D. H.; Yang, H. G.; Park, W.; Wagner, B. K.; Yasuda, K.; Summers, C. J. Uniform Nanoscale SiO_2 Encapsulation of ZnS Phosphors for Improved Aging Properties under Low Voltage Electron Beam Excitation. J. Electrochem. Soc. 2001, 148 (10), G548–G551. https://doi.org/10.1149/1.1397775.

(15) Labiadh, H.; Sellami, B.; Khazri, A.; Saidani, W.; Khemais, S. Optical Properties and Toxicity of Undoped and Mn-Doped ZnS Semiconductor Nanoparticles Synthesized through the Aqueous Route. Optical Materials 2017, 64, 179–186. https://doi.org/10.1016/j.optmat.2016.12.011.

(16) Zhou, D.-J.; Xie, X.-Y.; Zhang, Y.; Guo, D.-Y.; Zhou, Y.-J.; Xie, J.-F. Facile Synthesis of ZnS Nanorods in PEG and Their Spectral Performance. Mater. Res. Express 2016, 3 (10), 105023. https://doi.org/10.1088/2053-1591/3/10/105023.

(17) Liu, W.; Chen, S. An Investigation of the Tribological Behaviour of Surface-Modified ZnS Nanoparticles in Liquid Paraffin. Wear 2000, 238 (2), 120–124. https://doi.org/10.1016/S0043-1648(99)00344-0.

(18) Geszke, M.; Murias, M.; Balan, L.; Medjahdi, G.; Korczynski, J.; Moritz, M.; Lulek, J.; Schneider, R. Folic Acid-Conjugated Core/Shell ZnS:Mn/ZnS Quantum Dots as Targeted Probes for Two Photon Fluorescence Imaging of Cancer Cells. Acta Biomaterialia 2011, 7 (3), 1327–1338. https://doi.org/10.1016/j.actbio.2010.10.012.

(19) Kolmykov, O.; Coulon, J.; Lalevée, J.; Alem, H.; Medjahdi, G.; Schneider, R. Aqueous Synthesis of Highly Luminescent Glutathione-Capped Mn^{2+}-Doped ZnS Quantum Dots. Materials Science and Engineering: C 2014, 44, 17–23. https://doi.org/10.1016/j.msec.2014.07.064.

(20) Bwatanglang, I. B.; Mohammad, F.; Yusof, N. A.; Abdullah, J.; Hussein, M. Z.; Alitheen, N. B.; Abu, N. Folic Acid Targeted Mn:ZnS Quantum Dots for Theranostic Applications of Cancer Cell Imaging and Therapy. Int J Nanomedicine 2016, 11, 413–428. https://doi.org/10.2147/IJN.S90198.

(21) Sumboja, A.; Ge, X.; Goh, F. W. T.; Li, B.; Geng, D.; Hor, T. S. A.; Zong, Y.; Liu, Z. Manganese Oxide Catalyst Grown on Carbon Paper as an Air Cathode for High-Performance Rechargeable Zinc–Air Batteries. ChemPlusChem 2015, 80 (8), 1341–1346. https://doi.org/10.1002/cplu.201500183.

(22) Munk, M.; Brandão, H. M.; Nowak, S.; Mouton, L.; Gern, J. C.; Guimaraes, A. S.; Yéprémian, C.; Couté, A.; Raposo, N. R. B.; Marconcini, J. M.; Brayner, R. Direct and Indirect Toxic Effects of Cotton-Derived Cellulose Nanofibres on Filamentous Green Algae. Ecotoxicology and Environmental Safety 2015, 122, 399–405. https://doi.org/10.1016/j.ecoenv.2015.09.001.

(23) Ding, H.; Ma, Y. Controlling Cellular Uptake of Nanoparticles with PH-Sensitive Polymers. Sci Rep 2013, 3 (1), 2804. https://doi.org/10.1038/srep02804.

(24) Polonini, H. C.; Brandão, H. M.; Raposo, N. R. B.; Brandão, M. A. F.; Mouton, L.; Couté, A.; Yéprémian, C.; Sivry, Y.; Brayner, R. Size-Dependent Ecotoxicity of Barium Titanate Particles: The Case of Chlorella Vulgaris Green Algae.

Ecotoxicology 2015, 24 (4), 938–948. https://doi.org/10.1007/s10646-015-1436-6.

(25) Rodea-Palomares, I.; Gonzalo, S.; Santiago-Morales, J.; Leganés, F.; García-Calvo, E.; Rosal, R.; Fernández-Piñas, F. An Insight into the Mechanisms of Nanoceria Toxicity in Aquatic Photosynthetic Organisms. Aquatic Toxicology 2012, 122–123, 133–143. https://doi.org/10.1016/j.aquatox.2012.06.005.

(26) Haniu, H.; Saito, N.; Matsuda, Y.; Tsukahara, T.; Maruyama, K.; Usui, Y.; Aoki, K.; Takanashi, S.; Kobayashi, S.; Nomura, H.; Okamoto, M.; Shimizu, M.; Kato, H. Culture Medium Type Affects Endocytosis of Multi-Walled Carbon Nanotubes in BEAS-2B Cells and Subsequent Biological Response. Toxicology in Vitro 2013, 27 (6), 1679–1685. https://doi.org/10.1016/j.tiv.2013.04.012.

(27) Brayner, R.; Yéprémian, C.; Djediat, C.; Coradin, T.; Herbst, F.; Livage, J.; Fiévet, F.; Couté, A. Photosynthetic Microorganism-Mediated Synthesis of Akaganeite (β-FeOOH) Nanorods. Langmuir 2009, 25 (17), 10062–10067. https://doi.org/10.1021/la9010345.

(28) Planchon, M.; Ferrari, R.; Guyot, F.; Gélabert, A.; Menguy, N.; Chanéac, C.; Thill, A.; Benedetti, M. F.; Spalla, O. Interaction between Escherichia Coli and TiO_2 Nanoparticles in Natural and Artificial Waters. Colloids and Surfaces B: Biointerfaces 2013, 102, 158–164. https://doi.org/10.1016/j.colsurfb.2012.08.034.

(29) Polonini, H. C.; Brandão, H. M.; Raposo, N. R. B.; Mouton, L.; Yéprémian, C.; Couté, A.; Brayner, R. Ecotoxicological Studies of Micro- and Nanosized Barium Titanate on Aquatic Photosynthetic Microorganisms. Aquatic Toxicology 2014, 154, 58–70. https://doi.org/10.1016/j.aquatox.2014.05.005.

(30) Cheng, W.-W.; Lin, Z.-Q.; Wei, B.-F.; Zeng, Q.; Han, B.; Wei, C.-X.; Fan, X.-J.; Hu, C.-L.; Liu, L.-H.; Huang, J.-H. Single-Walled Carbon Nanotube Induction of Rat Aortic Endothelial Cell Apoptosis: Reactive Oxygen Species Are Involved in the Mitochondrial Pathway. The International Journal of Biochemistry & Cell Biology 2011, 43 (4), 564–572. https://doi.org/10.1016/j.biocel.2010.12.013.

(31) Pereira, M. M.; Mouton, L.; Yéprémian, C.; Couté, A.; Lo, J.; Marconcini, J. M.; Ladeira, L. O.; Raposo, N. R.; Brandão, H. M.; Brayner, R. Ecotoxicological Effects of Carbon Nanotubes and Cellulose Nanofibers in Chlorella Vulgaris. J Nanobiotechnol 2014, 12 (1), 15. https://doi.org/10.1186/1477-3155-12-15.

(32) Brayner, R.; Dahoumane, S. A.; Nguyen, J. N.-L.; Yéprémian, C.; Djediat, C.; Couté, A.; Fiévet, F. Ecotoxicological Studies of CdS Nanoparticles on Photosynthetic Microorganisms. Journal of Nanoscience and Nanotechnology 2011, 11 (3), 1852–1858. https://doi.org/10.1166/jnn.2011.3564.

(33) Brayner, R.; Ferrari-Iliou, R.; Brivois, N.; Djediat, S.; Benedetti, M. F.; Fiévet, F. Toxicological Impact Studies Based on Escherichia Coli Bacteria in Ultrafine ZnO Nanoparticles Colloidal Medium. Nano Lett. 2006, 6 (4), 866–870. https://doi.org/10.1021/nl052326h.

(34) Brayner, R.; Dahoumane, S. A.; Yéprémian, C.; Djediat, C.; Meyer, M.; Couté, A.; Fiévet, F. ZnO Nanoparticles: Synthesis, Characterization, and Ecotoxicological Studies. Langmuir 2010, 26 (9), 6522–6528. https://doi.org/10.1021/la100293s.

(35) da Rocha, A.; Menguy, N.; Yéprémian, C.; Couté, A.; Brayner, R. Ecotoxicological Studies of ZnO and CdS Nanoparticles on Chlorella Vulgaris Photosynthetic Microorganism in Seine River Water. Nanomaterials (Basel) 2020, 10 (2). https://doi.org/10.3390/nano10020227.

(36) Furger, C. Live Cell Assays for the Assessment of Antioxidant Activities of Plant Extracts. Antioxidants 2021, 10 (6), 944. https://doi.org/10.3390/antiox10060944.

(37) Boissière, M.; J. Meadows, P.; Brayner, R.; Hélary, C.; Livage, J.; Coradin, T. Turning Biopolymer Particles into Hybrid Capsules: The Example of Silica /Alginate Nanocomposites. Journal of Materials Chemistry 2006, 16 (12), 1178–1182. https://doi.org/10.1039/B515797H.

(38) Aubert, T.; Soenen, S. J.; Wassmuth, D.; Cirillo, M.; Van Deun, R.; Braeckmans, K.; Hens, Z. Bright and Stable CdSe/CdS@SiO_2 Nanoparticles Suitable for Long-Term Cell Labeling. ACS Appl. Mater. Interfaces 2014, 6 (14), 11714–11723. https://doi.org/10.1021/am502367b.

(39) Christophe, M.; Nicolas, S. Mitochondria: A Target for Neuroprotective Interventions in Cerebral Ischemia-Reperfusion. Current Pharmaceutical Design 2006, 12 (6), 739–757. https://doi.org/10.2174/138161206775474242.

Chapter III. Ecotoxicity of Mn doped ZnS quantum dots on Chlorella vulgaris microalgae. Influence of the size of the nanoparticles.

1. Introduction

The toxicity of materials depends mainly on their size, their shape, and their reactivity,[1] influenced in particular by the surface-to-volume ratio and the chemical state of their surface. All of these parameters can influence NP-algae or internalization of NPs by microalgae.[2,3] Based on previous research, it is already known that bulk materials are non-toxic or few toxic to cells.[1,4] In Chapter 2, we studied the toxicity of small size ZnS:Mn NPs (about 1-2 nm) on Chlorella vulgaris. However, what about the toxic effect of larger ZnS:Mn NPs? Therefore, we aimed at synthesizing larger ZnS:Mn NPs to study their toxicity on Chlorella vulgaris.

Therefore, this chapter presents the synthesis and structural characterization of quantum dots of ZnS:Mn, of blende structure, and the development of ecotoxicity tests, by measuring the photosynthetic activity, mitochondrial activity, SOD activity as well as the viability of Chlorella vulgaris algae.

2. Experimental

2.1. Synthesis of ZnS:Mn NPs using thioacetamide (TAA) as the source of sulfur, by microwave-assisted polyol method

All chemicals were of analytical grade and used without any further purification. Manganese acetate tetrahydrate (≥ 99%, $Mn(CH_3COO)_2.4H_2O$), ethylene glycol (EG) ($OH(CH_2)_2OH$), thioacetamide (TAA) (CH_3CSNH_2) were purchased from Sigma-Aldrich, and zinc acetate dihydrate ($Zn(CH_3COO)_2.2H_2O$, 98+%) was purchased from ACROS ORGANICS.

To obtain a larger ZnS:Mn NPs, we removed TOPO form the synthesis. To synthesize ZnS NPs containing 10% Mn, we mixed 1.08 g of zinc acetate dihydrate, 133.98 mg of manganese acetate tetrahydrate and 452.64 mg of thioacetamide in 80 mL of ethylene glycol. After 15 min of sonication with a water bath, the suspension was transferred to the microwave oven (Synthos 3000), then heated at 220 W for 30 min. Then we recovered the NPs by 3 cycles of centrifugation (22000 rpm), and washing in

ethanol then drying overnight at 60 °C. (The manganese mass used for other ZnS:Mn NPs are shown in Table 3).

Table 3. *The used manganese acetate tetrahydrate mass for ZnS:Mn (0.5%, 2.0%, 4.0%, 10.0%) NPs.*

Name	Mass
ZnS:Mn (0.5%)	6.06 mg
ZnS:Mn (2.0%)	24.61 mg
ZnS:Mn (4.0%)	50.24 mg
ZnS:Mn (10.0%)	133.98 mg

3. Results and discussion

3.1. Characterization of ZnS: Mn NPs

The X-ray diffraction patterns of these NPs are presented in Fig. 36. The diffraction peaks of these samples were matching well with the (111), (220), (311) crystal planes of the cubic ZnS phase (COD no. 5000088). The diffraction peaks were narrower than those observed in Chapter 2 and indicated that the size of the crystallites had indeed increased. We estimated the average crystal size of NPs using Scherrer's formula:[5,6]

$$D = \frac{k\lambda}{\beta cos\theta},$$

where D is the average size of the particles, k is the particles shape factor (0.89), λ is the X-ray wavelength (0.179 nm), β is the FWHM of the diffraction peak, θ is the diffraction Bragg angle. The average crystal sizes calculated for these NPs ranged from 6.3 nm to 6.6 nm.

The TEM images (Fig. 37) showed that the size of the nanoparticles is around 8.5 to 10.5 nm, values slightly higher than the average size estimated by Scherrer's formula. They also allowed us to confirm the crystal structure of ZnS NPs doped with different concentrations of Mn. The EDS analyzes (Fig. 38) made it possible to identify the presence of Zn, S, and Mn (whose peak intensity increased when the molar concentration introduced during the synthesis increased). Except for Cu (coming from the copper grid), no impurity was observed. Finally, in order to confirm the elemental composition of the ZnS:Mn NPs, X-ray fluorescence (XRF) measurements were carried out (Table 4): the Mn content in the NPs increased with the increase in the molar concentration of Mn, in agreement with the results obtained by EDS.

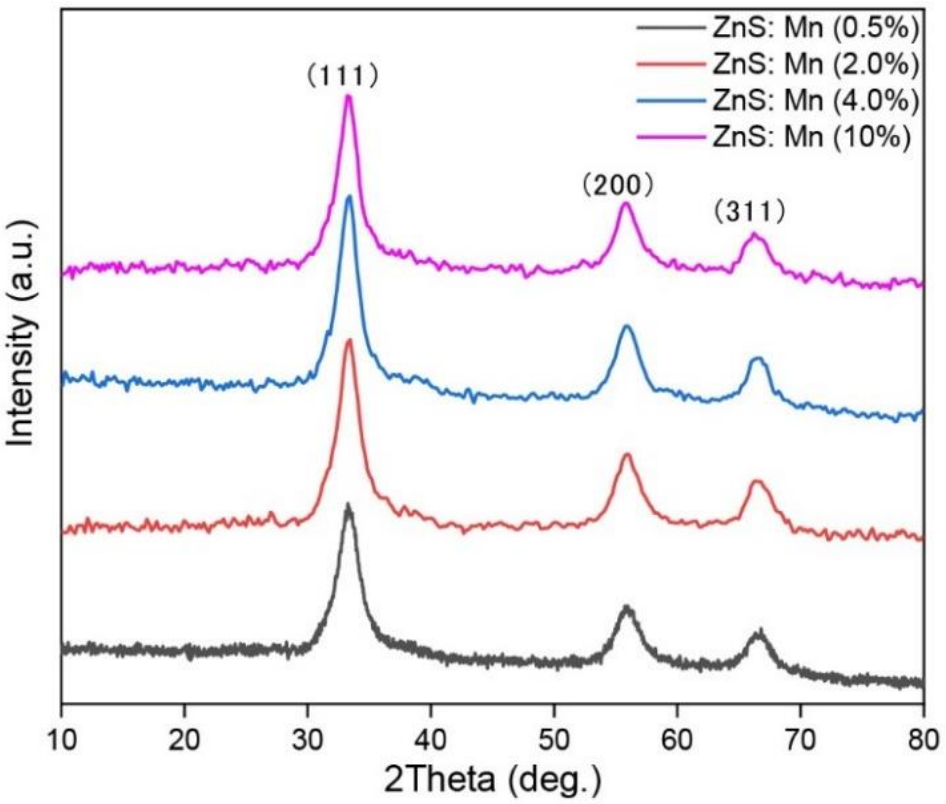

Fig. 36 *XRD patterns of the produced ZnS:Mn NPs.*

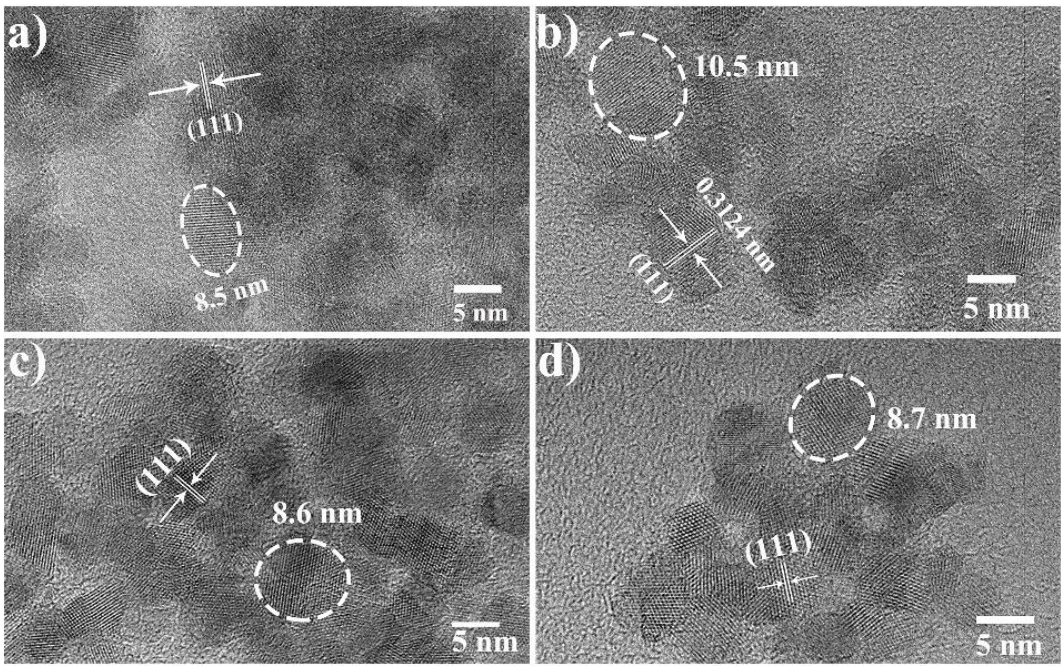

Fig. 37 *TEM images of ZnS:Mn NPs a) 0.5% Mn, b) 2% Mn, c) 4% Mn, d) 10% Mn.*

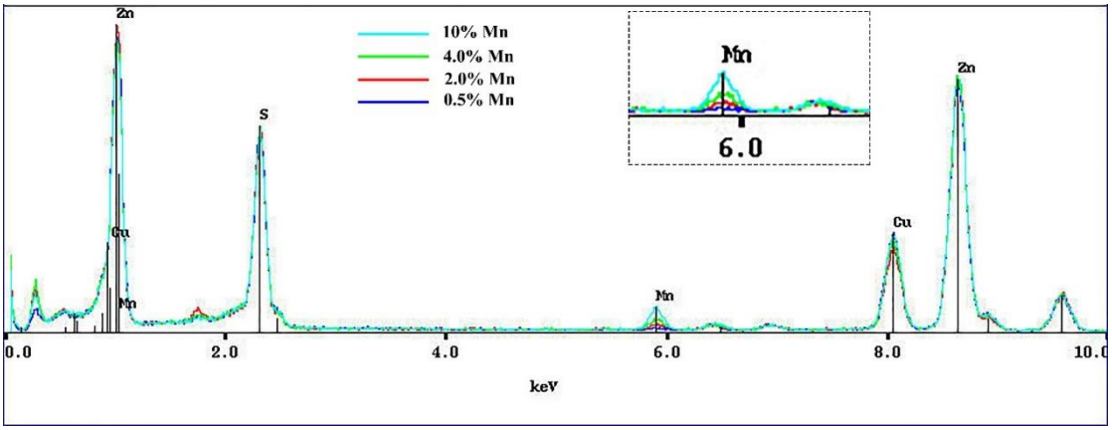

Fig.38 *EDS of ZnS:Mn NPs with different molar concentrations of Mn.*

Table 4 *Composition of the ZnS:Mn NPS from XRF measurements.*

Sample		Zn	S	Mn
0.5% Mn	mass (µg)	192.958	32.035	0.864
	percent (%mol)	74.4	25.2	**0.4**
2.0% Mn	mass (µg)	187.274	30.745	2.788
	percent (%mol)	73.9	24.8	**1.3**
4.0% Mn	mass (µg)	192.488	34.84	6.325
	percent (%mol)	71.0	26.2	**2.8**
10.0% Mn	mass (µg)	201.116	36.408	15.055
	percent (%mol)	68.6	25.3	**6.1**

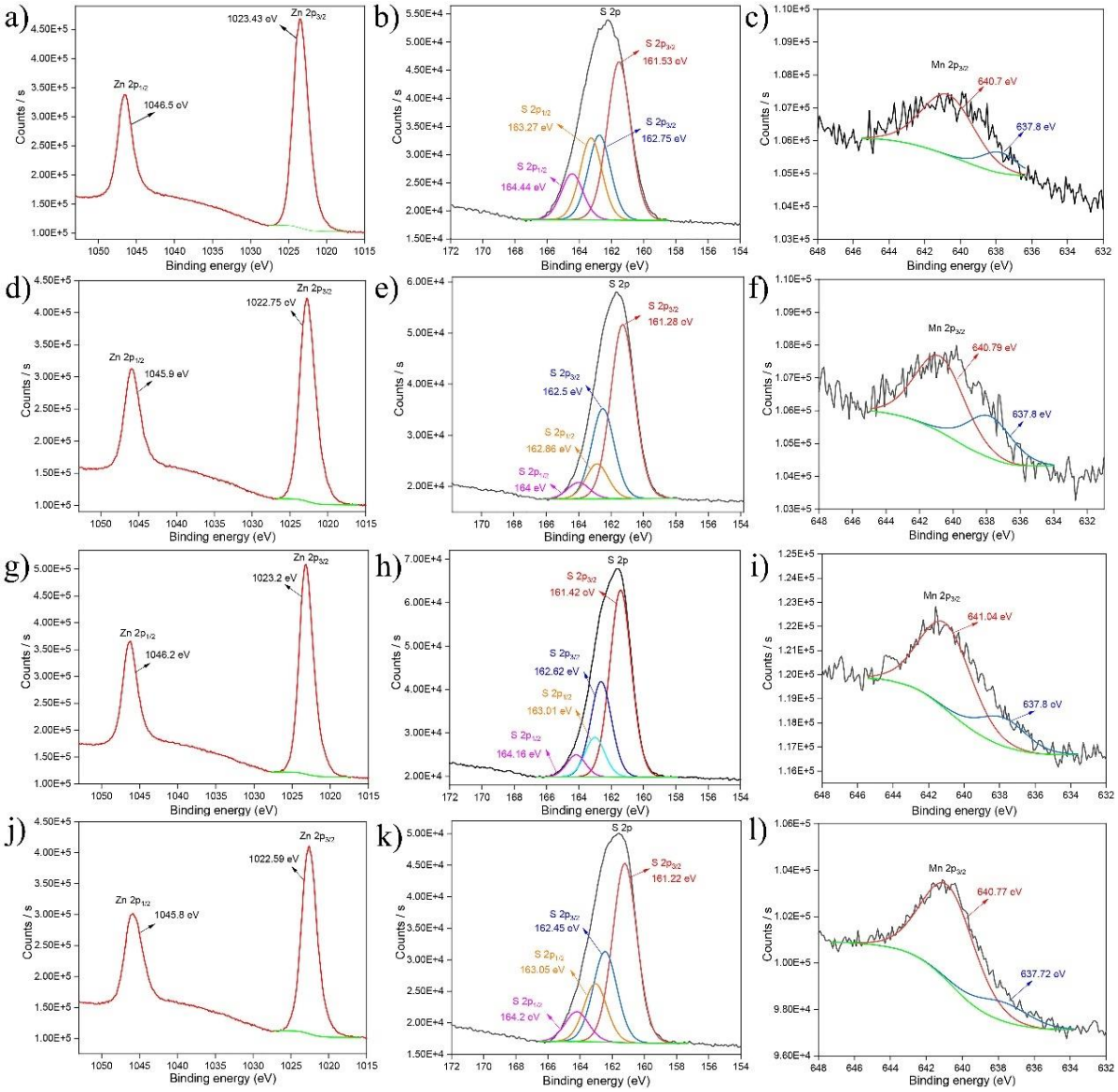

Fig. 39 *XPS spectra of Zn2p, S2p, Mn2p, a-c) ZnS:Mn (0.5%), d-f) ZnS:Mn (2.0%), g-i) ZnS:Mn (4.0%), j-l) ZnS:Mn (10%).*

XPS measurements were also performed to get more details on the elemental chemical composition of these samples and to confirm the chemical state of Mn, Zn, and S elements (Fig. 39). The two peaks located at binding energies of 1022 eV and 1045 eV (Fig. 39 a, d, g, j) correspond respectively to Zn 2P3/2 and Zn 2p1/2, which are the signature of Zn2+ in a cubic structure ZnS.[7–9]

The deconvolution of the high-resolution spectra of S 2p were shown in Fig. 39 b, e, h, k). The S 2p peaks can be fitted with 2 peaks at 161.2 eV and 162.5 eV, corresponding to S $2p_{3/2}$, and 2 peaks at 163.1 eV and 164.2 eV, corresponding to S $2p_{1/2}$.[10–12] And the deconvolution of the Mn 2p spectra showed two peaks at 637.8 eV and 640.7 eV, characteristic of the Mn^{2+} ion.[13]

Dynamic light-scattering (DLS) measurements were performed using the Zetasizer Nano ZS (Malvern) to determine the size and colloidal stability of the suspensions of ZnS:Mn (10%) NPs in BG11, Seine River water (SRW) and synthetic seawater (SSW), at pH values between 2 and 10. In BG11 (Fig. 40 a), we could see NPs of size 11 nm and others of 615 nm when the pH value is 2. The size was rather 250 nm in an alkaline medium (pH = 10), while the size of the NPs was greater than 1700 nm at pH 4, 6, and 8. In sea water (SSW) (Fig. 40 c), particles of 15 nm and aggregates of 712 nm were observed when the pH is 4, while it was greater than 2000 nm for other values. of pH, acid or alkaline. Furthermore, zeta potential measurements were performed in these aqueous media of different pH (Fig. 40 d).[14–16] The value of the zeta potential of these NPs varied from -20 to 5 almost independently of the acid or alkaline whether in BG11, SRW or SSW, which means that these colloids were rather unstable.[17] Therefore, we can confirm that ZnS:Mn (10%) NPs will have a propensity to aggregate very easily in the presence of Chlorella vulgaris (whose pH of the culture medium is around 8-9, see Table 2).

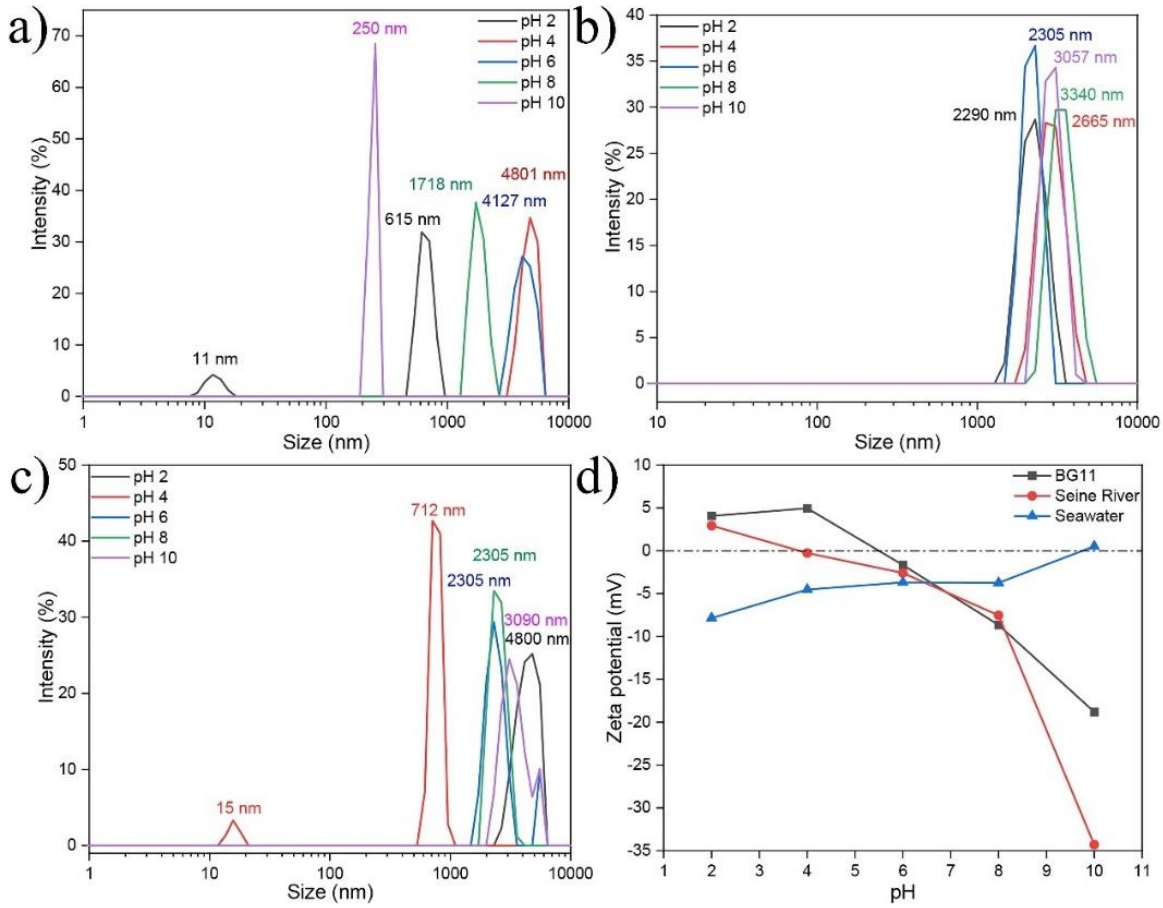

Fig. 40 *DLS data of ZnS:Mn (10%) NPs, size in a) BG11, b) SRW, c) SSW, d) Zeta potential in different waters.*

The magnetic properties of ZnS:Mn NPs were measured using a SQUID magnetometer and are shown in Fig. 41. Fig. 41 a) presents the magnetization of ZnS:Mn NPs, containing different molar concentrations of Mn, as a function of the applied external magnetic field at 300 K. All the samples exhibited paramagnetic characteristics at room temperature except the one containing 0.5% Mn, which presented diamagnetic properties (the amount of Mn was too low to induce macroscopic magnetization in the sample). The magnetization of ZnS NPs doped with 2%, 4% and 10% Mn increased linearly with the increasing molar concentration of Mn. Fig. 41 b) showed the susceptibility of these ZnS:Mn NPs, which was recorded at different temperatures under an external applied magnetic field of 500 Oe. For NPs containing 2% and 4% Mn, the curves were linear, evidencing paramagnetic properties; however, the slope of the curve varied for NPs containing 10% Mn, and reflected an antiferromagnetic behavior: clusters of Mn could form in the NPs, when the Mn concentration was increased.[18,19] In the NPs containing lower Mn amounts (2% and 4%), Mn^{2+} ions were more likely to replace Zn^{2+} cations in the host lattice, and therefore could be considered independent of each other, without forming Mn clusters, which explained paramagnetic properties.[18,20]

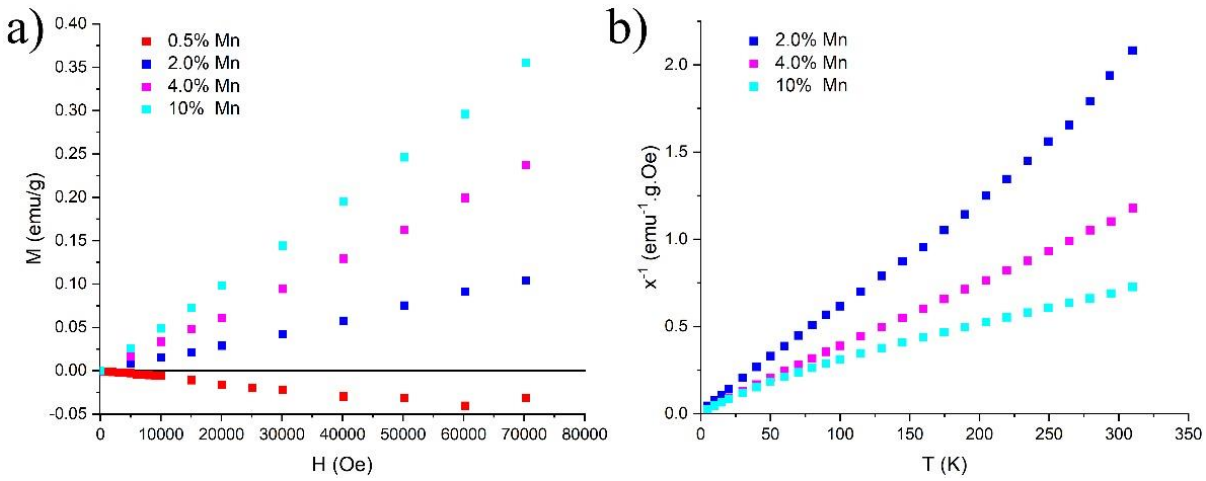

Fig. 41 *Magnetization versus magnetic field at 300K (a) and susceptibility versus temperature at 500 Oe (b) of Mn-doped ZnS NPs with different dopant concentrations.*

We studied the dissolution of Mn^{2+} and Zn^{2+} ions from ZnS:Mn (10%) NPs in different waters, by ICP-AES. For this, we dispersed the ZnS:Mn (10%) NPs in the 3 media: Milli-Q, SRW and SSW (0.01 mg/mL) by sonication for 30 min. Then, the suspensions were ultracentrifuged once a day for 5 days, using a 1 kDa filter (at 5000 rpm, for 20 min) by adding 50 µL nitric acid to the filtrate at each step. Moreover, we also recovered the powders of ZnS:Mn (10%) NPs in the different aqueous media after ultracentrifugation and drying on the 5th day, in order to characterize them to evaluate

potential phase, composition or magnetic properties changes by XRD, XRF and SQUID, respectively.

X-ray diffraction patterns of ZnS:Mn (10%) NPs after dispersion and extraction of different waters are shown in Fig. 42. The diffraction patterns of ZnS:Mn (10%) NPs after dispersion in Milli-Q and Seine River waters were unchanged and contained no impurity. However, the diffraction pattern of NPs dispersed in seawater presented a new phase, namely NaCl, which came from the salt present in synthetic seawater.

The composition of the ZnS:Mn (10%) NPs recovered after dissolution were analyzed by X-ray fluorescence (XRF). The results are gathered in Table 5. After the ultracentrifugation step, the amount of Mn decreased compared to the starting NPs while the amount of Zn remained almost the same (the Mn/Zn ratio changed from 0.09 to 0.06 in Milli-Q and SRW, and to 0.05 in SSW). Therefore, we can confirm that part of the Mn^{2+} ions were dissolved in the filtrate.

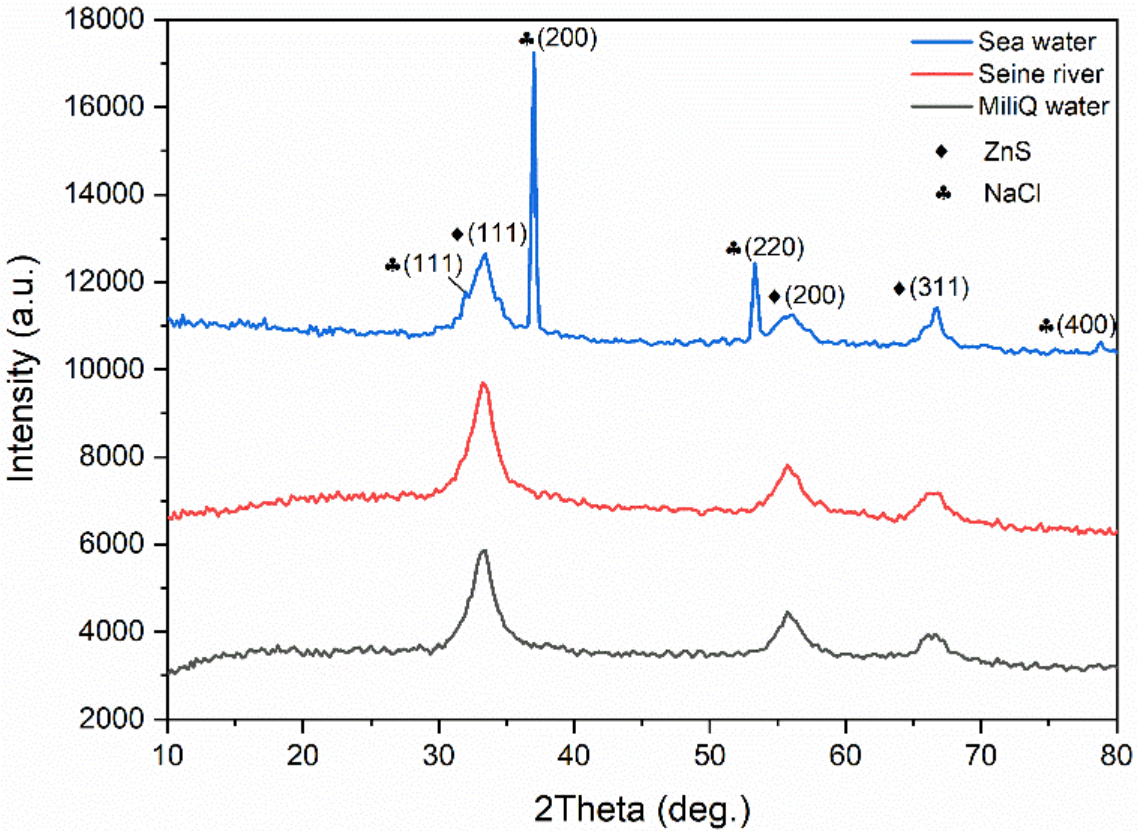

Fig. 42 *XRD of the ZnS:Mn NPs dispersed in Milli-Q water, SRW and SSW.*

Table 5 *XRF of ZnS: Mn (10%) NPs dispersed in Milli-Q water, SRW and SSW.*

Name		Zn	S	Mn
10% Mn	mass (µg)	201.116	36.408	15.055
	percent (%mol)	68.6	25.3	**6.1**
10% Mn -Milli-Q	mass (µg)	52.22	16.33	2.581
	percent (%mol)	58.9	37.6	**3.5**
10% Mn -SRW	mass (µg)	89.552	22.744	4.326
	percent (%mol)	63.5	32.9	**3.7**
10% Mn -SSW	mass (µg)	69.789	18.933	3.213
	percent (%mol)	62.2	34.4	**3.4**

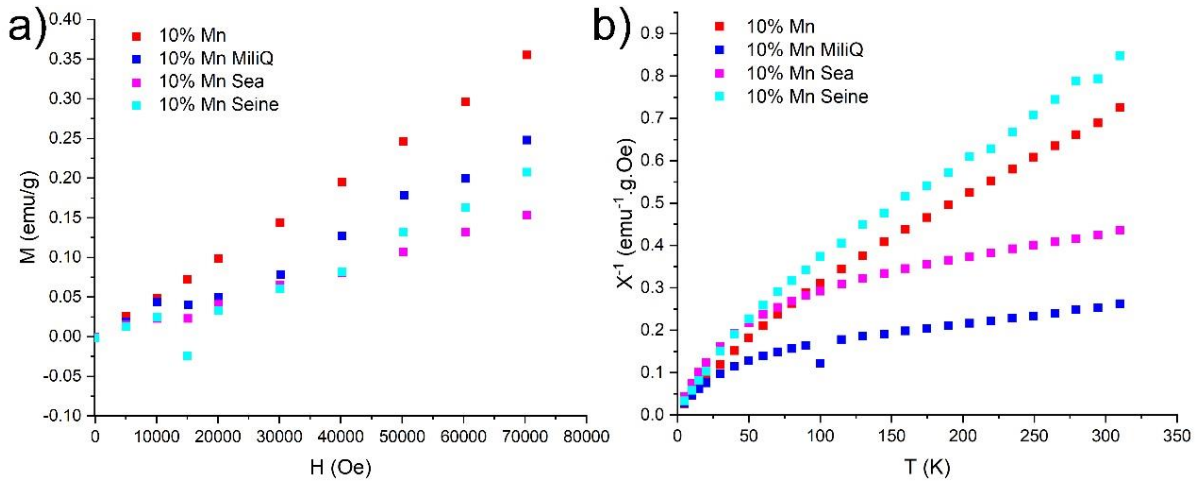

Fig. 43 *a) Magnetization versus magnetic field at 300K (a) and susceptibility versus temperature at 500 Oe (b) of ZnS:Mn (10%) NPs after ultracentrifugation.*

The magnetic properties of these NPs were measured by SQUID magnetometry (Fig. 43). Ultracentrifuged ZnS:Mn (10%) NPs still exhibited paramagnetic properties (Fig. 43a), but the magnetization of these NPs was weaker than that of the starting NPs. This was due to the loss of Mn^{2+} cations after ultracentrifugation. Fig. 43 b) shows the susceptibility of NPs as a function of temperature at 500 Oe. The curves corresponding to the NPs dispersed in the Milli-Q and SSW media presented a change in slope after T = 50 K; there are two possible reasons for this: Mn^{2+} has been oxidized to Mn^{3+} or Mn^{4+}, or Mn^{2+} ions have been lost after ultracentrifugation. The results of the XRF measurements tend to conclude that the change in slope was rather due to

the loss of Mn^{2+}. On the other hand, the magnetic properties of NPs from SRW did not seem to be influenced by the previous treatments.

The dissolution of Mn^{2+} and Zn^{2+} was measured by ICP-AES using the filtrates that we prepared previously for 5 days. The percentages of Mn^{2+} and Zn^{2+} dissolved in different waters for 5 days are shown in Fig. 44. The percentage of dissolution of Mn^{2+} and Zn^{2+} increased day after day and reached a maximum on the 4th day. The dissolution of Mn2+ in SRW was greater than that in Milli-Q and SSW; moreover, the dissolution of Zn2+ in Milli-Q and SRW was higher than in SSW. Therefore, we could confirm that part of ZnS:Mn NPs (10%) can dissolve in Milli-Q water, as well as SRW and SSW, resulting in increased dissolution of Mn and/or Zn in the 3 media. This can induce some toxicity for the microalgae.

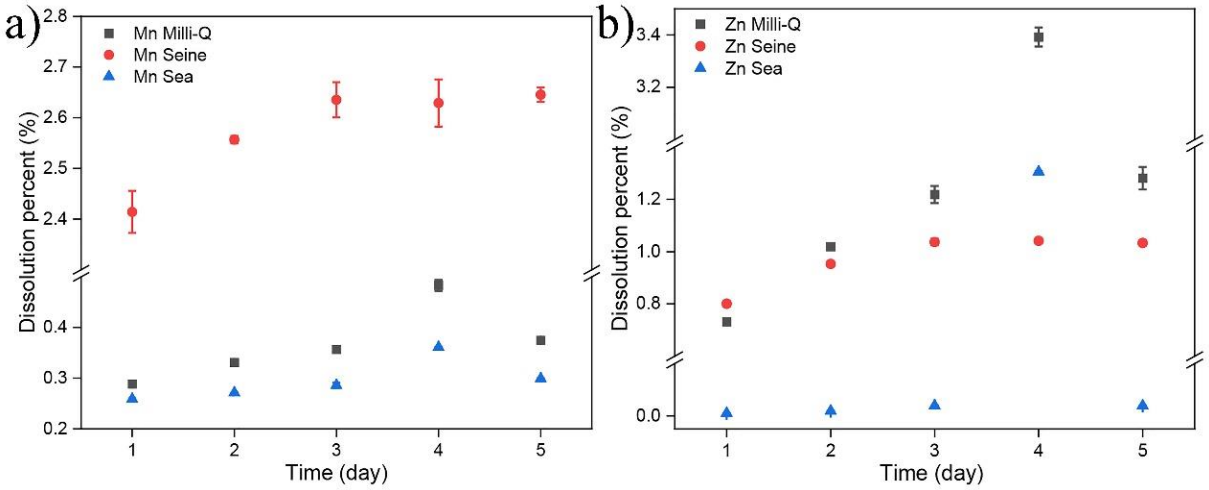

Fig. 44 *Dissolution of Mn^{2+} and Zn^{2+} in different waters.*

3.2. Toxicity analysis

As we wrote in chapter II, ZnS NPs doped with Mn, of small size (about 1.5 nm) have a toxic effect on Chlorella vulgaris. In this Chapter III, we intend to test the influence of NPs size on their toxicity for the algae Chlorella vulgaris; therefore, we prepared ZnS:Mn (10%) NPs of about 8-10 nm. The toxicity of ZnS:Mn (10%) NPs on Chlorella vulgaris was studied according to the same protocol, using the same concentrations (20 mg/L, 50 mg/L and 100 mg/L) of NPs in BG11, SRW and SSW. For each culture medium, we prepared 4 culture flasks (three research groups and one control group). In this Chapter III, we focused on the photosynthetic activity, viability, intracellular ATP content and SOD activity of Chlorella vulgaris.

The chlorella vulgaris culture still came from the Museum National d'Histoire Naturelle (MNHN), and we used the same cultivation protocol: 15 mL of culture from the Chlorella vulgaris collection was mixed in the cell culture flask (capacity 75 cm^2) with 45 mL of culture medium. All cultures were kept in an incubation cabinet with a controlled temperature of 25 ℃ and a daily cycle of 16 h of luminosity (50-80 µmol m^2 s^1 photosynthetic photon flux, PPF) under ambient CO_2 environment.[21] After one week of culture, 1.2 mg (20 mg/L), 3.0 mg (50 mg/L) and 6.0 mg (100 mg/L) of ZnS:Mn (10%) NPs were added to the culture bottles containing 60 mL of Chlorella vulgaris culture, respectively.

In BG11 (Fig. 45 a), the photosynthetic activity of Chlorella vulgaris decreased slightly from the 1st day of the test, in the presence of 100 mg/L of NPs, whereas it only decreased after 72 hours (i.e., 3 days of test) in the presence of 20 mg/L of NPs. In SRW (Fig. 45 b), the photosynthetic activity decreased on the second and third test day in all the research groups, then the algae seemed to have recovered from the toxic effect of the NPs 72h later. Indeed, we observed that they maintained the same photosynthetic activity as the control group. In SSW (Fig. 45 c), the photosynthetic activity increased significantly from the second day of the test, which was probably due to the adaptation of the algae to the presence of the NPs: they could harvest and store necessary elements or nutrients, coming from the NP in nutrient-deficient synthetic seawater.[2,17]

The viability of the algae varied in good agreement with their photosynthetic activity. In BG11 (Fig. 45 d), it decreased slightly on the first and fourth day of testing compared to the control group. In SRW (Fig. 45 e), the viability of Chlorella vulgaris decreased a little during the first two days of testing, after that the algae recovered and maintained

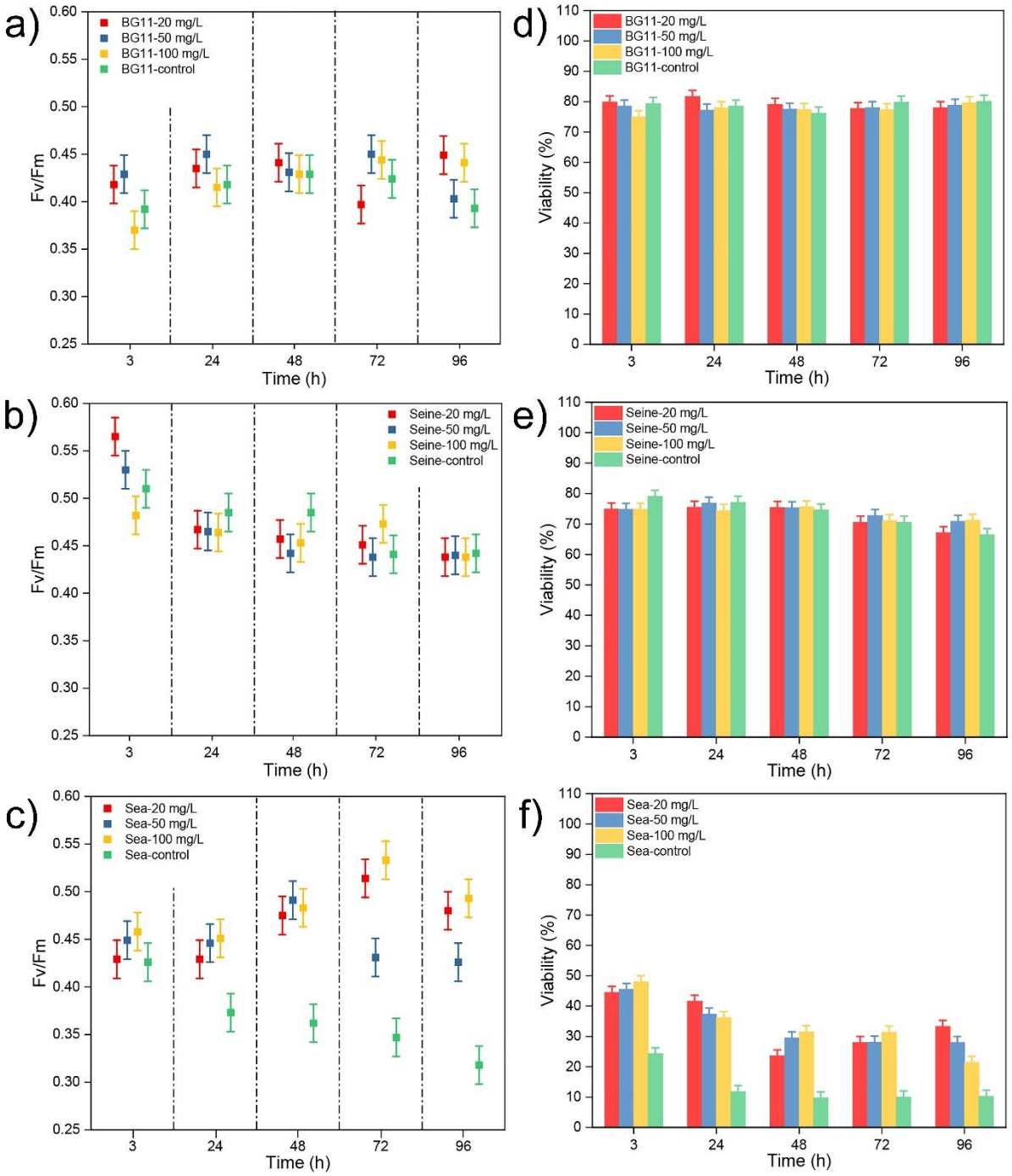

Fig. 45 *PAM data (a-c) and viability (d-f) of Chlorella vulgaris in different culture media contacted with ZnS:Mn (10%) NPs.*

the same level of viability as the control group. In contrast, in SSW (Fig. 45 f), viability increased significantly from the very first to the last day of testing. The most likely reason was that Chlorella vulgaris obtained its essential nutrients from ZnS:Mn (10%) NPs. Furthermore, we have also already mentioned (Fig. 40) the strong propensity of these NPs to aggregate into larger colloids (over 2000 nm), which tends to reduce the toxicity of the NPs for Chlorella Vulgaris.

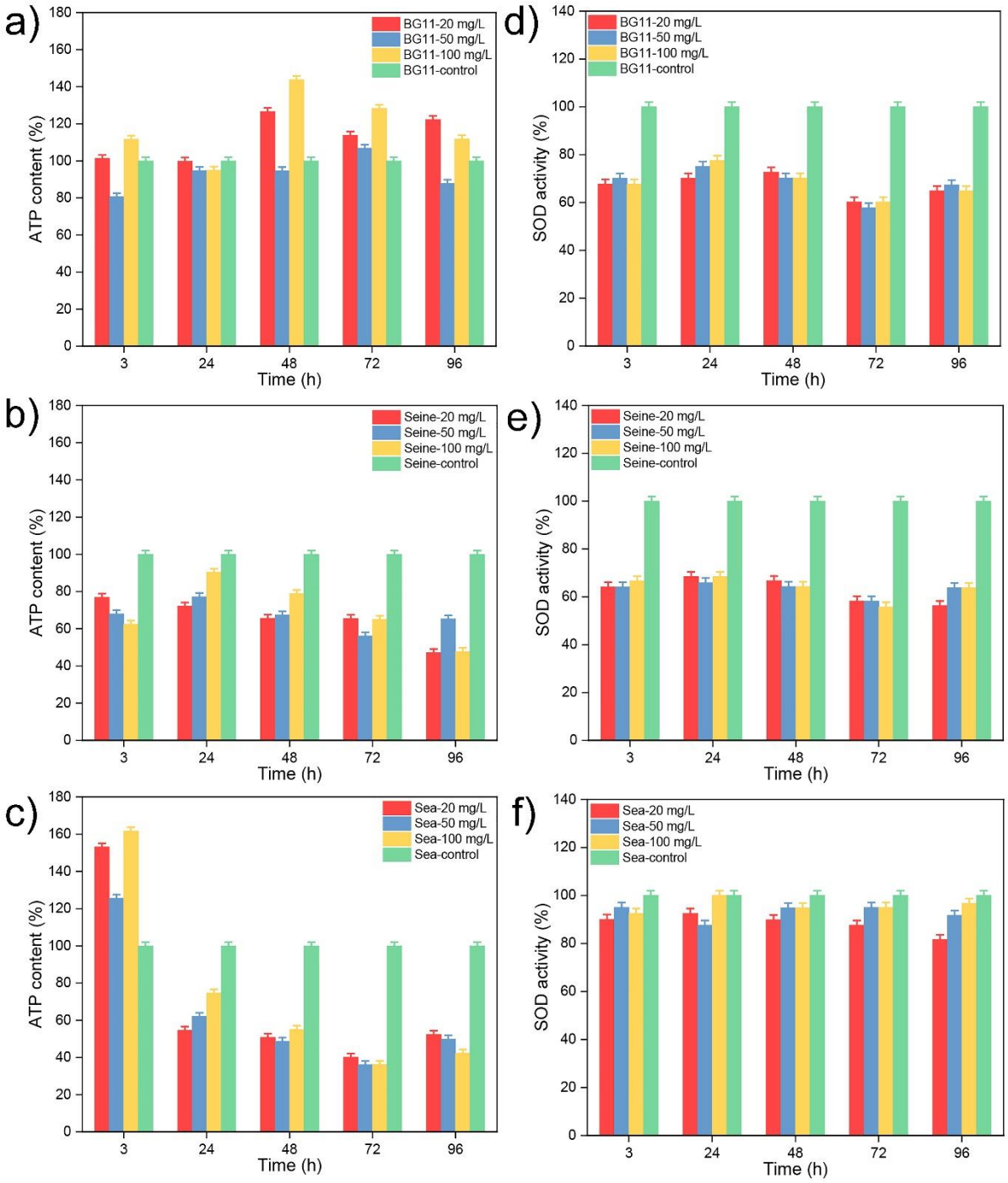

Fig. 46 *ATP (a-c) and SOD (d-f) measurements made on Chlorella vulgaris in different culture media contacted with ZnS:Mn (10%) NPs.*

Intracellular ATP content and SOD activity were also measured to test whether NPs induced ROS production and caused a toxic effect on mitochondrial activity. In BG11 (Fig. 46 a), the ATP content was slightly reduced on the second day of the test in the presence of 20 mg/L and 100 mg/L of NPs. In the presence of 50 mg/L of NPs, the ATP content clearly decreased on the first and last day of the test. In SRW (Fig. 46 b), the ATP content decreased significantly from the first to the last day of testing compared to the control group. In SSW (Fig. 46 c), the ATP content decreased significantly from

the second to the last day of testing. However, in SSW, the viability and photosynthetic activity of Chlorella vulgaris increased significantly. Hence, these results suggest that NPs had a toxic effect on the mitochondrial activity of Chlorella vulgaris, but that microalgae could also benefit from adequate nutrition or from the energy essential to their survival thanks to NPs.

Fig 46 d-f) shows the SOD activity of Chlorella vulgaris in the different media. We observed that the SOD activity decreased in the presence of NPs regardless of the research group, and regardless of the culture medium. Normally, NPs can induce the production of ROS, which causes oxidative stress of algae cells; indeed, to maintain the antioxidant balance of algae cells, SOD will be secreted to dismutate superoxide anions (O_2^-) to oxygen and hydrogen peroxide,[1,22,23] Two reasons could explain a decrease in SOD activity on contact with NPs: firstly, NPs aggregated very easily, as shown by DLS analyzes (Fig. 40), to form far too large colloids (more than 2000 nm) which could not surround the surface of the algae cell. Therefore, photosynthetic activity and viability were not influenced; moreover, the SOD activity did not increase following the production of ROS which would be due to the NPs. The other reason was that the NPs induced oxidative stress in the algae cell, causing the production of ROS to increase, while the excessive accumulation of hydrogen peroxide irreversibly inactivated SOD, which disrupted the synthesis of SOD in the algae cell.[2,24] Moreover, we know that these large ZnS:Mn (10%) NPs were less toxic for Chlorella vulgaris, although the activity of mitochondria was influenced by their presence; in particular, in SRW and SSW, the photosynthetic activity and viability of Chlorella vulgaris were not severely affected.

4. Conclusions

We successfully synthesized, by the polyol process, ZnS NPs doped with different molar concentrations of Mn, presenting a ZnS blende structure, and of size ranged between 8 nm and 10 nm (i.e., larger than the particles described in Chapter II). We were able to confirm that the amount of Mn increased well according to the theoretical molar concentration of Mn. DLS measurements showed that the NPs aggregated into larger colloids, greater than 1720 nm in the three types of medium when the pH was between 4 and 8. Zeta potential measurements confirmed that ZnS:Mn (10%) NPs presented low zeta potentials of -15 to 5 mV in BG11, SRW and SSW, whose pH varied between 2 to 10; these colloids were therefore unstable. Magnetometry measurements showed that most of the samples were paramagnetic materials except the one

containing 10% Mn, which exhibited antiferromagnetic behavior when the temperature was above 150 K, due to the formation of Mn clusters in presence of higher concentrations of Mn.

After that, the fate and behavior of ZnS:Mn (10%) NPs in different aqueous systems were studied. After an ultracentrifugation step, the magnetic properties of the NPs decreased, which means that some of the Mn^{2+} ions were released into the filtrate. XRF and ICP measurements confirmed this result. Thus, we were able to conclude that the Mn^{2+} and Zn^{2+} ions can dissolve in the three types of media.

Finally, we evaluated the toxicity of ZnS:Mn (10%) NPs on Chlorella vulgaris. Photosynthetic activity and algae viability were hardly affected in BG11 and SRW, while they increased in SSW. This is likely because ZnS:Mn (10%) NPs can provide energy or essential nutrients to keep Chlorella vulgaris alive in synthetic seawater. In addition, mitochondrial activity and SOD activity were also measured and we found that the mitochondrial activity of Chlorella vulgaris decreased in all three types of culture media, but more particularly in SRW and SSW. The SOD activity curiously did not increase, probably due to the excessive aggregation of the NPs into very large colloids (larger than 2000 nm), which are not toxic for the Chlorella vulgaris cells. We proposed another reason: it could also be due to an excessive accumulation of hydrogen peroxide which irreversibly inactivated SOD, or even disrupted the synthesis of SOD in algae cells. However, whatever the reason, we can conclude that **large-sized ZnS:Mn (10%) NPs are less toxic than particles of the same composition but of smaller size for Chlorella vulgaris**, since at least, they did not cause cell death.

5. References

(1) Rogers, N. J.; Franklin, N. M.; Apte, S. C.; Batley, G. E.; Angel, B. M.; Lead, J. R.; Baalousha, M. Physico-Chemical Behaviour and Algal Toxicity of Nanoparticulate CeO_2 in Freshwater. *Environ. Chem.* **2010**, *7* (1), 50. https://doi.org/10.1071/EN09123.

(2) Polonini, H. C.; Brandão, H. M.; Raposo, N. R. B.; Brandão, M. A. F.; Mouton, L.; Couté, A.; Yéprémian, C.; Sivry, Y.; Brayner, R. Size-Dependent Ecotoxicity of Barium Titanate Particles: The Case of Chlorella Vulgaris Green Algae. *Ecotoxicology* **2015**, *24* (4), 938–948. https://doi.org/10.1007/s10646-015-1436-6.

(3) Brayner, R.; Dahoumane, S. A.; Yéprémian, C.; Djediat, C.; Meyer, M.; Couté, A.; Fiévet, F. ZnO Nanoparticles: Synthesis, Characterization, and Ecotoxicological Studies. *Langmuir* **2010**, *26* (9), 6522–6528. https://doi.org/10.1021/la100293s.

(4) Djurišić, A. B.; Leung, Y. H.; Ng, A. M. C.; Xu, X. Y.; Lee, P. K. H.; Degger, N.; Wu, R. S. S. Toxicity of Metal Oxide Nanoparticles: Mechanisms, Characterization, and Avoiding Experimental Artefacts. *Small* **2015**, *11* (1), 26–44. https://doi.org/10.1002/smll.201303947.

(5) Ramachandran, R.; Saranya, M.; Kollu, P.; Raghupathy, B. P. C.; Jeong, S. K.; Grace, A. N. Solvothermal Synthesis of Zinc Sulfide Decorated Graphene (ZnS/G) Nanocomposites for Novel Supercapacitor Electrodes. *Electrochimica Acta* **2015**, *178*, 647–657. https://doi.org/10.1016/j.electacta.2015.08.010.

(6) Ramachandran, R.; Saranya, M.; Kollu, P.; Raghupathy, B. P. C.; Jeong, S. K.; Grace, A. N. Solvothermal Synthesis of Zinc Sulfide Decorated Graphene (ZnS/G) Nanocomposites for Novel Supercapacitor Electrodes. *Electrochimica Acta* **2015**, *178*, 647–657. https://doi.org/10.1016/j.electacta.2015.08.010.

(7) Labiadh, H.; Sellami, B.; Khazri, A.; Saidani, W.; Khemais, S. Optical Properties and Toxicity of Undoped and Mn-Doped ZnS Semiconductor Nanoparticles Synthesized through the Aqueous Route. *Optical Materials* **2017**, *64*, 179–186. https://doi.org/10.1016/j.optmat.2016.12.011.

(8) Elidrissi, B.; Addou, M.; Regragui, M.; Bougrine, A.; Kachouane, A.; Bernède, J. C. Structure, Composition and Optical Properties of ZnS Thin Films Prepared by Spray Pyrolysis. *Materials Chemistry and Physics* **2001**, *68* (1), 175–179. https://doi.org/10.1016/S0254-0584(00)00351-5.

(9) Jrad, A.; Naouai, M.; Abdallah, A.; Ammar, S.; Turki-Kamoun, N. Doping ZnS Films with Cobalt: Structural, Compositional, Morphological, Optical, Electrical, Magnetic and Photocatalytic Properties. *Physica B: Condensed Matter* **2021**, *603*, 412776. https://doi.org/10.1016/j.physb.2020.412776.

(10) Yiju, Li; Guiling, Wang; Tong Wei; Zhuangjun, Fan; Peng Yan. Nitrogen and Sulfur Co-Doped Porous Carbon Nanosheets derived from willow catkin for supercapacitors. Nanoenergy **2015**, 19, 165-175, https://doi.org/10.1016/j.nanoen.2015.10.038.

(11) Saavedra Rodríguez, G.; Carrillo Torres, R. C.; Sánchez Zeferino, R.; Álvarez Ramos, M. E. Stabilized Blue Emitting ZnS@SiO_2 Quantum Dots. *Optical Materials* **2019**, *89*, 396–401. https://doi.org/10.1016/j.optmat.2019.01.057.

(12) Adegoke, O.; Mashazi, P.; Nyokong, T.; Forbes, P. B. C. Fluorescence Properties of Alloyed ZnSeS Quantum Dots Overcoated with ZnTe and ZnTe/ZnS Shells. *Optical Materials* **2016**, *54*, 104–110. https://doi.org/10.1016/j.optmat.2016.02.024.

(13) Cao, J.; Yang, J.; Yang, L.; Wei, M.; Feng, B.; Han, D.; Fan, L.; Wang, B.; Fu, H. The Effects of Doping and Shell Thickness on the Optical and Magnetic Properties of Mn/Cu/Fe-Doped and Co-Doped ZnS Nanowires/ZnO Quantum Dots/SiO_2 Heterostructures. *Journal of Applied Physics* **2012**, *112* (1), 014316. https://doi.org/10.1063/1.4733948.

(14) Sousa, C. A.; Soares, H. M. V. M.; Soares, E. V. Chronic Exposure of the Freshwater Alga Pseudokirchneriella Subcapitata to Five Oxide Nanoparticles: Hazard Assessment and Cytotoxicity Mechanisms. *Aquatic Toxicology* **2019**, *214*, 105265. https://doi.org/10.1016/j.aquatox.2019.105265.

(15) Darbandi, M.; Urban, G.; Krüger, M. A Facile Synthesis Method to Silica Coated CdSe/ZnS Nanocomposites with Tuneable Size and Optical Properties. *Journal of Colloid and Interface Science* **2010**, *351* (1), 30–34. https://doi.org/10.1016/j.jcis.2010.07.043.

(16) Pereira, M. M.; Mouton, L.; Yéprémian, C.; Couté, A.; Lo, J.; Marconcini, J. M.; Ladeira, L. O.; Raposo, N. R.; Brandão, H. M.; Brayner, R. Ecotoxicological Effects of Carbon Nanotubes and Cellulose Nanofibers in Chlorella Vulgaris. *J Nanobiotechnol* **2014**, *12* (1), 15. https://doi.org/10.1186/1477-3155-12-15.

(17) Planchon, M.; Ferrari, R.; Guyot, F.; Gélabert, A.; Menguy, N.; Chanéac, C.; Thill, A.; Benedetti, M. F.; Spalla, O. Interaction between Escherichia Coli and TiO_2 Nanoparticles in Natural and Artificial Waters. *Colloids and Surfaces B: Biointerfaces* **2013**, *102*, 158–164. https://doi.org/10.1016/j.colsurfb.2012.08.034.

(18) Jahanbin, T.; Gaceur, M.; Gros-Dagnac, H.; Benderbous, S.; Merah, S. A. High Potential of Mn-Doped ZnS Nanoparticles with Different Dopant Concentrations as Novel MRI Contrast Agents: Synthesis and in Vitro Relaxivity Studies. *J Nanopart Res* **2015**, *17* (6), 258. https://doi.org/10.1007/s11051-015-3038-x.

(19) Tsujii, N.; Kitazawa, H.; Kido, G. Magnetic Properties of Mn- and Eu-Doped ZnS Nanocrystals. *Journal of Applied Physics* **2003**, *93* (10), 6957–6959. https://doi.org/10.1063/1.1540034.

(20) Sirkeli, V. P.; Nedeoglo, D. D.; Nedeoglo, N. D.; Radevici, I. V.; Sobolevskaia, R. L.; Sushkevich, K. D.; Lähderanta, E.; Lashkul, A. V.; Laiho, R.; Biethan, J.-P.; Yilmazoglu, O.; Pavlidis, D.; Hartnagel, H. L. Magnetic and Luminescent Properties of Manganese-Doped ZnSe Crystals. *Physica B: Condensed Matter* **2012**, *407* (18), 3802–3807. https://doi.org/10.1016/j.physb.2012.05.064.

(21) Dahoumane, S. A.; Yéprémian, C.; Djédiat, C.; Couté, A.; Fiévet, F.; Coradin, T.; Brayner, R. Improvement of Kinetics, Yield, and Colloidal Stability of Biogenic Gold Nanoparticles Using Living Cells of Euglena Gracilis Microalga. *J Nanopart Res* **2016**, *18* (3), 79. https://doi.org/10.1007/s11051-016-3378-1.

(22) Polonini, H. C.; Brandão, H. M.; Raposo, N. R. B.; Mouton, L.; Yéprémian, C.; Couté, A.; Brayner, R. Ecotoxicological Studies of Micro- and Nanosized Barium Titanate on Aquatic Photosynthetic Microorganisms. *Aquatic Toxicology* **2014**, *154*, 58–70. https://doi.org/10.1016/j.aquatox.2014.05.005.

(23) Munk, M.; Brandão, H. M.; Nowak, S.; Mouton, L.; Gern, J. C.; Guimaraes, A. S.; Yéprémian, C.; Couté, A.; Raposo, N. R. B.; Marconcini, J. M.; Brayner, R. Direct and Indirect Toxic Effects of Cotton-Derived Cellulose Nanofibres on Filamentous Green Algae. *Ecotoxicology and Environmental Safety* **2015**, *122*, 399–405. https://doi.org/10.1016/j.ecoenv.2015.09.001.

(24) Župan, G.; Vitezić, D.; Mršić, J.; Matešić, D.; Simonić, A. Effects of Nimodipine, Felodipine and Amlodipine on Electroconvulsive Shock-Induced Amnesia in the Rat. *European Journal of Pharmacology* **1996**, *310* (2), 103–106. https://doi.org/10.1016/0014-2999(96)00534-1.

Chapter IV. Ecotoxicological effects of Mn, Cu, Co monodoped ZnS quantum dots on Chlorella vulgaris. Influence of the transition metal cation.

1. Introduction

Heavy metal trace elements are also essential micronutrients for the many metabolic activities of living cells; these include copper (Cu), cobalt (Co), manganese (Mn) and zinc (Zn).[1–3] However, they can be very toxic to most prokaryotes and eukaryotes when the metal concentrations are excessive.[4] Ions like Mn^{2+}, Cu^{2+}, Co^{2+} and Cr^{3+} are also used as dopants of ZnS nanoparticles, widely used in gas-sensor, photocatalytic and optical applications,[5–7] in order to enhance their physico-chemical properties. Therefore, we wanted to study the toxicity of ZnS NPs containing different transition metal cations used as different dopants on Chlorella vulgaris algae.

We present here the synthesis of ZnS nanoparticles doped with Mn, Cu and Co, using the microwave-assisted polyol method. We varied the molar concentration of the transition metals: 0.5%, 1.0%, 1.5%, 5.0%, 10% and 20%. The NPs were all of cubic structure and size between 1.4 and 3 nm. These NPs exhibited interesting optical properties, in particular the ZnS:Mn (10%) NPs, which emitted yellow-orange light at the excitation wavelength of 330 nm.

2. Experimental

2.1. Synthesis of Mn, Cu, Co monodoped ZnS NPs by microwave-assisted polyol method

All chemicals were of analytical grade and used without any further purification. Manganese acetate tetrahydrate (≥ 99%, $Mn(CH_3COO)_2.4H_2O$), diethylene glycol (DEG) ($OH(CH_2)_2O(CH_2)_2OH$), and thioacetamide (TAA, CH_3CSNH_2) were purchased from Sigma-Aldrich, zinc acetate dihydrate (98+%, $Zn(CH_3COO)_2.2H_2O$), copper (II) acetate anhydrous ($Cu(OOCCH_3)_2$) were purchased from ACROS ORGANICS, cobalt (II) acetate anhydrous (98+%, $Co(OOCCH_3)_2$) was purchased from Thermo Scientific.

We synthesized ZnS NPs monodoped with Mn, Cu, and Co by the microwave-assisted polyol method.

Synthesis of ZnS:Mn. 87.8 mg of zinc acetate dihydrate were mixed with a variable amount of manganese acetate tetrahydrate (1.0 mg, 2.0 mg, 3.0 mg, 10.8 mg, 24.5 mg and 65.4 mg) in 80 ml of DEG, in the presence of 45.1 mg of TAA, to obtain ZnS:Mn NPs containing a molar concentration of Mn equal to 0.5%, 1.0%, 1.5%, 5%, 10% and 20% , respectively). After the reagents were dissolved by sonication in the polyol, the solutions were transferred to the microwave oven, heating at the power of 220 W for 30 min. Finally, the samples were recovered after 3 cycles of washing with ethanol and centrifugation (at 22,000 rpm) and drying at 60°C overnight.

Synthesis of ZnS:Cu and ZnS:Co. The ZnS:Mn synthesis protocol was adapted by just replacing manganese acetate tetrahydrate with copper acetate (Ⅱ) anhydrous (0.7 mg, 1.5 mg, 2.2 mg, 8.0 mg , 18.2 mg and 48.5 mg) or cobalt acetate (Ⅱ) anhydrous (0.7 mg, 1.4 mg, 2.2 mg, 7.8 mg, 17.7 mg and 47, 3mg). Due to the difficulties encountered in inserting the transition cations into the crystal lattice of ZnS, we introduced twice the theoretical masses during each synthesis.

2.2. Algae culture

The green algae Chlorella vulgaris came from a collection of the Museum National d'Histoire Naturelle (MNHN). Chlorella vulgaris is a single-cell eukaryotic planktonic green alga, which was cultivated in a 75 cm^2 cell culture flask purchased from Thermofisher, in (i) sterile BG11 medium (pH 7.30), (ii) Seine River water (SRW, pH 8.11) and (iii) synthetic seawater (SSW, pH 7.81). All cultures were incubated at a controlled temperature of 25 ℃ and a daily cycle of 16 h of luminosity (50-80 µmol m^2 s^1 photosynthetic photon flux, PPF) under ambient CO_2 environment was applied.[8]

3. Results and discussion

3.1. Characterization of Mn, Cu, Co monodoped ZnS NPs

Fig. 47 shows the XRD patterns of all the ZnS NPs doped with Mn, Co, and Cu. All the patterns presented rather broad peaks at 33.8°, 56.7°, 66.9°, which were matching well with the (111), (220), (311) crystalline planes of cubic ZnS phase (COD no. 5000088) and revealed a nanometer size. Moreover, no impurity was found.[9] The crystal sizes of 10% Mn, Cu, Co monodoped ZnS NPs were ranging from 1.4 nm to 1.8 nm as determined by computational Rietveld refinements using MAUD software. In addition, the average crystal size was also estimated by Scherrer's formula based on the diffraction peaks full-width maximum (FWHM):[10]

$$D = \frac{k\lambda}{\beta cos\theta},$$

where D is the average size of the particles, k is the particle shape factor (0.89), λ is the X-ray wavelength (0.179 nm), β is the FWHM of the diffraction peak, θ is the Bragg diffraction angle. The calculated average crystalline sizes of the 10% Mn, Cu, Co doped ZnS NPs were 2.6 nm, 3.0 nm and 2.9 nm respectively, which was in agreement with the average diameter deduced from TEM analysis (Fig. 50).

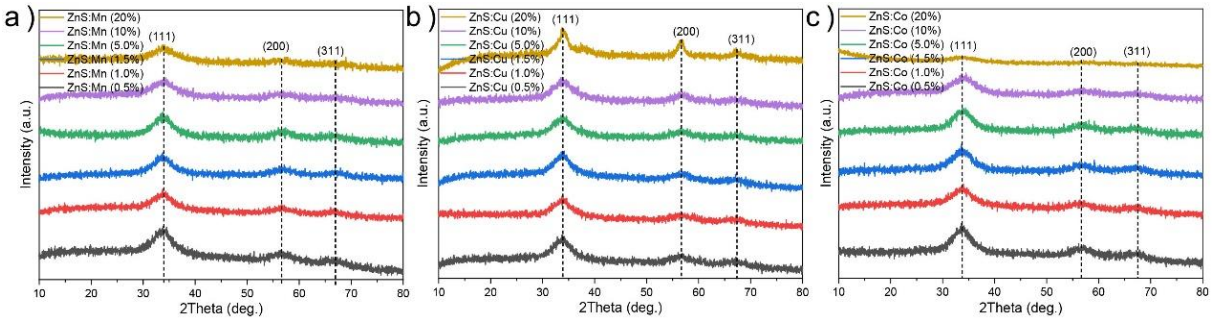

Fig. 47 *XRD patterns of different molar concentration Mn, Cu, Co monodoped ZnS NPs.*

X-ray fluorescence (XRF) measurements were performed to confirm the composition of the NPs. The Mn, Cu, and Co contents are shown in Table 6. We observe that the actual Mn content is lower than expected, despite the stoichiometric excess introduced during the synthesis. However, the actual Cu and Co contents are higher than the expected proportions due to the excess introduced.

Table 6 *XRF data: different molar concentration of Mn, Cu, Co in monodoped ZnS NPs.*

NPs		Mn	Cu	Co
ZnS: M (0.5%)	mass (µg)	0.075	0.487	0.618
	%mol	0.26	1.22	1.07
ZnS: M (1.0%)	mass (µg)	0.219	0.885	0.723
	%mol	0.68	2.31	2.03
ZnS: M (1.5%)	mass (µg)	0.653	1.1	0.862
	%mol	2.05	2.43	3.09
ZnS: M (5.0%)	mass (µg)	2.489	6.237	4.218
	%mol	6.27	10.99	10.04
ZnS: M (10%)	mass (µg)	4.176	10.811	8.348
	%mol	9.69	19.97	19.61
ZnS: M (20%)	mass (µg)	7.126	21.617	6.721
	%mol	26.98	50.99	31.46

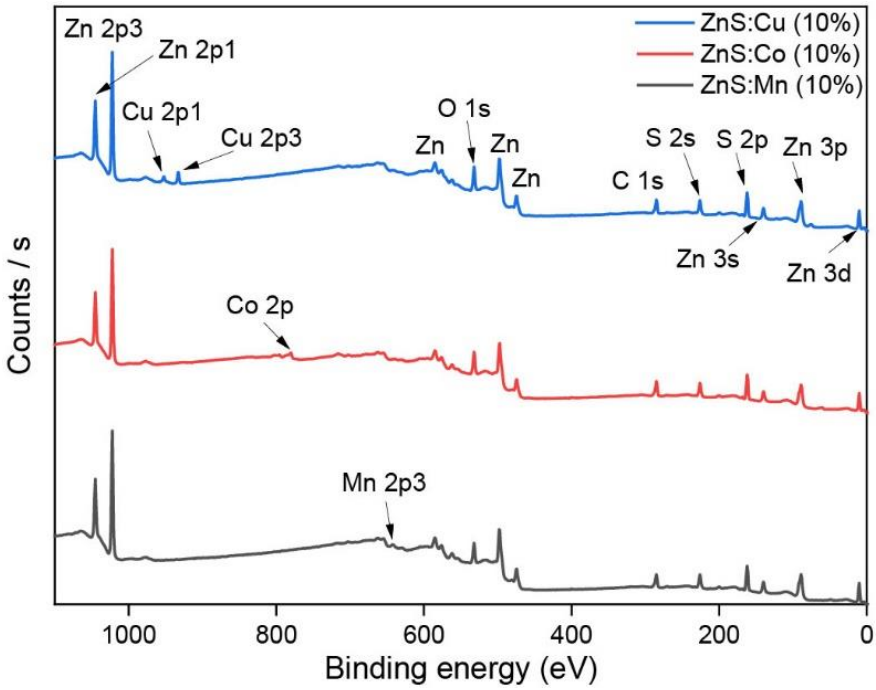

Fig.48 *XPS survey spectra of the 10% Mn, Cu, Co monodoped ZnS NPs, the spectra calibration was performed by setting the main C 1s at 285 eV.*

XPS measurements were performed to assess the elemental surface chemical composition of these NPs. [11] Survey spectra of ZnS NPs containing 10% Mn, Cu, Co are shown in Fig. 48, and clearly showed the peaks corresponding to Zn 2p, S 2p, Mn 2p, Cu 2p and Co 2p at binding energies of 1022, 162, 642, 933, 779 eV, respectively. The O 1s peak at 532 eV is attributed to chemisorbed oxygen species [12] or suggests mild surface oxidation of ZnS NPs. The peaks located at 475, 496 and 586 eV correspond to the Auger lines of Zn. [12,13]

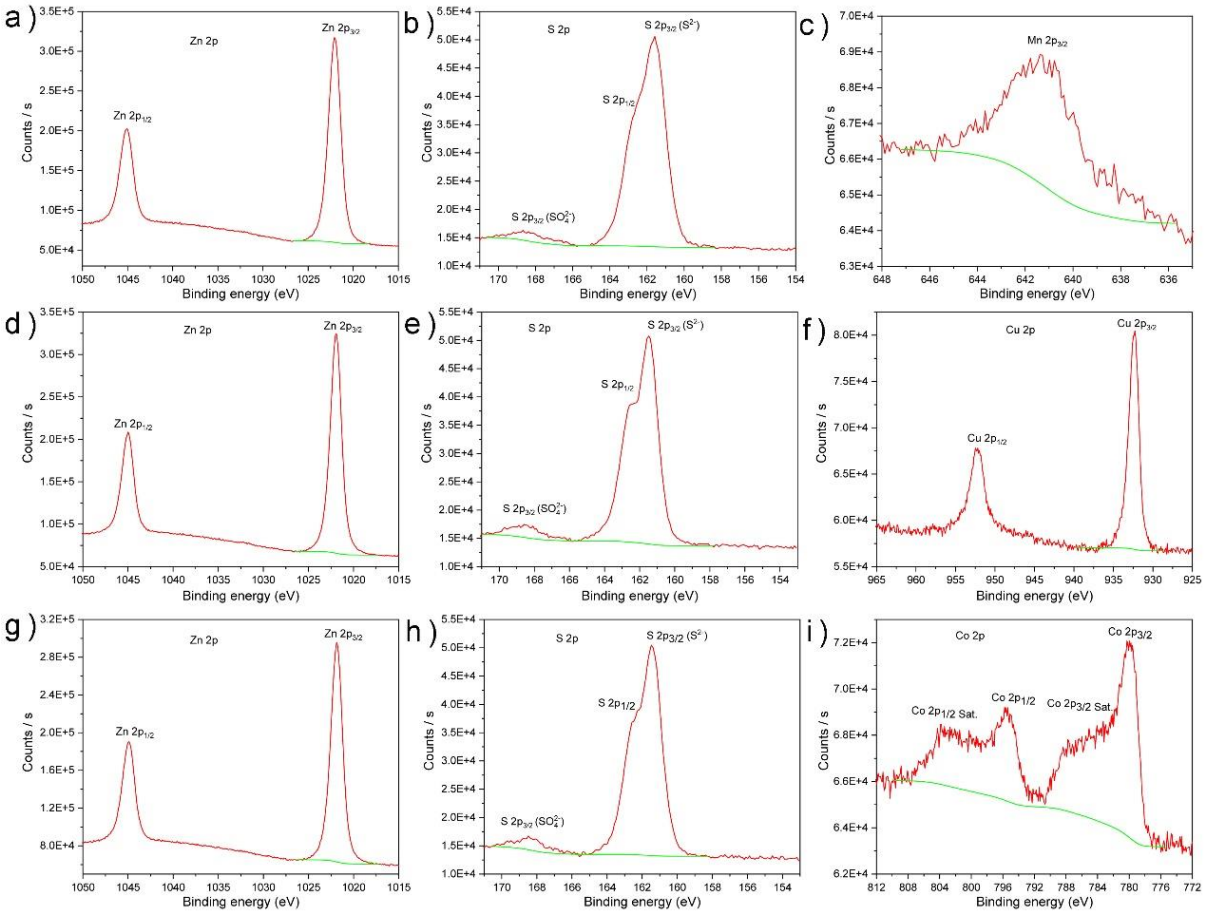

Fig. 49 *High resolution spectra of Zn 2p, S 2p, Mn 2p, Cu 2p, Co 2p signals recorded on ZnS: Mn (10%) (a-c), ZnS: Cu (10%) (d-f), ZnS: Co (10%) (g-i).*

High resolution XPS spectra of Zn, S, Mn, Cu, Co elements contained in ZnS nanoparticles (10%) are shown in Fig. 49. The peaks present at 1044.9 eV and 1021.8 eV, corresponding to Zn $2p_{1/2}$ and Zn $2p_{3/2}$ (Fig. 49 a, d, g) were characteristic of the presence of Zn^{2+} ions in ZnS: the difference between the two peaks, resulting from the spin-orbit coupling was approximately 23 eV.[12,14] The peak corresponding to S (Fig. 49 b, e, h) contained two components of different intensity. The one, of higher intensity, located at 161.4 eV, could be fitted by two peaks, corresponding to the binding energies of S $2p_{3/2}$ and S $2p_{1/2}$, at 161.4 eV and 162.5 eV, which are assigned to the anion S^{2-}. The other of lower intensity, at around 168.4 eV, was attributed to the oxidized form

SO_4^{2-} [11,15] suggesting the partial oxidation of the surface of the ZnS NPs. The peak corresponding to Mn $2p_{3/2}$ (Fig. 49 c) centered at 641.4 eV is a bit weak in intensity, due to the low concentration of Mn at the surface of the ZnS NPs.[16–18] The binding energies of Cu $2p_{1/2}$ and Cu $2p_{3/2}$ (Fig. 49 f) were centered at 952.2 eV and 932.3 eV respectively; the splitting corresponding to the spin-orbit coupling was 19.9 eV, characteristic of copper ions.[19] However, the presence of shake-up peaks around 946 eV and 958 eV, characteristic of Cu^{2+}, allows us to conclude on the oxidation state of copper.[20,21] The binding energies of Co $2p_{1/2}$ and Co $2p_{3/2}$ were centered at 795.7 eV and 779.9 eV (Fig. 49 i) and the energy splitting between these two peaks was 15.8 eV. Shake-up peaks of Co $2p_{1/2}$ and Co $2p_{3/2}$ were present at 803.9 eV and 787.7 eV, respectively, confirming the presence of Co^{2+} cations.[6,22,23]

The size and morphology of ZnS NPs doped with 10% Mn, Cu, or Co were evaluated by TEM (Fig. 50). The crystal lattice corresponded well to a blende structure, in agreement with the XRD patterns. Statistical analysis of the size distribution of NPs doped with 10% Mn, Cu and Co, gave sizes of 3.5 ± 1.1 nm, 3.8 ± 1.3 nm, and 3.3 ± 1 nm, respectively. The EDX analyzes revealed the presence of Zn, S and Mn, or Cu, or Co. The copper found during the observations of the NPs doped with Mn and Co came from the copper TEM grid, while the Ni found during the observation of ZnS:Cu NPs came from the Ni TEM grid. The presence of chromium in all samples came from the instrument. Therefore, we could confirm that no impurities were found in our samples.

Fig. 51 presents the UV-vis absorbance spectra of ZnS NPs doped with different molar concentrations of Mn, Cu, and Co and recorded at room temperature. The characteristic absorption peak of ZnS NPs is centered in the range of 250 to 320 nm and allows the determination of the bandgap of NPs.[24,25] It was centered at 302 nm for pure ZnS. The position of the absorption peak of ZnS NPs doped with transition metal cations varied depending on the metal and the doping rate. As shown in Fig. 51 a), the absorbance peaks of the ZnS NPs doped with low concentration of Mn (0.5%, 1.0% and 1.5%) were centered at 304 nm, 307 nm, 309 nm, respectively. However, when the Mn concentration was further increased (5.0%, 10% and 20%), the absorbance peak exhibited a blue shift, and was then centered at 307 nm, 304 nm and 298 nm respectively. ZnS NPs doped with Cu or Co behave similarly. ZnS:Cu absorption peaks were located at 306 nm, 311 nm, 316 nm, 312 nm, 310 nm and 258 nm, corresponding to increasing Cu doping concentrations (Fig. 51 b). The ZnS:Co absorption peaks were located at 310 nm, 312 nm, 314 nm, 304 nm, 302 nm and 282 nm corresponding to the different Co concentrations (Fig. 51 c).

Besides, the edge of the absorption peak slightly shifted to higher wavelength (red shift) using the lowest concentrations of dopant (0.5%, 1.0% and 1.5%) NPs. This revealed the progressive replacement of Zn^{2+} by M^{2+} (M = Mn, Cu, Co) in ZnS lattice, suggesting the insertion of new M^{2+} cations. [26,27] However, when the dopant concentration increased (5.0%, 10% 20%), the absorbance edge shifted to lower wavelength (blue shift), that could be ascribed to a reduction of the particle size, which could cause the quantum confinement effect of the excitons present in samples.[28–30]

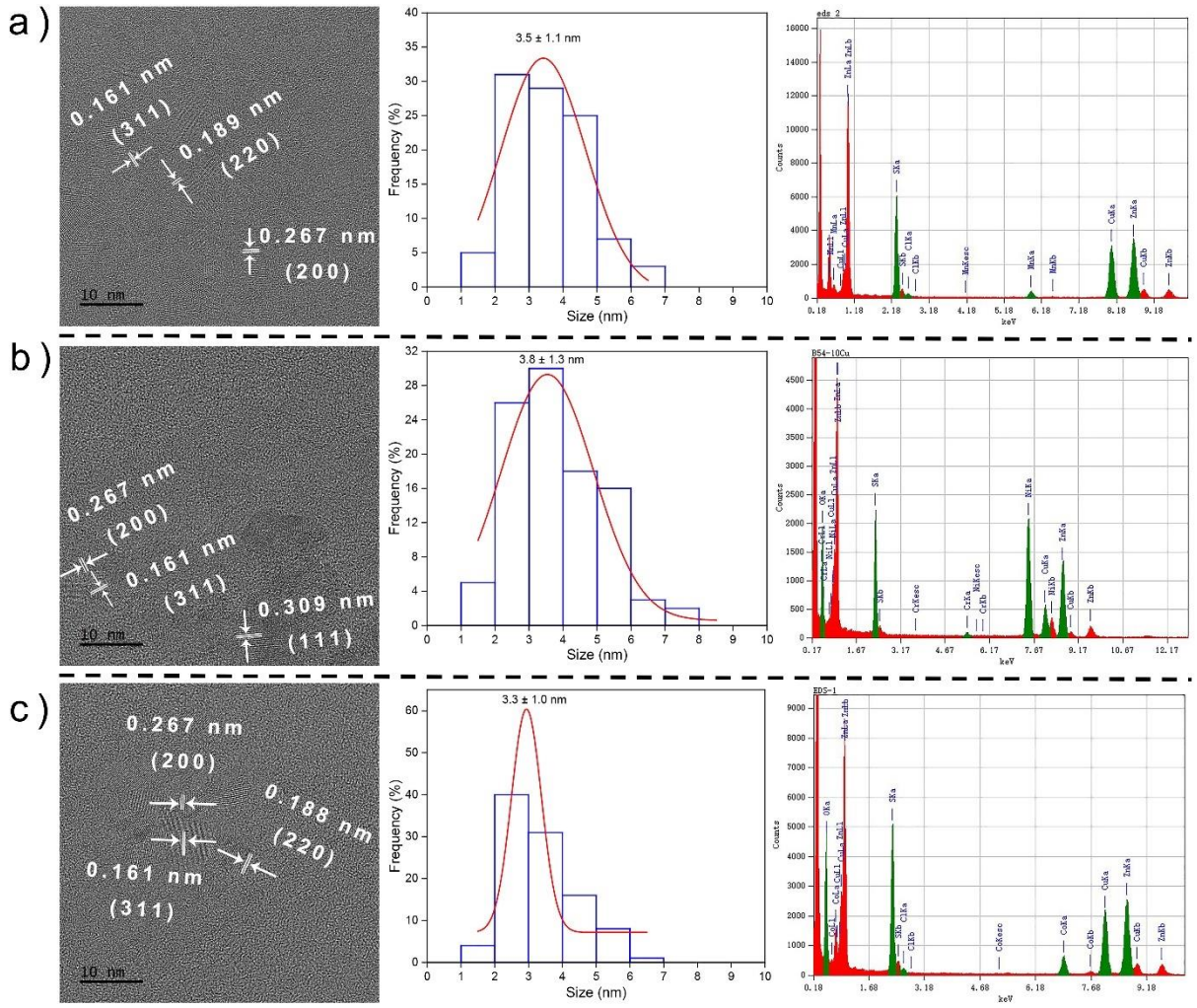

Fig. 50 *TEM images, size distribution and EDX analysis of 10% Mn, Cu, Co monodoped ZnS NPs a) ZnS:Mn, b) ZnS:Cu, c) ZnS:Co.*

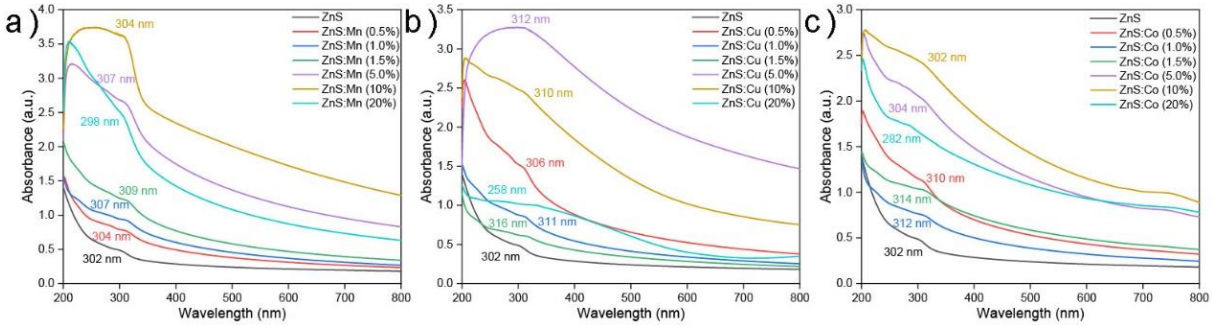

Fig. 51 *UV-vis absorbance spectra of ZnS NPs doped with different concentrations of a) Mn, b) Cu, c) Co.*

Photoluminescence (PL) measurement can provide information on the energy states of impurities and defects even in a very low concentrations; therefore, it is a useful technique to know the structure of defects in semiconductors.[31] The PL spectra of NPs doped with low concentrations (0.5%, 1.0%, 1.5% and 5.0%) of Mn, Cu, and Co are shown in Fig. 52. The excitation wavelength of ZnS:Mn NPs was 330 nm (Fig. 52 a); the emission peak is red-shifted compared to undoped ZnS NPs (peak centered at 389 nm). A high intensity peak was also observed at 585 nm (yellow-orange) and corresponded to the $^4T_1$-$^6A_1$ spin forbidden transition of Mn^{2+}.[5,24,32]

As the Mn dopant concentration increased, the emission wavelength did not present any noticeable change; we could assume that the energy level of the defect states or sulfur vacancies related to the valence band remained constant.[31] However, the intensity of the emission peak intensity increased first and then decreased, which could be attributed to a quantum quenching, observed for high concentrations of dopant.[24]

The PL spectra of ZnS:Cu NPs containing different Cu concentrations are shown in Fig. 52 b). Emission spectra were recorded at room temperature, at an excitation wavelength of 300 nm. The emission peak located at 437 nm (blue band), can be ascribed to the transition of electrons from the sulfur vacancy states to the valence band. Cu^{2+} doping resulted in the creation of additional sulfur vacancies.[33,34] However, since copper can act as a normal acceptor at lower concentration, the intensity first decreased (from 0.5% Cu to 1.0% Cu) and then increased with 5.0% Cu, because Cu can act as a normal acceptor at a lower concentration, hence a higher PL was observed.[34]

Fig. 52 c) shows the PL spectra of ZnS:Co NPs with different Co concentrations, obtained with an excitation wavelength of 344 nm. A weak emission peak was obtained, centered at 517 nm (green). This green emission must rather come from the impurities

than from the ZnS, due to a transition of the electrons from the states of the conduction band to t_2 level.[35,36]

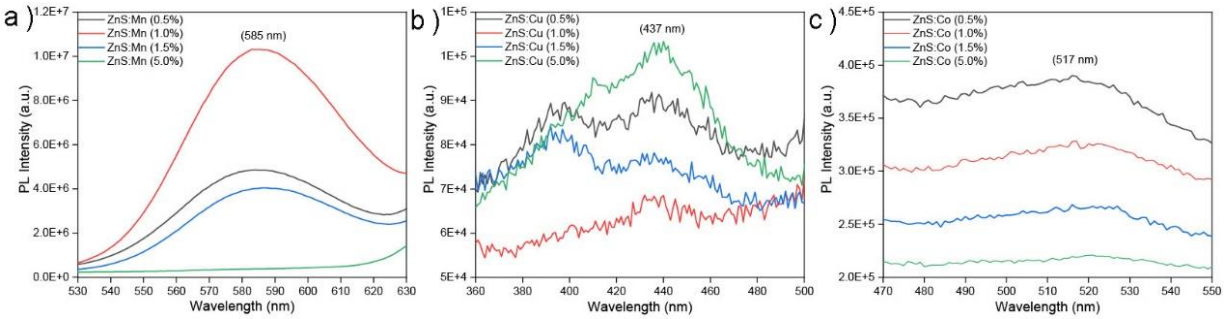

Fig. 52 *PL spectra of ZnS NPs doped with different molar concentrations a) Mn, b) Cu, c) Co.*

3.2. Toxicity analysis

According to the results of the characterizations of the optical properties by UV-vis and PL spectroscopies, it can be envisaged to use these ZnS NPs doped with different transition metal ions in luminescent devices (at a lower concentration of Mn, Cu or Co) or in magnetic bimodal imaging probes (with a higher concentration of Mn, Cu or Co).[37] However, as the potential toxicity of these ZnS NPs is not fully elucidated, we investigated the behavior of microalgae (Chlorella vulgaris) in the presence of ZnS NPs doped with 10% Mn, Cu and Co.

Fig. 53 a-c) shows the photosynthetic activity of Chlorella vulgaris in contact with different concentrations (20 mg/L, 40 mg/L and 60 mg/L) of ZnS NPs containing 10% of Mn in BG11, Seine River water (SRW), and synthetic seawater (SSW). In BG11, the photosynthetic activity (F_v/F_m) decreased slightly after 3h and 72h of contact with the NPs compared to the control group. Then, it increased again; this means that Chlorella vulgaris can recover from NPs toxicity.[38] In SRW, the photosynthetic activity decreased 3h, 48h and 72h later, and after 96h it recovered to the level of that of the control group. In SSW, photosynthetic activity significantly decreased 3h later compared to the control group. This decrease continued a long time and then the photosynthetic activity returned to the level of that of the control group 96 hours later. Photosynthetic activity is closely associated with ROS production,[39,40] which can be induced by NPs, as previously discussed. In this case, the decrease in photosynthetic activity can be attributed to the production of ROS (reactive oxygen species).

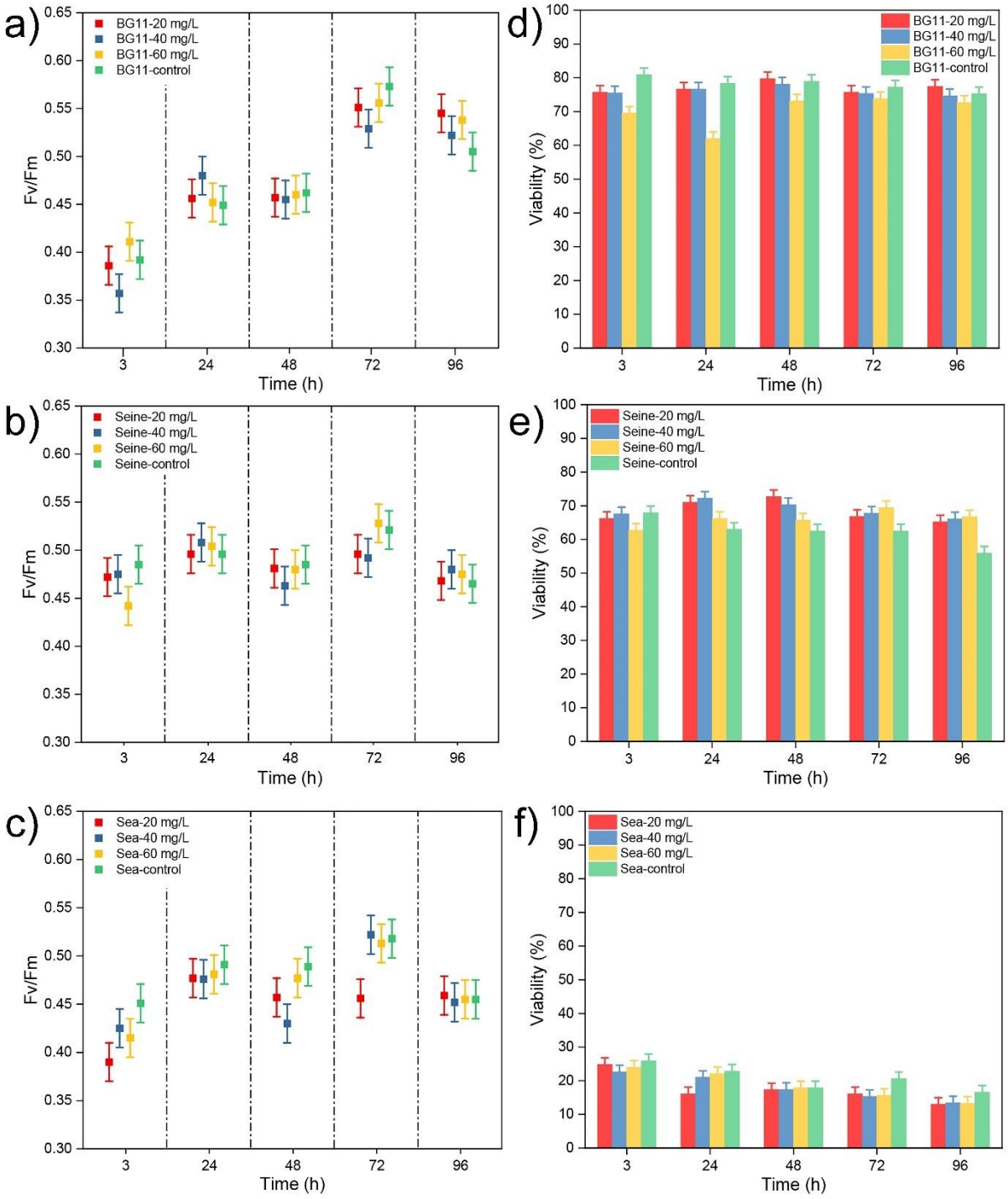

Fig. 53 *Toxicity tests carried out on ZnS:Mn (10%) in different water systems, a-c) PAM, d-f) viability.*

Fig. 53 d-f) shows the viability of Chlorella vulgaris in different aqueous systems after contact with the NPs in the culture medium. In BG11, the viability of Chlorella vulgaris clearly decreased after 3h of contact with ZnS:Mn (10%) whatever the concentration of NPs, but more particularly in the presence of 60 mg/L. The viability was systematically lower than the control group during the test period except in the presence of 20 mg/L of NPs. In SSW, the algal viability also decreased significantly, throughout the test period compared to the control group. It was always less than 30%

even in control group, which is probably due to nutritional deficiencies and the expression of cell membrane proteins that were influenced by the SSW medium.[8,41] Viability in SRW also decreased 3h later, before recovering the level of the control group. We can conclude that NPs can induce cell death whatever the culture medium. The reasons for cell death are complex: we can cite the production of ROS,[42] or the NPs attached to the algae can influence the cellular uptake of nutrients, causing cell death,[38] or the expression of cell membrane proteins.[8]

Mitochondrial activity of microalgae was measured through intracellular ATP content (Fig. 54 a-c). Mitochondria, as an important organelle, is responsible for the production of ATP, the production of ROS, and also the release of the proteins controlling the apoptosis. Therefore, mitochondria are directly related to cell death.[8,39] We observe that the ATP content decreased after 3h of contact with the NPs in all the media, even in the presence of low concentrations of NPs. In addition, the influence of NPs on the mitochondria continued over time (for 72h or 96 hours). The decrease in ATP content reduced the activity of mitochondria, which means that the ZnS:Mn NPs disrupted the energetic metabolism of the Chlorella vulgaris cell.

As we have already discussed, the production of ROS (which are the main cause of the toxicity of NPs), can be detected by the activity of superoxide dismutase (SOD) (Fig. 54 d-f). SOD is one of the most important antioxidant enzymes produced by cells, it can catalyze the dismutation of superoxide (O_2^-) anions into oxygen and hydrogen peroxide. SOD may therefore protect cells from ROS toxicity.[39,42] In Fig. 54, the activity of SOD clearly increased after the addition of NPs, and this, in all the culture media; the SOD activity was higher than that of the control group during the first three days of testing, and almost maintained at the lower steady state (compared to the control group) 72h later. Moreover, the SOD activity was consistent with the results obtained previously concerning the measurements of photosynthetic activity, viability, and activity of mitochondria.

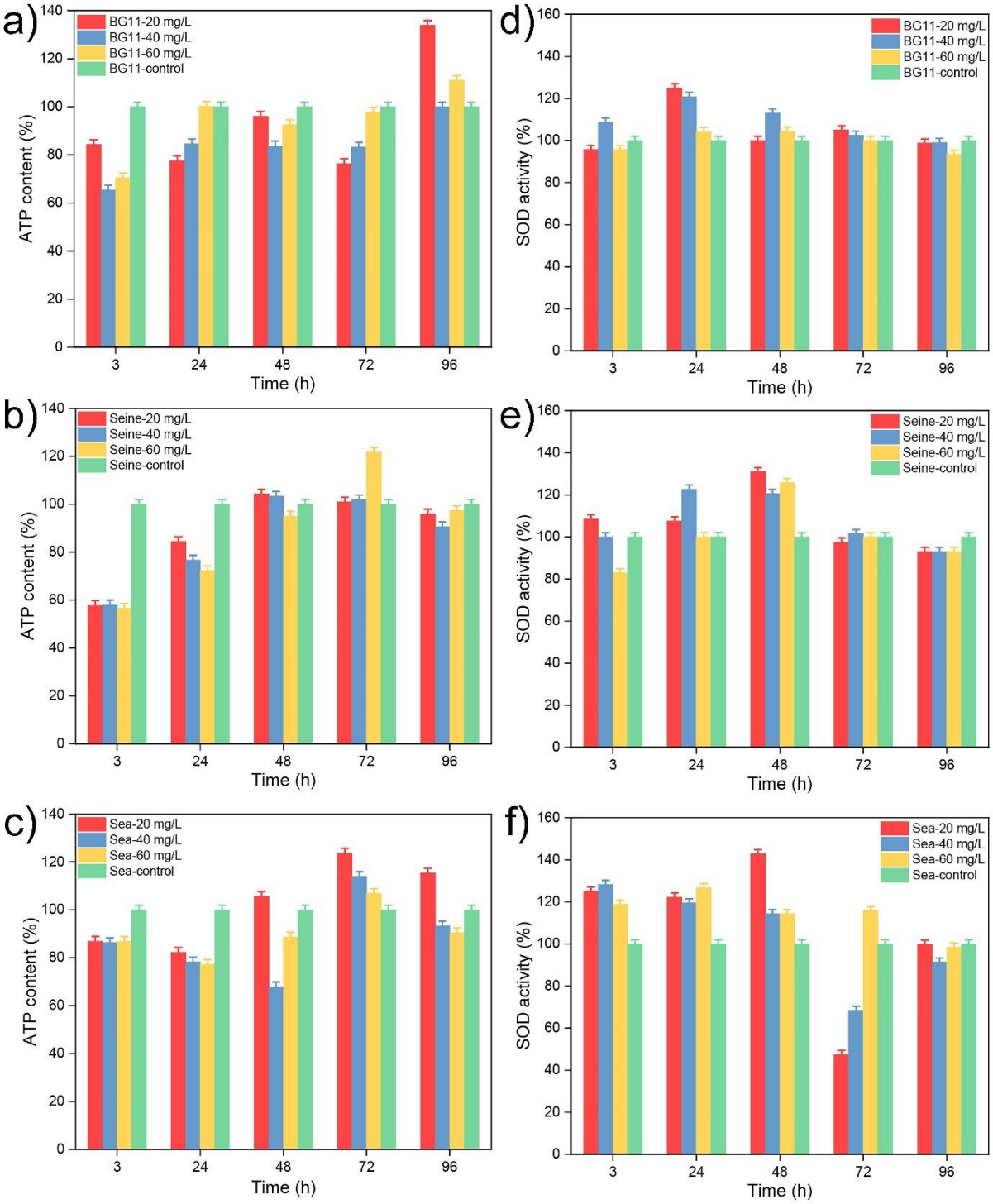

Fig. 54 *Toxicity tests carried out on ZnS:Mn (10%) in different water systems, a-c) ATP, d-f) SOD activity.*

The toxicity of ZnS:Cu NPs was also evaluated in different culture media in contact with Chlorella vulgaris (Fig. 55). Fig. 55 a-c) shows the photosynthetic activity (F_v/F_m) of Chlorella vulgaris in different media in the presence of 20 mg/L, 40 mg/L and 60 mg/L of ZnS:Cu (10%). One can see that the photosynthetic activity decreased 3 h later in BG11 and SRW, and toxic effect continued for 96h, compared to the control group. In SSW, the photosynthetic activity decreased 96h later.

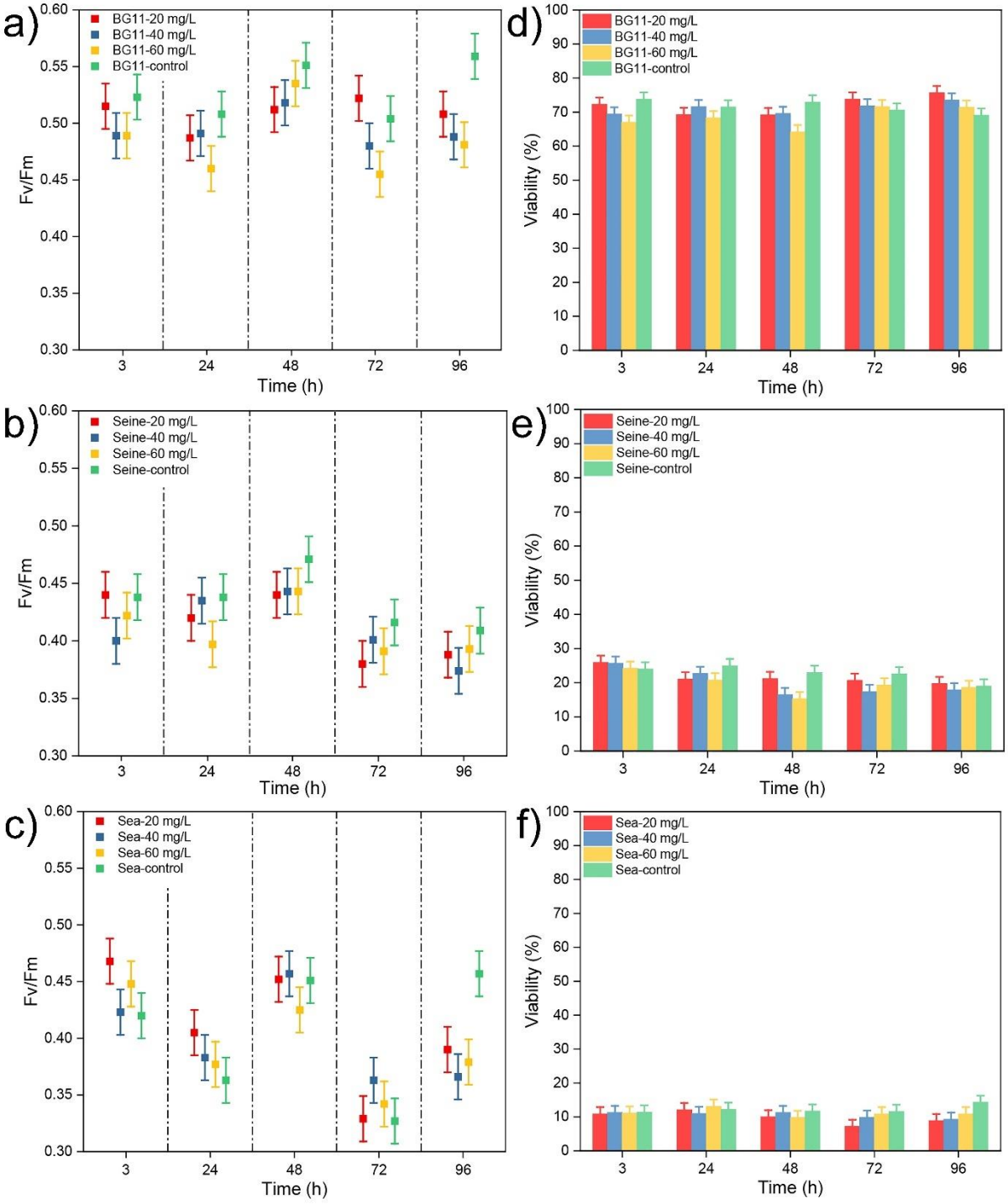

Fig. 55 *Toxicity test performed on ZnS:Cu (10%) in different water systems, a-c) PAM, d-f) viability.*

The viability of Chlorella vulgaris was measured in the three types of culture media (Fig. 55 d-f). In BG11, the viability decreased between 3 h and 72 h of test, then, it recovered from the toxic effect of NPs and reached the same level as the control group. On the other hand, the viability of the algae in SRW and SSW decreased 24 h after the beginning of the test and the toxic effect continued up to 96h in SSW.

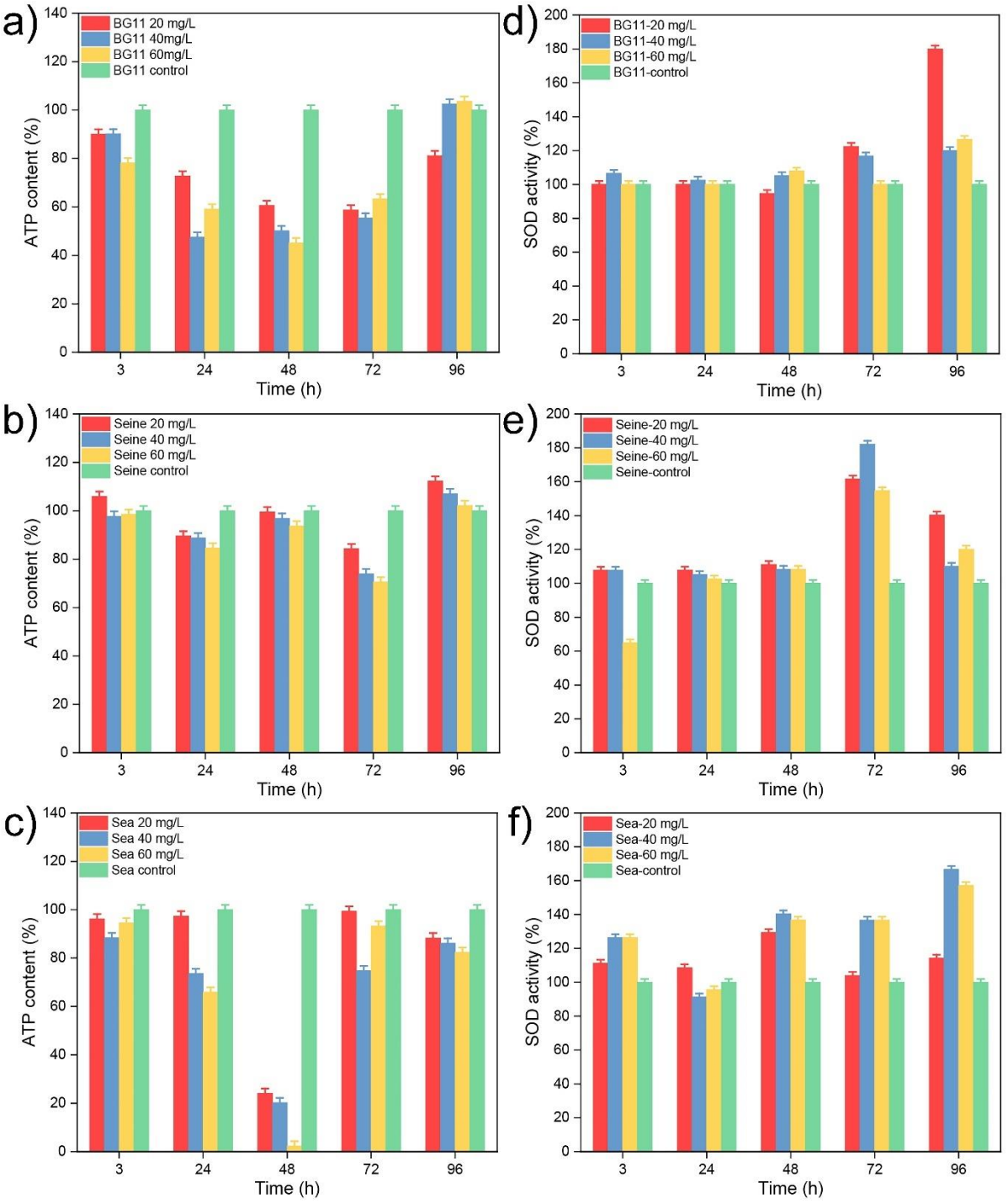

Fig. 56 *Toxicity tests carried out on ZnS:Cu (10%) in different water systems, a-c) ATP, d-f) SOD activity.*

The ATP content of algae cells was measured to check the activity of mitochondria (Fig. 56 a-c). In BG11, the ATP content decreased significantly after contacting with NPs, and it increased again to the same level as the control group 96 h later. The ATP content in SRW media also decreased 24 h later and then increased and until it became higher than that of the control group, 96 h later. The ATP content in SSW decreased clearly during the whole test period, and 48h later it almost decreased to 0. It recovered 72 h later but it can be assumed that NPs have a toxic effect on

mitochondria activity. After 48 hours, the microalgae gradually draw energy from the ZnS:Cu (10%) NPs; this is the reason why Chlorella algae can recover the activity of mitochondria at 72 hours. Mitochondrial activity evolves in good agreement with photosynthetic activity and viability.

Fig. 56 d-f) shows the SOD activity of Chlorella vulgaris, which increased 3 h after the introduction of NPs, Enzyme activity is abnormally active after 48h in all culture media compared to control group, indicating that NPs induced much of ROS production in algae cells, and then caused the toxic effect on photosynthetic activity, mitochondria activity and viability of Chlorella vulgaris.

We evaluated the toxicity of ZnS:Co (10%) NPs following the same protocol as before. Fig. 57 a-c) shows the photosynthetic activity of Chlorella vulgaris obtained by carrying out the PAM test. In BG11, photosynthetic activity decreased in the presence of 60 mg/L of ZnS:Co NPs (10%) after 3 h. On the other hand, a concentration of 40 mg/L of NPs has less toxic effect on photosynthetic activity, 48 hours later. Moreover, the microalgae almost recovered from the toxic effect of the NPs 96h later. In SRW, in the presence of 20 mg/L and 40 mg/L of NPs, the toxic effect appeared 24 h later; algae placed in contact with 20 mg/L quickly recovered from the toxic effect, while the toxic effect of NPs at a concentration of 40 mg/L continued for a long time. A concentration of 60 mg/L of NPs had a much more serious toxic influence on the photosynthetic activity of chlorella vulgaris, since the microalga could not recover, even 96 hours later. In SSW, the photosynthetic activity dropped rapidly after the addition of NPs in the medium, and the toxic effect continued for a long time although the algae could recover 48h later. Therefore, we concluded that ZnS:Co NPs (10%) presented a significantly toxic effect on the photosynthetic activity of Chlorella vulgaris, and it seemed that high concentrations of NPs are more toxic.

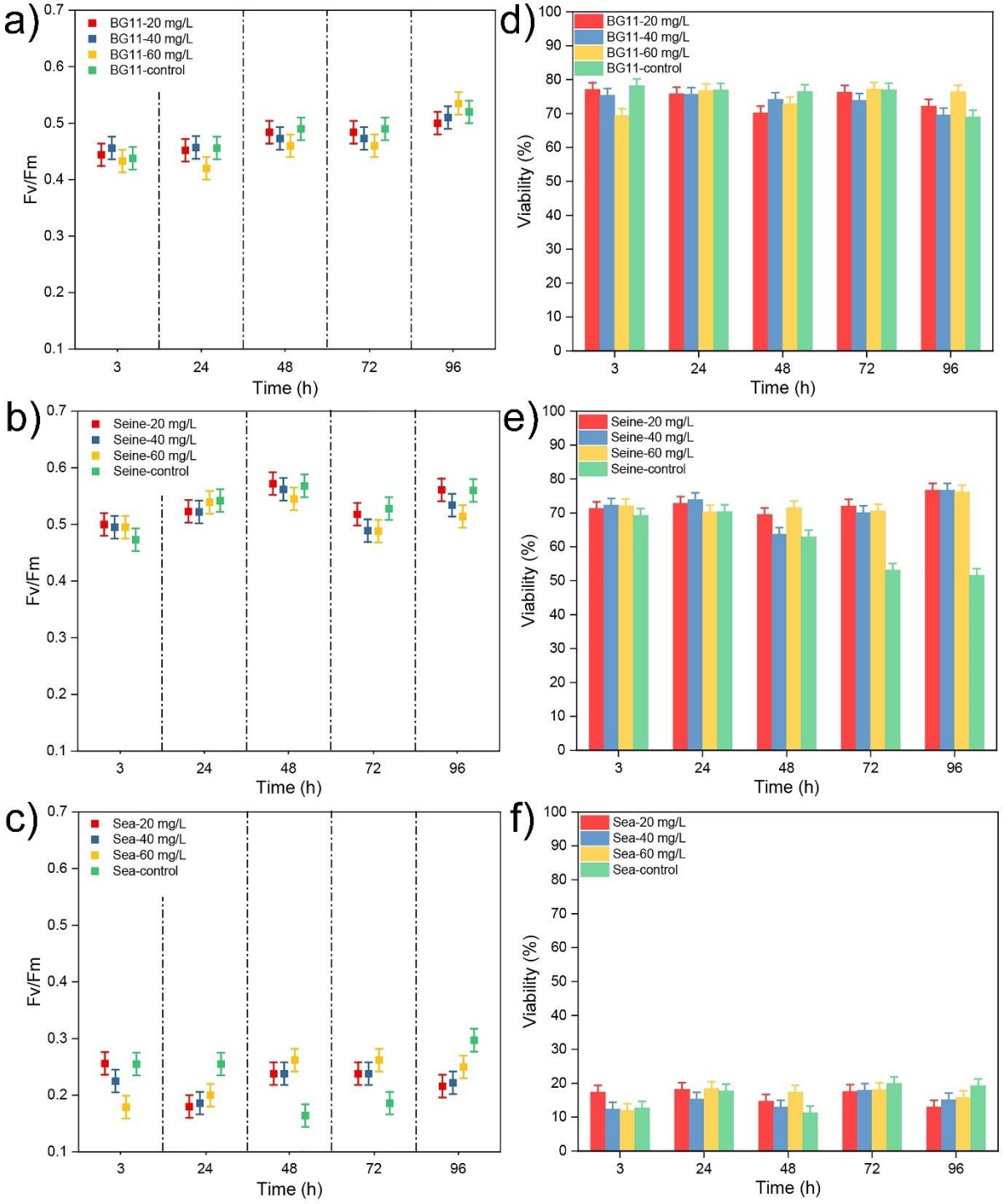

Fig. 57 *Toxicity tests carried out on ZnS:Co (10%) in different water systems, a-c) PAM, d-f) viability.*

The viability of Chlorella algae dropped 3 hours after they have been brought into contact with the NPs (Fig. 57 d-f). It seemed that a concentration of 60 mg/L exhibited significant toxicity compared to the control group. However, this toxic effect did not cause cell death. In SRW, it seemed that viability was not influenced by NPs; however, we could not say that NPs were not toxic to algae in SRW since, if they did not lead to cell death, they altered the initial photosynthetic activity (Fig. 57 b). In SSW, the decline in viability appeared after 72h in all research groups, and concentrations of 40 mg/L

and 60 mg/L were toxic for algae 3h after contacting. **The higher the concentration of NPs the stronger the toxic effect on the microalgae**.

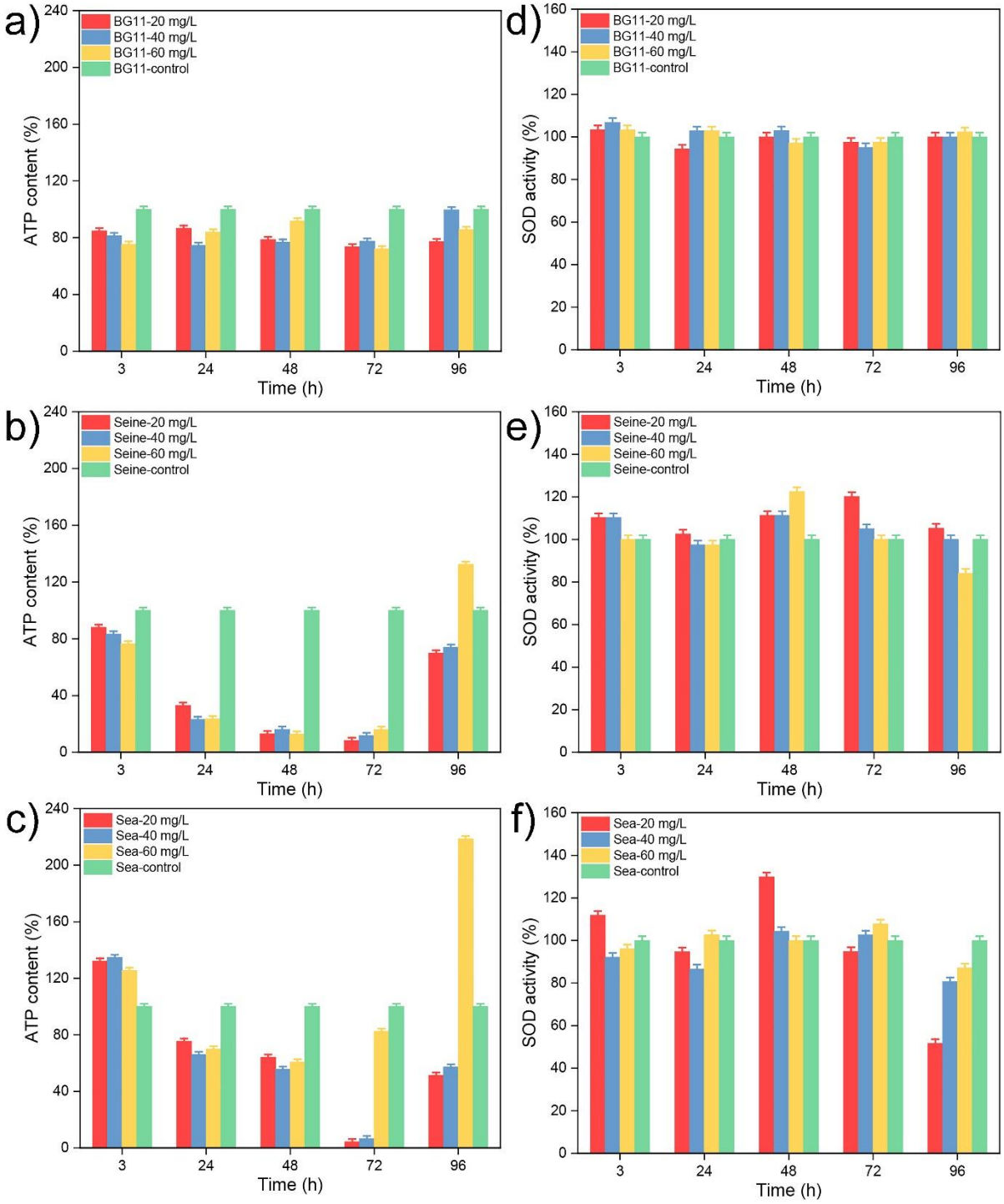

Fig. 58 *Toxicity tests carried out on ZnS:Co (10%) in different water systems, a-c) ATP, d-f) SOD activity.*

In Fig. 58 a-c), a significant decrease in intracellular ATP content could be seen in all culture media and in all research groups. In BG11 and SRW, the ATP content decreased throughout the test period, and 60 mg/L of NPs was more toxic than the other two NPs concentrations on the mitochondrial activity of microalgae. While the

ATP content of chlorella vulgaris decreased quickly after 24h in SRW and SSW media, and the algae maintained the lower ATP content for 48h, indicating that the mitochondria activity of microalgae was very low, during this period, microalgae could only obtain energy from NPs. This was also the reason why the algae were not completely dead and still maintained some photosynthetic activity.

The SOD activity of the microalgae slightly increased in BG11 from the first day of testing (Fig. 58 d-f), and the microalgae were able to recover from the toxic effect of ROS production 48 h later. In SRW and SSW, the SOD activity increased significantly from the first day of testing compared to the control group, especially in the media containing 20 mg/L and 60 mg/L of NP, and the SOD activity decreased on the last day of testing (96 h later) in media containing 60 mg/L of NP. To explain the decrease in SOD activity in Chlorella algal cells exposed to the highest concentration (60%) of NPs, we assumed that oxidative stress and hydrogen peroxide accumulation irreversibly inactivated the SOD, or disrupted SOD synthesis by destroying the functions of mitochondria. Moreover, we could conclude that the NPs of ZnS:Co (10%) had a strong toxic effect on the cells of Chlorella algae, especially on the activity of the mitochondria, because these NPs could induce the production of ROS, which influenced the function of mitochondria. The production of ATP decreased, then influenced the necessary cellular metabolic activity, such as photosynthetic activity and finally the process of apoptosis.

4. Conclusions

We synthesized successfully ZnS nanoparticles with a cubic structure, monodoped with transition metal cations: Mn^{2+}, Cu^{2+} and Co^{2+}, using the microwave-assisted polyol method. The size of these NPs was about 1.4 to 1.8 nm. XRF measurements evidenced that Cu^{2+} and Co^{2+} cations inserted more easily than Mn^{2+} into the crystal lattice, probably replacing Zn^{2+} ions. Indeed, using the same synthesis protocol, the Mn contents were always lower than those of Cu and Co. The XPS analyzes confirmed that all the cations were divalent and that the nanoparticles could be very slightly oxidized on the surface.

Moreover, these NPs exhibited interesting optical properties for their further use in luminescent devices, in particular those doped with Mn which emitted yellow-orange light under an excitation wavelength of 330 nm. ZnS:Mn NPs (10%) still presented toxicity on Chlorella vulgaris even when the NPs concentration decreased from (20 mg/L, 50 mg/L, and 100 mg/L) to (20 mg/L, 40 mg/L, and 60 mg/L). Although

photosynthetic activity decreased slightly, viability decreased drastically in BG11 during the first two days of testing. Moreover, NPs still induced a net increase in ROS production during the first three days of testing, affecting the activity of Chlorella vulgaris mitochondria. ZnS:Cu (10%) NPs also had a serious toxic effect on Chlorella vulgaris; the photosynthetic activity and the viability were clearly reduced after the introduction of the NPs, compared to the control group. Mitochondrial activity was severely affected by ZnS:Cu (10%) NPs, particularly in BG11 and SSW. SOD activity increased significantly over the last three days of testing, which was equivalent to a net increase in ROS production, leading to disorder in mitochondrial activity and then cell death. Finally, ZnS:Co NPs (10%) also affected the metabolic activity of Chlorella vulgaris; photosynthetic activity and viability were slightly reduced. However, the activity of mitochondria was severely influenced, especially for Chlorella vulgaris in SRW and SSW. SOD activity did not increase in BG11, whereas it markedly increased in SRW and SSW.

Finally, we can confirm that all these ZnS NPs monodoped with Mn, Cu, Co can induce a toxic effect on Chlorella vulgaris. Cu- and Co-doped NPs exhibited more severe toxic effects on mitochondrial activity, and these effects were enhanced in SRW and SSW.

5. References

(1) Leal, P. P.; Hurd, C. L.; Sander, S. G.; Armstrong, E.; Roleda, M. Y. Copper Ecotoxicology of Marine Algae: A Methodological Appraisal. *Chemistry and Ecology* **2016**, *32* (8), 786–800. https://doi.org/10.1080/02757540.2016.1177520.

(2) Moenne, A.; González, A.; Sáez, C. A. Mechanisms of Metal Tolerance in Marine Macroalgae, with Emphasis on Copper Tolerance in Chlorophyta and Rhodophyta. *Aquatic Toxicology* **2016**, *176*, 30–37. https://doi.org/10.1016/j.aquatox.2016.04.015.

(3) Saavedra, R.; Muñoz, R.; Taboada, M. E.; Vega, M.; Bolado, S. Comparative Uptake Study of Arsenic, Boron, Copper, Manganese and Zinc from Water by Different Green Microalgae. *Bioresource Technology* **2018**, *263*, 49–57. https://doi.org/10.1016/j.biortech.2018.04.101.

(4) Ciurli, A.; Di Baccio, D.; Scartazza, A.; Grifoni, M.; Pezzarossa, B.; Chiellini, C.; Mariotti, L.; Pardossi, A. Influence of Zinc and Manganese Enrichments on Growth, Biosorption and Photosynthetic Efficiency of Chlorella Sp. *Environ Sci*

Pollut Res **2021**, *28* (7), 8539–8555. https://doi.org/10.1007/s11356-020-11033-2.

(5) Longo, A. V.; Notebaert, B.; Gaceur, M.; Patriarche, G.; Sciortino, A.; Cannas, M.; Messina, F.; von Bardeleben, H. J.; Battaglini, N.; Ammar, S. Photo-Activated Phosphorescence of Ultrafine ZnS:Mn Quantum Dots: On the Lattice Strain Contribution. *J. Phys. Chem. C* **2022**, *126* (3), 1531–1541. https://doi.org/10.1021/acs.jpcc.1c09687.

(6) Jrad, A.; Naouai, M.; Abdallah, A.; Ammar, S.; Turki-Kamoun, N. Doping ZnS Films with Cobalt: Structural, Compositional, Morphological, Optical, Electrical, Magnetic and Photocatalytic Properties. *Physica B: Condensed Matter* **2021**, *603*, 412776. https://doi.org/10.1016/j.physb.2020.412776.

(7) Hao, X.; Wang, Y.; Zhou, J.; Cui, Z.; Wang, Y.; Zou, Z. Zinc Vacancy-Promoted Photocatalytic Activity and Photostability of ZnS for Efficient Visible-Light-Driven Hydrogen Evolution. *Applied Catalysis B: Environmental* **2018**, *221*, 302–311. https://doi.org/10.1016/j.apcatb.2017.09.006.

(8) Polonini, H. C.; Brandão, H. M.; Raposo, N. R. B.; Brandão, M. A. F.; Mouton, L.; Couté, A.; Yéprémian, C.; Sivry, Y.; Brayner, R. Size-Dependent Ecotoxicity of Barium Titanate Particles: The Case of Chlorella Vulgaris Green Algae. *Ecotoxicology* **2015**, *24* (4), 938–948. https://doi.org/10.1007/s10646-015-1436-6.

(9) Murugadoss, G. Synthesis and Photoluminescence Properties of Zinc Sulfide Nanoparticles Doped with Copper Using Effective Surfactants. *Particuology* **2013**, *11* (5), 566–573. https://doi.org/10.1016/j.partic.2012.11.003.

(10) Sakthivel, P.; Prasanna Venkatesan, G. K. D.; Subramaniam, K.; Muthukrishnan, P. Structural, Optical, Photoluminescence and Electrochemical Behaviours of Mg, Mn Dual-Doped ZnS Quantum Dots. *J Mater Sci: Mater Electron* **2019**, *30* (13), 11984–11993. https://doi.org/10.1007/s10854-019-01551-2.

(11) Chaguetmi, S.; Chaperman, L.; Nowak, S.; Schaming, D.; Lau-Truong, S.; Decorse, P.; Beaunier, P.; Costentin, C.; Mammeri, F.; Achour, S.; Ammar, S. Photoelectrochemical Properties of ZnS- and CdS-TiO_2 Nanostructured Photocatalysts: Aqueous Sulfidation as a Smart Route to Improve Catalyst Stability. *Journal of Photochemistry and Photobiology A: Chemistry* **2018**, *356*, 489–501. https://doi.org/10.1016/j.jphotochem.2018.01.038.

(12) Zhu, Y.-P.; Li, J.; Ma, T.-Y.; Liu, Y.-P.; Du, G.; Yuan, Z.-Y. Sonochemistry-Assisted Synthesis and Optical Properties of Mesoporous ZnS Nanomaterials. *Journal of Materials Chemistry A* **2014**, *2* (4), 1093–1101. https://doi.org/10.1039/C3TA13636A.

(13) Brayek, A.; Chaguetmi, S.; Ghoul, M.; Assaker, I. B.; Chtourou, R.; Decorse, P.; Beaunier, P.; Nowak, S.; Mammeri, F.; Ammar, S. The Structural and the Photoelectrochemical Properties of ZnO–ZnS/ITO 1D Hetero-Junctions Prepared by Tandem Electrodeposition and Surface Sulfidation: On the Material Processing Limits. *RSC Advances* **2018**, *8* (21), 11785–11798. https://doi.org/10.1039/C8RA00176F.

(14) Ramachandran, R.; Saranya, M.; Kollu, P.; Raghupathy, B. P. C.; Jeong, S. K.; Grace, A. N. Solvothermal Synthesis of Zinc Sulfide Decorated Graphene (ZnS/G) Nanocomposites for Novel Supercapacitor Electrodes. *Electrochimica Acta* **2015**, *178*, 647–657. https://doi.org/10.1016/j.electacta.2015.08.010.

(15) Chaguetmi, S.; Mammeri, F.; Nowak, S.; Decorse, P.; Lecoq, H.; Gaceur, M.; Naceur, J. B.; Achour, S.; Chtourou, R.; Ammar, S. Photocatalytic Activity of TiO_2 Nanofibers Sensitized with ZnS Quantum Dots. *RSC Advances* **2013**, *3* (8), 2572–2580. https://doi.org/10.1039/C2RA21684A.

(16) Geszke, M.; Murias, M.; Balan, L.; Medjahdi, G.; Korczynski, J.; Moritz, M.; Lulek, J.; Schneider, R. Folic Acid-Conjugated Core/Shell ZnS:Mn/ZnS Quantum Dots as Targeted Probes for Two Photon Fluorescence Imaging of Cancer Cells. *Acta Biomaterialia* **2011**, *7* (3), 1327–1338. https://doi.org/10.1016/j.actbio.2010.10.012.

(17) Kolmykov, O.; Coulon, J.; Lalevée, J.; Alem, H.; Medjahdi, G.; Schneider, R. Aqueous Synthesis of Highly Luminescent Glutathione-Capped Mn^{2+}-Doped ZnS Quantum Dots. *Materials Science and Engineering: C* **2014**, *44*, 17–23. https://doi.org/10.1016/j.msec.2014.07.064.

(18) Bwatanglang, I. B.; Mohammad, F.; Yusof, N. A.; Abdullah, J.; Hussein, M. Z.; Alitheen, N. B.; Abu, N. Folic Acid Targeted Mn:ZnS Quantum Dots for Theranostic Applications of Cancer Cell Imaging and Therapy. *Int J Nanomedicine* **2016**, *11*, 413–428. https://doi.org/10.2147/IJN.S90198.

(19) Lee, G.-J.; Chen, H.-C.; Wu, J. J. (In, Cu) Co-Doped ZnS Nanoparticles for Photoelectrochemical Hydrogen Production. *International Journal of Hydrogen Energy* **2019**, *44* (1), 110–117. https://doi.org/10.1016/j.ijhydene.2018.02.112.

(20) Madhusudan, P.; Wang, Y.; Chandrashekar, B. N.; Wang, W.; Wang, J.; Miao, J.; Shi, R.; Liang, Y.; Mi, G.; Cheng, C. Nature Inspired ZnO/ZnS Nanobranch-like Composites, Decorated with $Cu(OH)_2$ Clusters for Enhanced Visible-Light Photocatalytic Hydrogen Evolution. *Applied Catalysis B: Environmental* **2019**, *253*, 379–390. https://doi.org/10.1016/j.apcatb.2019.04.008.

(21) Daskalakis, I.; Vamvasakis, I.; T. Papadas, I.; Tsatsos, S.; A. Choulis, S.; Kennou, S.; Armatas, G. Surface Defect Engineering of Mesoporous Cu/ZnS Nanocrystal-Linked Networks for Improved Visible-Light Photocatalytic Hydrogen Production. *Inorganic Chemistry Frontiers* **2020**, *7* (23), 4687–4700. https://doi.org/10.1039/D0QI01013H.

(22) Liu, H.; Wei, G.; Xu, Z.; Liu, P.; Li, Y. Quantitative Analysis of Fe and Co in Co-Substituted Magnetite Using XPS: The Application of Non-Linear Least Squares Fitting (NLLSF). *Applied Surface Science* **2016**, *389*, 438–446. https://doi.org/10.1016/j.apsusc.2016.07.146.

(23) Poornaprakash, B.; Chalapathi, U.; Kumar, M.; Vattikuti, S. V. P.; Rajitha, B.; Poojitha, P. T.; Park, S.-H. Tailoring the Optical and Magnetic Properties of ZnS Nanoparticles via 3d and 4f Elements Co-Doping. *Materials Science in Semiconductor Processing* **2021**, *121*, 105395. https://doi.org/10.1016/j.mssp.2020.105395.

(24) Murugadoss, G. Luminescence Properties of Co-Doped ZnS:Ni, Mn and ZnS:Cu, Cd Nanoparticles. *Journal of Luminescence* **2012**, *132* (8), 2043–2048. https://doi.org/10.1016/j.jlumin.2012.02.011.

(25) Raksha, K. R.; Ananda, S.; Madegowda, N. M. Study of Kinetics of Photocatalysis, Bacterial Inactivation and •OH Scavenging Activity of Electrochemically Synthesized Se^{4+} Doped ZnS Nanoparticles. *Journal of Molecular Catalysis A: Chemical* **2015**, *396*, 319–327. https://doi.org/10.1016/j.molcata.2014.10.005.

(26) Sakthivel, P.; Muthukumaran, S. Crystallographic, Structural and Band Gap Tailoring of $Zn_{0.98}Mn_{0.02}S$ Quantum Dots Co-Doped with Cu by Co-Precipitation Method. *J Inorg Organomet Polym* **2016**, *26* (3), 563–571. https://doi.org/10.1007/s10904-016-0341-7.

(27) Sakthivel, P.; Muthukumaran, S. Structural, Photoluminescence and Magnetic Properties of Mn, Cr Dual-Doped ZnS Quantum Dots: Influence of Cr

Concentration. *Journal of Physics and Chemistry of Solids* **2018**, *120*, 183–189. https://doi.org/10.1016/j.jpcs.2018.04.037.

(28) Lakshmi, P. V. B.; Raj, K. S.; Ramachandran, K. Synthesis and Characterization of Nano ZnS Doped with Mn. *Crystal Research and Technology* **2009**, *44* (2), 153–158. https://doi.org/10.1002/crat.200800271.

(29) Rahdar, A. Effect of 2-Mercaptoethanol as Capping Agent on ZnS Nanoparticles: Structural and Optical Characterization. *J Nanostruct Chem* **2013**, *3* (1), 10. https://doi.org/10.1186/2193-8865-3-10.

(30) Bansal, N.; Mohanta, G. C.; Singh, K. Effect of Mn^{2+} and Cu^{2+} Co-Doping on Structural and Luminescent Properties of ZnS Nanoparticles. *Ceramics International* **2017**, *43* (9), 7193–7201. https://doi.org/10.1016/j.ceramint.2017.03.007.

(31) Poornaprakash, B.; Amaranatha Reddy, D.; Murali, G.; Madhusudhana Rao, N.; Vijayalakshmi, R. P.; Reddy, B. K. Composition Dependent Room Temperature Ferromagnetism and PL Intensity of Cobalt Doped ZnS Nanoparticles. *Journal of Alloys and Compounds* **2013**, *577*, 79–85. https://doi.org/10.1016/j.jallcom.2013.04.106.

(32) Sabitha, C.; Kumar, K. D. A.; Valanarasu, S.; Saranya, A.; Joe, I. H. Cu:ZnS and Al:ZnS Thin Films Prepared on FTO Substrate by Nebulized Spray Pyrolysis Technique. *J Mater Sci: Mater Electron* **2018**, *29* (6), 4612–4623. https://doi.org/10.1007/s10854-017-8412-2.

(33) Poornaprakash, B.; Chalapathi, U.; Poojitha, P. T.; Vattikuti, S. V. P.; Reddy, M. S. P. (Al, Cu) Co-Doped ZnS Nanoparticles: Structural, Chemical, Optical, and Photocatalytic Properties. *J Mater Sci: Mater Electron* **2019**, *30* (10), 9897–9902. https://doi.org/10.1007/s10854-019-01327-8.

(34) Belache, B.; Khelfaoui, Y.; Bououdina, M.; Souier, T.; Cai, W. Photoluminescence of ZnS: Cu Quantum Dots Embedded in Silica Thin Films. *Journal of Luminescence* **2019**, *207*, 258–265. https://doi.org/10.1016/j.jlumin.2018.11.029.

(35) Hu, Y.; Hu, B.; Yang, D.; Wei, Z. Suppression of Blue Photoluminescence and Enhancement of Green Photoluminescence by Mn and Cu Co-Doped ZnS Quantum Dots. *J Mater Sci: Mater Electron* **2020**, *31* (3), 2617–2624. https://doi.org/10.1007/s10854-019-02800-0.

(36) Lin, K. B.; Su, Y. H. Photoluminescence of Cu:ZnS, Ag:ZnS, and Au:ZnS Nanoparticles Applied in Bio-LED. *Appl. Phys. B* **2013**, *113* (3), 351–359. https://doi.org/10.1007/s00340-013-5497-z.

(37) Gaceur, M.; Giraud, M.; Hemadi, M.; Nowak, S.; Menguy, N.; Quisefit, J. P.; David, K.; Jahanbin, T.; Benderbous, S.; Boissière, M.; Ammar, S. Polyol-Synthesized $Zn_{0.9}Mn_{0.1}S$ Nanoparticles as Potential Luminescent and Magnetic Bimodal Imaging Probes: Synthesis, Characterization, and Toxicity Study. *Journal of Nanoparticle Research* **2012**, *14* (7). https://doi.org/10.1007/s11051-012-0932-3.

(38) Munk, M.; Brandão, H. M.; Nowak, S.; Mouton, L.; Gern, J. C.; Guimaraes, A. S.; Yéprémian, C.; Couté, A.; Raposo, N. R. B.; Marconcini, J. M.; Brayner, R. Direct and Indirect Toxic Effects of Cotton-Derived Cellulose Nanofibres on Filamentous Green Algae. *Ecotoxicology and Environmental Safety* **2015**, *122*, 399–405. https://doi.org/10.1016/j.ecoenv.2015.09.001.

(39) Polonini, H. C.; Brandão, H. M.; Raposo, N. R. B.; Mouton, L.; Yéprémian, C.; Couté, A.; Brayner, R. Ecotoxicological Studies of Micro- and Nanosized Barium Titanate on Aquatic Photosynthetic Microorganisms. *Aquatic Toxicology* **2014**, *154*, 58–70. https://doi.org/10.1016/j.aquatox.2014.05.005.

(40) Rodea-Palomares, I.; Gonzalo, S.; Santiago-Morales, J.; Leganés, F.; García-Calvo, E.; Rosal, R.; Fernández-Piñas, F. An Insight into the Mechanisms of Nanoceria Toxicity in Aquatic Photosynthetic Organisms. *Aquatic Toxicology* **2012**, *122–123*, 133–143. https://doi.org/10.1016/j.aquatox.2012.06.005.

(41) Haniu, H.; Saito, N.; Matsuda, Y.; Tsukahara, T.; Maruyama, K.; Usui, Y.; Aoki, K.; Takanashi, S.; Kobayashi, S.; Nomura, H.; Okamoto, M.; Shimizu, M.; Kato, H. Culture Medium Type Affects Endocytosis of Multi-Walled Carbon Nanotubes in BEAS-2B Cells and Subsequent Biological Response. *Toxicology in Vitro* **2013**, *27* (6), 1679–1685. https://doi.org/10.1016/j.tiv.2013.04.012.

(42) Pereira, M. M.; Mouton, L.; Yéprémian, C.; Couté, A.; Lo, J.; Marconcini, J. M.; Ladeira, L. O.; Raposo, N. R.; Brandão, H. M.; Brayner, R. Ecotoxicological Effects of Carbon Nanotubes and Cellulose Nanofibers in Chlorella Vulgaris. *J Nanobiotechnol* **2014**, *12* (1), 15. https://doi.org/10.1186/1477-3155-12-15.

General conclusion and prospective

With the wide application of nanomaterials due to their specific physiochemical properties, their potential ecotoxicity to microorganisms or even human beings has gradually attracted research's attention. ZnS NPs as a promising alternative semiconductor material, which can be widely applied in photoluminescent, electroluminescent, and optoelectronic devices, therefore, we researched the ecotoxicological effect of the ZnS NPs doped with different dopants (e.g., Mn, Cu, Co) on *Chlorella vulgaris*, we studied the toxicity of ZnS NPs with different molar concentration dopants, different size, different dopants and the function of the silica shell on preventing the toxicity of ZnS NPs.

The different concentrations of Mn-doped ZnS NPs (0.5%, 2.0%, 4.0%, 10%) were synthesized by the polyol method, and all presented a zinc sulfide blende structure. The crystal size was around 1.1-1.5 nm but the NPs aggregated in larger colloids, in the three aqueous media (BG11, SRW, and SSW), of at least 300 nm. This size could be bigger than 1000 nm when the pH was 2 or 10; when the pH of the NPs suspension was almost equal to that of Chlorella vulgaris culture (from 6 to 8), the colloidal size was around 400 or 600 nm. Moreover, the zeta potential of these colloids ranged between 5 and -20 mV, which evidenced a certain instability, and a propensity to aggregate. Aggregated NPs could surround the surface of the algae, and thus influence the photosynthetic activity and the uptake of the nutrients. And these NPs induced the increase of the ROS production, and caused the decrease of the mitochondria activity; sometimes, it caused even cell death, evidenced by TEM pictures of Chlorella vulgaris thin sections, since the NPs were observed to be inside the algae cells. The higher the concentration of Mn-doped NPs, the higher the toxicity for Chlorella vulgaris. In addition, to prevent the toxic effect of NPs, we successfully coated the Mn-doped ZnS nanoparticles with a shell of silica, using the sol-gel process: the toxic effect of ZnS:Mn (10%) for Chlorella vulgaris decreased compared to ZnS:Mn (10%) without silica shell.

Then, we evaluated the influence of the size of the nanoparticles on the toxicity of microalgae under the same conditions. We synthesized larger ZnS:Mn NPs, presenting the same blende structure, whose size was around 10 nm. DLS experiments showed that these NPs could also aggregate easily, to form colloids bigger than 2000 nm at pH 6 to 8. The toxicity investigations allowed us to conclude that the larger the NPs, the lower the toxicity. The photosynthetic activity and viability

of Chlorella vulgaris were barely influenced by the presence of NPs in BG11 and SRW, while it increased in SSW, probably because the ZnS:Mn NPs could provide some essential nutrients or energy to the Chlorella vulgaris in the harsh synthetic seawater. ICP and XRF experiments proved that Mn^{2+} and Zn^{2+} ions dissolved in the three aqueous media, and were available as nutrients to promote algae growth in the appropriate concentration range. Meanwhile, the intracellular ATP content decreased, because the mitochondria function was affected. However, the SOD activity did not increase. We suggested two reasons for that: first, the NPs did not cause the increase in ROS production, so the larger size of ZnS:Mn (10%) NPs did not induce oxidation stress to Chlorella vulgaris and were not too toxic for the algae. The other reason may be the excessive accumulation of hydrogen peroxide that irreversibly inactivated SOD, and affected the synthesis of SOD in algae cells. However, for one or other reason, we could confirm that larger ZnS:Mn (10%) NPs were not too toxic, since the viability did not decrease. And we could also conclude that the mitochondria were more sensitive to the toxicity of the NPs.

Finally, Mn^{2+}, Cu^{2+}, and $Co^{2+}$are very important for the microalgae, as trace elements, even if they may be also very toxic to the algae cells when they exceed a threshold. Meanwhile, these transition metal ions are also widely used as dopants in ZnS to enhance their physicochemical and optical properties. Therefore, we also investigated the toxic effect of the Mn, Cu, and Co monodoped ZnS NPs, presenting also a blende structure, and whose size was around 1.4-1.8 nm. These Mn, Cu, and Co monodoped ZnS NPs presented good luminescence properties (e.g., ZnS:Mn NPs emitted an orange-yellow light at the excitation wavelength of 330 nm). In addition, we evaluated the toxic effect of the 10% Mn, Cu, Co monodoped ZnS NPs, using the same protocol as previously; but, as knew that high concentrations of NPs presented high toxicity on Chlorella vulgaris, we decreased the concentrations of NPs contacted with Chlorella vulgaris to 20 mg/L, 40 mg/L and 60 mg/L. For the photosynthetic activity, ZnS:Mn (10%) NPs had a slightly toxic effect on Chlorella vulgaris in the three media, ZnS:Co (10%) NPs had a significant toxic effect on Chlorella vulgaris in SSW media, while the ZnS:Cu NPs had a heavy toxic effect on Chlorella vulgaris in the three media. Meanwhile, the ZnS:Mn, Cu, and Co NPs all caused the algae cell death in the three kinds of media to some extent, except for the microalgae living in the SRW water treated with ZnS:Co NPs. Moreover, the ZnS:Mn NPs caused a serious toxic effect on the mitochondria of Chlorella vulgaris during the first 3 test days, which is consistent with the SOD activity result, the NPs induced a heavy ROS production during the first

three test days in all the media. ZnS:Cu NPs also heavily affected the mitochondria activity of Chlorella vulgaris in the three media, even causing the inactivity of the mitochondria in SSW 48 h later; and the ZnS:Cu NPs also induced a serious ROS production, especially during the last two test days. ZnS:Co NPs had a more serious toxic effect on mitochondria activity in all the media, especially in SRW and SSW media, the intracellular ATP level was even less than 20% 72 h later in these two media; and the ZnS:Co NPs also induced the increase of the ROS production in SRW and SSW media. Therefore, we can conclude that the ZnS:Mn and ZnS:Cu NPs seem more toxic than ZnS:Co NPs to Chlorella vulgaris in the three kinds of media, and the ZnS:Co NPs have a much more toxic effect on the mitochondria activity of Chlorella vulgaris.

Nanotoxicity is being questioned by more and more researchers, due to large-scale applications of engineered nanoparticles; Therefore, their potential toxicological effects require increased attention. In our work, we only investigated some basic toxicological effects of nanoparticles on microalgae, such as photosynthesis, mitochondrial activity, and SOD activity. All these results showed that it is possible to develop a methodology for evaluating the toxicity of nanoparticles in different aqueous media and to obtain valuable results. However, further studies would be needed to understand other toxicological mechanisms, as well as the toxic effects of nanoparticles on mammals or animal cells. A multidisciplinary approach is more than ever necessary to study subsequent toxicological mechanisms, which require the collaborative effort of ecotoxicologists, toxicologists, biologists, and chemists.

Nevertheless, as discussed in the introduction, there are many organisms living in river and sea waters. Therefore, it is necessary to be able to obtain and then cultivate these organisms in sufficient quantity to carry out the numerous tests described in this manuscript. Moreover, the quantities of manufactured nanomaterials produced are constantly increasing and it will become difficult to test in lab, not only all the compositions, sizes and shapes of nanomaterials but also the surface functionalization that are sometimes carried out.

With the emergence of machine learning and artificial intelligence, the toxicity effect of the numerous NPs can be simulated or measured, the ecotoxicity measurements of the NPs aim to know the toxicity mechanism instead of to forbidden using the NPs in our life. However, only when we know the toxicity mechanism clearly, we can prevent the toxicity effect of NPs and use it safely in the future.

Annex

1. Algae culture

1.1. Blue-Green medium (BG11)

According to the recipe Sendersky & al, bio-protocol, 2017 with three main changed for the buffer concentration, the pH, the copper concentration (modified by Claude Yepremian, MNHN, 2020)

N° solution Stock	Component	Mass (g) for 200 mL	Molar concentration	Notes
1.	$MgSO_4.7H_2O$	1.3	0.284 mM	Don't autoclave!
	$CaCl_2.2H_2O$	0.72	0.245 mM	
2.	$K_2HPO_4.3H_2O$	0.80	0.175 mM	Storage 3 months at 4 ℃
	EDTA (Na_2)	0.02	2.26 µM	
3.	Citric Acid	0.12	31.2 µM	Storage 10 days in the dark
	Ammonium Ferric Citrate Green	0.12	30.0 µM	
4. Metal trace solution	H_3BO_3	572	46.3 µM	Storage 2 years at 4 ℃
	$MnCl_2.4H_2O$	362	9.15 µM	
	$ZnSO_4.7H_2O$	44	0.77 µM	
	$Na_2MoO_4.2H_2O$	78	1.61 µM	
	$CuSO_4.5H_2O$	4	0.08 µM	
	$CO(NO_3)2.6H_2O$	10	0.17 µM	
5. Vitamin solution (optional)	Cyanocobalamin (B12)	8		Vitamin solution n° 7 of JM/JM2 media, vitamins are dissolved in ultrapure Water pH=4
	Thiamine HCl (B1)	8		
	Biotin	8		

Table 6. *Preparation of stock solutions.*

For the 5 stock solutions: Adjust to 200 mL with ultrapure water

For the stock solution 2, 3, 4, 5: Autoclave at 121 ℃ for 20 minutes

Preparation of BG11 medium with stock solutions:

(1) Add 950 mL ultrapure water in 1 L bottle,

(2) Add 1.5 g of $NaNO_3$ (17.6 mM)

(3) Add the stock solution according to the table 7.

N° solution stock	Volume (mL) for 1 L
1	10
2	10
3	10
Metal trace solution (4)	1
Vitamin solution (5)	1
HEPES (5 mM)	1.19 g

Table 7. *Preparation of BG11 medium*

Adjust pH=7.30 with ≈2 mL NaOH (1 M)

Adjust the volume to 1 L with ultrapure water

Autoclave at 121 ℃ for 15-20 minutes

1.2. Seine River water (SRW) medium

The Seine River water was taken from the river close the *Université Paris Diderot*, France (GPS: 48.828335°N, 2.385351°E), then it was filtered immediately with a 0.22 µm acetate membrane (Millipore), the autoclave was used to kill all the microorganisms (121 ℃ for 20 minutes), and stored at 4 ℃ in fridge. The average chemical composition of Seine River water was shown in table 8.[1]

$\times 10^{-3}$ mol/L	Na^+	Mg^{2+}	Ca^{2+}	K^+	Cl^-	Alkalinity	SO_4^{2-}	NO_3^-	SiO_2	pH	DOC (mg/L)
Seine River water	0.429	0.189	2.366	0.077	0.617	3.807	0.334	0.382	0.06	8.05	2.445

Table 8. *Chemical composition of Seine River water.*

1.3. Synthetic seawater (SSW) medium

The seawater was synthesized according to the Alexandre Gelabert's paper,[2,3]

Na^+ (mmol L^{-1})	Mg^{2+} (mmol L^{-1})	Ca^{2+} (mmol L^{-1})	K^+ (mmol L^{-1})	Cl^- (mmol L^{-1})	HCO_3^- (mmol L^{-1})	SO_4^{2-} (mmol L^{-1})	H3BO4 (mmol L^{-1})	pH
486	54.7	10.8	10.6	569	0.699	29.27	0.066	7.6-8.3

***Table 9**. Chemical composition of synthetic seawater*

2. Techniques

X-Ray Diffraction (XRD) patterns of the nanoparticles (NPs) have been recorded on an X'Pert Pro PANanalytical diffractometer, using the Co Kα radiation, in the range 10-80° (2θ) with a scan step of 0.016°. The peak indexing was performed using the Highscore Plus software and the Database ICSD-Panalytical. The cell parameter and the size of the coherent diffraction domain were determined with MAUD software, based on the Rietveld method.

X-ray photoelectron spectroscopy (XPS) is performed in the range of 0 eV-1100 eV using THERMO-VG ESCALAB 250 system with RX Kα Al (1486.6 eV) source, spot size of 500 µm and energy step size of 1.000 eV.

The morphology of the NPs has been determined by Transmission Electron Microscopy (TEM), using a JEOL-100 CX II microscope operating at 100 kV. The mean diameter and standard deviation were inferred from image analysis of ca. 100 particles using ImageJ software.

The surface chemical composition of as prepared and functionalized NPs has been checked by X-ray Photoelectron Spectroscopy (XPS) using a Thermo VG ESCALAB 250 instrument equipped with a micro-focused monochromatic Al Kα X-ray source (1486.6 eV) and a magnetic lens. The X-ray spot size was 500 µm (15 kV, 150 W). The spectra were acquired in the constant analyzer energy mode with pass energy of 100 and 40 eV for the survey spectra and the narrow high-resolution regions, respectively. The "Avantage" software (version 4.67) was used for data acquisition and processing. The C1s peak at 285 eV, due to the adventitious contamination, was used as a reference to calibrate the binding energies for charge correction.

Dynamic Light Scattering (DLS) and zetametry were performed using Zetasizer from Malvern to determine the size distribution and the surface charge of the NPs; their ζ

potential was measured at room temperature starting from their aqueous solution (0.5 g L^{-1}), after vigorous sonication for 15 min.

Absorption measurements were performed at 25 °C on a Cary 4000 spectrophotometer equipped with a Peltier-thermostated cell-carrier. Fluorimetric measurements were performed at 25 °C on an Aminco-Bowman series 2 luminescence spectrometer thermostated by external water circulation.

ICP-AES (ICAP 6200 Thermo Fisher, Thermo Fisher Scientific, Waltham, MA, USA). Detection and quantification limits were of 0.20 ppb and 0.67 ppb respectively, and of 0.02 ppb and 0.07 ppb respectively, for Zn and Mn. The standard deviation associated with the measurements was smaller than 5%.

The thermal variation magnetization of Mn doped ZnS NPs was measured at 4 K to 300 K temperature range using a Quantum Design MPMS-XL SQUID magnetometer in field cooling (FC) conditions with an applied magnetic field of 500 Oe, and the magnetization variation as a function of the magnetic field M(H) was measured from 0 Oe to 70 KOe at 300 K temperature.

The photosynthetic activity of microalgae was measured by the pulsed amplitude modulation (PAM) method using a Handy PEA fluorometer (Hansatech instruments, UK). The microalgae can receive a short beam of light which will saturate the photosystem II (PS II) through the pulse saturation mode in this method. And the photochemical quenching will be eliminated during this process, then the maximum fluorescence yield can be reduced. Therefore, the fluorescence ratio (Fv/Fm) can be measured.

Viability test has been done using the Cellometer Auto T4 manufactured by Nexcelom.

SOD enzymatic activity measurements were performed using 19,160 SOD determination kit from Sigma-Aldrich (France). SOD enzymatic activity was determined using colorimetric measurements by a kinetic method and then read at 450 nm using an Envision Multilabel Plate Reader (Perkin-Elmer, USA).

Adenosine-5’-triphosphate (ATP) level of the samples were detected using the luciferase-luciferin enzymatic assay kit BacTiter-Glo™ ordered from Progema (France). The ATP can be released from algae cell easily with the cell lysis in this kit, and we do not need to wash cells or remove the medium, the reagent can be added to the microplate well directly. The plate reader will be used to quantitative determinate the ATP, and the relative luminescent units were detected with an Envision Multilabel Plate

Reader equipped with a luminescent optical filter. All experiments were done in triplicate.

Biomass transmission electron microscopy (TEM) imaging was performed with a Hitachi H-700 (Tokyo, Japan) operating at 75 kV equipped with a Hamatsu camera.

3. References

(1) Rocha, A. D.; Sivry, Y.; Gelabert, A.; Beji, Z.; Benedetti, M. F.; Menguy, N.; Brayner, R. The Fate of Polyol-Made ZnO and CdS Nanoparticles in Seine River Water (Paris, France). *j nanosci nanotechnol* **2015**, *15* (5), 3900–3908. https://doi.org/10.1166/jnn.2015.9276.

(2) Gelabert, A.; Sivry, Y.; Ferrari, R.; Akrout, A.; Cordier, L.; Nowak, S.; Menguy, N.; Benedetti, M. F. Uncoated and Coated ZnO Nanoparticle Life Cycle in Synthetic Seawater: ZnO Nanoparticle Life Cycle in Synthetic Seawater. *Environ Toxicol Chem* **2014**, *33* (2), 341–349. https://doi.org/10.1002/etc.2447.

(3) Dickson, A. G. Thermodynamics of the Dissociation of Boric Acid in Synthetic Seawater from 273.15 to 318.15 K. *Deep Sea Research Part A. Oceanographic Research Papers* **1990**, *37* (5), 755–766. https://doi.org/10.1016/0198-0149(90)90004-F.